Fluorescent Chemosensors for Metal Ions Based on Photoinduced Electron Transfer (PET) from Sulfur

Dissertation

zur

Erlangung der naturwissenschaftlichen Doktorwürde

(Dr. sc. nat.)

vorgelegt der

Mathematisch-naturwissenschaftlichen Fakultät

der

Universität Zürich

von

Mireille Vonlanthen

von

Schmitten FR

Promotionskomitee

Prof. Dr. Jay S. Siegel (Vorsitz)

PD Dr. Nathaniel S. Finney (Leitung der Dissertation)

Prof. Dr. Karl-Heinz Ernst

Zurich, 2013

Abstract of the Dissertation

Fluorescent Chemosensors for Metal Ions Based on Photoinduced Electron Transfer (PET) from Sulfur

by Mireille Vonlanthen
University of Zurich, 2013

The use of fluorescence for the detection of metal ions is a very powerful technique since it allows the analysis of traces amounts of specific analytes by a simple optical method. However, metal ions are not fluorescent, and in order to detect non-emissive targets using fluorescence spectroscopy small organic compounds capable of signal transduction need to be developed. Such compounds are named chemosensors when they are of abiotic origin. They will have to present two different states in their fluorescence emission indicating the occurrence of a supramolecular binding event via a transduction mechanism.

A photophysical mechanism is required for the signal transduction, and the most commonly used is photoinduced electron transfer (PET) quenching. In the majority of the examples found in the literature, PET based chemosensors focus on the use of the lone pair of electron from a benzylic nitrogen atom as electron donor for the quenching of the fluorescence. Upon coordination with metal ions, or protonation, the energy of the lone pair of electron is lowered and electron transfer is no longer thermodynamically favored. This gives rise to an increase of the fluorescence emission giving a visual indication of the presence of the target. In this thesis, the use of a sulfur atom as electron donor for PET quenching was investigated.

First, the case of a thioether functional group was studied with either a naphthalimide or a coumarin as fluorophore. The obtained compounds were not showing reduced quantum yields as expected in the case of an efficient PET quenching. This behavior could be explained by high redox potential of the thioether moiety leading to thermodynamically disfavored PET quenching process.

The second case studied was the integration of a thiourea moiety as electron donor for PET quenching process with a naphthalimide fluorophore. In this case, low quantum yields in

comparison with a non-quenched analog were observed indicating that PET quenching is occurring. A typical distance dependence of the efficiency of the process was observed and the study of the thermodynamics of the process indicates that PET is feasible. Subsequent addition of metal ions in methanol and in a water:methanol mixture was investigated and leads to recovery of the fluorescence. The addition of Hg^{2+} is showing the strongest affinity with an apparent binding constant of 1 μM and with a 10- to 20-fold increase of the fluorescence emission for all the compounds.

The affinity of the thiourea based chemosensor to various metal ions can be modulated by variation of the appended binding domain. The introduction of a di-2-pycolylamine (DPA), which is a well-known ligand for Zn^{2+}, as well as the introduction of other pyridine containing analogs is inducing interesting behavior. When DPA is placed very close in space to the thiourea, the chemosensor interacts with Zn^{2+} with only one of the pyridine, leading to 13 folds increase of the fluorescence but with lower affinity, as it would be expected for typical DPA-Zn^{2+} interaction. This hypothesis was confirmed by the crystal structure of a zinc complexe of an analog of our chemosensor bearing a phenyl group instead of the fluorophore. The addition of an ethyl bridge in the system gives more space between the DPA moiety and the sulfur atom leading to lower increase of the fluorescence enhancement but increased affinity for the interaction with Zn^{2+}.

Further modifications of the binding domain, for example by the addition of crown ethers containing oxygen or sulfur bridging atoms were investigated, and lead to interesting responses to various metal ion as for example Ag^{+} and Pb^{2+} in methanol and aqueous media.

This work demonstrates that modulation of PET quenching by thioureas provides a basis for the development of metal-responsive fluorescent chemosensors in protic media. High affinity and intensity response to the addition of Hg^{2+} as well as very interesting variation of the response to the addition of Zn^{2+} depending on the additional binding domain was observed.

Zusammenfassung der Dissertation

Fluoreszierende Chemosensoren für Metallionen Basierend auf Photoinduziertem Elektronentransfer (PET) von Schwefel

von Mireille Vonlanthen
Universität Zürich, 2013

Fluoreszenz ist eine sehr effiziente Methode für den Nachweis von Metallionen, weil es die Analyse von sehr geringen Mengen durch eine einfache und visuelle Methode erlaubt. Allerdings sind die Metallionen selbst nicht fluoreszierend und deshalb braucht es die Entwicklung von kleinen organischen Verbindungen, die fähig sind, einen Unterschied in der Fluoreszenz-Emission zu zeigen. Wenn diese Verbindungen eine abiotische Herkunft haben, werden sind sie Chemosensoren genannt. Es braucht zwei verschiedene Zustände in der Fluoreszenz-Emission um das supramolekulare Ereignis zwischen dem Metall und dem Chemosensor durch einen Transduktionsmechanismus zu zeigen.

Ein photophysikalischer Prozess ist die Grundlage für den Unterschied in Fluoreszenz-Emission und der meistgebrauchte Mechanismus ist die Fluoreszenzlöschung oder Quenching durch photoinduzierten Elektronentransfer (PET). Die Mehrheit der Beispiele von PET Chemosensoren in der Literatur funktionieren mit einem freien Elektronpaar von benzylischem Stickstoff als Elektronendonor. Wenn dieses Elektronpaar in einer Koordinationsbindung mit Metallionen involviert ist oder protoniert ist, ist der photoinduzierte Elektronentransfer nicht mehr thermodynamisch begünstigt. Das verursacht die Zunahme der Fluoreszenz-Intensität und ist deswegen eine visuelle Indikation, dass das Metallion anwesend ist. In dieser Dissertation wird der Gebrauch von Schwefel als Elektronendonor untersucht.

Zuerst wurde die funktionelle Gruppe der Thiolether als Elektronendonor für Naphthalimide- und Cumarin- Fluorophore studiert. Die erhaltenen Verbindungen haben keine Reduktion der Quantenausbeute gezeigt, wie es für einen effizienten PET Fluoreszenzlöschungsprozess zu erwarten war. Dieses Verhalten wurde durch das hohe Redoxpotentiale von Thiolethern erklärt, woraus ein thermodynamisch ungünstiger Prozess resultiert.

Dann wurde der Gebrauch einer Thiourea-Funktion als Elektronendonor für PET Fluoreszenzlöschung mit einem Naphthalimide-Fluorophore untersucht. Dieses Mal wurden im Vergleich zu nicht fluoreszenzgelöschten Analogen niedrige Quantenausbeuten beobachtet, was darauf hinweist, dass effiziente Fluoreszenzlöschung stattfindet. Ein Studium der Distanzabhängigkeit des Prozesses sowie Untersuchung der thermodynamischen Machbarkeit haben gezeigt, dass der PET-Prozess in unseren Molekülen möglich ist. Nachfolgende Zugabe von verschiedenen Metallionen in Methanol oder in einer Methanol:Wasser 90:10 Mischung hat gezeigt, dass die Fluoreszenz wieder ansteigt. Die Addition von Hg^{2+} zeigt die höchste Affinität mit einer Bindungskonstant von 1 μM und eine Zunahme der Fluoreszenz-Intensität von 10 bis 20 Mal mit allen Verbindungen.

Die Affinität unseres Systems für verschiedene Metallionen kann durch Variation des Bindungsbereichs angepasst werden. Der Gebrauch von di-2-pycolylamine (DPA), das bekannt ist als Ligand für Zn^{2+}, sowie der Gebrauch von anderen Pyridinresten hat interessantes Verhalten gezeigt. Wenn DPA sehr nah am Thiourea lag, konnte nur eines der beiden Pyridine an Zn^{2+} binden und deshalb war die Affinität für eine DPA-Zn^{2+} Interaktion geringer als erwartet. Diese Hypothese wurde mit einer Kristallstruktur eines Analogs unseres Chemosensors bestätigt. Eine Ethylbrücke wurde zwischen DPA und dem Thiourea eingesetz, sodass es mehr Platz für die Koordinationsbindung gab. Eine Erhöhung der Affinität für Zn^{2+} mit geringer Fluoreszenzzunahme wurde beobachtet.

Weitere Strukturmodifikationen, wie zum Beispiel der Gebrauch von Kronenethern mit Sauerstoff oder Schwefel als Heteroatome wurden getestet. Zudem wurden verschiedene interessante Zunahmen der Fluoreszenz in Gegenwart von Metallionen wie Ag^{+} und Pb^{2+} in Methanol oder in wässerigen Lösungen beobachtet.

Acknowledgement

I would like to start my thesis by thanking all the people who made it possible for me to reach this day. First of all, I want to thank my PhD supervisor PD Dr. Nathaniel Finney for allowing me to join his group and for providing me a perfect place to develop my research and teaching skills. I would like to thank him as well for teaching me his chemistry knowledge and for his support.

I would also like to thank Professor Jay Siegel and Professor Kim Baldridge for teaching me a lot of chemistry and as well for their great support especially at the end of my PhD and at time of taking decision for my future.

I would like to express my gratitude to Professor Karl-Heinz Ernst for being part of my PhD committee.

I would like to thank the NMR service, Simon Jurt and Nadia Bross for the great facilities and help solving NMR problems. I am also grateful to the mass analysis team, PD Laurent Biegler and Urs Stalder for all the measurements of mass analysis with a special thank to Jean-Christophe Prost for answering all my questions about mass analysis and being a great friend since the beginning of our studies in Neuchâtel.

I would like to thank Professor Anthony Linden for solving my crystal structure and his coworker Peter Uebelhart who was also very helpful sharing the lab and teaching me lab technics at the beginning of my PhD thesis.

During the 4 years of this thesis I have met many people and I would like to thank all the Finney, Siegel, Stuparu and Hessen PhD students past and present for the great working environment that we have shared in the lab and for all the nice moment that we have spent together. I would like to mention especially the Finney group members Eoin, Sergey, Silvia and Rahul for their collaboration and friendship as well as Yazmin, Fabienne, Caroline, Karla and Paola for their very nice friendship.

A very special person made all this work possible by giving me the motivation and making me smile everyday, so I would like to thank Fabián for his love and for being always ready to help me.

Finally I would like to thank my family, my parents and my sister for their unlimited support, patience and love.

Table of Contents

List of Figures

List of Schemes

List of Tables

Chapter 1

Introduction to Fluorescent Chemosensors

1.1 Introduction

The biochemical behaviors of living organisms like self-replication, information processing, and metabolism is based on specific interactions between targets and guests (as for example metal ions binding cellular receptors). The understanding of the selectivity and reversibility of molecular recognition is thus a fundamental issue. Since the recognition events are occurring in a world that is not directly observable for the human eyes, the development of devices capable of information transmission from the molecular level to the observable level is needed. Such devices are called chemical sensors or biochemical sensors. According to the Gold Book of the IUPAC, the definition of a chemical sensor is *a device that transforms chemical information, ranging from the concentration of a specific sample component to a total composition analysis, into an analytically useful signal*.[1] The basis of this device is a molecule of abiotic origin capable of signaling called chemosensor.[2] In the case where the basis of the device is of biotic origin it will be called biosensor. Chemosensors are more robust than biosensors and the target analytes of interest for chemosensors are not limited. They have the potential of information transmission and can be applied by analytical and environmental chemists, analytical biochemists and medical scientist as well as information technologist.[3,4]

A versatile phenomenon to visualize two different states of a chemical sensor is the observation of light, more particularly modification of the luminescence of the chemosensor.[5] The development of fluorescent chemosensors includes the study of photophysical properties for the visual modifications and supramolecular chemistry for the interactions between chemosensors and targets. Those topics will be developed in the following sections.

1.2 Photophysical Processes

All the phenomena that are occurring in a molecule starting from the absorption of a photon of light but are not leading to chemical modifications are referred as photophysical processes and are depicted in the Jablonski diagram (Figure 1.1). This diagram was first proposed by Jablonski in 1935.[6] It depicts the ground state S_0, the first and second singlet excited electronic state S_1 and S_2 as well as the first triplet excited electronic state T_1. Each state can exist in various vibrational energy levels, due to the variety of nuclear geometries, represented by the numbers 0, 1, 2 and 3. According to the Frank-Condon principle, the transitions of electrons between the states occur in a shorter time (10^{-15} s) than the displacement of the nuclei (10^{-12} s) and therefore can be represented as vertical lines.

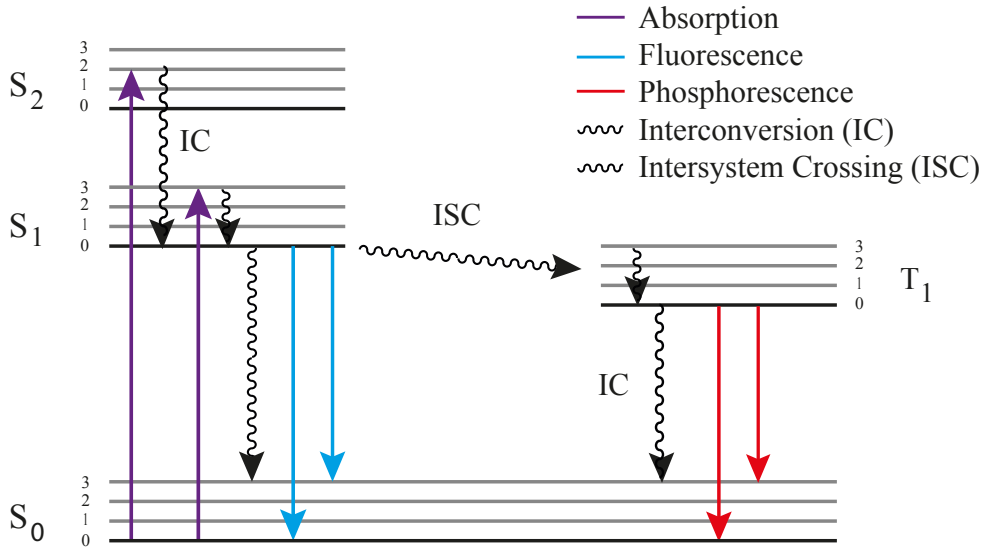

Figure 1.1: Jablonsky diagram, the straight arrows indicate radiative processes and wavy arrows indicate non radiative processes.

Light absorption promotes one electron from the ground state S_0 to one of the vibrational energy level of one of the singlet excited electronic states S_1 or S_2. It is followed by a rapid radiationless relaxation process (10^{-12} s) called internal conversion (IC) to the lowest vibrational energy level of S_1. This result in a thermally equilibrated long-lived excited state. Intersystem crossing (ISC) is a radiationless transition that can occurs between states of different multiplicity, it takes place from the lowest vibrational energy level of the singlet excited electronic state S_1 to one of the vibrational energy level of the first triplet excited electronic state T_1. In this process the spin of the electron is inverted and this process is formally symmetry forbidden because triplet and singlet wavefunctions are orthogonal.

However ISC is favored by spin-orbit coupling, which is an interaction between orbital angular momentum and spin angular momentum. The presence of heavy atom and halogens is increasing the spin-orbit coupling and consequently the rate of ISC.[7]

Fluorescence and phosphorescence are radiative deactivations processes from the lowest vibrational energy level of the singlet and triplet electronic excited state, respectively, to the ground or vibrational excited state of S_0. This is known as Kasha's rule since he first postulated that $S_n \rightarrow S_1$ internal conversion will be faster than $S_1 \rightarrow S_0$ emission because the exited stated are closer in energy to each other than they are to the ground state.[8] A photon with an energy corresponding to the difference in energy between the 2 states is emitted. Fluorescence emission is a spin allowed transformation from the singlet excited electronic state S_1 occurring with typical lifetime of 10^{-9} to 10^{-5} s. It occurs at a higher wavelength than the absorption and the observed Stokes shift represent a measure of the structural distortion between the ground and the excited electronic state. Phosphorescence emission is a spin forbidden process from the triplet excited electronic state T_1 occurring with a smaller rate constant and typical lifetime of 10^{-4} to 10^{1} s. The energy of the emitted photon is lower in comparison with the fluorescence emission, and therefore phosphorescence is observed at higher wavelength in the emission spectra.[7]

1.3 Principles and Design of Fluorescent Chemosensors

There are several aspects of fluorescence emission that make it especially suitable as a signal output for chemosensors. The advantages are the high sensitivity of detection down to single molecule and even routine experiments only need micromolar level of active molecules. Other advantages are the on-off switchability, the subnanometer spatial resolution and the millisecond temporal resolution in the present supramolecular context.[3,9] In order to use this phenomenon for visual detection of binding event, fluorescent chemosensors, which are molecules able to present two different states in their fluorescence emission properties, have to be developed.

A key concept in the development of fluorescent chemosensors is the fact the binding event to the analytes must be reversible. It will be characterized by an equilibrium constant and will allow dynamic optical response with the change of the analyte concentration. The dissociation constant (K_d) of the complex formed should be approximately equal to the mean concentration of the guest of interest.[2]

In case of biomedical applications, other requirements for the development of fluorescent chemosensors are first to have an excitation wavelength higher than 340 nm to avoid cell damage by UV and second to have an emission wavelength higher than 500 nm in order to be distinguishable from the auto-fluorescence of the cell.[10] Furthermore a large increase in the fluorescence quantum yield is desirable in order to be observable by microscopy.

The chemosensors devices are built of two distinct moieties, the recognition moiety and the signaling moiety.[11] The recognition moiety is responsible for the selectivity and the efficiency of the binding event between the sensor and the target. For each class of targets, different binding domains presenting specific interactions have to be developed. Hydrogen bonds and π-interactions will be involved in the recognition of neutral molecules, coordinative interactions in the case of metal ions and electrostatic interactions in the case of anions. The nature of the solvent will also contribute to the binding event. The research of novel specific and reversible interactions is in the field of supramolecular chemistry. The signaling moiety acts as signal transducer and is responsible for the conversion of the recognition event into a change in the photophysical properties of the chemosensor. This happens because the chemical and structural properties of the excited state are very different than the ones of the ground state and various processes such as photoinduced electron transfer (PET), energy transfer (ET), excimer and exciplex formation can occur in the excited state. They are the basis of the photophysical changes and will be studied in more details in Chapter 1.5. The topology of the link between those two units has also an important role in the overall detection process. The functioning of an OFF-ON chemosensor is depicted in Figure 1.2. The most desirable configuration is to have a chemosensor which is non-fluorescent in its unbound state (OFF-state) and is recovering fluorescence emission upon binding with the analyte (ON-state). The other configuration starting from a fluorescent chemosensor showing turning-off of the fluorescent emission is also possible.

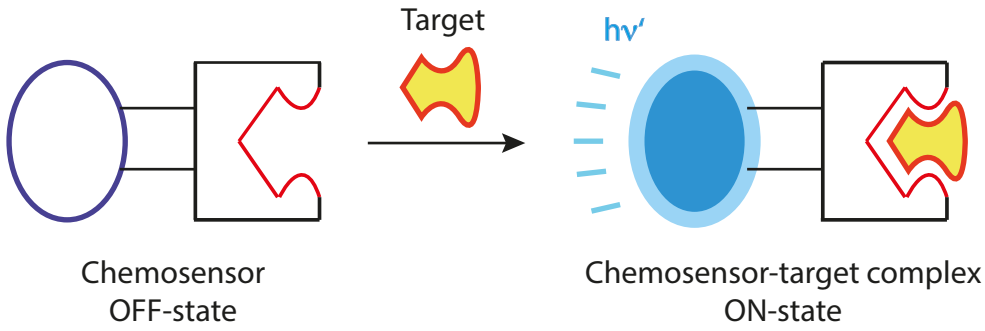

Figure 1.2: Principle of fluorescent chemosensor. Fluorescence emission is turned-on upon binding with the target.

1.4 Early Fluorescent Chemosensors

In the middle of the 19th century, George Stokes reported the fact that fluorescence emission occurs at higher wavelength than the excitation, phenomenon named Stokes shift. In addition, he proposed that fluorescence could be used for the detection of organic substances because of his various observations of variations of the fluorescence intensity due to the presence of foreign substances.[12,13] The observation of fluorescence is the experimental key to the development of fluorescent chemosensors. The theoretical background about exciplex formation and photoinduced electron transfer explaining the observations was developed by Weller in 1970 and will be discussed in Section 1.5.

In the development of fluorescent chemosensors, a class of proton-responsive compounds was first investigated and the difference in fluorescence by the change of the pH was the most obvious analysis.[14] Later the development of the chemosensors for the detection of cations and anions was possible leading to useful applications.

The first example of fluorescence sensing by application of supramolecular receptors was published by Sousa in 1977.[15,16] The chemosensors **1** and **2** are based on naphthalene fluorophore bearing crown ether as receptor for alkali metal ions.

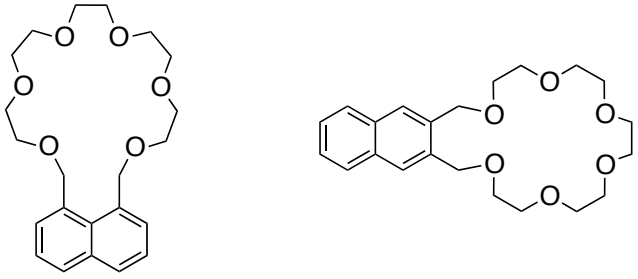

1 **2**

Figure 1.3: First examples of fluorescent chemosensors reported by Sousa in 1977.[15]

The work of Selinger shows the phenomenon of intramolecular fluorescence quenching though a propylene chain spacer in compound **3** and subsequent annulation of this process through protonation of the nitrogen center.[14] Then Shizuka in Japan studied a library of phenyl alkylamines **4** with variation of the chain length from 1 to 3 methyl groups. Their fluorescence is pH dependent and a relation with their relative pK_a was studied. The quenching was observed without excimer formation and it depends on the number of methylenes units, on the polarity of the solvent and on the temperature.[17]

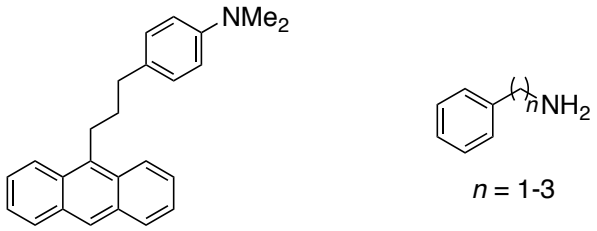

3 **4**

Figure 1.4: Structures of the chemosensors studied by Selinger and Shizuka.[14,17]

Bouas-Laurent, Desvergnes and Lehn in collaboration have published in 1985 an example of fluorescence enhancement due to the interaction of a neutral receptor **5** with a target that was different than a proton.[18,19] In the following years, the application of the observation of fluorescence enhancement for sensing purposes started to be generalized by the discoveries of A.P. de Silva. He could demonstrate that the interactions of **6** with protons and **7** with alkali metal ions were leading to modifications of the fluorescence output and were possible to monitor.[20,21]

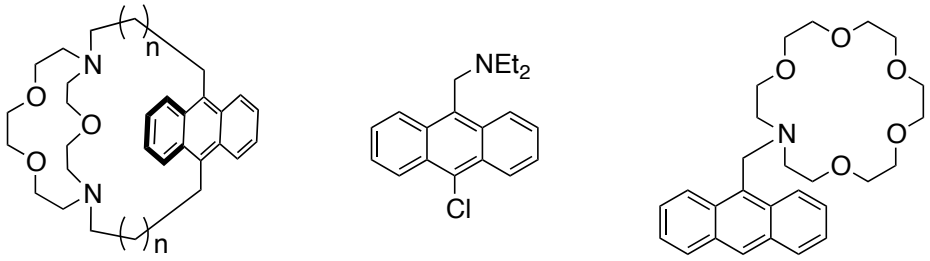

5 **6** **7**

Figure 1.5: Structures of the first chemosensors proposed by Bouas-Laurent, Desvergnes, Lehn and de Silva.[18,20]

Czarnik was able to show that fluorescent probe can also be used in order to sense anions. His compound **8** is showing high fluorescence enhancement upon addition of phosphate and other anions (Figure 1.6).[22] He has produced a lot of contribution in the development of fluorescent chemosensors. At the time when he was studying metal ion catalyzed amide hydrolysis with compound **9**, he observed for he first time a peculiar fluorescence behavior after exposition to Zn^{2+}.[23] Further detailed study of the properties of **9** showed in 1988 a very large enhancement of the fluorescence emission in acetonitrile after addition of zinc chloride (Figure 1.6).[24]

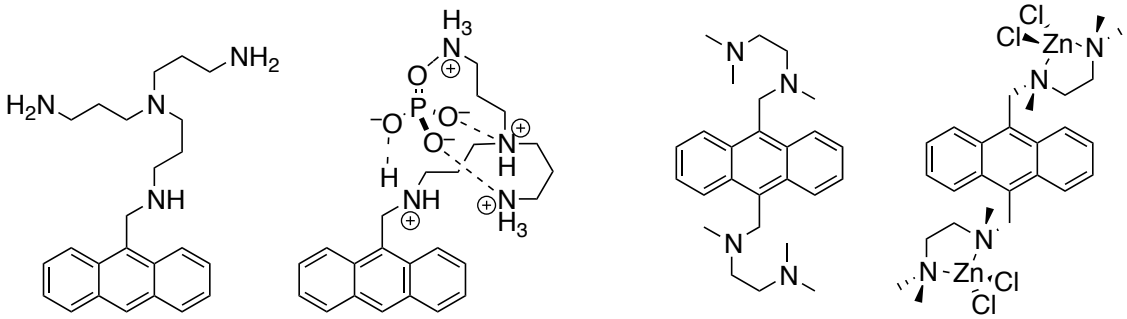

8 **8-Phosphate** **9** **9-Zn**

low fluorescence high fluorescence low fluorescence high fluorescence

Figure 1.6: Anion sensor **8** and Zn^{2+} sensor **9** reported by Czarnik.[22,24]

The disadvantage of those compounds is their insolubility in water, for this reason Czarnik developed different sensor bearing polyazamacrocycle **10** and **11**.[25,26] In this series of compounds, changes in the fluorescence emission are observed, while changing the pH of the solution, supporting the idea of a photoinduced electron transfer mechanism. Those compounds are responding as well to metal ions. For ions like Zn^{2+} and Cd^{2+}, a 20 to 190

folds increase of the fluorescence is observed after the addition of one equivalent. For metal ions like Hg^{2+}, a decrease of the fluorescence is observed.[25]

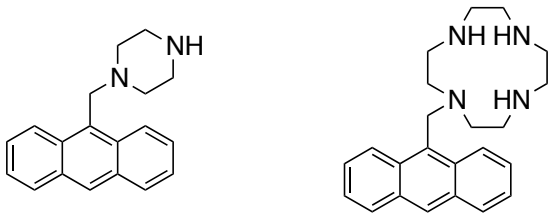

10 **11**

Figure 1.7: Aqueous chemosensors based on polyazamacrocycle from Czarnik.[25]

Since those first reports, fluorescent chemosensors have evolved and many groups have made important contributions, which were recently reviewed in the literature.[4,27,28]

1.5 Mechanisms of Signal Transduction

The process of molecular recognition happens in the ground electronic state of the two interacting atoms or molecules. This recognition event has to induce a modification of the fluorescence emission in order to be observable and therefore changes in the excited electronic state of the fluorophore as electronic structure or energy variations are needed. The coupling between the recognition and the reporting event is called transduction. There are many mechanisms of signal transduction, which can be use for the design of fluorescent chemosensors.

Apart from non-radiative internal conversion, and radiative processes fluorescence and phosphorescence emission, an excited state can participate to many inter- and intramolecular reactions. Examples of intramolecular processes are photoionization, photodecomposition and photoisomerization. For the intermolecular pathways, reactions with molecules in the ground state are taking place as for example addition reaction, hydrogen abstraction, energy transfer and electron transfer.[29]

Various ways to modify fluorescence have been studied for the development of fluorescent chemosensor. The most common ones are photoinduced electron transfer (PET) and photoinduced internal charge transfer (ICT) and they will be the subject of the following sections. Other mechanisms have been studied as for example electronic energy transfer

(EET) and conformational restriction but those mechanism will not be discussed in this thesis.[3]

1.5.1 Photoinduced Electron Transfer (PET)

1.5.1.1 Theory of PET

A species in the electronic excited state has a better ability to donate or capture electrons from other sites as the same species is in the ground electronic state. The excited species is therefore acting as strong oxidizing or reducing agent inducing chemical changes in a neighboring ground state molecule through photoinduced electron transfer (PET).[30]

The reductive or oxidative electron transfer processes according the equations (1) and (2) and their respective frontier orbital energy diagram are represented in Figure 1.8.

$$A^* + D \rightarrow A^{\cdot -} + D^{\cdot +} \quad (1)$$

$$D^* + A \rightarrow D^{\cdot +} + A^{\cdot -} \quad (2)$$

In the case of a reductive electron transfer (1) the fluorophore is reduced by the quencher and in the case of an oxidative electron transfer (2) the quencher is reduced by the fluorophore. The direction of the transfer is directed by the redox potential of both components of the molecule.

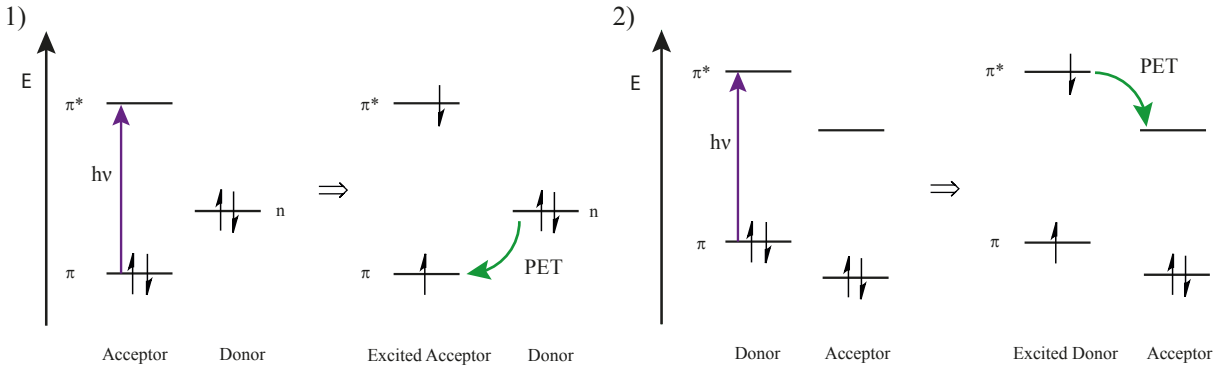

Figure 1.8: Frontier orbital energy diagram of a fluorophore-receptor pair, illustrating the thermodynamics of PET. 1) reductive electron transfer with the fluorophore as electron acceptor and receptor as electron donor. 2) oxidative electron transfer with the fluorophore as electron donor and receptor as electron acceptor.

The photoinduced electron transfer is a fundamental early event of the photosynthesis process, when, following light absorption, fast electron transfers create charge separation in a photosynthetic reaction center.[31] This phenomenon is of great interests and is the most commonly used signaling mechanism for fluorescent chemosensors.

There are three important factors to determine the feasibility of an excited electron transfer. The first factor is an electronic factor; the redox potential of the donor and the acceptor should match to allow the electron transfer. The direction of the transfer is determined by the oxidation and reduction potentials of the ground and excited state of the donor and acceptor. The second and third factors are structural factors. The electron donor and the electron acceptor have to be close in space because the transfer needs crossing of the electronic wavefunctions of the initial excited state and the product state. It can be achieved by covalent bonding through a short spacer. Moreover the transfer of electron will be favored only in the case when the molecular orbitals involved in the transfer are from the same symmetry. Those factors will be detailed in the following sections.

a) Thermodynamics of PET

The work of Rehm and Weller in 1970 provides the thermodynamic and kinetic basis for the process of excimer formation and photoinduced electron transfer.[32,33] In order to predict the feasibility of the process, the free energy of electron transfer ΔG_{el}^{0} is calculated by the Rehm-Weller equation:

$$\Delta G_{el}^{0} = E(D^{+}/D) - E(A/A^{-}) - \Delta E_{00} - \frac{e^{2}}{\varepsilon\, d} \qquad (3)$$

In this equation, $E(D^{+}/D)$ describes the reduction potential of the electron donor depicted in equation (4) and $E(A/A^{-})$ the reduction potential of the acceptor depicted in equation (5). ΔE_{00} is the energy of the 00 band of the $S_0 \rightarrow S_1$ transition of the fluorophore.

$$D^{+} + e^{-} \rightarrow D \qquad (4)$$

$$A + e^{-} \rightarrow A^{-} \qquad (5)$$

The last term of the Rehm-Weller equation represent the coulombic interaction between the formed charges derived from Coulomb's Law where ε is the static dielectric constant of the solvent and *d* the center-to-center separation distance in Ångströms between the charges. The formation of a radical anion from the acceptor and a radical cation from the

donor is inducing electrostatic interactions. The contribution of this force is depending on the solvent through its dielectric constant but is only a small contribution in the overall estimation of ΔG_{el}^{0}.[6,34]

A negative ΔG_{el}^{0} indicates an exergonic reaction and will be favored with a rate constant k_{el} depending on the free energy of activation $\Delta G_{el}^{\neq}$.

$$k_{el} = A\ exp\{-\Delta G_{el}^{\neq}/RT\} \quad (6)$$

According to the Marcus theory, $\Delta G_{el}^{\neq}$ can be derived from ΔG_{el}^{0} and the reorganizational energy.[35-37] This theory predicts a quadratic dependence of $\Delta G_{el}^{\neq}$ with ΔG_{el}^{0} (7).

$$\Delta G_{el}^{\neq} = \frac{\lambda}{4}\left(1 + \frac{{\Delta G_{el}^{0}}^{2}}{\lambda}\right) \quad (7)$$

It predicts that the distortion of the reactants, products and solvents is described by identical parabolas that are shifted according to the driving force of the process (ΔG_{el}^{0}). In the Marcus inverted region, a high ΔG_{el}^{0} leads to increase of the activation energy and therefore a less favored process. Quenching of the fluorescence emission will be observed when electron transfer occurs during the lifetime of the excited state.

b) Distance dependence of the electron transfer

The distance dependence has been postulated by Davidson, if the donor is far from the acceptor in the ground state, several bond rotation must occur to place the two part in the ideal configuration for the electron transfer to occur.[38] It has been shown that a linker up to 14 atoms can be used.[38,39] The geometry is an important parameter determining the efficiency of PET since an overlap of the electronic wavefunction is needed. The formation of exciplex in aminoalkylnaphthalenes have been studied by Chandross, Thomas and Davidson.[40,41]

The expression for the distance dependence of PET rates which assume an exponential decay with the increasing of the distance is given in equation (8) where *k* is the rate constant, R_0 the Van der Waals separation and β a constant scaling the distance dependence.[42]

$$k = k_0\ exp[-\beta(R - R_0)] \quad (8)$$

This equation indicates that an increase of the distance between the donor and the acceptor is decreasing the rate of PET and therefore lowering the probability of fluorescence quenching with the distance.

c) Orbital symmetry dependence of the electron transfer

The prediction of rate constant only from energetic considerations present some restriction in the case of ridged systems.[43] The symmetry of the orbitals involved in the electron transfer has to be considered to evaluate its feasibility. This parameter will have less influence in the case of flexible molecules that can modify its configuration to reach the correct orbital symmetry interaction for PET.

1.5.1.2 PET in Fluorescent Chemosensors

The quenching of fluorescence by PET is a property that is used in the development of fluorescent chemosensors. In the off state of the sensor, the photophysical processes are described as follow. After absorption of light one π-electron from the π orbital of the fluorophore is excited to its π^* orbital. In case that the thermodynamics and kinetics parameter are in favor of an electron transfer, one electron from the donor will be transferred to the ground state of the fluorophore leading to charge separation (radical anion and radical cation). The reaction of electron transfer is reversible, the excited electron is returning to the ground state of the donor via a non-emissive back electron transfer (ET) pathway and therefore the fluorescence of the fluorophore appears quenched (Figure 1.9).

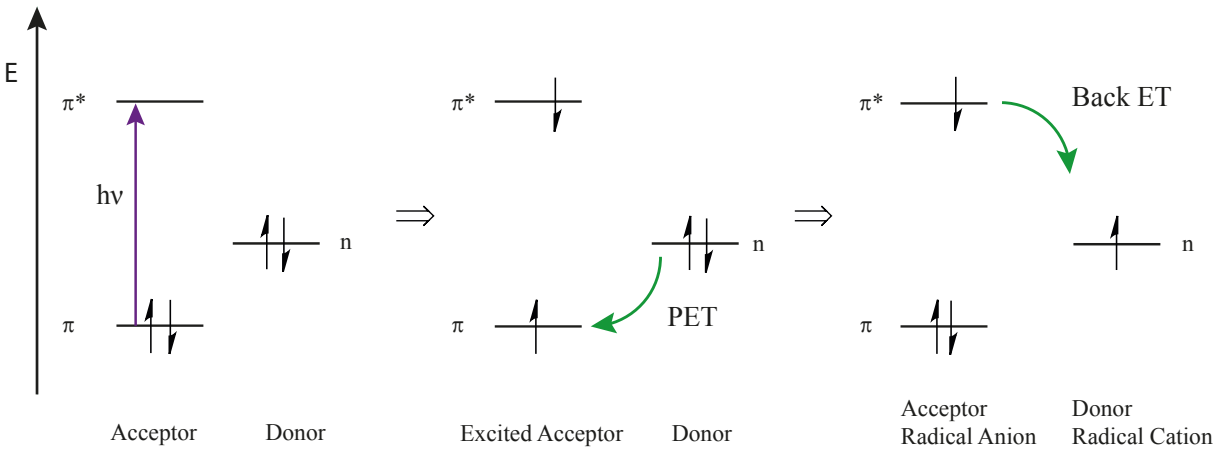

Figure 1.9: Frontier orbital energy diagram of a fluorophore (acceptor) receptor (donor) pair, illustrating the thermodynamics of PET and back electron transfer (ET).

By influencing the redox potential of one of the two partners, it is possible so avoid the transfer of an electron in the system and an enhancement of the fluorescence will be observed. The use of a benzylic nitrogen as electron donor for the quenching of the fluorescence is commonly reported. When a benzylic nitrogen is attached to a fluorophore,

the lone pair of electron from the nitrogen in its unbounded state is involved in the quenching of the fluorescence emission by PET. Protonation or coordination of the receptor will suppress this quenching by changing the redox properties of the nitrogen. The energy level of the n orbital of the nitrogen will be lowered and an enhancement of the fluorescence will be observed (Figure 1.10).[38,44]

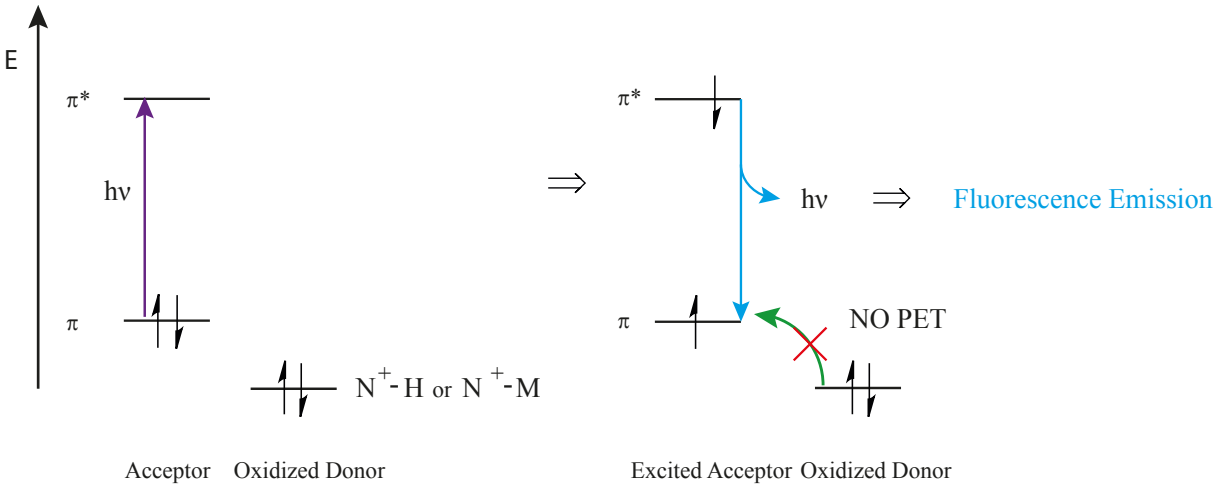

Figure 1.10: Frontier orbital energy diagram illustrating fluorescence enhancement due to interaction of the donor with protons or metal ions, lowering the energy level of the HOMO of the donor.

This configuration is the most commonly used in the development of fluorescent chemosensors but cases where the electron donor is the excited fluorophore are also leading to efficient PET quenching (Figure 1.11).

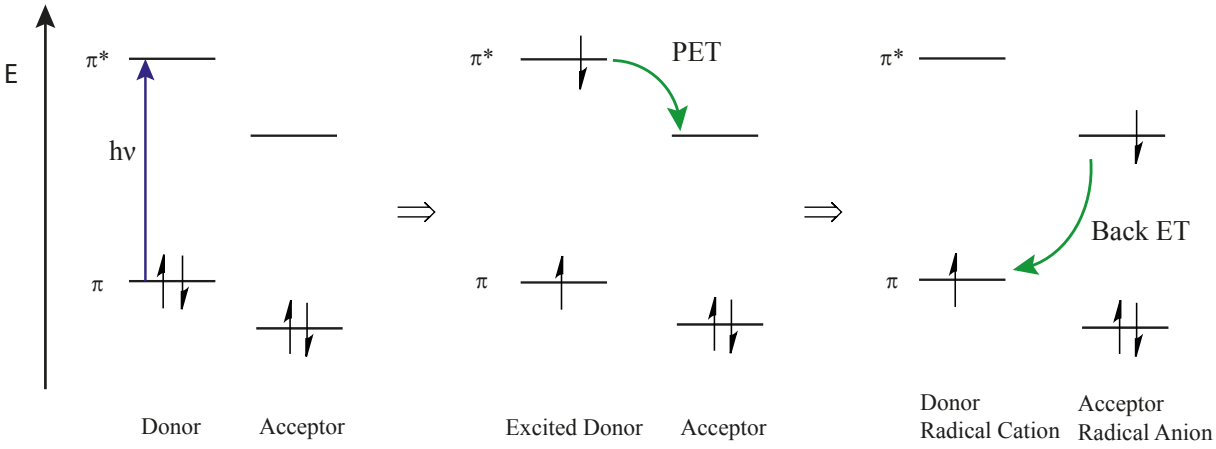

Figure 1.11: Frontier orbital energy diagram of a fluorophore (donor) receptor (acceptor) pair, illustrating the thermodynamics of PET and back electron transfer (ET).

The first chemosensors reported by de Silva for protons **6** and metal ions **7**, described in Chapter 1.4 are working by PET quenching mechanism.[45] Afterwards PET quenching has been the most commonly used mechanism for the development of fluorescent chemosensors. A typical example of a new developed chemosensor for metal ions is a series of compounds synthesized and studied by Lippard **Zinpyr-1**, **Zinpyr-2** and **ZP4**.[46-49] Their structures are containing fluorescein as fluorophore linked to a di-2-picolylamine (DPA) moiety as receptor for Zn^{2+} sensing (Figure 1.12).

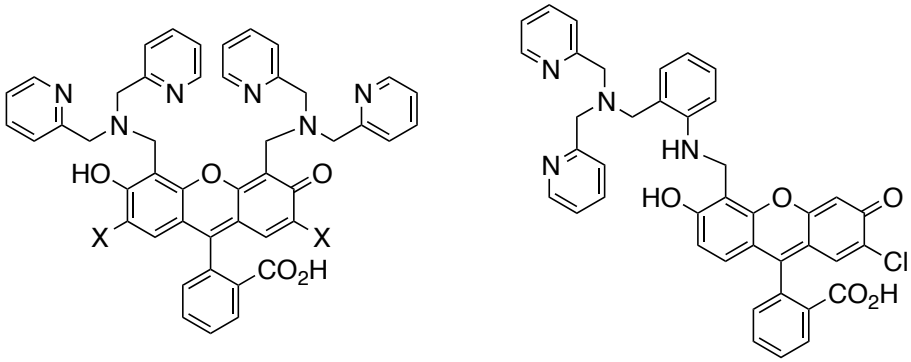

Zinpyr-1: X = Cl
Zinpyr-2: X = H

ZP4

Figure 1.12: PET based chemosensors for Zn^{2+} from Lippard.[47,48]

The first two published sensors **Zinpyr-1** and **Zinpyr-2** are presenting dissociation constants for Zn^{2+} complexes in the nM range. The obtained quantum yield is reaching 0.9 with a 2- to 3-fold enhancement of the fluorescence under physiological conditions and membrane permeability was shown but their initial quantum yield under those conditions is quite high.[47] To overcome this problem, different generations of sensors were prepared and **ZP4** is showing lower quantum yield under physiological conditions and the same affinity for Zn^{2+}, as well as membrane permeability.[48]

The sensors based on fluorescein have the advantage of absorbing light in the visible region. They can be used in water showing large variation of the quantum yield upon binding with Zn^{2+}. However the major drawback is its sensitivity to pH changes, which reduce its possible application in cellular systems.[47]

The studies of Czarnik on compound **12** with variation of the chain length from 1 to 3 methyl groups show that benzylic amines are uniquely positioned for PET quenching.[38] In those compounds the most efficient quenching was observed when a tertiary amine is linked

to anthracene though a methylene bridge. With a longer spacer the quenching still occurs but with lower efficiency.

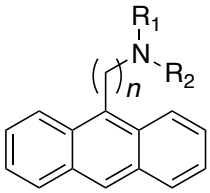

n = 1,2,3

12

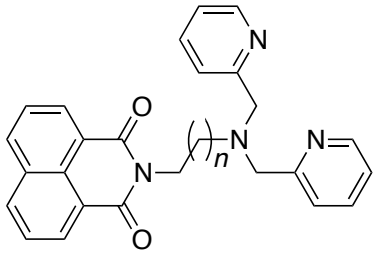

n = 1,2,3

13

Figure 1.13: Anthacene and naphthalimide based chemosensors showing distance dependent PET quenching.[38,50]

A naphthalimide-based chemosensor containing a di-2-pycolylamine binding domain for Zn^{2+} ions with variation of the chain length **13** (Figure 1.13) has been investigated and the same increase of the quantum yield was observed indicating less efficient PET quenching with the increasing of the distance.[50] This sensor and is selective for Zn^{2+} ions (K_d = 1 μM) and a 5-fold fluorescence enhancement is observed in HEPES buffer. The compound shows as well response to Cd^{2+} with lower fluorescence enhancement and higher dissociation constant (K_d = 14 μM). Other systems with variations of the length of the spacer have all shown increase in the quantum yield with the increase of the spacer length.[17,51,52]

1.5.2 Photoinduced Internal Charge Transfer (ICT)

1.5.2.1 Theory of ICT

Signaling via internal charge transfer (ITC) is based on electron transfer occurring within the same electronic system or between systems presenting a high level of conjugation. Molecules containing heteroatom π-electron systems with an electron withdrawing group on one side and electron donating group on the other side present a large difference in their dipole moment between their ground electronic state and their lowest energy singlet excited state.[3] Since the acceptor moiety becomes a stronger acceptor in the electronic excited state and the donor becomes a better donor, the pull-push mechanism leads to a larger charge polarization in the electronic excited state.

The dipole moment generated by excitation is interacting with the dipole moment of the solvent generating high sensitivity to the solvent polarity.[29] According to the Frank-Condon principle, the solvent dipole orientational distribution will be conserved upon absorption. The Frank-Condon S_1 excited state is populated but is presenting the same dipole orientation. Therefore no significant changes in the absorption band upon the polarity of the solvent are observed in the absorbance spectra (Figure 1.14a).

Since the emission process is slower, reorganization of the solvent dipoles can then occur leading to equilibrated S_1 excited state. In polar solvent the equilibrated S_1 excited state is stabilized and at the same time its equilibrated ground state is destabilized. Under cryogenic conditions or in low-polar solvent, emission from the Frank-Condon S_1 excited state will be observed, it corresponds to the $\pi^* \rightarrow \pi$ transition or locally excited state (LE) band. In polar solvent a red shift of the fluorescence emission band (ICT emission band) will be induced through stabilization of the excited state (Figure 1.14b).[3] The lifetime and the quantum yield will be lowered as well in polar media.

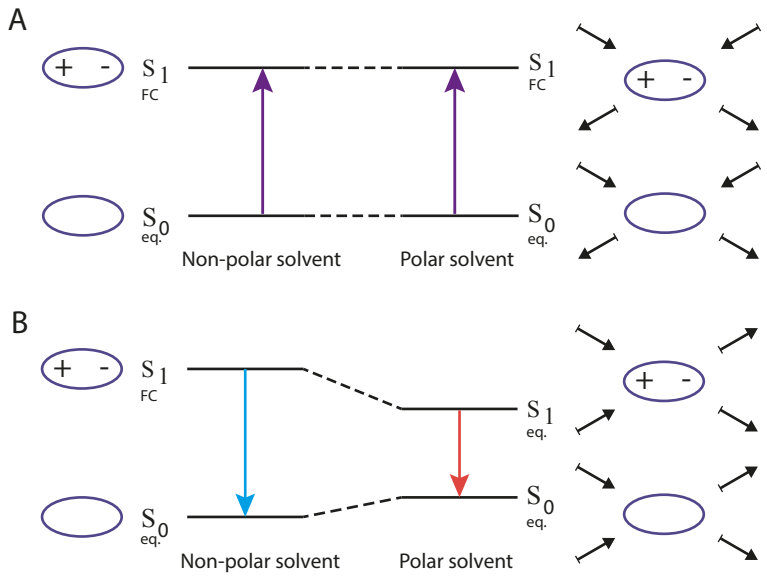

Figure 1.14: Solvent effect on a compound presenting ICT state. a) Effect on the absorbance; b) Effect on the fluorescence emission. FC represent a Frank-Condon excited state and eq. represent a thermally equilibrated state.

An example of compounds presenting a construction corresponding to the requirement of ICT is compound **14**. It shows a high red shift form apolar to polar media, the maximum of fluorescence emission is 455 nm in cyclohexane and 549 nm in water.[53]

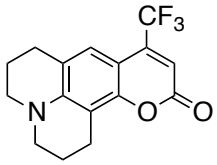

14

Figure 1.15: Coumarin-based fluorophore presenting ICT.

If the donor and the acceptor are connected through a single bond, they can adopt an orthogonal geometry in the excited state leading to full charge separation.[54,55] This excited state is then called twisted internal charge transfer (TICT) and emits a dual fluorescence with the first emission band coming from the locally exited state (LE) and a longer wavelength emission band from the charge transfer (CT) state. This phenomenon is very sensitive to the solvent polarity. The TICT emission band is appearing only in polar media due to the very polar character of the charge separated state. The most commonly studied compound presenting both ICT and TICT emission band is 4-(dimethylamino)benzonitrile **15** (Figure 1.16). It has a planar skeleton and therefore an ICT-type excited state, but the formation of a dimethylamino radical cation and bezonitrile radical anion leads to a 90° angle twist and therefore an TICT-type excited state.[56,57]

15

Figure 1.16: Representation of TICT state in **15**.

1.5.2.2 ICT in Fluorescent Chemosensors

The electronic excited states subject to ICT and TICT are very sensitive to the electric fields and therefore to the presence of metal ions. This property can be used to build a fluorescent chemosensor for metal ions when either the electron-rich side or the electron poor side of the fluorophore is functionalized with a cation receptor.

When a partial positive charge is generated by the addition of a cation close to the electron donor side, the exited state is destabilized and a blue shift of the absorption and fluorescence emission band are observed. On the contrary when the cation receptor is introduced on the electron poor side, a red shift of the absorption and fluorescence emission is

expected due to the stabilization of the electronic excited state through enhanced electron-withdrawing character of the acceptor (Figure 1.17).[11] In both cases, changes in quantum yield and lifetime are also observed. The absorption band is in general more shifted than the emission band. If the cation receptor is at the positively charged side of the chemosensor, the cation can be ejected during the lifetime of the excited state and no recognition will be observed.

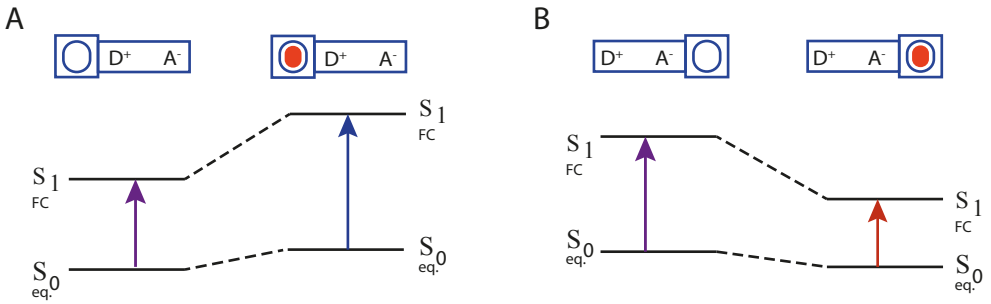

Figure 1.17: Cation (red dot) effect on the absorption wavelength for a fluorophore with an ICT exited state. a) Receptor on the donor side; b) Receptor on the acceptor side of the fluorophore.

The first studies base on ICT chemosensors were done by Valeur and Lapouyarde with structures containing an azacrown ether as cation receptor.[58,59] The nitrogen atom was then conjugated with various electron-withdrawing groups and form for example **16** and **17** chemosensors. The absorption spectra are shifted to the blue upon addition of Ca^{2+} indicating destabilization of the complex. However the fluorescence emission spectra shows only a small shift due to the effect of photodisruption of the interaction between the metal ion and the chemosensor.[60] Variation of the size of the crown ether is leading to response to different metal ions.[61]

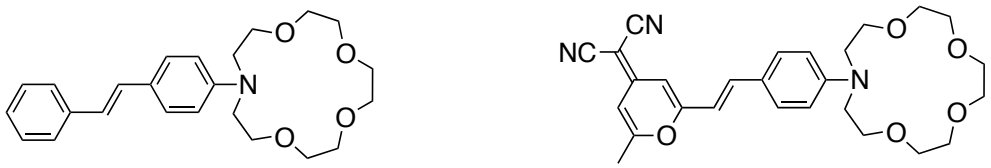

16 **17**

Figure 1.18: Crown ether containing sensors based on ICT mechanism.[58,59]

In the further development of this kind of sensor, different well-known chelator moieties were introduced in the scaffold. The most famous examples are **Indo-1** and **Fura-1** (Figure 1.19) developed by Tsien for the detection of Ca^{2+}.[62-64] In those examples the electron

donating group is again involved in the coordination leading to significant blue shift in the absorbance spectra whereas less influence is observed on the fluorescence emission spectra.

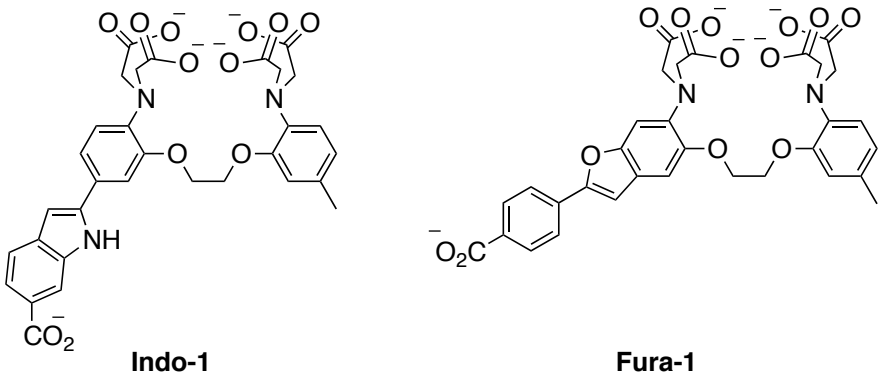

Figure 1.19: Chemosensors for Ca^{2+} based on ICT mechanism.[64]

1.6 Thesis Objective

In the chemosensor literature using PET quenching as transduction mechanism, the reporting element of an important majority of examples is the nitrogen atom. Its ability as electron donor and its changes in redox properties upon protonation and coordination are the major advantages of this element. However other elements should be able to be involved as well in PET quenching and sensing application. Since all the main group of elements have there own characteristics regarding to the redox and coordination properties, the development of fluorescent chemosensor based on different reporting elements would expand their range of metal recognition domain.

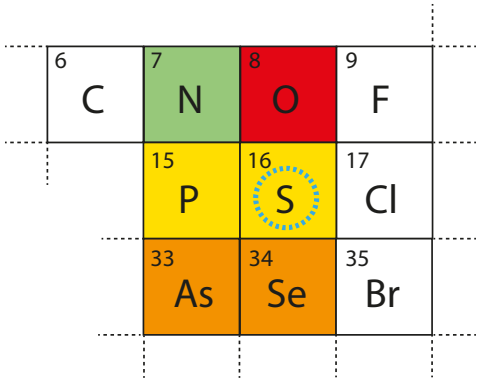

Figure 1.20: Non-metal elements of the periodic table.

Among the other elements of the same group as nitrogen, phosphorus was studied and a few examples of compounds showing different states in their fluorescence emission are described in the literature.[65-67] In all those compounds fluorescence recovery was observed upon oxidation from the phosphorus to the phosphine oxide. Since phosphorus undergoes oxidation, it use in the development of fluorescent chemosensors for metal ions is restricted. The use of arsenic remains almost unexplored due to its toxicity but one recent example shows the development of FlAsH fluorescent probe for the labeling of proteins in intact cells and the use of arsenic would be worth to study it in more details.[68,69]

In the elements of the sixth main group, oxygen is not a good candidate due to its poor electron donor properties and sulfur and selenium remain almost unexplored. In this thesis efforts will be done on the development of PET based sensors with sulfur as reporting element. Its redox properties and its ability of making soft donor interactions with metal ions could be involved in a PET quenching switch to form fluorescent chemosensors. However no clear examples of metal-responsive chemosensors based on sulfur have been reported in the literature. Sulfur could be incorporated to chemosensors in various forms. The first idea which is going to be explored in this thesis is the use sulfur from a thioether function. The study of the photophysical processes in a construct based on a naphthalimide or a coumarin as fluorophore linked to a chain containing a thioether functionality as electron donor will be the subject of the study in Chapter 2. Another possibility of involving sulfur in a PET chemosensor is to incorporate it as a thiourea moiety. In Chapter 3, the first constructs based on naphthalimide as fluorophore linked to a thiourea moiety as well as various responses upon addition of metal ions will be presented and Chapter 4 will show possible modifications of this structures leading to modulation of the fluorescence response. All the experimental procedures and characterizations of the obtained compounds will be detailed in Chapter 5.

Chapter 2

Study of thioethers as Donor for PET Quenching

2.1 Introduction

The research objectives described in this Chapter are the syntheses and the investigation of the photophysical properties of series of molecules designed in order to test the possibility of using thioether as donor for a PET quenching signaling mechanism in fluorescent chemosensors. All the compounds investigated in this Chapter will contain a thioether receptor and different fluorophores. First a phthalimide fluorophore will be tested and following the encouraging results obtained a naphthalimide fluorophore based sensor will be studied. In the last part of the Chapter, a construct based on a coumarin fluorophore will also be investigated. In the cases where effective PET quenching is observed, subsequent responses to the addition of different metal ions will be investigated in order to test the chemosensor capacity of the obtained compounds.

2.1.1 Background on Thioether Coordination Chemistry and the Chemosensors

The use of sulfur as reporting element in fluorescence chemosensors for metal ions could open new possibilities of ion selectivity due to its coordination properties, which are different than those of nitrogen. Sulfur has low electronegativity, can be easily oxidized, is highly polarizable and has low-lying empty orbitals.[70,71] Those criteria correspond to the definition of a soft base and following the empirical principle of hard and soft acid and base (HSAB), it will preferentially interact with soft acids. This means that it will interact with acceptor metal of low positive charge, large size and containing polarizable outer electrons like Hg^{2+}.[72,73]

The use of a sulfur atom as reporting element for PET based chemosensors for the detection of metal ions has not been reported in the literature to the best of our knowledge. However, some reported observations of variations of the fluorescence intensity in the presence of a sulfur atom and an oxidized sulfur atom supports the idea that a compound

constructed from a fluorophore and a quenching element containing a sulfur atom could lead to the development of new metal-responsive chemosensors.

More precisely, a publication from Griesbeck reports the observation of a low quantum yield for a compound based on a phthalimide fluorophore linked to a thioether side chain **18**.[74] Moreover the oxidation of the sulfur atom was leading to an increase of the fluorescence of the compound **19** (Figure 2.1). The reason for this observation could be that the sulfur atom is acting as a donor for PET and therefore is quenching the fluorescence of the phthalimide. In the case of the oxidation from the sulfur to the sulfoxide, the quenching effect is may be suppressed and the recovery of the fluorescence could be observed.

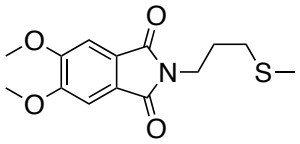

18

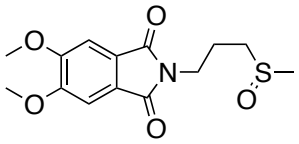

19

Figure 2.1: Griesbeck's Structures.[74]

2.2 First Target: Bis-Phthalimide as Fluorophore

2.2.1 Introduction

The initial target molecule of this project, the bis-phthalimide compound **20** (Figure 2.2), is inspired by the observations made with Griesbeck's system. It is composed of a bis-phthalimide fluorophore linked to a thioether containing chain through an ethyl group spacer. This compound was chosen because it has the advantage that a bis-phthalic anhydride core is commercially available.

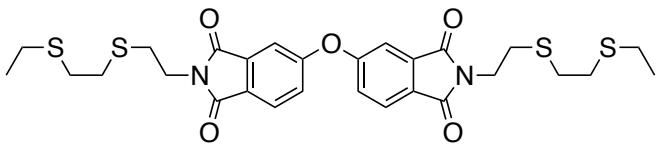

20

Figure 2.2: Bis-phthalimide based target compound.

2.2.2 Synthesis of the first target 20

The synthesis of the sulfur-containing moiety **25** containing two thioether functions was accomplished in three steps following the synthetic way shown in Scheme 2.1.

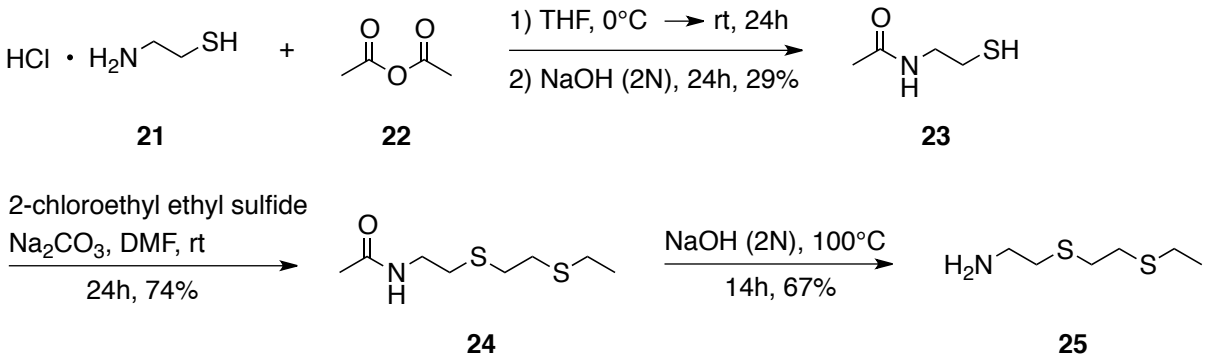

Scheme 2.1: Synthesis of the thioether containing chain **25**.

The synthesis starts from cysteamine hydrochloride **21**. The amine function was protected with an acetyl group **23**.[75] Cysteamine is reacting first to form the *S*-acetyl compound, which is then stirred in basic conditions to accomplish a sulfur to nitrogen acetyl transfer in 29% yield.[76,77] The free thiol **23** is sensitive to oxidation and has to be kept under nitrogen atmosphere.[i] In the next step, it reacts with the commercially available 2-chloroethylethyl sulfide to give **24** in 75% yield. Extreme precautions have to be taken for this reaction because of the toxicity of the starting material, which is an analogue to mustard gas. The product **24** was then deprotected under basic conditions to give the free amine **25** in good yield (Scheme 2.1).

The thioether containing chain **25** can be attached to different kind of fluorophores in order to try to quench their fluorescence. The phthalimide **20** was synthesized in one step starting from the commercially available 4,4'-oxydiphthalic anhydride **26** in 46 % yield and obtained as a white solid (Scheme 2.2).[78] A mass spectra analysis could be obtained form acetonitrile confirming the obtaining of **20** but even very small amount of methanol added to the analysis was leading to decomposition of the product. This means that no analysis of this compound can be done in polar protic solvents. However the compound is very stable as a solid or in apolar and polar aprotic solvents.

[i] Since 2012 compound **23** is commercially available.

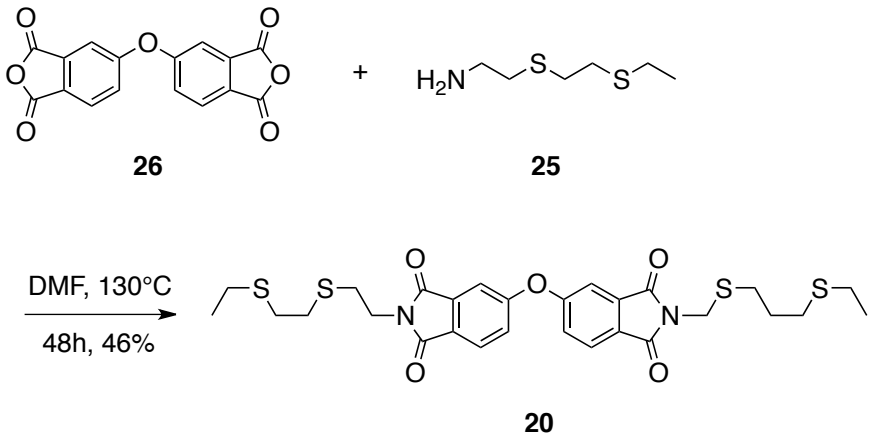

Scheme 2.2: Synthesis of the first target **20**.

The synthesis of compound **20** was not obtained through the first reaction pathway tested. Other reaction pathways have been explored and will be described shortly in the next paragraphs.

The compound **27** could be obtained from the reaction of the commercially available 4,4'-oxydiphthalic anhydride **26** and 2-bromoethylamine heating at 130°C in DMF for 2 days. The next step was the introduction of a thiol to the compound. This can be done by introducing a thioester through the reaction with thioacetic acid in the presence of a base in THF. Compound **28** could be isolated, but the deprotection of the thioester did not lead to the isolated free thiol. A one-pot reaction with deprotection followed by substitution by 2-chloroethyl ethyl sulfide was attempted without success (Scheme 2.3).

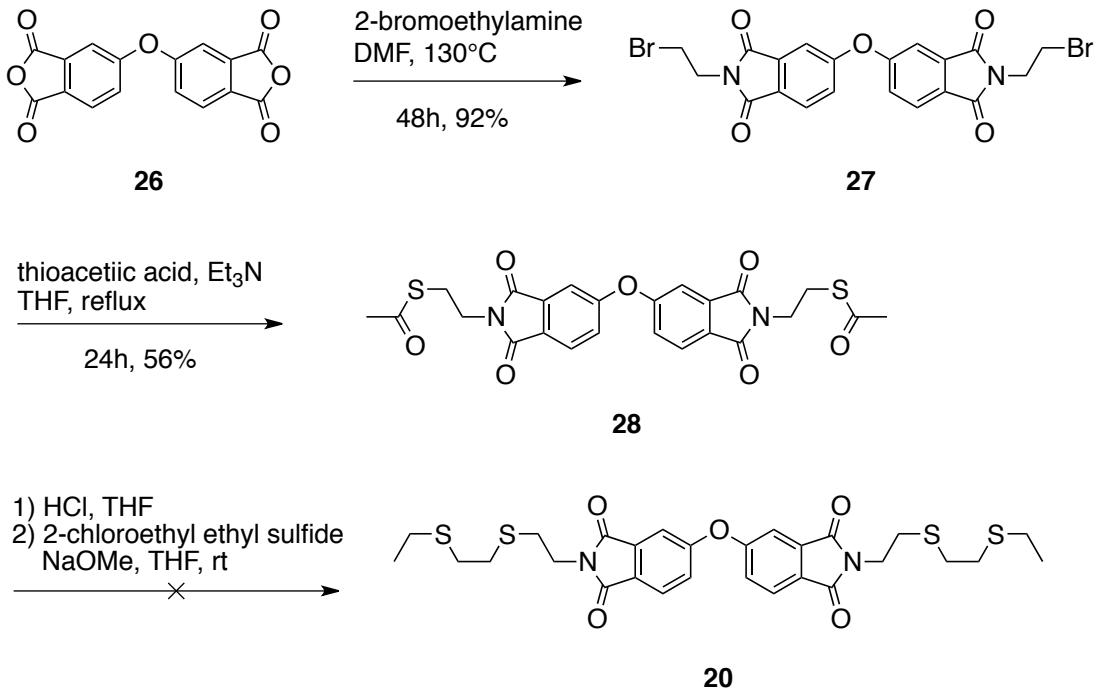

Scheme 2.3: Unsuccessful synthetic pathway for compound **20**.

In order to avoid the use of the very toxic mustard gas analogue 2-chloroethylethyl sulfide, ethyl 2-hydroxyethyl sulfide **29** was used. Unfortunately the reaction with thiourea did not lead to the formation of the thiol **30** and the reaction with p-toluensulfonyl chloride also did not lead to the formation of the tosylated **31** (Scheme 2.4).

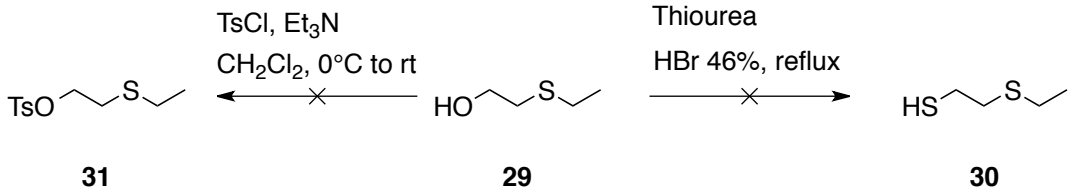

Scheme 2.4: Unsuccessful synthetic pathways from ethyl 2-hydroxyethyl sulfide **29**.

2.2.3 Photophysical Properties of Compound 20

The photophysical properties of compound **20** were investigated in CH_2Cl_2 and in acetonitrile. The UV-visible absorption spectrum is showing a high-energy band at 240 nm and the last emissive band appears at about 310 to 330 nm in both solvents (Figure 2.3). The fluorescence emission spectrum is showing no emission band in both solvents.

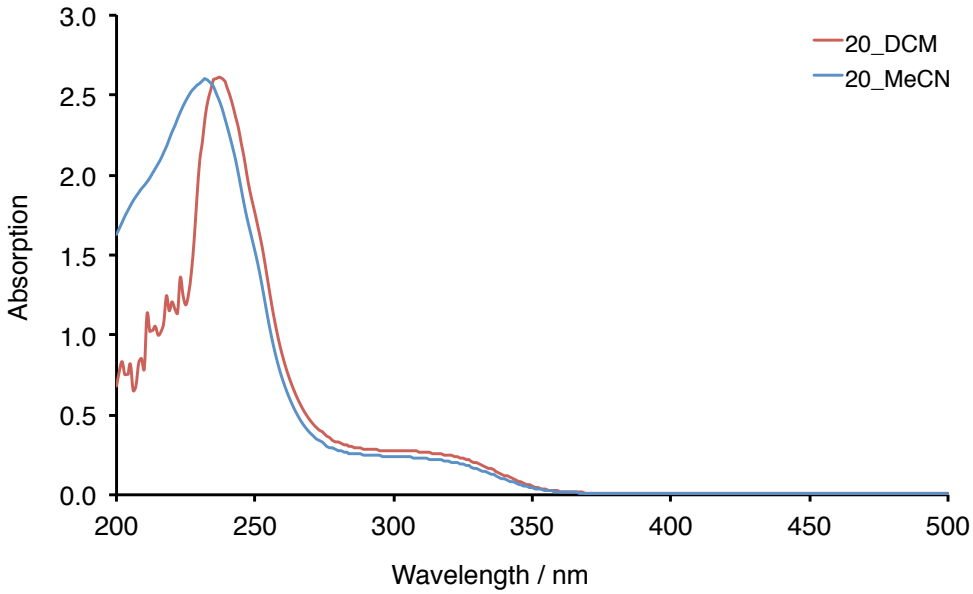

Figure 2.3: Absorbance spectra of **20** in CH_2Cl_2 and in acetonitrile.

The measurements of the photophysical properties for compound **20** could not be determined in protic polar solvent like methanol and water for stability reason. This proved to be a problem for the detection of metal ions because they are more soluble in polar solvents and practical applications require aqueous conditions.

2.2.4 Fluorescence Titration of the Compound 20 with Metal Ions

The fluorescence titration of compound **20** was carried out in CH_2Cl_2 but the metal ions were added as solution in DMSO. The metal ions tested are Li^+, Na^+, K^+, Mg^{2+}, Ca^{2+}, Ag^+, Zn^{2+}, Cd^{2+}, Hg^{2+} and Pb^{2+}. The anions used are Cl^-, ClO_4^- or NO_3^-. The only response by appearance of a large fluorescent band at 400 nm was observed after the addition of Hg^{2+} (Scheme 2.5). However the addition of more Hg^{2+} was leading to rapid decrease of the fluorescence. It is probably due to the effect of the solvent because the Hg^{2+} salt was added in DMSO and the presence of this solvent is inhibiting the complexation with the metal leading to decrease of the fluorescence.

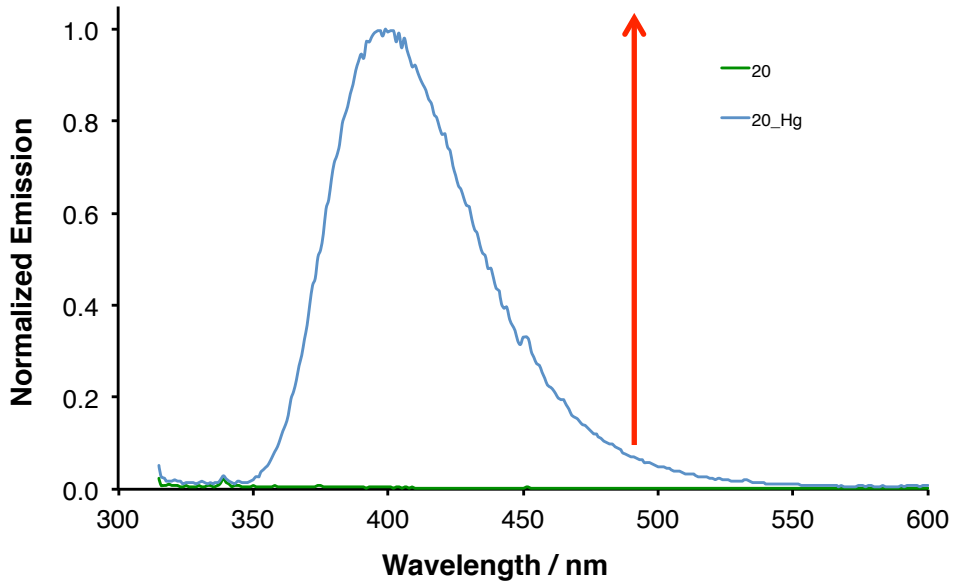

Scheme 2.5: Fluorescence emission increase of **20** after addition of 1 equivalent of Hg^{2+}.

2.2.5 Conclusions

The obtained phthalimide compound was not stable in protic polar solvents and for this reason it is difficult to titrate it with metal ions. An increase of the fluorescence emission was observed upon addition of Hg^{2+} in CH_2Cl_2 but no conclusion on the quenching mechanism could be done with this only data point. Therefore we decided to improve the stability of the chemosensor by changing the compound to a naphthalimide based fluorophore.

2.3 Naphthalimide Based Series of Targets

2.3.1 Naphthalimide Based Chemosensors

The naphthlimide core was chosen as fluorophore because of its high fluorescence, high photostability and large Stokes shift.[50] Additionally the stability of naphthlimides towards hydrolysis has been proved to be higher than the stability of phthalimides in polar solvents.[79]

Absorption and emission properties of various substitution pattern of the naphthalimide core have been studied.[80] Derivatives bearing no substituent at the 4-position of the naphthalimide core are not a very emissive fluorophores but the addition of various substituents are modifying their photophysical properties. Various amino-substituents at the

4-position are showing a yellow color corresponding to absorption band around 450 nm with a very high quantum yield of 0.7 to 0.8.[81]

4-amino-1,8-naphthalimide possess a internal charge transfer excited state (ICT). This structure favors PET from electron rich receptors positioned at the 4-position rather than at the imide side position.[82,83] However, Gunnlaugsson is showing the bidirectionality of the process.[84,85] He has designed and studied compounds based on naphthalimide and thiourea as sensor for anions (See structures in Chapter 3, Figure 3.2) and he observed that PET quenching is effective in both directions of the naphthalimide core. Moreover studies on 4-methoxy substituted naphthalimides are showing high quantum yields in compoud **32** and are showing PET quenching of the fluorescence by the addition of an amine linked to the imide side through an ethyl spacer **33**.[86] The quantum yield is lowered from 0.76 for **32** to 0.065 for **33** by PET quenching of the amine. In the case of the absence of the methoxy group on this construct, the fluorescence is much lower for the analogue to **32** but still quenched by the amine linked to the imide side of the naphthalimide. In both case, the quenching is observed to be distance dependent as explained in the Chapter 1.5.1.[50]

$\phi = 0.76$ $\phi = 0.065$

32 **33**

Figure 2.4: Structures and quantum yields of naphthalimide based chemosensors.[86]

2.3.2 Design of the Target Compounds

The targets were designed by analogy to the first target from Chapter 2.2.1 in order to improve the stability of the sensor in polar solvents. We have selected a 1,8-naphthalimide fluorophore substituted at the amine position and at the 4-position with a thioether containing side chain to test its ability for PET quenching of the naphthalimide fluorescence.

In order to test the directionality of the process observed by Gunnlaugsson, two types of compounds were designed. The first compounds are containing a 2-methoxy ethoxy group at the 4-position and the thioether containing chain linked though the nitrogen of the naphthalimide with variation of the chain length (**34** and **35**, Figure 2.5). The second group of

compounds is constructed in the opposite direction for the electron transfer. The thioether chain is placed on the aromatic ring at 4-position with variation of the length of the chain and the amine of the naphthalimide is bearing a propyl chain (**36** and **37**, Figure 2.5).

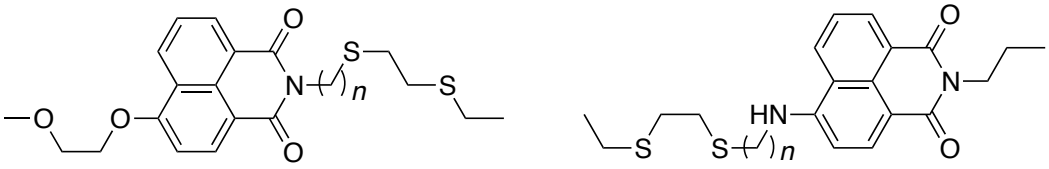

34: $n = 2$
35: $n = 3$

36: $n = 2$
37: $n = 3$

Figure 2.5: Structures of the targets based on a naphthalimide fluorophore with different position of the chain and different spacer lengths.

2.3.3 Synthesis of the Target compounds 34-37

The thioether containing chain **25** was prepared as described in the Chapter 2.2.2. In the next reaction step, it was solved in DMF and heated to 100°C with the commercially available 4-bromo-naphthalic anhydride **38** to form compound **39** in 76 % yield (Scheme 2.6). The bromine is then substituted by refluxing **39** for 2 hours in methoxyethanol in presence of K_2CO_3 as a base to give the target **34** in 53 % yield. This procedure is exempt of transition metal catalyst, which is an advantage in the synthesis of fluorescent chemosensor for metal ions. With this procedure we are sure that the obtained pure material is free of traces of metal contaminants. The product **34** is purified by column on silica gel deactivated with triethylamine because of its instability towards acids on silica.

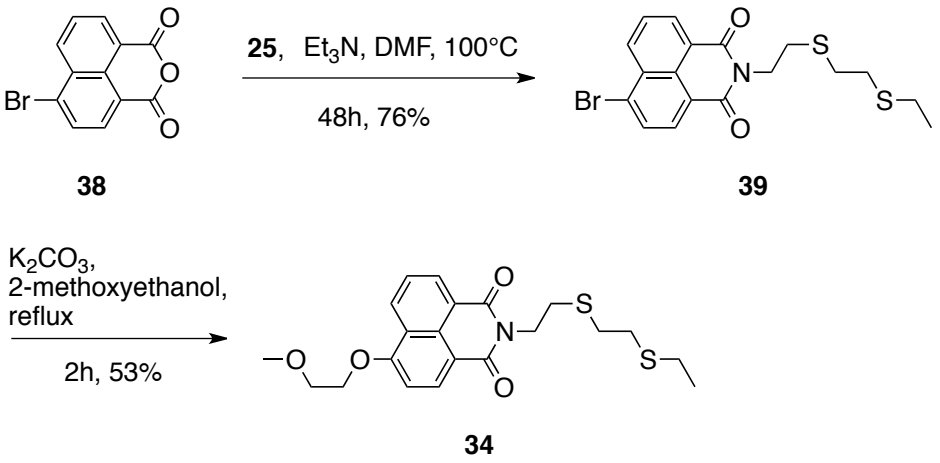

Scheme 2.6: Synthetic scheme of the target compound **34**.

A different synthetic route had to be investigated to obtain a propyl spacer between the fluorophore and the sulfur quenching element. The synthesis starts with the commercially available 3-bromopropylamine **40** and potassium thioacetate **41**. Compound **42** is obtained after heating at reflux overnight in THF. A substitution of the bromine by the thioacetate occurs first and is followed by a sulfur to nitrogen acetyl transfer as described in Chapter 2.2.2 for the synthesis of **23**. This reaction has a very low yield probably due to the instability of the product towards oxidation. Then compound **43** was formed by the reaction with 2-chloroethyl ethyl sulfide in DMF in the presence of a base. The starting material of this reaction is commercially available and it is important to repeat that it has to be handled with extreme precautions because of its acute toxicity. The compound **43** is deprotected under basic conditions to give the free amine **44** in 74% yield (Scheme 2.7).

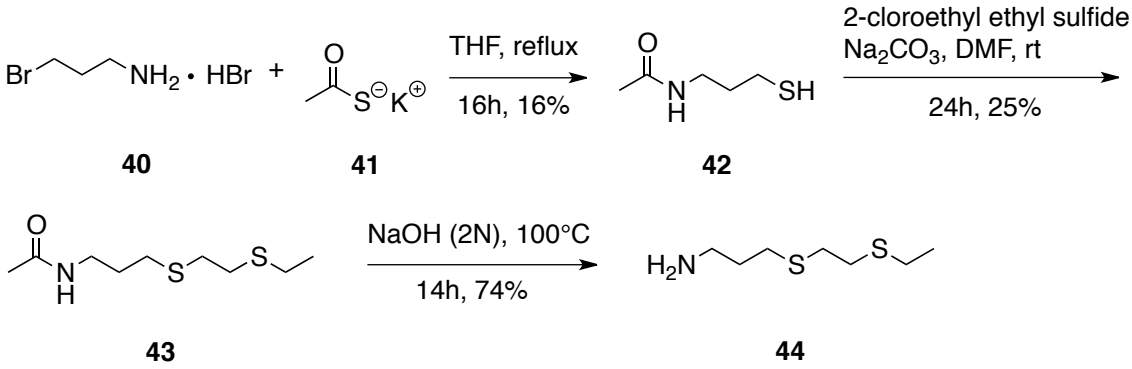

Scheme 2.7: Synthetic scheme of the thioether chain with a propyl chain spacer **44**.

The obtained thioether containing chain with a propyl spacer **44** was heated to 100°C in DMF with the commercially available 4-bromo-naphthalic anhydride **38** to form compound **45** in 55% yield. The bromine is then substituted in the same way as described for **34** to get compound **35** in 40% yield (Scheme 2.8). The product **35** is purified by column on silica gel deactivated with triethylamine because of its instability towards acids on silica.

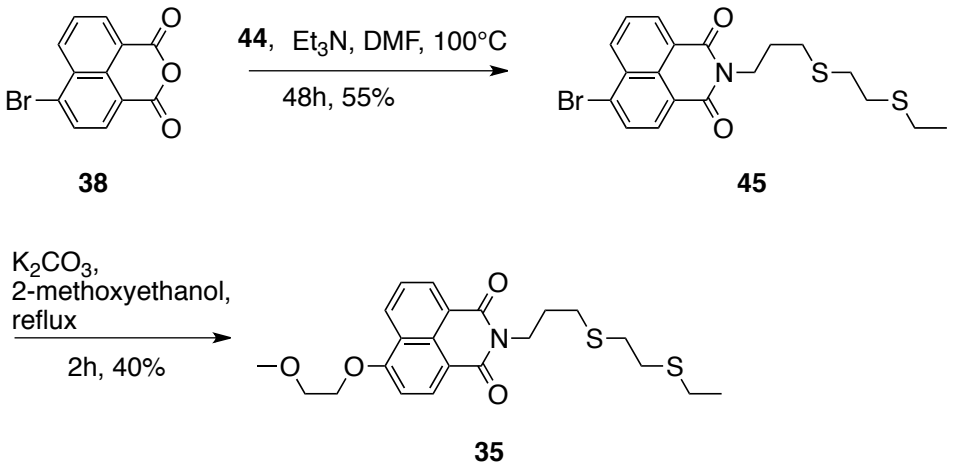

38 **45** **35**

Scheme 2.8: Synthetic scheme of the target compound **35**.

In order to invert the position of the substituents on the naphthalimide and obtain the target compounds **36** and **37**, 4-bromo-naphathalic anhydride **38** was heated to reflux with 1-aminopropane in ethanol overnight to form the precursor **46**. Then the bromine was substituted by the chain **25** or **44**, heating at 80°C in DMSO overnight, to give the target compounds **36** and **37** respectively (Scheme 2.9).

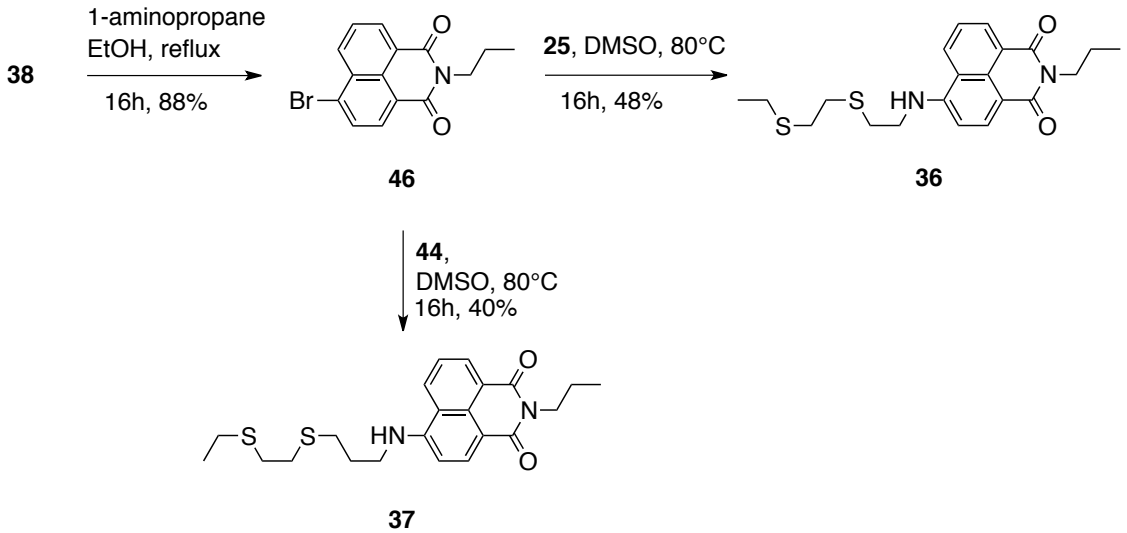

46 **36** **37**

Scheme 2.9: Synthetic scheme of the target compounds **36** and **37**.

A control compound **47** was synthesized to evaluate the quenching of the fluorescence by the thioether moiety. This compound is expected to show very high quantum yield since no quenching element is attached. The synthesis is done starting form **46** and 1-aminobutane in hot DMSO overnight to yield **47** (Scheme 2.10).

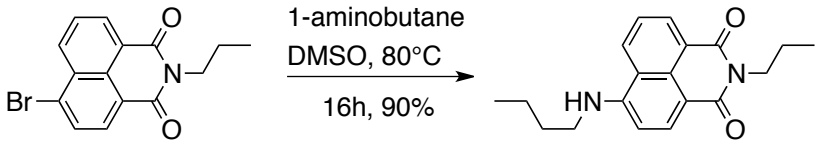

46 **47**

Scheme 2.10: Synthetic scheme of the control compound **47**.

An alternative target containing a methoxy instead of a 2-methoxyethoxy group at the 4-position of the naphthalimide fluorophore was also explored. The reaction of **39** with a base in methanol in order to form **48** was not successful. The use of phenanthroline and copper iodide was intended in methanol but the product could not be isolated.[87,88] The problem was that decomposition of the product was catalyzed by cupper and the boiling point of methanol was too low for the reaction to occur without catalyst.

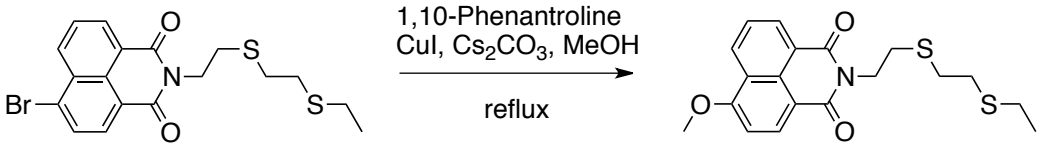

39 **48**

Scheme 2.11: Intended substitution of the 4-position of **39** by a methoxy group.

2.3.4 Photophysical Properties of 34-37

The photophysical properties of the target compounds **34** and **35** were investigated in CH_2Cl_2. The UV-visible absorption spectrum of both compounds is characterized by a broad band with a maximum at 365 nm. The fluorescence emission spectrum is characterized by a broad band with a maximum at 425 nm. Compound **34** is showing high quantum yield of 0.15 while **35** with a longer spacer is showing an even higher quantum yield of 0.24 (Table 2.1). This observation is consistent with modest distance-dependent PET quenching.

Table 2.1: Photophysical properties of **34** and **35** in CH_2Cl_2.

Compounds	λ_{abs} / nm	ε^a / $M^{-1}cm^{-1}$	λ_{em} / nm	$\phi_F{}^b$
34	365	15200	425	0.15
35	365	14800	425	0.24
47	425	14800	500	0.55

[a] For longest wavelength λ_{max} . [b] Relative to anthracene in methanol $\phi = 0.30$. [89]

At the time of the design of **35,** we were predicting that a compound with propyl spacer would be more efficiently quenched than with an ethyl spacer, if the sulfur atom is not in an appropriate position in the case of **34** and is not close enough in space to the fluorophore for an efficient PET quenching, as depicted in Figure 2.6. The position of the sulfur quencher in the case of a propyl chain could be more appropriate.

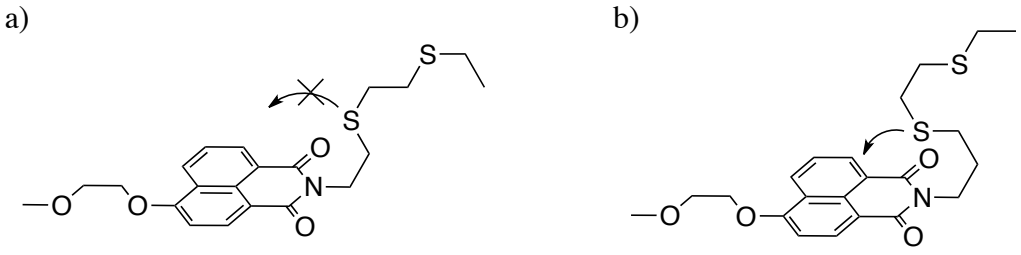

Figure 2.6: Hypothesis to explain the non-efficient PET quenching in the compound **34**. a) Sulfur atom is not close enough to the fluorophore to allow ET or contact mediated fluorescence quenching. b) Sulfur atom is close enough to the fluorophore to allow ET or contact mediated fluorescence quenching.

This prediction appeared to be erroneous after the observation that **35** shows similar UV-visible and fluorescence emission spectra but higher quantum yield than the parent compound **34** (Table 2.1). This observation of distance dependence is not a surprising result since it is in accord with the literature (see Chapter 1.5.1).

The photophysical properties of the target compounds **34** and **35** were investigated as well in methanol. The UV-visible absorption spectrum of both compounds is similar as in CH_2Cl_2. The fluorescence emission spectrum is characterized by a broad band showing a bathochromic shift in comparison with CH_2Cl_2 with a maximum at 445 nm. Compound **34** is

showing similar quantum yield in both solvent while the quantum yield of **35** is lower in methanol (Table 2.2).

Table 2.2: Photophysical properties of **34** and **35** in methanol.

Compounds	λ_{abs} / nm	ε^a/ $M^{-1}cm^{-1}$	λ_{em} / nm	$\phi_F{}^b$
34	365	12500	445	0.13
35	365	13200	445	0.15
47	425	14800	500	0.55

[a] For longest wavelength λ_{max} . [b] Relative to anthracene in methanol $\phi = 0.30$.[89]

The thioether containing chain was attached on the 4-position of the naphthalimide to check the directionality of the quenching because maybe from this side the quenching by sulfur could be more efficient. This prediction turned out to be incorrect as well.

For both spacer length **36** and **37**, the photophysical properties were investigated in CH_2Cl_2. The UV-visible absorption spectra are characterized by a broad emission band at 425 nm and the fluorescence emission spectra by long wavelength emission band with a maximum at 500 nm (Table 2.3). This represents a bathochromic shift from 80 nm for the absorption and the emission in comparison with **34** and **35**. The fluorescence emission band of the compounds **36** and **37** is coming from an internal charge transfer from the amine to the fluorophore. A bright green fluorescence can be observed by eye (Figure 2.7), corresponding to quantum yields of 0.43 and 0.52 respectively. Both quantum yields are higher than the ones observed for **34** and **35** indicating that no efficient quenching of the fluorescence by the thioether moiety is taking place from this side.

The control compound **47** has the same absorption and emission characteristics as the compound of this series **36** and **37**. The quantum yield of **47** is not higher confirming that no quenching by sulfur can take place in this kind of construct.

Table 2.3: Photophysical properties of **36** and **37** in CH_2Cl_2.

Compounds	λ_{abs} / nm	ε^a/ $M^{-1}cm^{-1}$	λ_{em} / nm	$\phi_F{}^b$
36	425	14200	500	0.43
37	425	13800	500	0.52
47	425	14800	500	0.55

[a] For longest wavelength λ_{max} . [b] Relative to SPA in water ϕ = 0.57.[89]

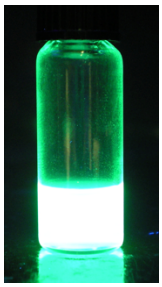

Figure 2.7: Green fluorescence of target compound **37**.

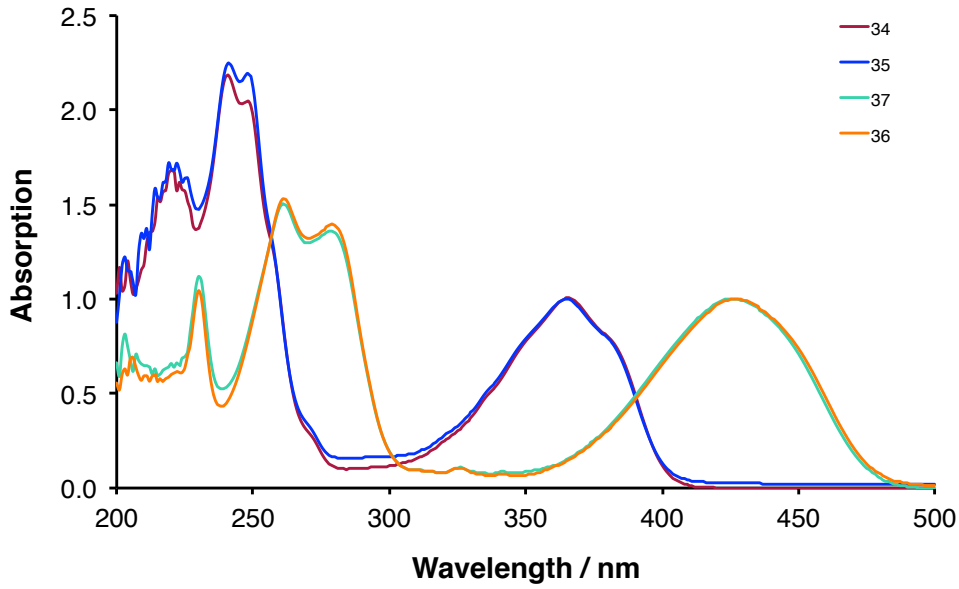

Figure 2.8: UV-visible absorption spectra from **34-37** in CH_2Cl_2.

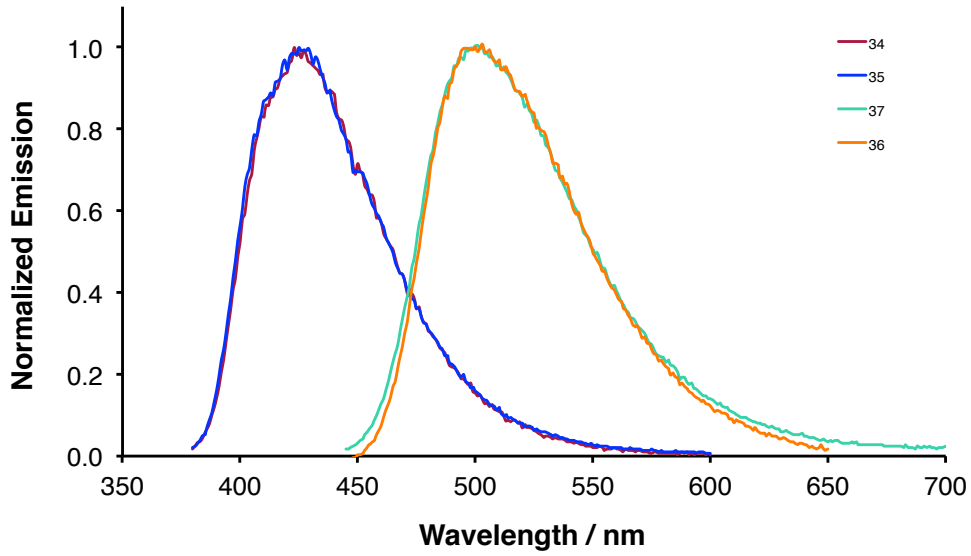

Figure 2.9: Fluorescence emission spectra from **34-37** in CH_2Cl_2.

2.3.5 Fluorescence Titrations with Various Metal Ions

Despite the high fluorescence quantum yield observed, some titrations with metal ions were intended in various solvents. For compounds **34** and **35** the fluorescence is not so high as for **37** and **36** so some modifications in the fluorescence intensity upon titration with metal ions were foreseen but it could not be observed experimentally.

2.3.6 Electrochemical Properties

In order to check the feasibility of an electron transfer between the thioether fragment and the naphthalimide fluorophore, electrochemistry studies have been done. Two fragments shown in Figure 2.10 were prepared and their CV measured. The results are shown in **Figure 2.11**.

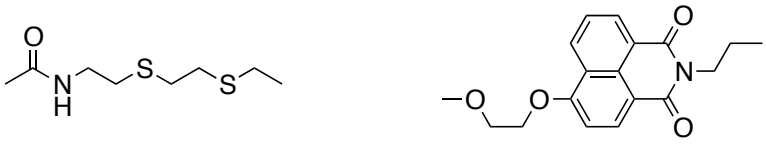

24 **49**

Figure 2.10: Fragments used for the measurements of cyclic voltammetry.

The oxidation and reduction potentials of both parts have been measured by cyclic voltammetry and the free energy of electron transfer ΔG_{el}^{0} is calculated by the Rehm-Weller equation (see Chapter 1.5.1[33]). The E^0 value for the oxidation of the thioether fragment **24** is taken as the absolute HOMO energy of the thioether and is obtained to be 1.50 eV from cyclic voltammetry measurements (**Figure 2.11**a). The E^0 value for the reduction of the naphthalimide moiety is taken as the absolute LUMO of the naphthalimide and is obtained as -1.8 eV from cyclic voltammetry measurement (**Figure 2.11**b). The difference in the electron affinities between the ground state and the excited state E_{00} has been determined to be 3.15 eV (394 nm) using the crossing of the UV and the emission spectra.[31] The ΔG_{el}^{0} was calculated to be + 0.15 eV, which correspond to an energy of 3.45 kcal/mol. This is an indication that an electron transfer between the thioether and the excited state of the naphthalimide is endothermic.

a) b)

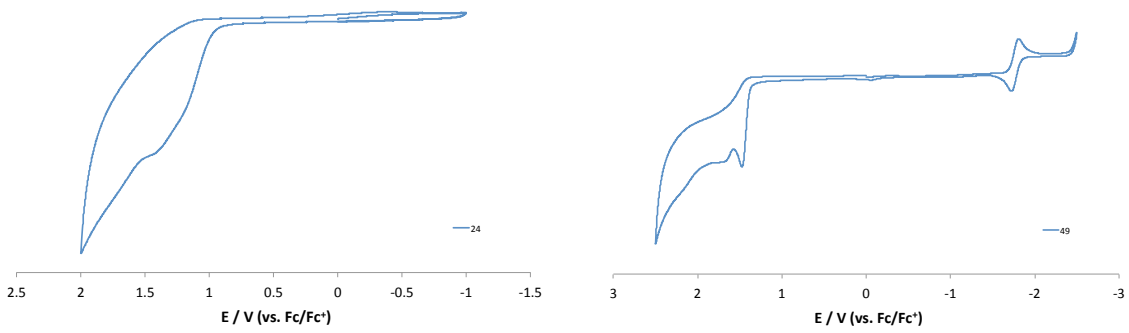

Figure 2.11: CV from thioether fragment **24** (a) and from naphthalimide fragment **49** (b). Conditions: 1mM compound, 0.1 M Bu_4NClO_4 as supporting electrolyte in CH_3CN, scan rate 100 mV s^{-1}, glassy carbon working electrode, Pt wire counter electrode, Ag/AgCl reference electrode, added ferrocene (Fc) as internal standard.

2.3.7 Conclusions

The measurement of the electrochemical properties of the component of the compounds designed in this section is in accordance with the observation of fluorescence quantum yields. While the quantum yields of **34** and **35** indicates that modest PET quenching does occur, the effect is not strong enough to exploit in chemosensor development. In compounds **36** and **37**, no efficient PET quenching was observed, which indicates that generalization of the bidirectional PET process in naphthalimide type compounds does not appear to hold in this case. The difference in quantum yields between the two different

geometries indicates that other factors are also important and to take in consideration. For the design of new PET based fluorescent chemosensors, the redox properties of the individual component should be taken in account.

2.4 Coumarin Based Series of Targets

2.4.1 Coumarin Based Chemosensors

Another fluorophore was chosen to test the feasibility of PET quenching from sulfur. Derivatives of coumarin were chosen because of their photostability and solubility in water. It has a long excitation wavelength and a large Stokes shift. This kind of compounds has low toxicity and is commonly used in pharmaceutical industry as well as in food and material science.[27]

The photophysical properties of the coumarin derivatives depend on the substitution pattern and the rigidity of the molecule. Many example of fluorescent chemosensors based on coumarin as fluorophore are using the internal charge transfer (ICT) mechanism with an electron donating group in the 7-position and an electron withdrawing group in the 3-position (See Chapter 1).

A comparison was made between compound **50** and **51**.[90] They are showing different behavior upon addition of Zn^{2+}. While compound **50** is showing a typical response to the addition of metal according to a PET quenching mechanism, compound **51** is a ratiometric response characteristic of an ICT mechanism.

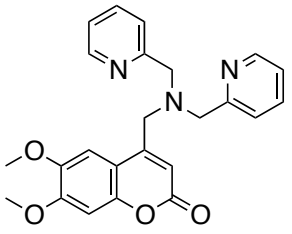

50

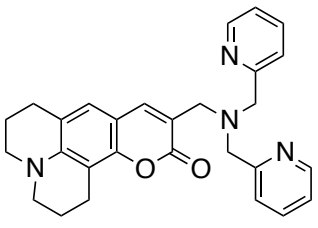

51

Figure 2.12: Examples of coumarin based chemosensors.[90]

2.4.2 Design of the Target Compounds Based on Coumarin Fluorophore

The series based on a coumarin fluorophore was designed by analogy to the generation of target based on a naphthalimide fluorophore. We have selected a coumarin with a methoxy group at the 7-position and the thioether containing chain at the 3-position. To facilitate the synthesis the last group was linked to the fluorophore via amide functionality. The influence of the chain length will be studied in this case as well with a variation from ethyl to propyl chain length **52** and **53**. The effect of methylation to obtain a tertiary amide **54** will also be studied (Figure 2.2.13).

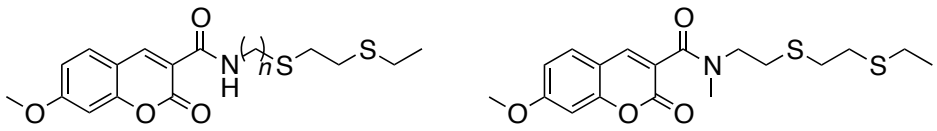

52: *n* = 2
53: *n* = 3

54

Figure 2.2.13: Structures of the targets based on a coumarin fluorophore with the different spacer lengths and substitution pattern.

An alternative substitution pattern with a methoxy group in the 7-position and a thioether containing side chain directly linked to the 4-position of the coumarin without any nitrogen or functionality in between was also designed (Figure 2.14). However the compound could not be obtained in this work and the effort towards its synthesis will be described only briefly.

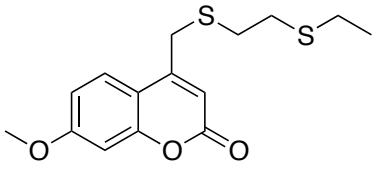

55

Figure 2.14: Structure of the target based on a coumarin fluorophore with direct connection from the thioether chain to the coumarin.

2.4.3 Synthesis of the Target Compounds 52-54

The synthesis of the coumarin derivatives starts with the commercially available 2,2-dimethyl-1,3-dioxane-4,6-dione, commonly named Meldrum's acid **56**, which reacts with 2-hydroxy-4-methoxybenzaldehyde **57**, as well commercially available, via Knoevenagel

condensation. 7-methoxycoumarin-3-carboxylic acid **58** is obtained in 2 hours with a good yield following a known procedure (Scheme 2.12).[91]

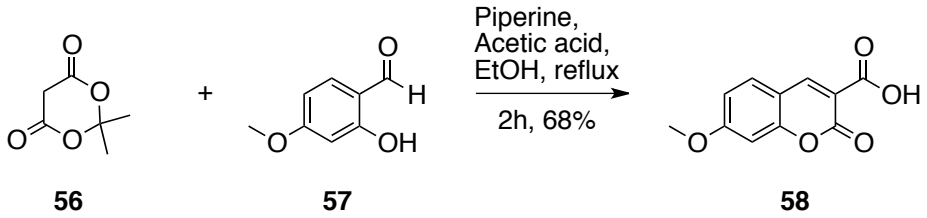

56 **57** **58**

Scheme 2.12: Synthesis of 7-methoxycoumarin-3-carboxylic acid **58**.

Using the free amines **25** and **44** from the previous synthesis (Scheme 2.1 and Scheme 2.7), compounds **52** and **53** were synthesized using standard conditions by coupling with 4-dimethylaminopyridine (DMAP) and *N*,*N*'-dicyclohexylcarbodiimide (DCC) (Scheme 2.13). The reactions are giving the target compounds in good yields. However they are not stable to acid on column chromatography. The purification of **52** could be done by recrystallization in cyclohexane and the purification of **53** had to be done on deactivated silica gel explaining the lower yield obtained.

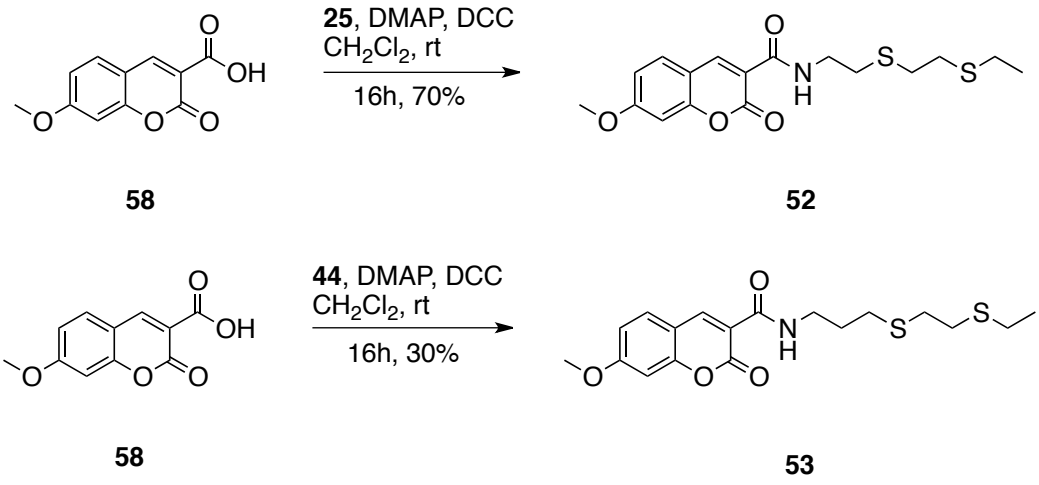

58 **52**

58 **53**

Scheme 2.13: Synthesis of target compounds **52** and **53**.

To obtain the tertiary amine containing target **54**, the acetyl protected chain **24**, which is an intermediate of the synthesis of **25** (Scheme 2.1), is methylated using methyliodide and butyl lithium as a base in THF to give **59**. After deprotection under basic conditions, the secondary amine **60** was obtained in 57 % yield. In the next step, it reacts with 7-methoxycoumarin-3-carboxylic acid **58** as described for **52** to give the tertiary amide **54**

(Scheme 2.14). The ^{1}H-NMR of **54** is showing the presence of two rotamers in a 2 to 1 ratio but the identity of the major one was not determined.

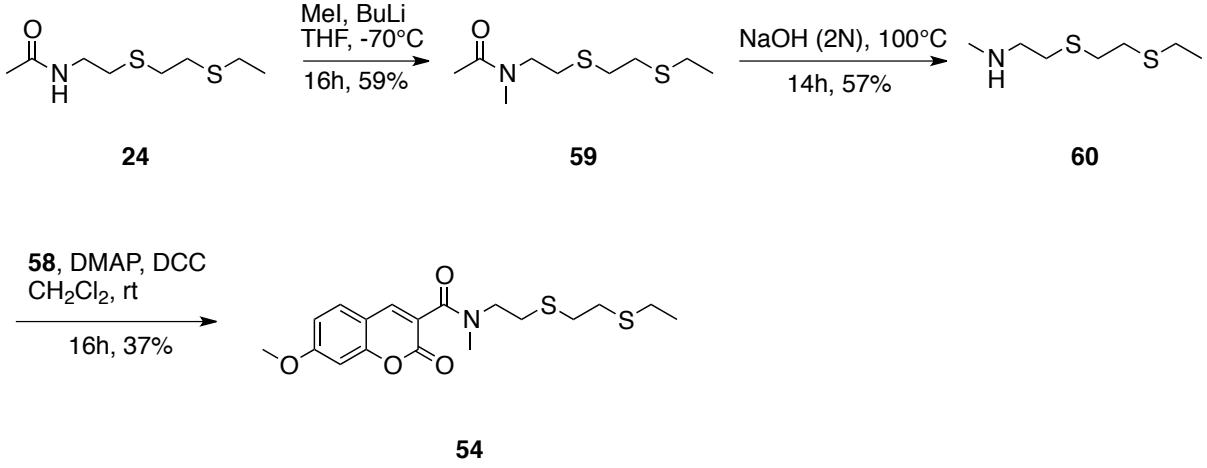

Scheme 2.14: Synthesis of target compound **54**.

The synthesis of the target compound **55** with a different substitution pattern was intended starting from the commercially available 3-methoxyphenol **61** and ethyl-4-chloroacetoacetate **62**. Both starting material were mixed in concentrated sulfuric acid and stirred over night giving the product **63** as reported in the literature.[92] This paper is also reporting the next step, which is the insertion of a thiol functional group via reaction with thioacetic acid in the presence of diisopropylethylamine (DIEPA). The product **64** could be isolated in 50 % yield but the deprotection in basic conditions followed by the reaction with 2-chloroethylethyl sulfide did not led to the isolation of the target compound. This synthesis did not lead to a clean product and was not investigated more because of the extreme toxicity of the starting material already mentioned in the synthesis of **25** (Chapter 2.2.2).

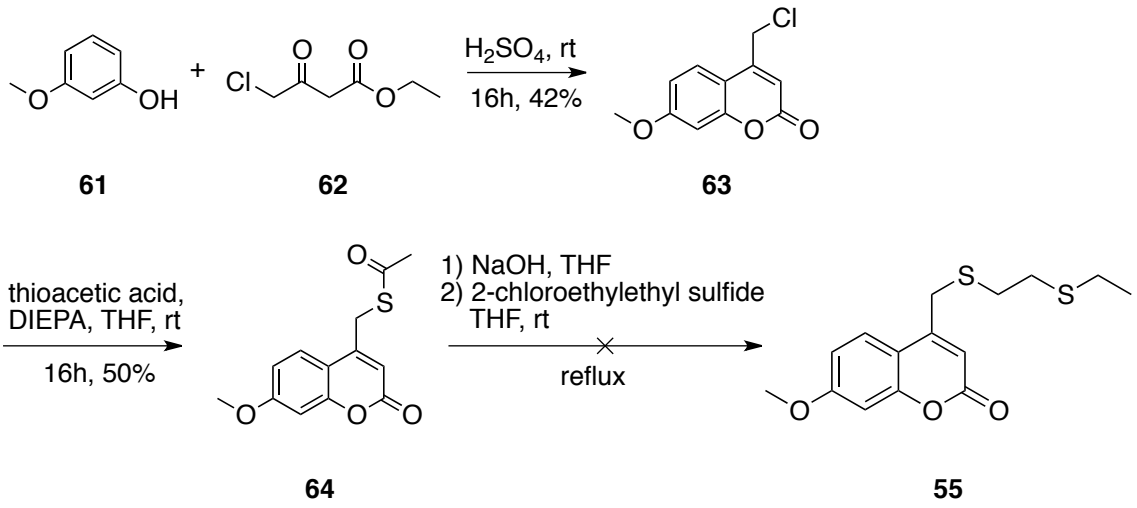

Scheme 2.15: Synthetic scheme towards the synthesis of **55**.

2.4.4 Photophysical properties

The photophysical properties of compound **52**, **53** and **54** were investigated in CH_2Cl_2. The UV-visible absorption spectrum is characterized by a broad band with a maximum at about 348 nm for compound **52** and **54** and at 335 nm for compound **54**. The fluorescence emission spectrum is characterized by broad band with a maximum at 390 nm indicating a small Stokes shift. The quantum yield increases with the length of the spacer as previously observed for the naphthalimide-based targets in Chapter 2.3.4. However, the lowest quantum yield is observed for compound **54** corresponding to the tertiary amide (Table 2.4). In this compound the presence of rotamers in the ^{1}H NMR spectroscopy could be a reason for the difference in the photophysical behavior.

Table 2.4: Photophysical properties of targets **52**, **53** and **54** in CH_2Cl_2.

Compounds	λ_{abs} / nm	ε^a / $M^{-1}cm^{-1}$	λ_{em} / nm	$\phi_F{}^b$
52	348	23800	390	0.11
53	347	23500	390	0.15
54	335	15200	392	0.007

[a] For longest wavelength λ_{max} . [b] Relative to anthracene in methanol $\phi = 0.30$.[89]

2.4.5 Fluorescence Titrations with Various Metal Ions

The evaluation of the response of the photophysical properties of the obtained compounds upon addition of various metal ions was done first in CH_2Cl_2. The first addition of Hg^{2+} to **54** is leading to an increase of the fluorescence emission but the addition of more Hg^{2+} is leading to subsequent decrease of the fluorescence emission. The problem is most probably the fact that the metal ions was not solved in CH_2Cl_2 and the effect of methanol added at the same times as the metal ions is having a high impact as we observed for the compounds of the next Chapter (see Chapter 3.2.5, Figure 3.13). In this case the titration in pure methanol did not lead to significant fluorescence enhancement.

2.4.6 Conclusions

The maximum of the fluorescence of non-quenched coumarin are not vey high and we estimated that no PET quenching processes were occurring in our compounds of this series. The behavior of the tertiary amine-containing compound is interesting but must rely on other mechanisms that remain unclear.

Chapter 3

Study of Thiourea Moiety as Electron Donor for PET Quenching

3.1 Introduction

The research objectives described in this chapter are the design, synthese and investigation of the photophysical properties of series of compounds composed from a napthalimide fluorophore and thiourea containing receptor. An effective PET quenching is observed and subsequent responses to the addition of different metal ions are investigated in order to test the chemosensor capacity of the obtained compounds in methanol as well as in aqueous systems. Variation of the receptor ligand will be studied in order to modulate the response of the chemosensor to various metal ions.

3.1.1 Background on Thioureas

Thioureas are known to have strong antifungal as well as antimicrobial and insecticidal properties.[93-96] It could have as well radiation protective effect attributed to its ability of metal binding and to the thione-thiol equilibrium.[97] Thioureas are also ligands of general interest in molecular recognition because of their various potential donor sites. The sulfur atom acts as soft donor for the complexation of soft cations whereas the NH groups are able to make hydrogen bonding.

Various thiourea and thiourea derivative ligands forming metal complexes with Hg^{2+}, Cd^{2+}, Zn^{2+} and Ni^{2+} have been isolated and crystal structures have been obtained.[98-100] The most stable conformation for the interaction between metal ion and thiourea is the eclipsed conformation with a torsion angel M-S-C-N close to 0° (Figure 3.1a). In this configuration, the orbitals from the metal are overlapping with the lone pair of electron of the sulfur. Thiourea can also coordinate in a staggered configuration with torsion angle M-S-C-N of 90° or in a distorted conformation when steric effects influence the structure (Figure 3.1b). In this conformation, the orbitals for the metal are overlapping with the π-orbitals of the C=S double bond making it weaker. It was calculated that in a AgCl:thiourea complex, the difference in energy between the staggered and the eclipsed conformation is 4.75 kcal/mol which is consistent with the possibility of steric destabilization.[101]

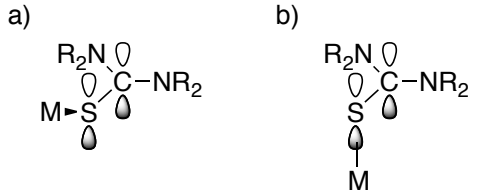

Figure 3.1: Representation of the torsion angle M-S-C-N in a thiourea metal complex; a) eclipsed conformation with 0° torsion angle, b) staggered conformation with 90° torsion angle.

Thioureas as well as ureas have the ability to make hydrogen bond with anions. Since thioureas are more acidic than ureas they are better recognition elements for anions and they also undergo faster deprotonation.[102,103] Two different isomers by rotation about the C-N bond are the s-*cis* and the s-*trans* isomer depicted in Figure 3.2. They have to be in a s-*cis* conformation, in order to bind anions through both NH group meaning that their behavior is dependent on their rotation energy barriers, which are about 11 to 13 kcal/mol and are depending on the substituent.[104-106] This ability and topology for anion binding is similar to the interactions found in active sites of enzymes and these properties have lead to the use of thiourea (and ureas) as metal free catalysts.[107,108]

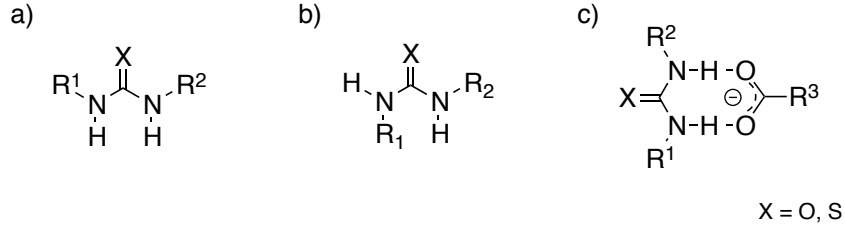

Figure 3.2: a) s-*cis* conformation of urea or thiourea, b) s-*trans* conformation of urea or thiourea, c) representation of urea or thiourea binding anions.

3.1.2 Thioureas as Chemosensors

The possibility of involving both thiourea or urea in fluorescent chemosensors has been investigated. Costero has observed changes in the absorption spectra and in the NMR for different N-benzylthiourea and one N-ethylthiourea after addition of acetate ions in DMSO.[109] It is also shown that most of the thioureas with a single *N* substituent are showing a strong thermodynamic preference for the *s*-cis conformation. But since the barrier to interconversion of the *s*-cis and *s*-trans isomer is low, a rapid interconversion is occurring. Strong color changes are observed when the thiourea is acidic enough to be involved in acid base reaction with fluoride or acetate ions.

Thioureas have been used in the development of PET based fluorescent chemosensors targeting biologically relevant anions such as acetate, phosphate amino acids and halides. Such sensors are working according to the following principle: An electron rich complex anion:receptor is formed though hydrogen bonding and the augmentation of the effective electron density on thiourea cause an increase in the rate of electron transfer. Therefore a decrease in the fluorescence emission will be observed upon addition of anion. The pioneering work of Gunnlaugsson in this field is based on anthracene or 1,8-naphthalimide as fluorophore linked to thiourea moiety to detect anions.[110] His compounds **65-69** shown in Figure 3.3 have high initial quantum yields and show decrease of the fluorescence emission after interaction with anions in DMSO.[84,111,112]

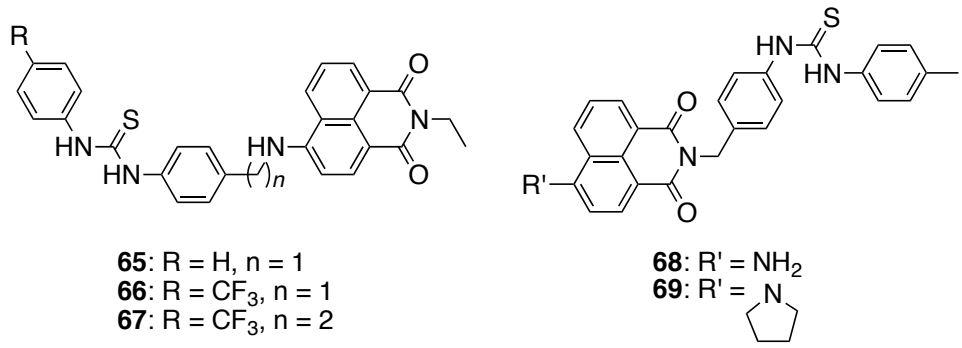

65: R = H, n = 1
66: R = CF_3, n = 1
67: R = CF_3, n = 2

68: R' = NH_2
69: R' = N

Figure 3.3: Anion sensors reported by Gunnlaugsson.[84]

Different compounds based on boron dipyrromethene dyes conjugated to urea and thiourea were investigated by Ziessel, revealing interesting redox and photophysical properties.[113] However the presence of the sulfur atom of thiourea **70** instead of the oxygen atom of urea **71** leads to only a slight decrease of the quantum yield, meaning that no PET quenching from the sulfur of the thiourea is observed in this case. This can be explained by the fact that the electron donor is conjugated to the electron acceptor and therefore the quenching of the fluorescence through PET mechanism can't take place.

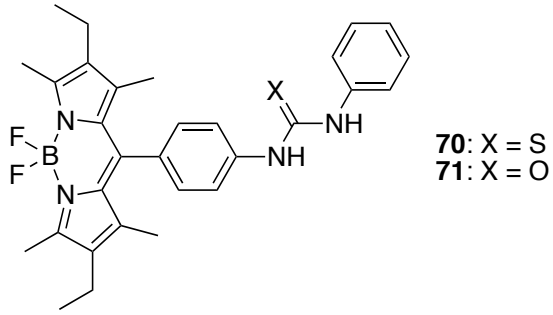

Figure 3.4: Bodipy containing urea and thiourea moiety investigated by Ziessel.[113]

Thioureas are soft donors and have the potential of metal ion binding. However their potential has not been previously exploited in the field of chemosensors for metal ions. Only few examples of thiourea compounds used for metal sensing have been studied.

The group of Bren made studies of cyclovoltametric properties of fluorescent compound based on thiourea and anthracene fluorophore (Figure 3.5) and postulated the use of those compounds as fluorescent chemosensors.[114,115] In the first paper they correlate the free energy of electron transfer ΔG_{el}^{0} obtained from cyclovoltammetric measurements with the observed quantum yield. The compound showing the more negative value for ΔG_{el}^{0} is showing the lowest intensity of fluorescence I_0. After addition of various metal ions, they have observed that the response of thiourea to Hg^{2+} is showing the highest increase in fluorescence and the best affinity. The compound showing the lowest I_0 is also the one showing the highest increase upon addition of Hg^{2+}. A 77-fold increase of the fluorescence was observed for compound **74**.[114,115]

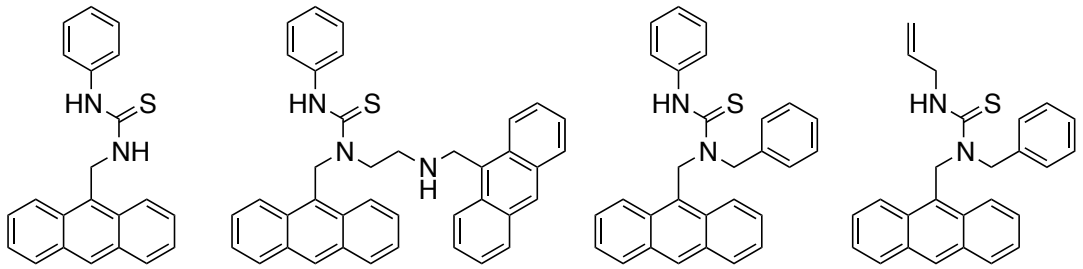

72 **73** **74** **75**

Figure 3.5: Series of compounds studied by Bren.[115]

The operating mechanism in Bren's sensors is proposed to be PET quenching but according to Elisei no direct investigations are showing that it is effectively the mechanism of quenching. After complete studies (nano and femto second time resolved spectroscopy) of the compounds shown in Figure 3.6, they conclude that there is no PET process occurring in this case because they could not observe the charge transfer intermediate necessary involved in PET processes.[116]

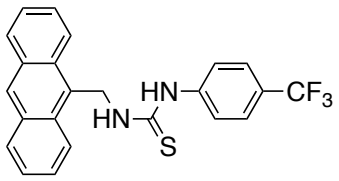

76

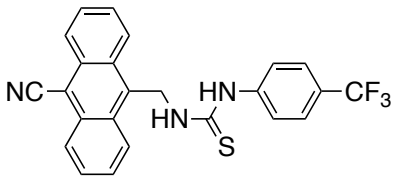

77

Figure 3.6: Structures studied by Elisei.[116]

Chemosensors bearing thiourea moieties have also been studied in the design of chemodosimeter for Hg^{2+} and Ag^{+}. In this type of sensors, the structure of the compound is irreversibly modified by chemical reaction following the interaction with the metal.[117-120] Some of the chemdosimeter reported in the literature are working with an N-acyl group as additional chelating element.[121]

In our group, derivatives of thiourea have been involved in chemosensors but were not involved in a PET quenching mechanism.[122] The ability of thiourea to bind Hg^{2+} was used to increase the fluorescence emission of a biarylpyridine based compound by a conformational restriction mechanism (Figure 3.7).

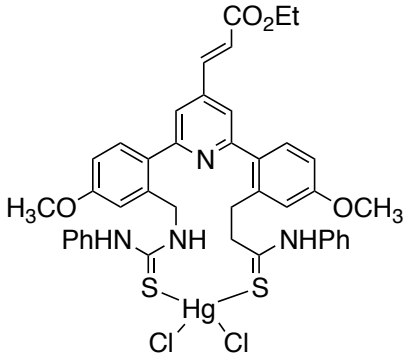

78

Figure 3.7: Chemosensor based on conformational restriction mechanism.[122]

3.2 First Target: Thiourea as Electron Donor for Naphthalimide

3.2.1 Introduction

The first target in the series based on a thiourea as electron donor for PET quenching was constructed in analogy to the targets presented in Chapter 2.3. The knowledge about the stability of the naphthalimide fluorophore discussed in Chapter 2.3.1 was taken in account for the design of the new targets. The substitution of the naphthalimide core by a 2-methoxyethoxy group in 4-position was also carried over from the compounds previously synthesized in this thesis. In this new series of compounds, the sulfide component, which was not reducing enough to transfer an electron to the excited state of the naphthalimide fluorophore, was replaced by a thiourea moiety. Different lengths of the spacer between the two components, from two carbon atoms to four carbon atoms **PTU**-**PTU4C**, were designed to observe the effect on the quantum yield. As introduced in Chapter 1.5.1 and reported for the compounds shown in Chapter 2, an increase in the fluorescence quantum yield with the increase of the chain length is expected for a PET quenching mechanism. A control compound **49**, lacking the thiourea electron donor was designed as well to evaluate the efficiency of the quenching of the thiourea residue (Figure 3.8).

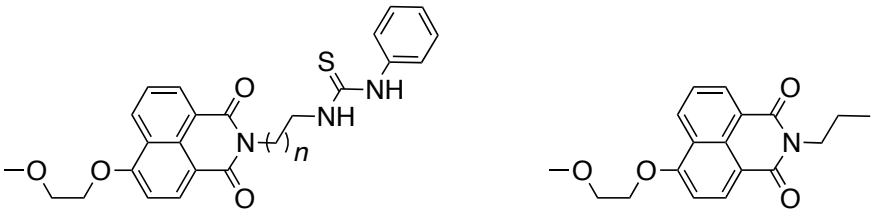

PTU: $n = 2$
PTU3C: $n = 3$
PTU4C: $n = 4$

49

Figure 3.8: Structures of the first naphthalimide-thiourea compounds with different spacer lengths **PTU**-**PTU4C** and the control compound without thiourea moiety **49**.

3.2.2 Synthesis of the Target Compounds PTU-PTU4C and 49

The targets **PTU**, **PTU3C** and **PTU4C** were prepared in a 5 steps synthesis starting from the commercially available 4-bromo-1,8-naphthalic anhydride **38** and the corresponding amine. The general synthesis is shown in Scheme 3.1. For **PTU** the synthesis start with N-Boc-1,2-diaminoethane **79**, prepared according to the literature,[123] heated at 100°C reacts

with 4-bromo-1,8-naphthalic anhydride **38** in DMF in the presence of triethylamine to form **82** in good yield.[124] The bromine was substituted by a 2-methoxyethoxy group by heating **82** at reflux for 2 hours in 2-methoxyethanol with K_2CO_3 as a base but without any catalyst. After deprotection of **85** using TFA in dichloromethane, the amine **88** was reacted with phenyl isothiocyanate, yielding the target **PTU** in 65 % yield after precipitation out of the reaction mixture and purification by recrystallization from isopropanol.

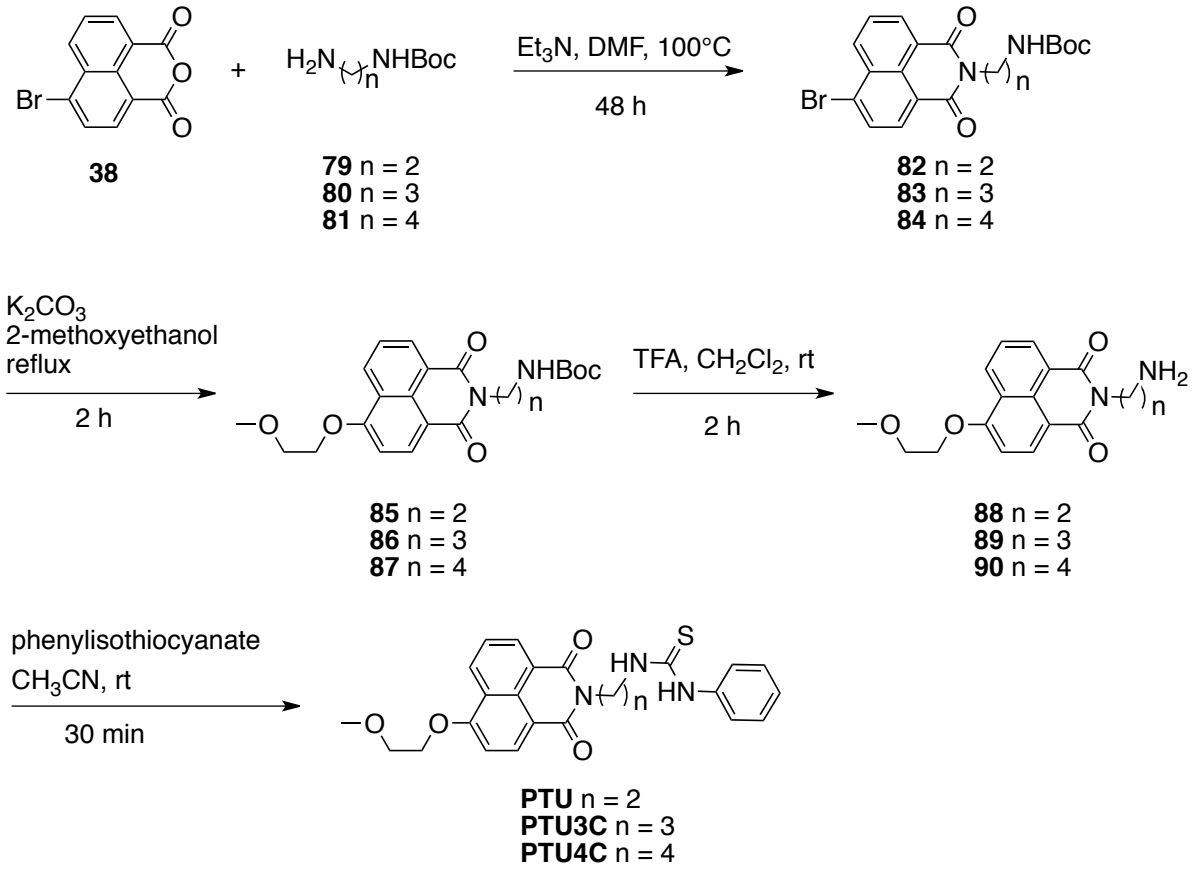

Scheme 3.1: Synthetic scheme of the series **PTU** to **PTU4C**.

The same pathway was followed for the synthesis of **PTU3C** and **PTU4C**. The Boc-protection of 1,3-diaminopropane and of 1,4-diaminobutane respectively were done according to the literature.[125,126] **PTU3C** and **PTU4C** were obtained following the general procedures in good yields.

In the first approach of this synthesis, the thiourea was introduced before the 2-methoxyethoxy substituent on the 4-position of the naphthalimide by analogy to the synthesis presented in Chapter 2. The Boc-protected amine **79** was mixed with phenylisothiocyanate to give the product **91**. After deprotection of the amine, it was

introduced on the commercially available 4-bromo-1,8-naphthalic anhydride **38** to give the product **92**. But as last step of this pathway, the substitution of the bromine was leading to a major byproduct. Substitution from the sulfur of the thiourea is occurring and two 2-methoxyethoxy chains are introduced to yield product **93** (Scheme 3.2). The order of the steps was changed as described in Scheme 3.1 to avoid this undesired reaction.

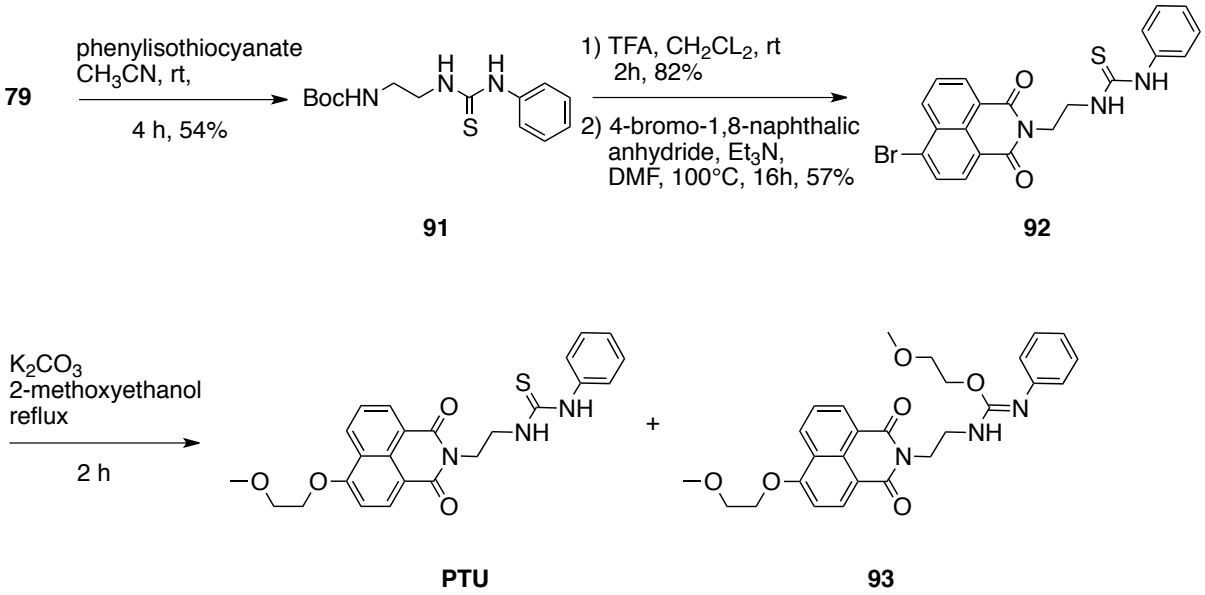

Scheme 3.2: Synthetic scheme of **PTU** leading to the undesired byproduct **93**.

The control compound **49** was synthesized as well from 4-bromo-1,8-naphthalic anhydride **38** (Scheme 3.3). The first step was done with propylamine at reflux in ethanol over night and product **46** was obtained in 88 % yield. In the next step, the substitution of the bromine was done as described in Scheme 3.1 for compounds **PTU**-**PTU4C**.

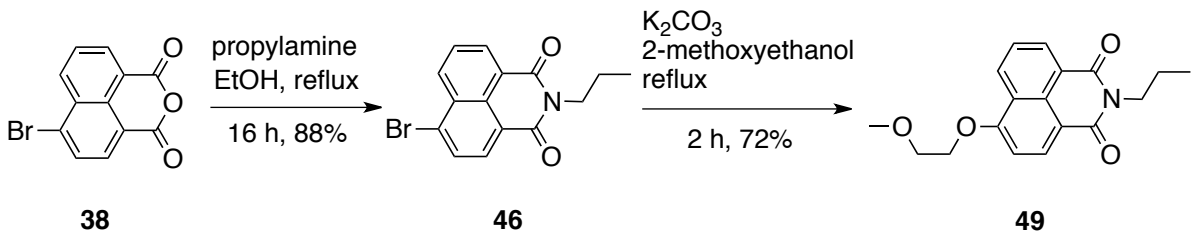

Scheme 3.3: Synthetic scheme of the control compound **49**.

3.2.3 Photophysical Properties of PTU-PTU4C and 49

The photophysical properties of **PTU**, **PTU3C** and **PTU4C** were investigated in methanol. The UV-visible absorption spectrum of the three compounds is characterized by a broad band with a maximum at 366 nm. The fluorescence emission spectrum is characterized by broad band with a maximum at 446 mn (Table 3.1).

Table 3.1: Photophysical properties of **PTU**, **PTU3C**, **PTU4C**, **85** and **49** in methanol.

Compounds	λ_{abs} / nm	ε^{a}/ $M^{-1}cm^{-1}$	λ_{em} / nm	ϕ_F [b]
PTU	366	11100	446	0.02
PTU3C	366	12800	446	0.08
PTU4C	366	12800	446	0.15
85	366	13300	446	0.92
49	366	13400	446	0.92

[a] For longest wavelength λ_{max} . [b] Relative to anthracene in methanol $\phi = 0.30$.[89]

A distance dependence of the intensity of the fluorescence emission was observed. If the distance between the thiourea and the naphthalimide is 2 carbon atoms, the quenching is the most efficient ($\phi_F = 0.02$). When one or two carbon atoms are added to the chain of the spacer, the quantum yield shows a 4-fold, respectively, or 8-fold increase of the fluorescence emission (Table 3.1). As described in the Chapter 1.5.1, this is an indication of the PET quenching mechanism.

As a comparison, the photophysical properties of non-quenched analogues **49** and **85** were investigated. The same general shape of the absorption and emission spectra, and similar extinction coefficients, were obtained. The observed quantum yields are 0.92 for both compounds, which shows that the fluorescence has been efficiently quenched by the thiourea moiety in all the target compounds. Even the fluorescence of **PTU4C**, which has the longest investigated spacer, has been quenched by comparison of the control compound **49**.

The photophysical properties of **PTU**, **PTU3C** and **PTU4C** were investigated as well in different solvents. The UV-visible absorption spectrum of the three compounds is showing the same characteristics in every solvent. The maximum of the fluorescence emission band is

dependent on the polarity of the solvent. The optical properties are listed in Table 3.2 and represented in Figure 3.9 for **PTU** as representative compound for the series.

Table 3.2: Photophysical properties of **PTU** in CH_2Cl_2, CH_3CN and MeOH and DMSO.

Solvent	CH_2Cl_2	CH_3CN	MeOH	DMSO
λ_{abs} / nm	366	366	366	366
λ_{em} / nm	434	443	446	452

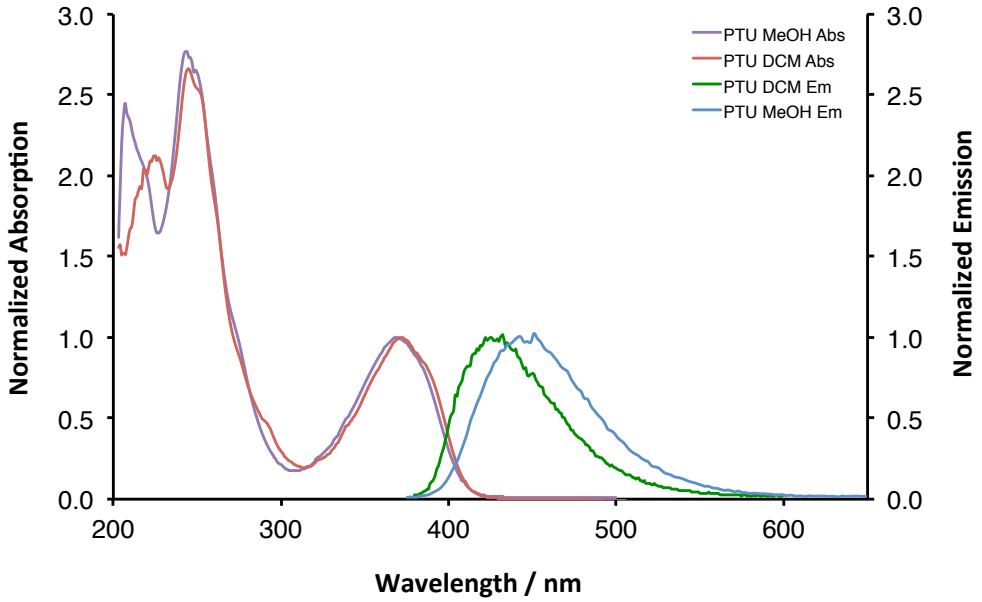

Figure 3.9: UV-visible absorbance and fluorescence emission spectra from **PTU** in methanol and dichloromethane.

3.2.4 Fluorescence Titrations of PTU with Various Metal Ions in Methanol

The response of the potential chemosensor **PTU** to addition of various metal ions was investigated. The metal ions tested were Li^+, Na^+, K^+, Mg^{2+}, Ca^{2+}, Ag^+, Zn^{2+}, Cd^{2+}, Hg^{2+} and Pb^{2+}. The counter ions used are Cl^-, ClO_4^- or NO_3^-. The titrations were carried out with a 3 µM solution of the fluorophore in methanol. The salts were added as 5 µl aliquots of solutions in methanol with an increasing concentration from 20 µM to 2 M depending on the response observed. When solubility problems were encountered for the preparation of the most concentrated salt solutions in methanol, some drops of water were added until a clear solution

was obtained. The detailed general procedure for the titration with metal ion is reported in Chapter 5 (p.127).

The first target compound **PTU** is showing a strong, low affinity response in methanol after the addition of Zn^{2+}. A maximum increase of the fluorescence emission of about 20 times was observed, with no changes in the wavelength for the emission maximum (Figure 3.10). The recurring deflexion at about 450 is a Wood's anomaly characteristic of our fluorimeter.[127] No differences in the absorption spectra were observed upon addition of the metal indicating that no change of the ground state electronic structure is occurring.

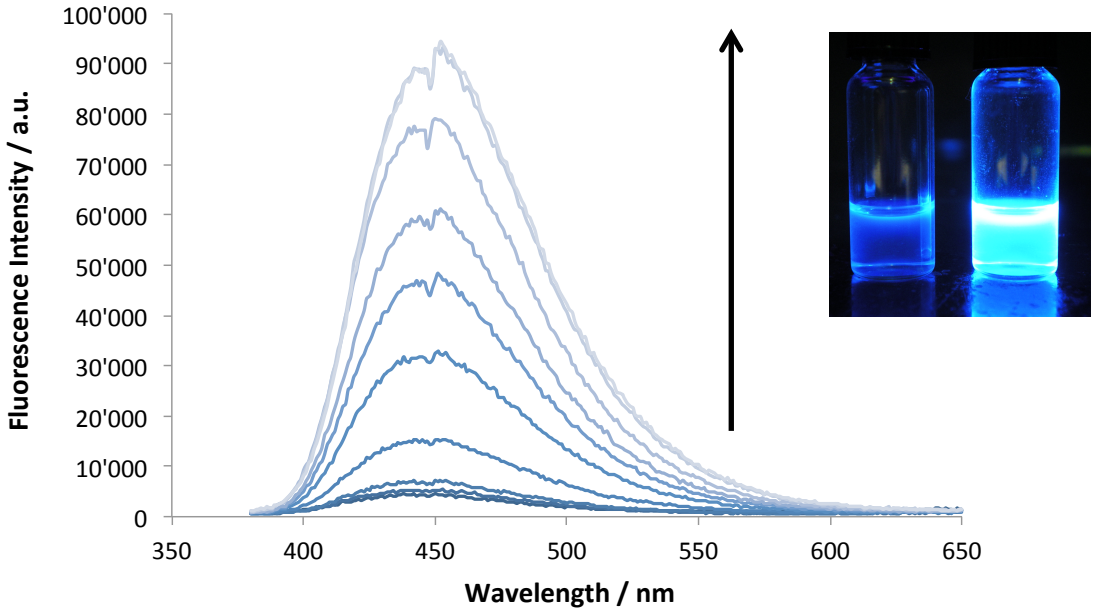

Figure 3.10: Fluorescence titration of **PTU** (3 µM in methanol) with $ZnCl_2$. The picture is representing the visual difference between the on and off state at higher concentration.

By the addition of Zn^{2+} to the thiourea ligand **PTU**, a complex between the two components is formed, and the energy level of the HOMO of quenching element is lowered by the complexation with Zn^{2+}. Therefore the PET is no longer occurring, leading to recovery of the fluorescence emission. The observed increase of the fluorescence emission is function of the concentration of the metal and for a 3 µM solution of the fluorophore in methanol the maximum of fluorescence emission increase observed correspond to a maximum quantum yield (ϕ_{max}) of 0.4 ($\phi_{max} = \phi_{initial} \times (I/I_0)_{max}$). The picture shown in Figure 3.10 is illustrating the

difference observable under a UV-visible lamp with a 1 mM concentration of the chemosensor **PTU**.

The relative integrated fluorescence emission intensity was plotted as a function of log [Zn^{2+}] and a sigmoidal curve was obtained (Figure 3.11). The dissociation constants of the complex formed between the metal and the chemosensor was calculated by fitting this curve by non-linear least-square using the program Prism6.

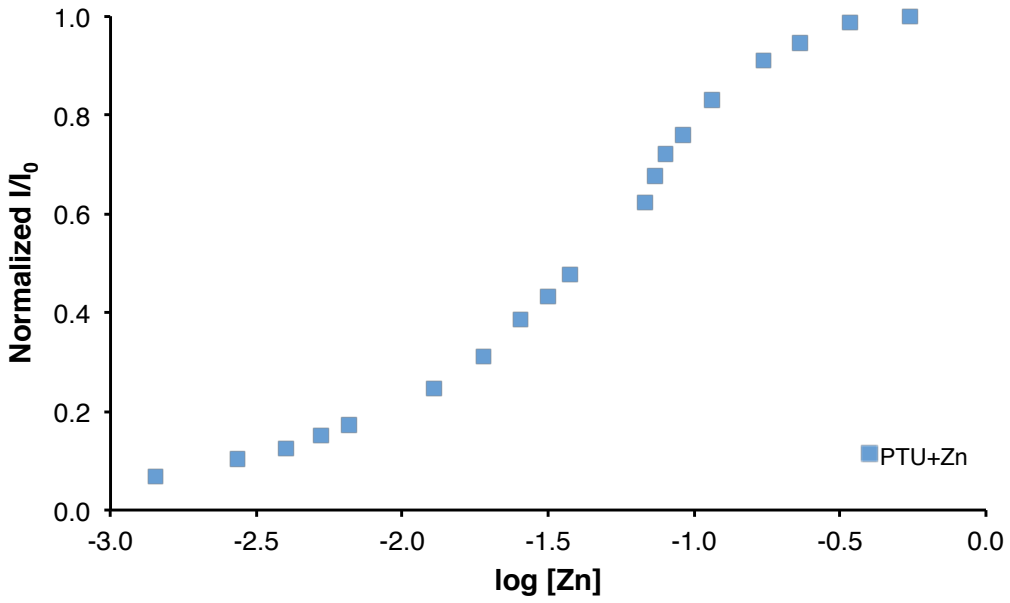

Figure 3.11: Ratiometric enhancement for the titration of **PTU** in methanol with $ZnCl_2$.

In the case of **PTU** with Zn^{2+} in methanol, the logarithm of the association constant (log K_d) was calculated to be -1.2 (calculated from Figure 3.11). In methanol **PTU** is responding as well to Cd^{2+} with a slightly higher affinity (log K_d = -1.6) but lower increase of the fluorescence emission (5 times increase) (Figure 3.12).

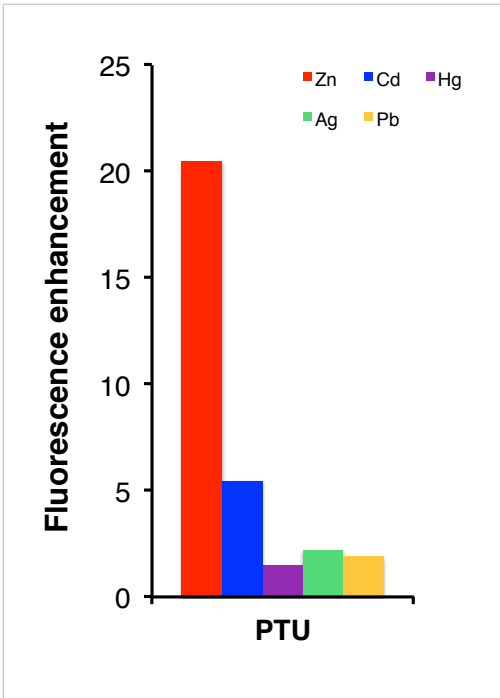

Figure 3.12: Metal-induced ratiometric fluorescence enhancement of **PTU** in methanol.

The other metals tested in methanol were showing no changes in the fluorescence emission. It is surprising that thiophilic metals surveyed like Hg^{2+} and Ag^{+} don't show coordination to **PTU** in methanol.

3.2.5 Fluorescence Titrations of PTU with Various Metal Ions in Different Solvents

The solvent has a very large influence on the binding affinity of the ligand **PTU** to metal ions. In the case of formation of a Zn^{2+} complex, the binding affinity is increasing considerably with the decreased polarity of the solvent. The dissociation constants observed in CH_3CN and in CH_2Cl_2 between **PTU** and Zn^{2+} are respectively $3.2 \cdot 10^{-4}$ M (log K_d = -3.5) and $2 \cdot 10^{-6}$ M (log K_d = -5.7) showing a higher affinity in apolar solvents (Figure 3.13). The maximum increase of the fluorescence emission is similar in the three tested solvents (about 20- to 23-fold increase of the fluorescence intensity). In the case of CH_2Cl_2, the binding is likely much tighter than the apparent K_d suggests because at the concentration of fluorophore used for this experiment, a lower K_d cannot be determined.

It is important to note that a very small amount of methanol in the titration of **PTU** with Zn^{2+} in CH_2Cl_2 has an important effect. The fluorescence intensity decreases drastically after addition of 10 µl of methanol at the end of the titration in CH_2Cl_2 (Figure 3.14).

Therefore the solution of Zn^{2+} used in the titration in CH_2Cl_2 has to be prepared as well in CH_2Cl_2. The same is true for the titration in CH_3CN; the salt has to be dissolved in the same solvent as the chemosensor.

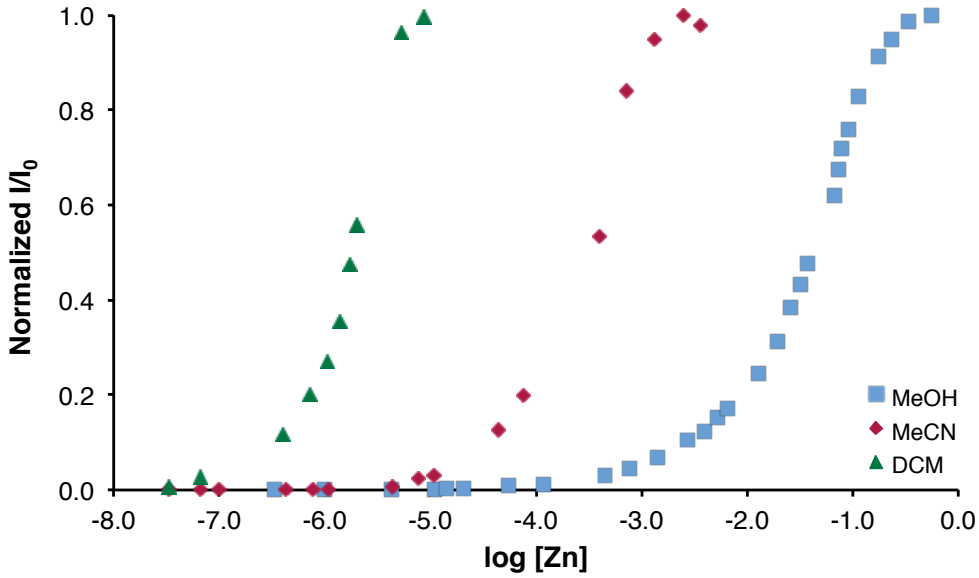

Figure 3.13: Comparison of the ratiometric enhancement for the titration of **PTU** in CH_2Cl_2, CH_3CN and methanol with $ZnCl_2$.

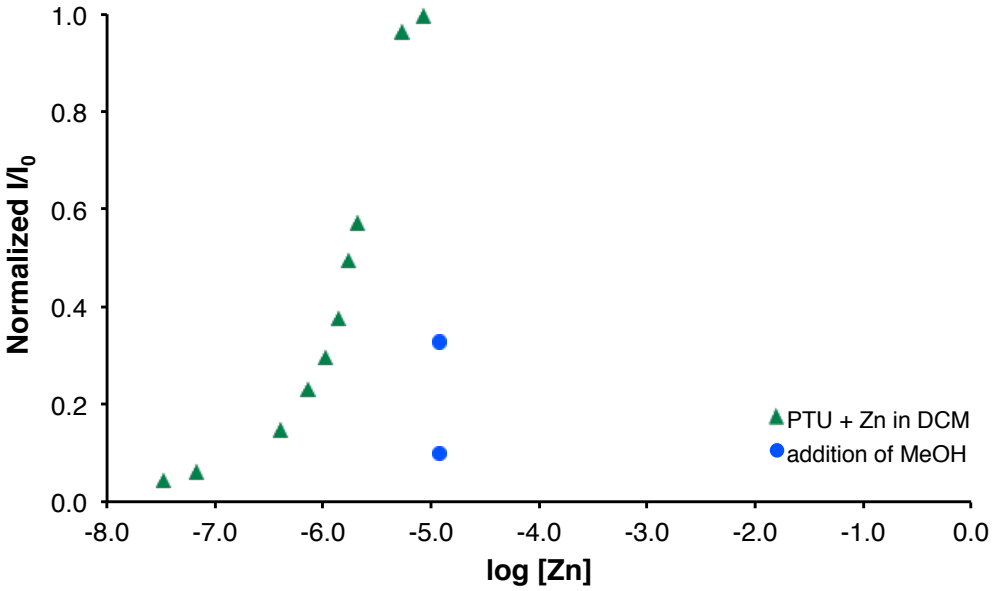

Figure 3.14: Effect of the addition of methanol to the titration of **PTU** in CH_2Cl_2 with Zn^{2+}.

In the case of the titration of **PTU** with Hg^{2+}, changing the solvent to CH_2Cl_2 leads to a 20-fold enhancement of the fluorescence even though the experiment in methanol was not showing any response as previously described. The logarithm of the dissociation constant was estimated to be -6.1. However, once the maximum of the fluorescence increase was reached, the fluorescence intensity decreased by the addition of further amount of Hg^{2+}. The fluorescence emission decreases dramatically when 10 µl of methanol was added at the end of the titration. This is consistent with the observation that no fluorescence enhancement was observed in methanol.

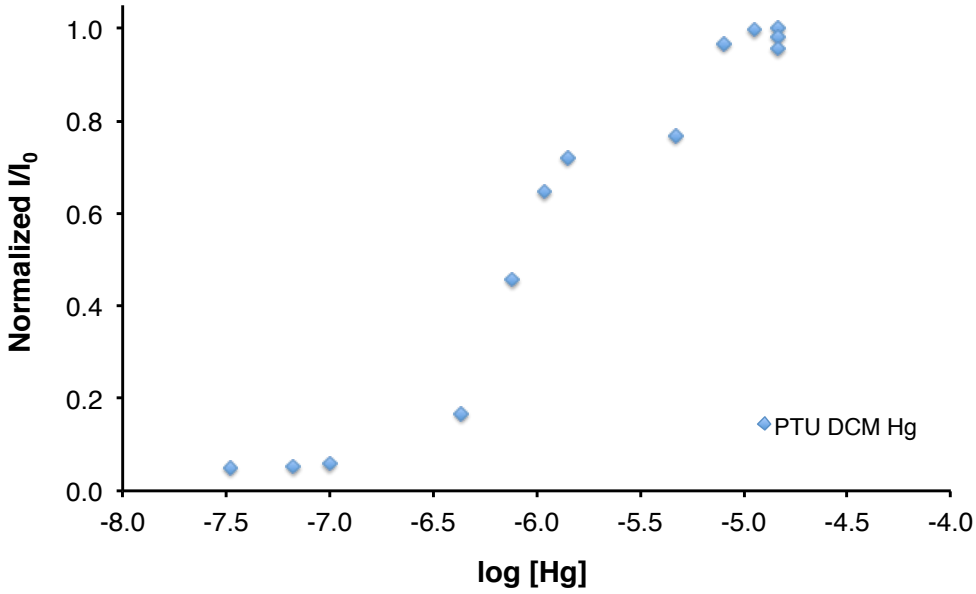

Figure 3.15: Ratiometric enhancement for the titration of **PTU** with $HgCl_2$ in CH_2Cl_2.

3.2.6 Electrochemical Properties

In order to prove that an electron transfer effectively occurs between the thiourea fragment and the naphthalimide fluorophore, electrochemistry studies have been done. The CV of fragment **91** (Figure 3.16) and the final compound **PTU** were measured and shown in **Figure 3.17**.

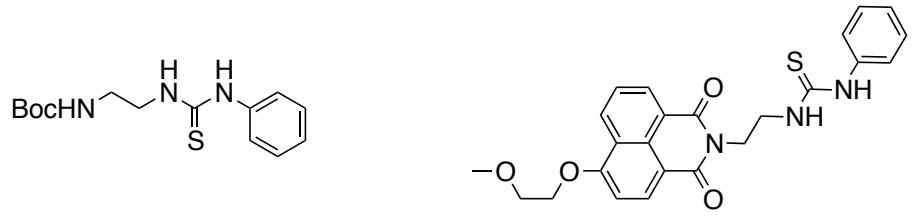

91 **PTU**

Figure 3.16: Fragments used for the measurements of cyclic voltammetry.

The oxidation and reduction potentials of both parts have been measured by cyclic voltammetry and the free energy of electron transfer ΔG_{el}^{0} is calculated by the Rehm-Weller equation (see Chapter 1.5.1[33]). The E^0 value for the oxidation of the thiourea fragment **91** is taken as the absolute HOMO energy of the thiourea and is found to be 0.9 eV from cyclic voltammetry measurements (**Figure 3.17**). The E^0 value for the reduction of the naphthalimide moiety is taken as the absolute LUMO of the naphthalimide and is obtained as -1.8 eV from cyclic voltammetry measurement (**Figure 3.17**). The difference in the electron affinities between the ground state and the excited state E_{00} has been determined to be 3.13 eV (396 nm) using the crossing of the UV and the emission spectra.[31] The ΔG_{el}^{0} was calculated to be -0.43 eV, which correspond to an energy of 9.91 kcal/mol. This is an indication that an electron transfer between the thiourea and the excited state of the naphthalimide is possible and therefore the quenching of the fluorescence can occur via a PET quenching mechanism.

a) b)

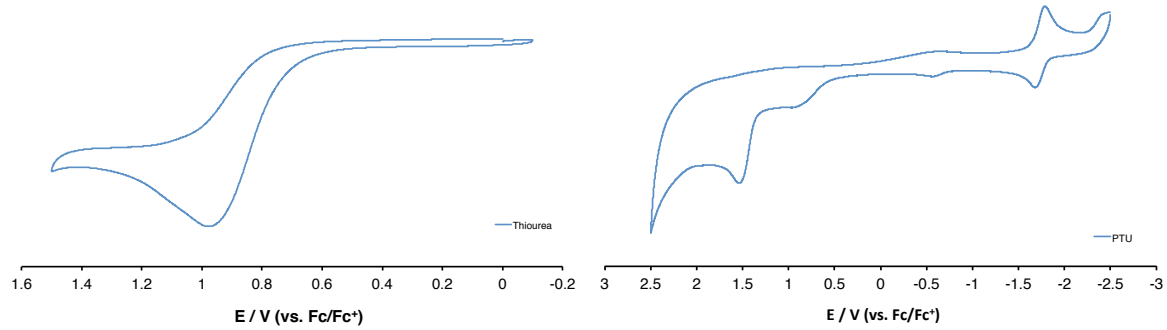

Figure 3.17: CV from thiourea fragment **91** (a) and from **PTU** (b). Conditions: 1mM compound, 0.1 M Bu_4NClO_4 as supporting electrolyte in CH_3CN, scan rate 100 mV s^{-1}, glassy carbon working electrode, Pt wire counter electrode, Ag/AgCl reference electrode, added ferrocene (Fc) as internal standard.

3.2.7 Conclusions

In this part of the chapter, we proved that we have obtained a chemosensor based on PET quenching mechanism from thiourea to a naphthalimide fluorophore by making distance dependence comparison of the fluorescence quantum yield and by cyclic voltammetry measurements. The ligand **PTU** itself with thiourea as binding domain is not a strong ligand in methanol for the metal ions tested, even for thiophilic metals like Hg^{2+} and Ag^{+}. However it has been shown that it is a viable reporting element for metal ions detection, showing a large increase of the fluorescence intensity in case of the titration with Zn^{2+}. The associated ϕ values of 0.4 upon metal:ligand formation are indicating substantial recovery of fluorescence emission.

3.3 First Series of PET Chemosensors: Modulation from the Thiourea as Binding Domain

3.3.1 Introduction

Following the promising results obtained with the simple phenyl substituted thiourea **PTU**, a series of modified compounds with different substituents on the thiourea moiety were designed to modulate the binding affinities of our sensor (Figure 3.18).[128]

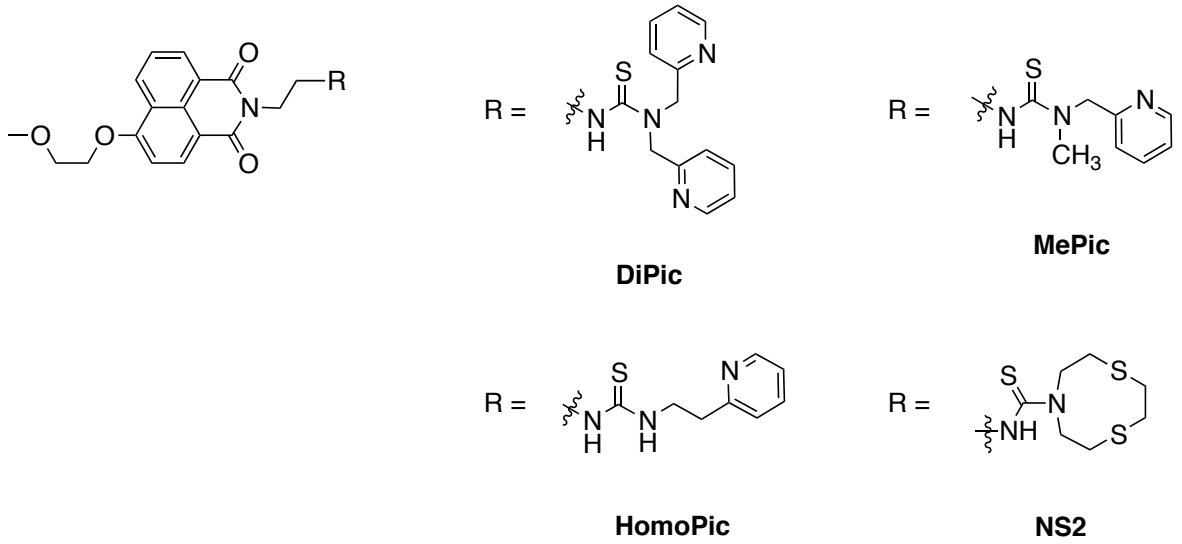

Figure 3.18: Structures of the target compounds of the first series of thiourea-naphthalimide based system, containing an additional metal binding moiety in comparison with **PTU**.

The binding moiety introduced in the compound **DiPic** is a di-2-picolylamine (DPA). This moiety was chosen because it is one of the most efficient binding moiety in the development of fluorescence chemosensors for Zn^{2+}.[129] As mentioned in Chapter 1.5.1, it has been incorporated for example in Zinpyr sensors taking based on the fluorescein fluorophore.[130] Bodipy fluorophores, as well as a tricarbocyanine fluorophores sensing in the near infrared with a turn on fluorescence response at 780 nm were reported with DPA as binding domain for Zn^{2+}.[131,132]

The level of zinc present in the body is regulated by transport proteins, and is minimized because free Zn^{2+} ions are toxic. The limit of detection of a Zn^{2+} sensor for medical application should be in the subnanomolar range and DPA has a corresponding high affinity for Zn^{2+}. Its apparent K_d value is 70 nM.[133] The secondary amine of DPA can be

easily used to link the moiety to different fluorophores as for example the compounds designed by Lippard and described in the Chapter 1.5.1.[47,48]

The binding moiety introduced in compound **MePic** presents only one pyridine in comparison with **DiPic**. We were expecting **MePic** to show a lower interaction with Zn^{2+} as **DiPic**. For compound **HomoPic**, the pyridine moiety is one methyl group more away from the thiourea. So for this compound we will observe influence the topology of the linked pyridine moiety. It was also expected to show lower affinity to Zn^{2+} in comparison with **DiPic**.

For the last target **NS2** a different binding moiety was chosen. As previously described in our group, 7-aza-1,4-dithiacyclononane appeared to be a good ligand in fluorescent chemosensors for Hg^{2+} and Ag^{+}.[122] As the thiourea moiety is a soft ligand, adding more soft coordination moiety to the sensor could improve the coordination with a specific class of metal ion. [134,135]

3.3.2 Synthesis of the Target Compounds DiPic, MePic, HomoPic and NS2

The modified targets were synthesized starting from 1,1-thiocarboxydiimidazole mixed with the amine **88** previously synthesized (Chapter 3.2.2) in acetonitrile at room temperature to give the mono-substituted thiourea **94** (Scheme 3.4). This compound can be isolated easily because it precipitates from the reaction mixture, preventing the substitution of the second imidazole moiety. In the second step, our different targets **DiPic, MePic, HomoPic and NS2** were synthesized by heating **94** and the corresponding amine at 80 degrees in acetonitrile (Scheme 3.4).

This synthetic pathway is very efficient and gives rapid access to a wide range of target chemosensors when the corresponding amine is commercially available or can be synthesized in a few steps. This general procedure will be used for all the target compounds of the following Chapters.

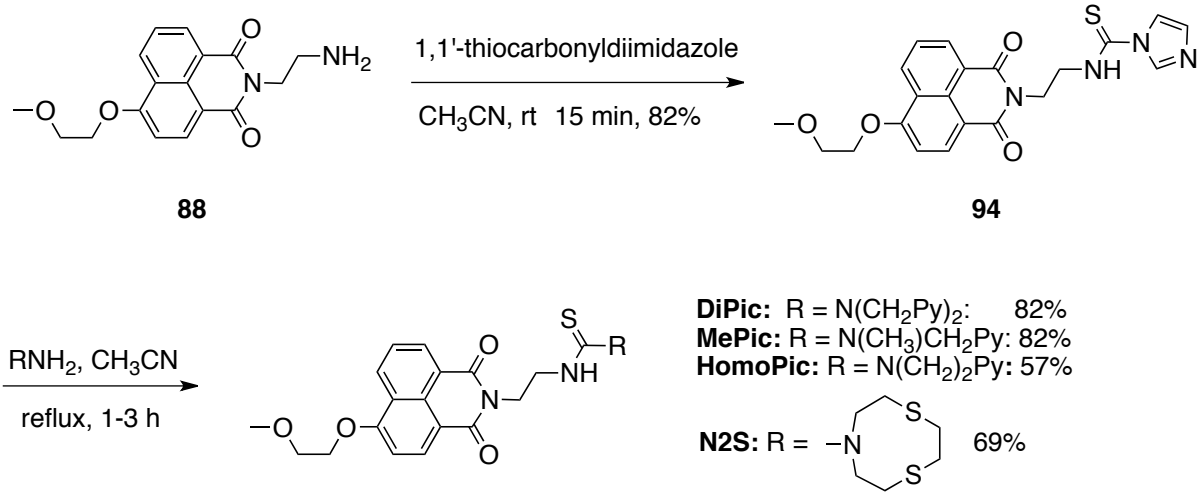

Scheme 3.4: Synthesis of the first series of naphthalimide-thiourea based targets; Py = 2-pyridyl.

For the first three targets of this chapter **DiPic**, **MePic** and **HomoPic**, di-2-picolylamine **97**, 2-[(methylamino)methyl] pyridine **99** and 2-aminoethylpyridine are commercially available. However the first two can be accessed by reductive amination from 2-pyridine carboxaldehyde **96** and the corresponding amine (Scheme 3.5).[136]

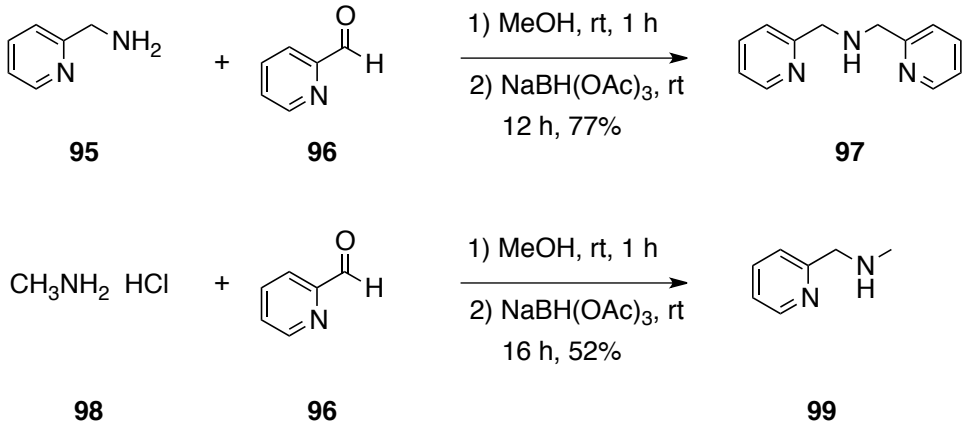

Scheme 3.5: Scheme of the reductive aminations.

The last amine, the 7-aza-1,4-dithiacyclononane, needed for the synthesis of the target **NS2** was synthesized as previously done in our group following a procedure from van de Water for bigger thiacrown ethers.[137] This synthesis starts from the commercially available bis-(2-chloroethyl) amine hydrochloride **100** and 1,2-ethanedithiol with an overall yield of 11 % (Scheme 3.6). Extreme precautions are needed for this reaction because of the high toxicity and the unpleasant smell of the starting materials.

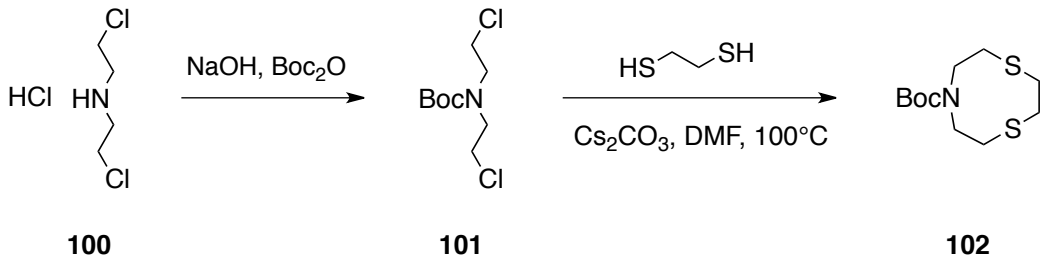

100 **101** **102**

Scheme 3.6: Synthesis of the Boc protected 7-aza-1,4-dithiacyclononane **102**.

The target **MePic** was not designed with a methyl group from the beginning. Compound **103** was designed and the synthesis of this compound was intended. The problem was that **103** was very unstable. The pyridine could be serving as an intramolecular base, helping to the formation of the imidazopyridine **105** as decomposition product via the isothiocyanate intermediate **104** (Scheme 3.7) as it has been previously described in the literature.[138]

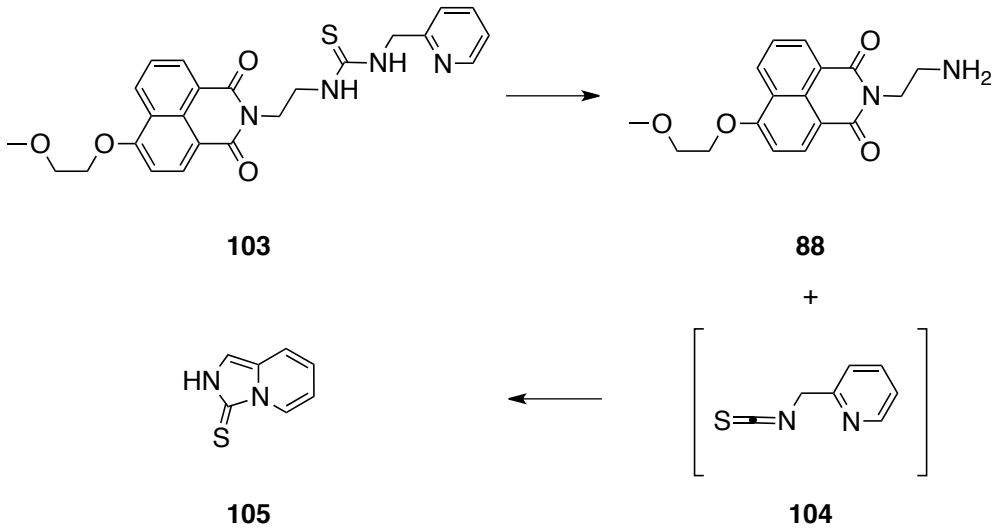

103 **88** + **105** **104**

Scheme 3.7: Proposed decomposition products of **103**.

In the reaction between 1,1- thiocarbonyldiimidazole **106** and the amine **95**, the mono or disubstituted products were not observed and the imidazopyridine **105** was isolated instead (Scheme 3.8). It could be characterized by ^{1}H-NMR spectroscopy data, which were consistent with data previously reported in the literature.[139]

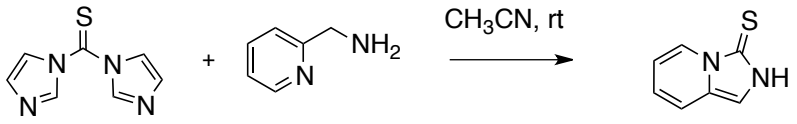

106 **95** **105**

Scheme 3.8: Control reaction for the formation of the imidazopyridine **105**.

3.3.3 Photophysical Properties of DiPic, MePic, HomoPic and NS2

The photophysical properties of **DiPic**, **MePic**, **HomoPic** and **NS2** were investigated in methanol. The UV-visible absorption spectrum is characterized by a broad band with a maximum at 368 nm. The fluorescence emission spectrum is characterized by broad band with a maximum at 446 mn (Table 3.3). All the compounds are showing relatively low quantum yield. The photophysical properties of those compounds are similar to those of the first thiourea **PTU**.

Table 3.3: Photophysical properties of **DiPic**, **MePic**, **HomoPic** and **NS2** in methanol.

Compounds	λ_{abs} / nm	ε^a/ $M^{-1}cm^{-1}$	λ_{em} / nm	ϕ_F [b]
DiPic	368	12600	446	0.05
MePic	368	13500	446	0.03
HomoPic	368	13300	446	0.05
NS2	368	13000	446	0.03

[a] For longest wavelength λ_{max} . [b] Relative to anthracene in methanol $\phi = 0.30$.[89]

Very similar photophysical properties were observed for those compounds in a water:methanol 90:10 mixture as solvent. The UV-visible spectra was showing the same absorption band as in methanol and the fluorescence emission band was bathochromically shifted to 454 nm.

3.3.4 Fluorescence Titrations of the First Series of Targets with Metal Ions in Methanol

The response of the compounds of the first series of chemosensors was investigated by addition of various metal ions in the same way as previously described for **PTU**. The metal ions tested are Li^+, Na^+, K^+, Mg^{2+}, Ca^{2+}, Ag^+, Zn^{2+}, Cd^{2+}, Hg^{2+} and Pb^{2+} and the anions are Cl^-, ClO_4^- or NO_3^-. The titrations were carried out in a 3 µM solution of the fluorophore in methanol. The salts were added as 5 µl aliquots of solutions in methanol with an increasing concentration from $2 \cdot 10^{-4}$ M to 2 M depending on the response observed. All the titrations presented in this section are showing modifications in the fluorescence intensities but no modification of their absorbance. This indicates that no changes in the ground state electronic structure of the fluorophore are occurring after interaction from the chemosensors with the metals since the thiourea moiety is the receptor.

The thiourea containing DPA as additional binding domain, **DiPic**, is showing a 13-fold increase of the fluorescence emission (Figure 3.19) in a very similar way as previously observed for the titration of **PTU** upon addition of Zn^{2+}. However **DiPic** shows an increased affinity to Zn^{2+} in comparison with the affinity of **PTU**. The logarithm of the dissociation constant was calculated to be -2.9 compared to -1.3 for **PTU** (Table 3.4).

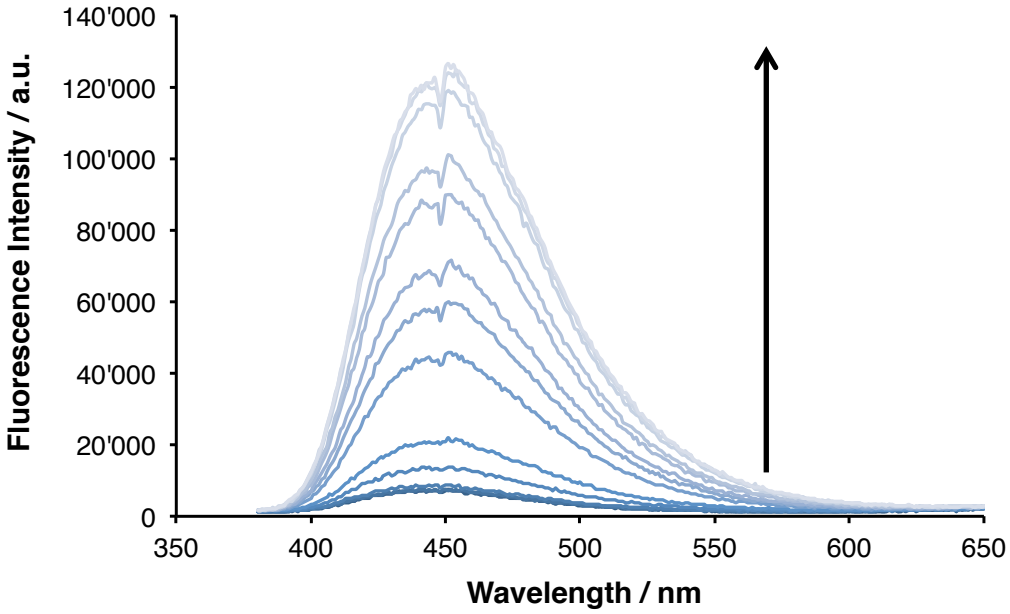

Figure 3.19: Fluorescence titration of **DiPic** (3 µM in methanol) with $ZnCl_2$.

Titrations with various metal ions were done in methanol with the four chemosensors of the first series **DiPic**, **MePic**, **HomoPic** and **NS2**. The dissociation constants were obtained in the same way as described for **PTU** using the program Prism6, fitting the sigmoidal curves obtained after plotting the normalized integrated fluorescence emission intensity as function of log [M]. The results are summarized in Table 3.4 for the binding affinities and in Figure 3.20 for the maximum of the fluorescence enhancement.

Table 3.4: Apparent log K_d (M) for the titrations of **PTU**, **DiPic**, **MePic**, **HomoPic** and **NS2** in methanol with responsives metal ions.

Compounds	Zn^{2+}	Cd^{2+}	Hg^{2+}	Ag^{+}	Pb^{2+}
PTU	-1.3	-1.6	–	–	–
DiPic	-2.9	-3.1	-6.1	–	–
MePic	-3.2	-3.2	-5.8	–	-2.5
HomoPic	-2.1	-2.3	-5.3	-2.3	–
NS2	-1.2	–	-5.2	-4.4	–

Titration at 3 µM of the chemosensor in methanol. Entries marked ”-“ indicate an absence of fluorescence response

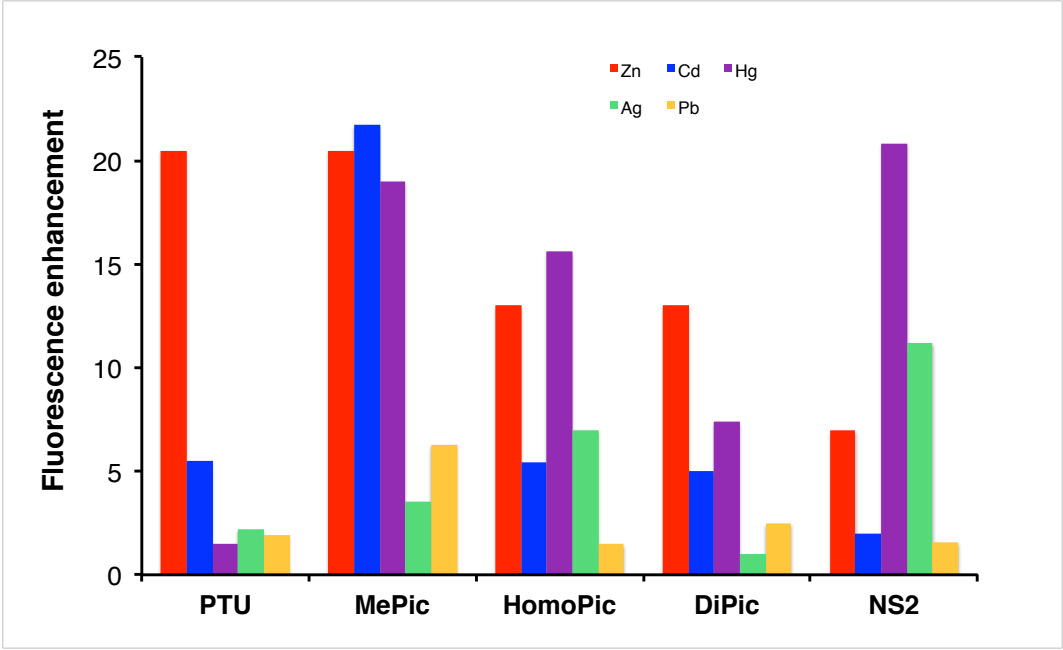

Figure 3.20: Metal-induced ratiometric fluorescence enhancement of **PTU**, **DiPic**, **MePic**, **HomoPic** and **NS2** in methanol.

Table 3.5: Values of $(I/I_0)_{max}$ and (ϕ_{max}) for titrations of **PTU**, **DiPic**, **MePic**, **HomoPic** and **NS2** in methanol.[a,b,c]

Compounds	Zn^{2+}	Cd^{2+}	Hg^{2+}	Ag^{+}	Pb^{2+}
PTU	20.5 (0.41)	5.5 (0.11)	–	–	–
DiPic	13 (0.65)	5 (0.25)	7.4 (0.37)	–	–
MePic	20.5 (0.62)	21.7 (0.65)	19 (0.57)	–	6.3 (0.19)
HomoPic	13 (0.65)	5.4 (0.27)	15.6 (0.78)	7 (0.35)	–
NS2	7 (0.21)	–	20.8 (0.62)	11.2 (0.33)	–

[a] Maximum observed I/I_0 as shown in Figure 3.20. [b] $\phi_{max} = \phi_{initial} \times (I/I_0)_{max}$. ϕ_{max} in parentheses. [c] Entries marked '–' indicate that saturated binding, and thus I/I_0(max), was not reached.

The identity of the additional metal coordinating group(s) determines the metal binding affinity and selectivity. The highest affinities for the titrations of all compounds of the first series of chemosensors in methanol are observed for the addition of Hg^{2+}. The sigmoidal titration curves of the normalized integrated fluorescence enhancement in function of log [Hg^{2+}] are represented in Figure 3.21.

For the addition of Zn^{2+}, the variations of the binding affinities are instructive. The comparison from **MePic** with **DiPic** shows that both compounds have a very similar response to the addition of Zn^{2+} (Figure 3.22). The observed log K_d (-3.1) of the complex between **DiPic** and Zn^{2+} is indicating a much weaker complex than the one expected between a DPA moiety and Zn^{2+}. Those two observations suggest that only one of the *N*-pyridine substituent on the thiourea in **DiPic** contributes to metal binding. Affirmation of this hypothesis was obtained by crystal structure of a related ligand (see Chapter 3.3.7). Furthermore the comparison of **MePic** with **HomoPic** shows the effect of the addition of one more methyl group between the thiourea and the pyridine indicating that even a small variation in the orientation of the coordinating heteroatom lone pairs has a significant impact on metal binding affinity (Figure 3.22).

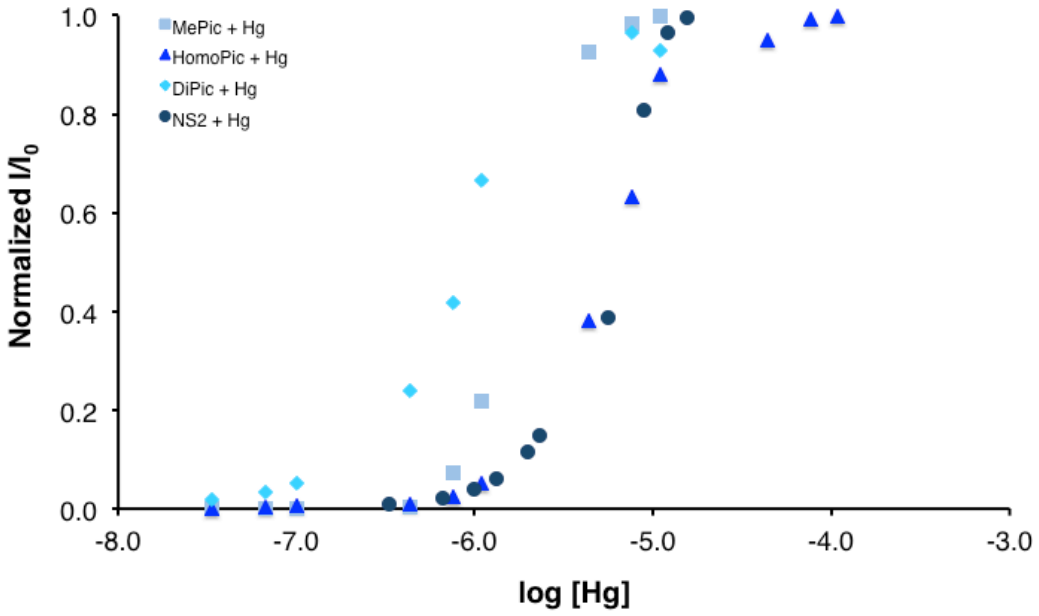

Figure 3.21: Ratiometric fluorescence enhancement for the titrations of **DiPic**, **MePic**, **HomoPic** and **NS2** with $HgCl_2$ in methanol.

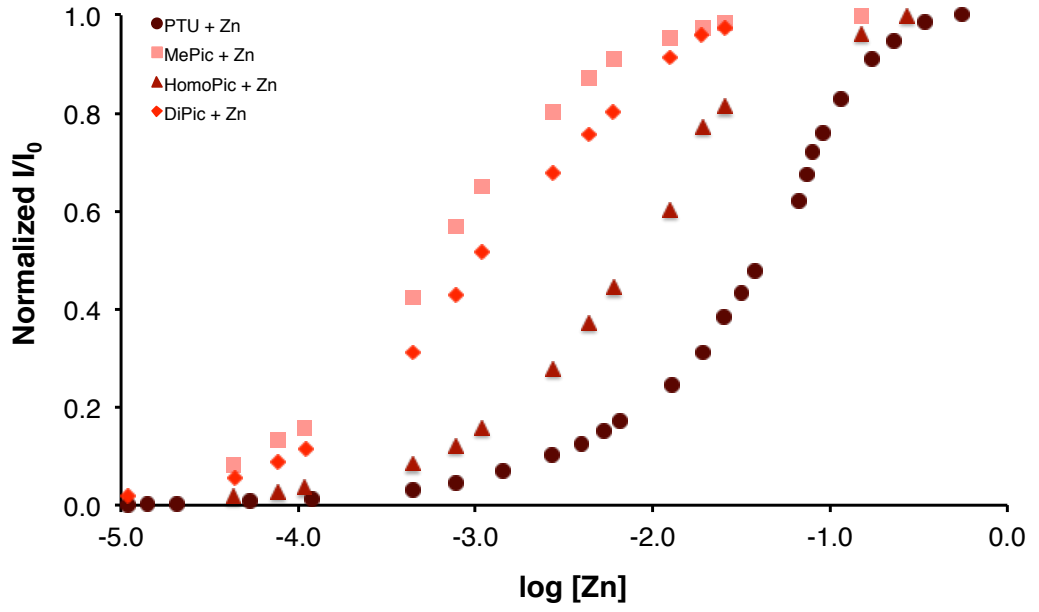

Figure 3.22: Ratiometric fluorescence enhancement for the titrations of **PTU**, **DiPic**, **MePic** and **HomoPic** with $ZnCl_2$ in methanol.

All of those chemosensors respond to Cd^{2+} with an affinity comparable to their affinity for Zn^{2+}. The difference lies in the maximum of the fluorescence emission enhancement. As shown in Table 3.5, a zinc complex as for example DiPic:Zn^{2+} is more emissive than its cadmium analog DiPic:Cd^{2+}. This indicates that coordinated metals do not have an equal intrinsic impact on PET quenching as previously observed for example by Lippard in **Zinpyr** chemosensors (Figure 1.12).[140]

The chemosensor **NS2** has a different structure than the other compounds of the series with a thiacrown ether moiety as additional binding domain instead of pyridines. This influences its binding affinities to various metal ions. The binding affinities of the thiacrown ether for Ag^{+} and Hg^{2+} previously observed in our group were confirmed with a low dissociation constant of the formed complexes (Table 3.4).[122]

The affinity of **NS2** for Zn^{2+} is similar to the affinity of the benzyl substituted thiourea **PTU** for Zn^{2+}, which is coherent with the absence of Zn^{2+} coordinating moieties. However the increase of the fluorescence emission in response to Zn^{2+} is much lower than in the case of **PTU**. In the case of Cd^{2+} with **NS2** no visible enhancement of the fluorescence could be observed.

The isolated responses to Ag^{+} or Pb^{2+} are intriguing but their origins are still unclear. The addition of various other metals did not lead to observable modifications of the fluorescence emission indicating that no disruption of the PET quenching process occurs from the thiourea to the fluorophore but interactions with other coordinating moiety of the chemosensors are not excluded.

The fact that there is no clear correlation between the variation of the fluorescence enhancement $(I/I_0)_{max}$ with the metal affinity (Table 3.5) indicates that other factors have to be taken in account to understand the behavior of our chemosensors. It is important to note that the presence of an additional ligand is not only affecting the binding constant but also the fluorescence enhancement. It indicates that the metal coordination environment beyond thiourea binding must also play a role in the fluorescence response.

The position of the s-cis/s-trans conformational equilibrium of non-emissive metal-complexed species in which thiourea is not ligated as well as the geometry of the conformation are important factors inducing differences in the behavior of our chemosensors towards metal ions.

An increase in the relative population of the s-cis configuration should be accompanied by an increase in the population of emissive thiourea-coordinated state, increasing the observed fluorescence enhancement (Figure 3.23).

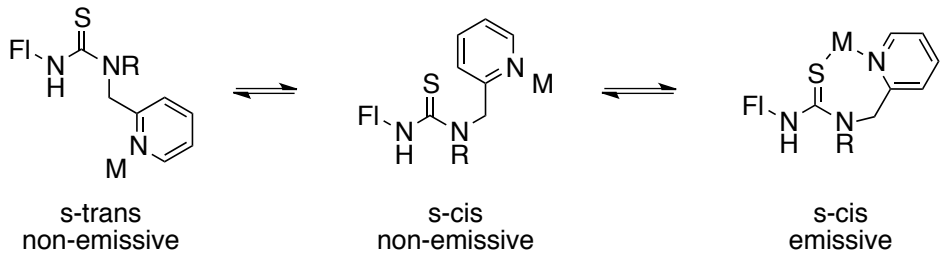

Figure 3.23: Minimal form of the s-*cis*/s-*trans* equilibria in metal complexes. (Fl = naphthalimide fragment.

The potential response to the interaction of the chemosensor with the counter ions was investigated by the addition of various cation non-responsive salts. Potassium salts as KCl, $KClO_4$ were chosen and titrations were done showing no significant changes in the fluorescence emission in methanol. This is leading to the conclusion that interactions with anions are not showing decrease in the fluorescence emission in methanol but the possibility of interaction with anion in DMSO as reported in the literature was not explored.

The reversibility of the binding was tested by dilution of the sample once the half-maximum of the increase in fluorescence was reached. The result of the sample dilution is the lowering of the fluorescence intensity. Further addition of the metal ion to the dilute sample leads to augmentation of the fluorescence emission. The reversibility of the binding was also tested by NMR and mass analysis. The possibility of desulfurization of the thiourea was excluded in the conditions of our analysis. A ^{13}C NMR of the complex prepared in order to obtain a crystal structure (see Chapter 3.3.7) is showing a peak at 180 ppm characteristic of the thiourea carbon atom which is still present in the Hg^{2+} complex and after washing the solution with EDTA.

The stoichiometry of the binding could not be analyzed by a traditional Job plot analysis in this series of compounds. To obtain it for the interaction with Zn^{2+} an unreasonably concentrated solution of the chemosensor was needed due to very low affinity. For the interaction with Hg^{2+}, the results were not reliable because of a systematic decrease of the fluorescence emission with time after the completion of the titrations. However the results obtained for the NMR titration (Chapter 3.3.6) and from the mass analysis of the

complexes (Zn^{2+}:MePic complex is represented in Figure 3.24) are consistent with reversible formation of 1:1 metal:ligand complex.

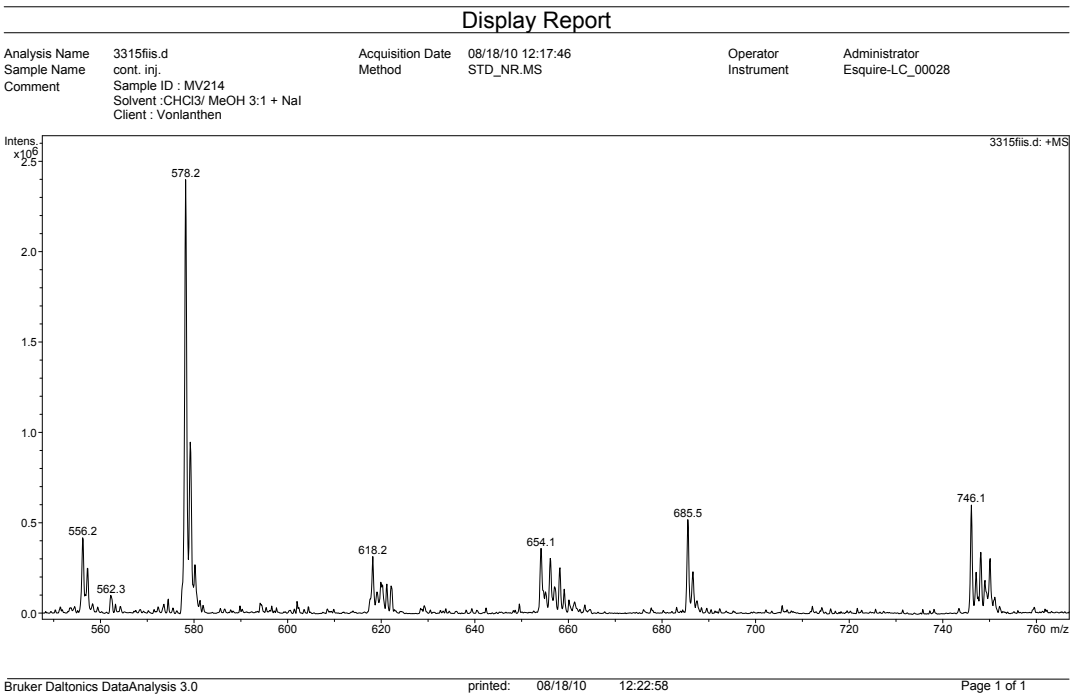

Figure 3.24: Mass spectra of **DiPic**:Zn complex; M^+ : 556; $M + Na^+$: 578; $M + Zn^{2+} - H^+$: 618; $M + Zn^{2+} + Cl^-$: 654; $M + 2H^+ + I^-$: 685; $M + Zn^{2+} + I^-$: 746.

3.3.5 Fluorescence Titrations of the First Series of Targets with Metal Ions in Water

The titrations done in Chapter 3.3.4 were repeated in a water:methanol 90:10 solvent mixture. The compounds **DiPic**, **MePic**, **HomoPic** and **NS2** were not directly soluble in water and for this reason the solutions used in this chapter were prepared by serial dilution with water from a 30 µM solution of the chemosensors in methanol. The titrations were done in the same way as reported for the titrations in methanol and the dissociation constants were calculated for all the experiment showing response to the added salt using the program Prism6. The results are summarized in Table 3.6 for the binding affinities and in Figure 3.25 for the maximum of the fluorescence enhancement.

Table 3.6: Apparent log K_d (M) for the titrations of **DiPic**, **MePic**, **HomoPic** and **NS2** in a mixture water:methanol 90:10 with responsives metal ions.

Compounds	Zn^{2+}	Cd^{2+}	Hg^{2+}
DiPic	-0.9	-2.3	-6.0
MePic	-1.1	-2.1	-5.9
HomoPic	-0.4[a]	-1.7	-5.8

Titration at 3µM of the chemosensor in water:methanol 90:10; Entries marked ”-“ indicate an absence of fluorescence response; a) Data extrapolated from incomplete titration because of sample volume limitation.

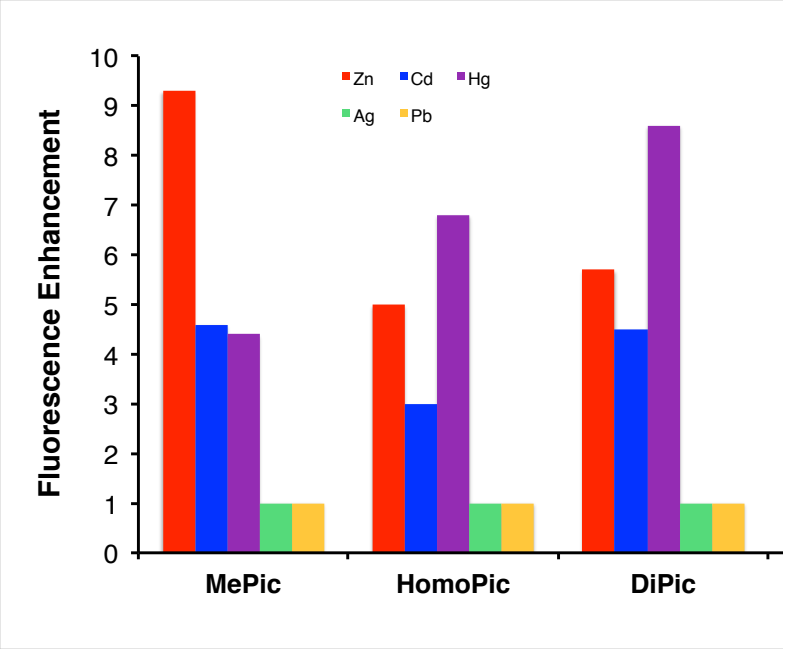

Figure 3.25: Metal-induced ratiometric fluorescence enhancement of **DiPic**, **MePic**, **HomoPic** and **NS2** in water:methanol 90:10.

Table 3.7: Values of $(I/I_0)_{max}$ and (ϕ_{max}) for titrations of **DiPic**, **MePic** and **HomoPic** in water:methanol 90:10.[a,b]

Compounds	Zn^{2+}	Cd^{2+}	Hg^{2+}
DiPic	5.7 (0.29)	4.5 (0.23)	8.6 (0.43)
MePic	9.3 (0.28)	4.6 (0.14)	4.4 (0.13)
HomoPic	5 (5.05)	3 (0.15)	6.8 (0.34)

[a] Maximum observed I/I_0 as shown in Figure 3.25. [b] $\phi_{max} = \phi_{initial} \times (I/I_0)_{max}$. ϕ_{max} in parentheses.

The titration in a water:methanol 90:10 media are showing for all the compounds the same affinity for Hg^{2+} as in methanol but with a approximately two times lower maximum of increase of the fluorescence (Figure 3.25 and Figure 3.26).

For the complexation of **DiPic**, **MePic** and **HomoPic** with Zn^{2+}, the dissociation constants observed in aqueous media were increased from about 10^2 M in comparison with the one previously observed in methanol (Table 3.4), indicating a response with lower affinity

for Zn^{2+} in an aqueous media (Figure 3.27). The maximum enhancement of the fluorescence intensity, as well as for Hg^{2+}, was lower by approximately a factor of two for the response to Zn^{2+}.

The affinities of the binding to Cd^{2+} are as well lower in the aqueous media in comparison with methanol but they are differentiated from the responses to Zn^{2+}, as the affinity for Cd^{2+} is slightly higher than the affinity for Zn^{2+} in water.

No response was observed to the addition of other metal ions as it was observed previously in methanol. Isolated response to Ag^{+} or Pb^{2+} were not observed in the water:methanol 90:10 mixture.

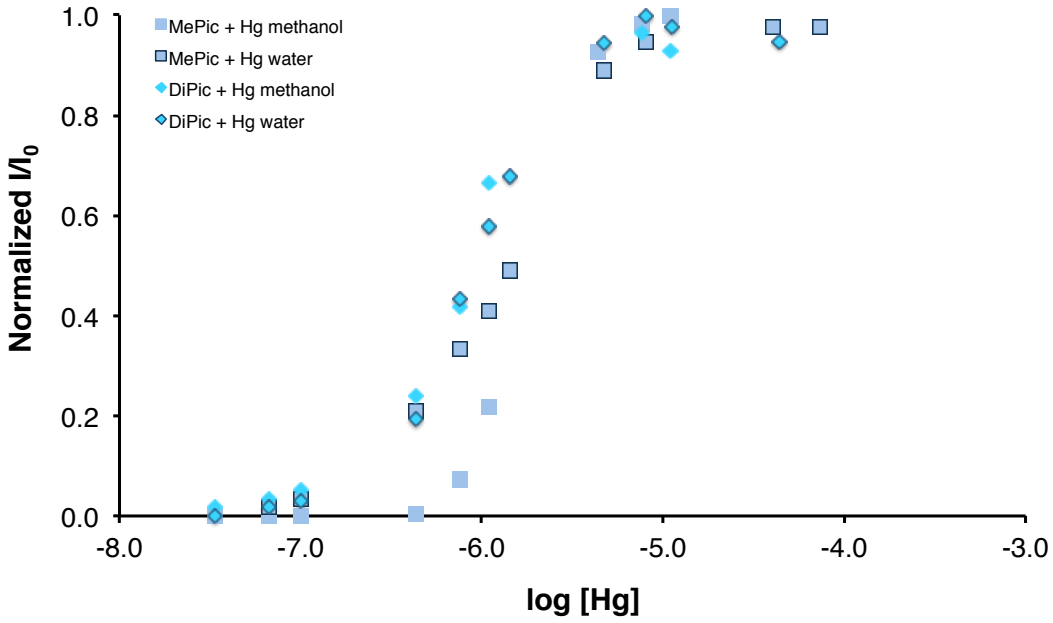

Figure 3.26: Comparison of the ratiometric fluorescence enhancement for the titrations of **DiPic** and **MePic** with $HgCl_2$ in water:methanol 90:10 and in methanol.

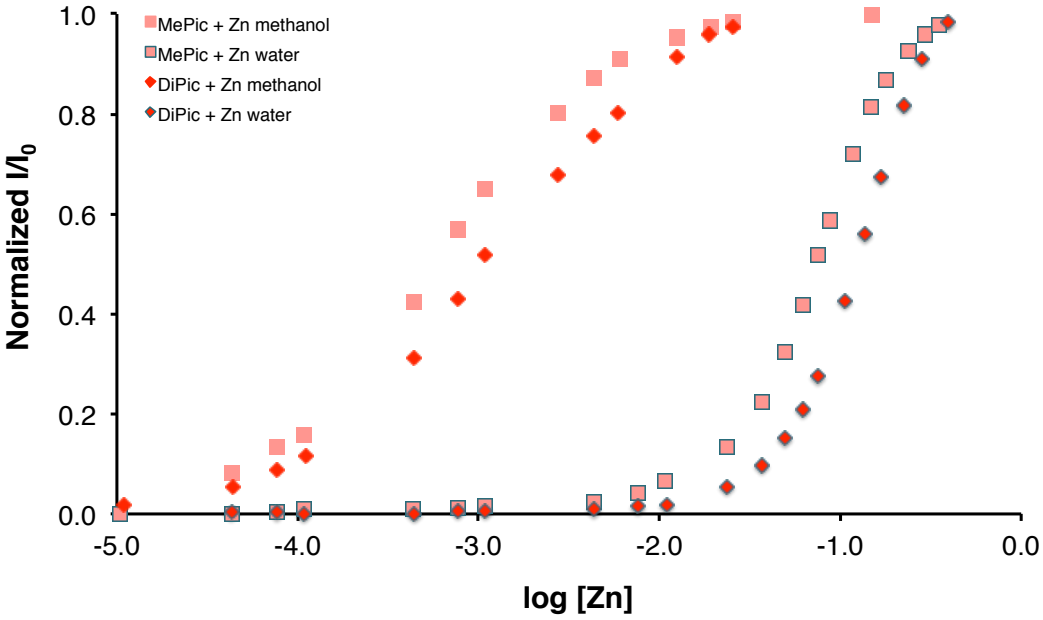

Figure 3.27: Comparison of the ratiometric fluorescence enhancement for the titrations of **DiPic** and **MePic** with $ZnCl_2$ in water:methanol 90:10 and in methanol.

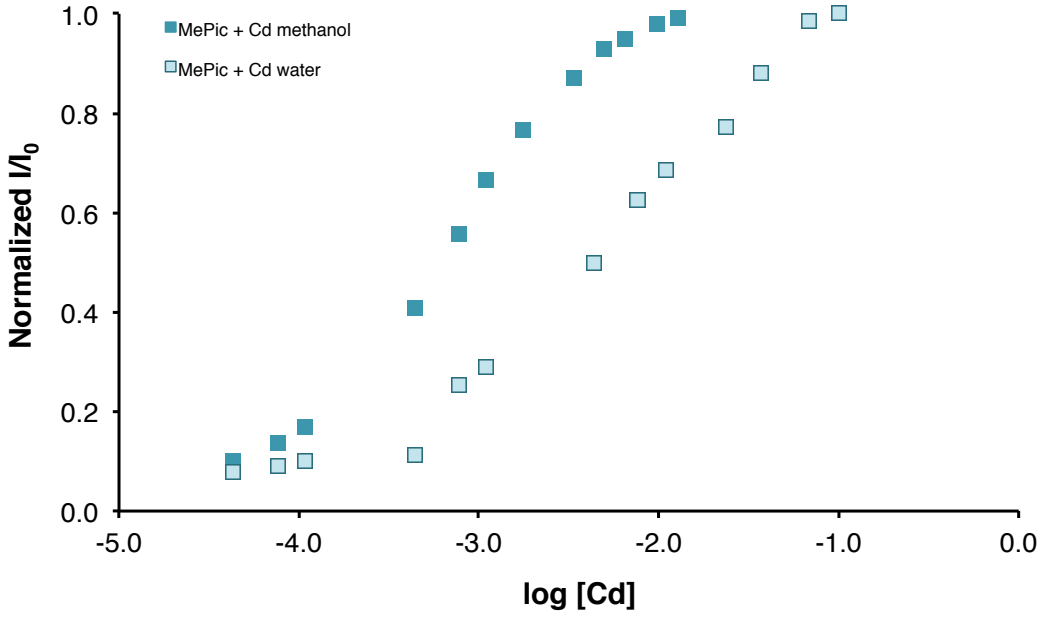

Figure 3.28: Comparison of the ratiometric fluorescence enhancement for the titrations of **MePic** with $CdCl_2$ in water:methanol 90:10 and in methanol.

3.3.6 NMR Titrations of MePic with Zn^{2+} and Hg^{2+}

The binding between the compounds of the first series of targets and metal ions was investigated by ^1H NMR. The exchange between the free and the metal bound conformation of the receptor is a reversible dynamic process that can have different effect on the appearance of the NMR spectra. It gives rise to two distinct sets of ^1H NMR signals. Two different limiting cases are commonly observed which are the fast or slow exchanges on the NMR timescale. If the exchange rate k is slow on the chemical shift timescale, two different sets of signal are visible. If the exchange rate k is fast on the chemical shift time scale, only one signal is observed at an average chemical shift of the two conformations.[141]

The compound used for this study is **MePic**, it was chosen because of its characteristic signal for the methyl group at 3.1 ppm and its well-defined pyridine signals. The titrations were done with an 8 mM solution of the compound in $CDCl_3$ at 500 MHz. The titrations were done with Zn^{2+} and Hg^{2+} and are representative for the compounds of the first series of targets.

The behavior of **MePic** was different depending on the metal ion added. In the case of the titration with Zn^{2+}, a slow exchange rate was observed (Figure 3.29) and in the case of the titration with Hg^{2+}, a fast exchange rate was observed (Figure 3.30).

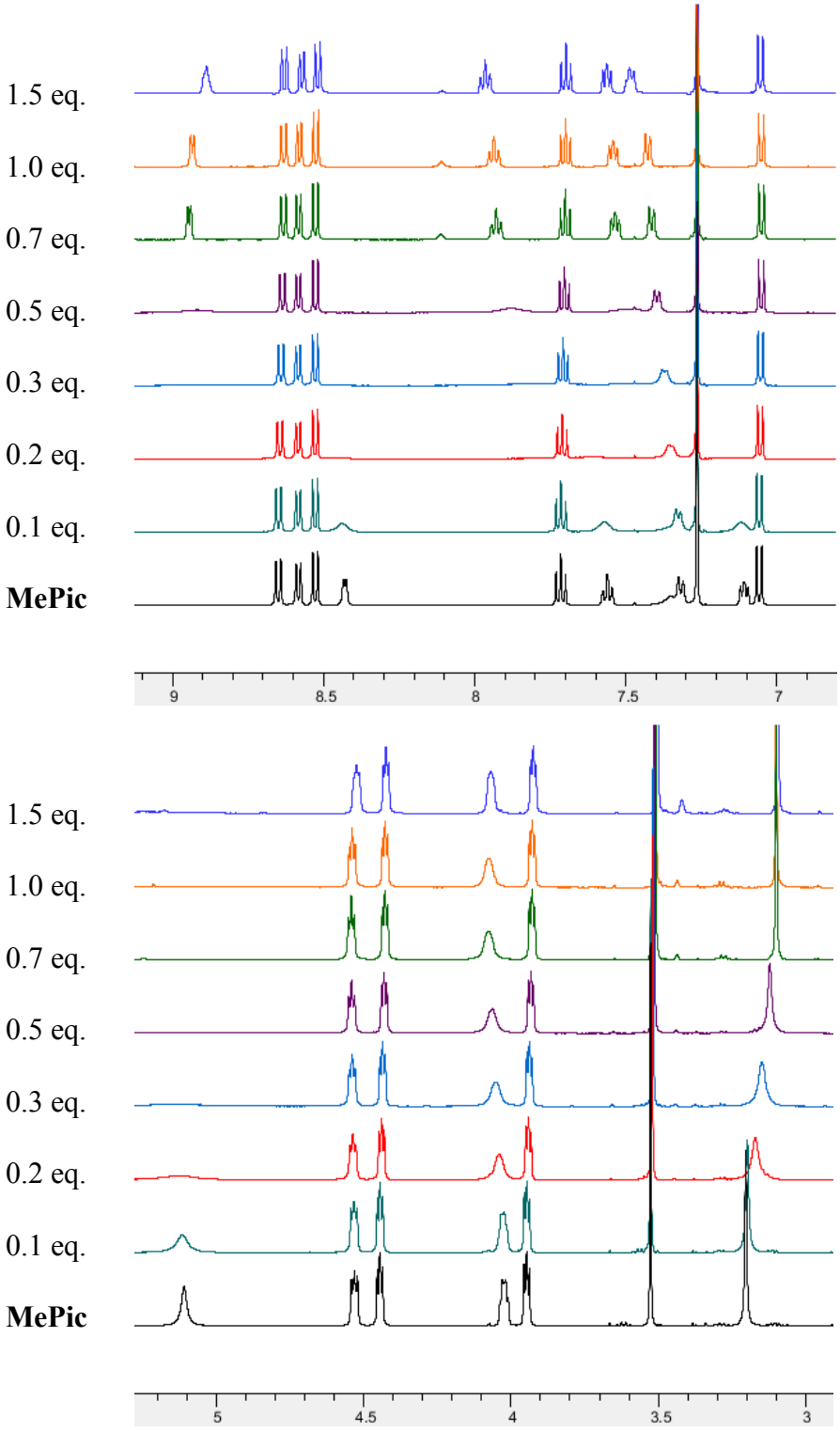

Figure 3.29: NMR Titration of **MePic** with Zn^{2+} in $CDCl_3$.

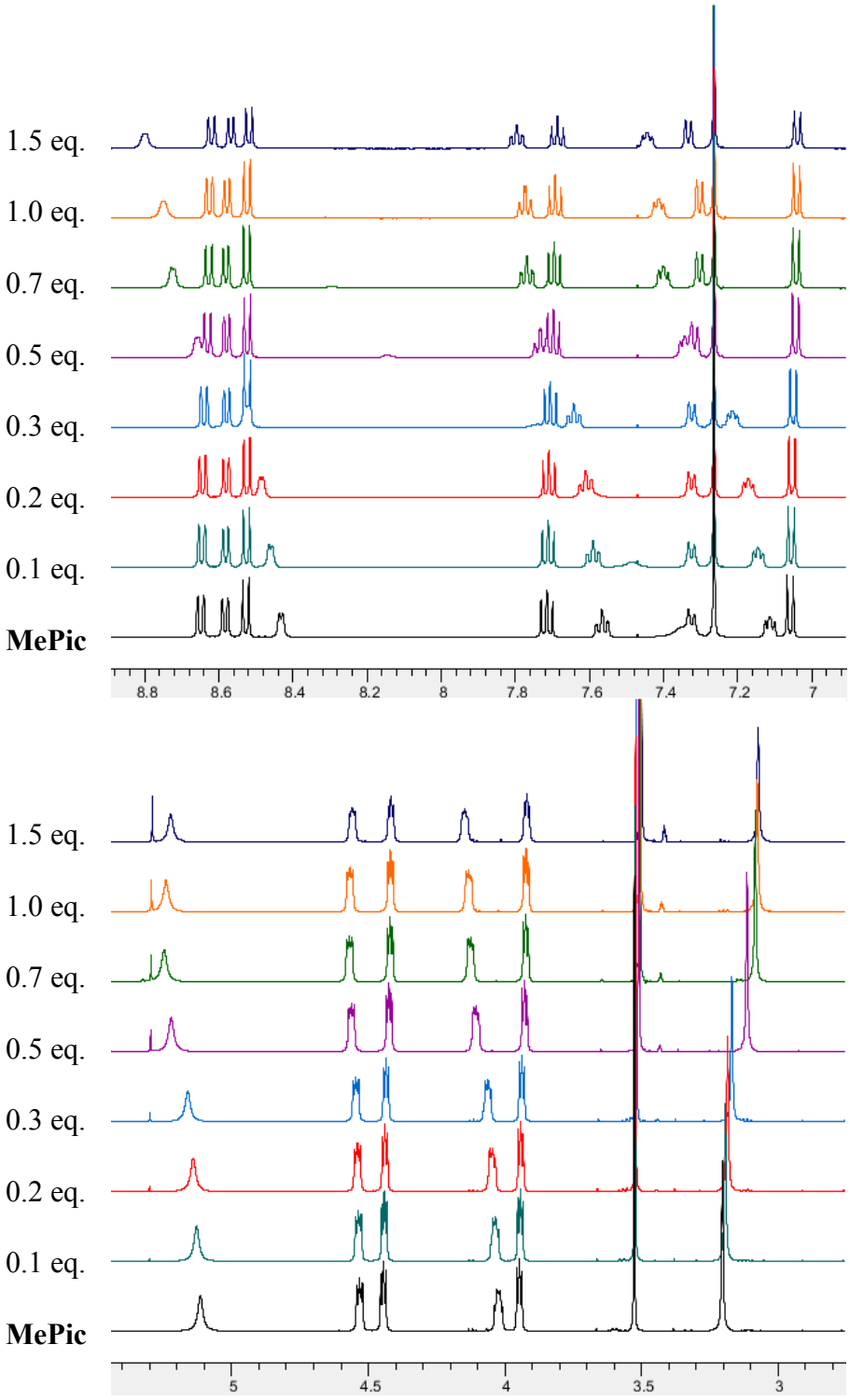

Figure 3.30: NMR Titration of **MePic** with Hg^{2+} in $CDCl_3$.

3.3.7 Crystal Structure

In order to determine the coordination geometry and the stoichiometry of our complexes formed during titrations with metal ions, they were synthesized and crystallization of the obtained compounds was attempted. Since the quantities of the obtained compounds were very low and the obtained compounds were more amorphous than crystalline solids, no crystals were obtained in this way.

A model ligand **107** was synthesized, containing the thiourea with a simple benzyl group instead of the naphthalimide fluorophore and the binding domain mimicking **DiPic** (Scheme 3.9). The Zn^{2+} complex of this new ligand was obtained by stirring a 1:1 ratio of the two components in acetonitrile for 30 minutes. The product was precipitated by addition of methanol and was filtered to obtain a white crystalline solid.

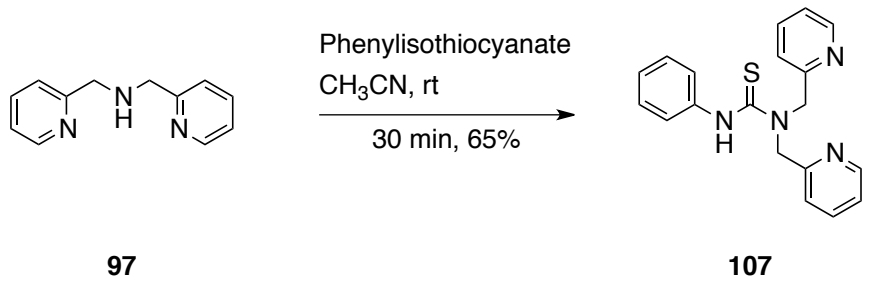

97 **107**

Scheme 3.9: Synthesis of the model ligand **107**.

Crystals of the **107**:Zn^{2+} complex could be grown by slow diffusion of hexane into dichloromethane and the crystal structure was determined via X-ray analysis (Figure 3.31). The crystal structure shows the interaction of Zn^{2+} with the sulfur atom from the thiourea, a nitrogen atom of one pyridine and two chlorine atoms. The nitrogen atom of the second pyridine is involved in a hydrogen bond with the NH group of the thiourea. This result nicely confirmed the observation done in the fluorescence titration showing almost no difference in binding affinity between **DiPic** and **MePic**, which was proposed to reflect the fact that only one pyridine of **DiPic** was involved in the coordination of Zn^{2+} instead of a both.

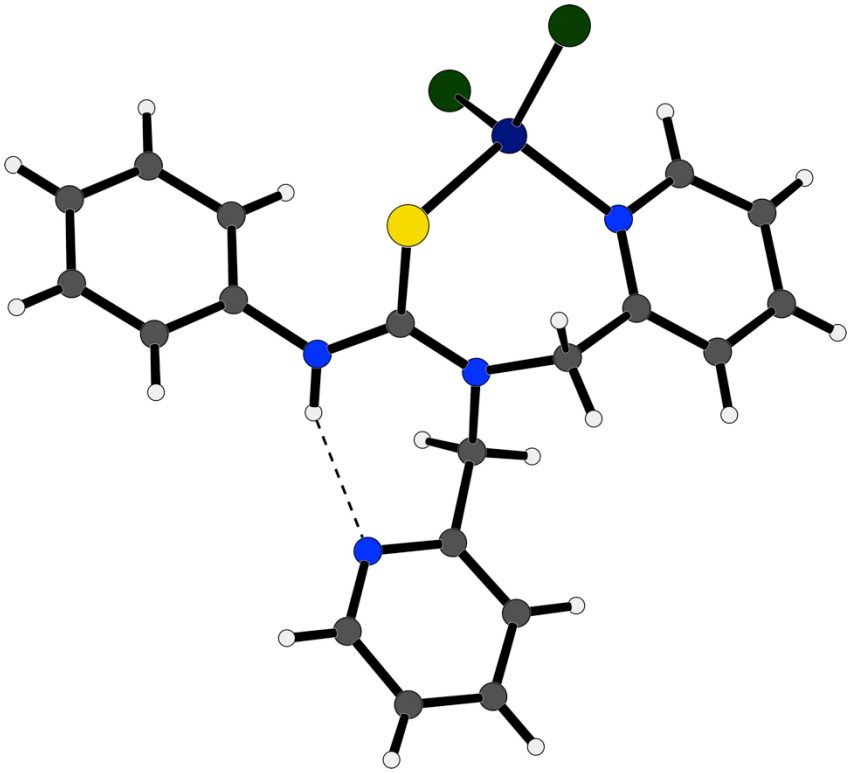

Figure 3.31: Crystal structure of **107**:Zn^{2+} complex. Blue: nitrogen, yellow: sulfur, dark blue: zinc, green: chloride.

It is interesting to note that the torsion angle obtained for Zn-S-C-N in this structure is 75° (Figure 3.32), which is not what we would expect to give to most stable configuration (See Chapter 3.1.1, Figure 3.1). It seems that the stabilization induced by the hydrogen bond formation between the thiourea NH and the non-coordinating pyridine is inducing more stabilization in the complex. This torsion angle involve the fact that the metal is interacting with the π-electron system of the C=S double bond rather than with the sulfur free electron pair. The bond length of this double bond is also longer (1.724) than a normal C=S double bond (1.693). We suppose that this geometry is also having an influence in the observed fluorescence enhancement but crystal structures of other complexes with different metal and ligand are needed in order to make a better conclusion.

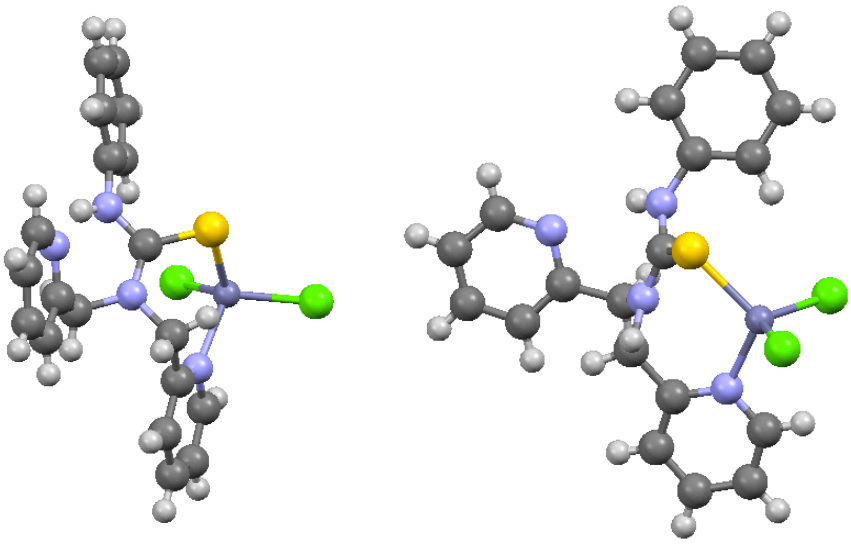

Figure 3.32: Different view of the crystal structure of **107**:Zn^{2+} complex. Blue: nitrogen, yellow: sulfur, dark blue: zinc, green: chloride.

3.3.8 Conclusions

The results presented in this Chapter demonstrate that modulation of PET quenching by thioureas provides a basis for the development of metal-responsive fluorescent chemosensors. The described compounds could be claimed as Hg^{2+} selective chemosensors; however, the apparent affinities are insufficient for practical use. The dissociation constant of the obtained complex between **DiPic** and Zn^{2+} was higher than expected for a complex of a free di-2-picolylamine moiety with Zn^{2+} and therefore compounds with different ligand geometry will be developed in the next section.

3.4 Second Series of PET Chemosensors: Modulation of the Distance between Thiourea and Binding Domain

3.4.1 Introduction

To improve the effect of the metal-coordinating site of the chemosensor, we designed a second series of naphthalimide-thiourea based chemosensors. Since we have observed that for the compound **DiPic** of the first series, the di-2-picolylamine moiety was not coordinating Zn^{2+} with both pyridines, we introduced an ethylene bridge between the thiourea and the metal coordinating sites. In this construct, the di-2-picolylamine moiety should be more free to bind Zn^{2+} with both pyridines and affect the fluorescence of the chemosensor by the additional coordination of Zn^{2+} with the sulfur atom of the thiourea.

Two targets of this series **EnDiPic** and **EnMePic** were obtained (Figure 3.33) and their responses to metal ions were tested in the same way as previously described for the compounds of the first series. The synthesis of the last two targets **EnHomoPic** and **EnNS2** (Figure 3.34) were not completed during this work, but the effort towards their synthesis will be discussed.

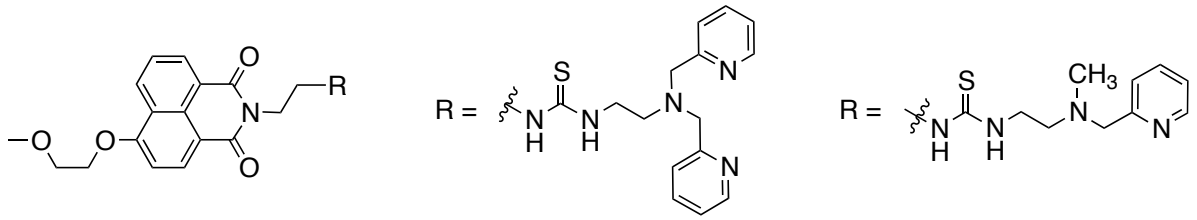

Figure 3.33: Structures of the obtained target compounds of the second series of thiourea-naphthalimide based system, containing an ethylene bridge between the thiourea and the metal binding moiety.

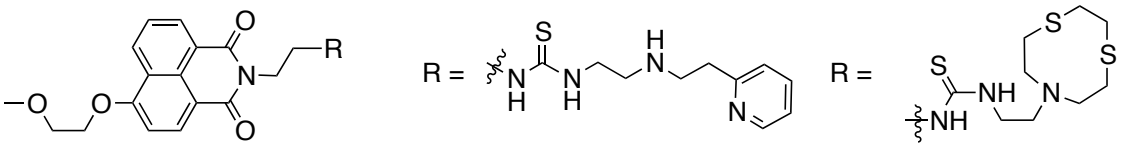

EnHomoPic **EnNS2**

Figure 3.34: Structures of the two target compounds of the second series of thiourea-naphthalimide based systems, containing an ethylene bridge between the thiourea and the metal binding moiety, that were not obtained.

3.4.2 Synthesis of the Targets of the Second Series of Chemosensors

To achieve the synthesis of the proposed compounds, the corresponding amines have to be synthesized first and then be coupled to the fluorophore by substitution of the imidazole of **94** in the same way as previously described in Chapter 3.3.2 for the first series of chemosensors based on naphthalimide-thiourea system.

The amine **110** for the synthesis of **EnDiPic**, analogue of **DiPic** with a DPA biding moiety and an ethyl spacer, was synthesized starting from the mono Boc-protected 1,2-aminoethane **79** and 2-chloromethylpyridine **108**. The reaction in methanol in presence of Na_2CO_3 as a base gave compound **109**, which could be deprotected using TFA following the general procedure to give the desired amine **110** (Scheme 3.10).[142]

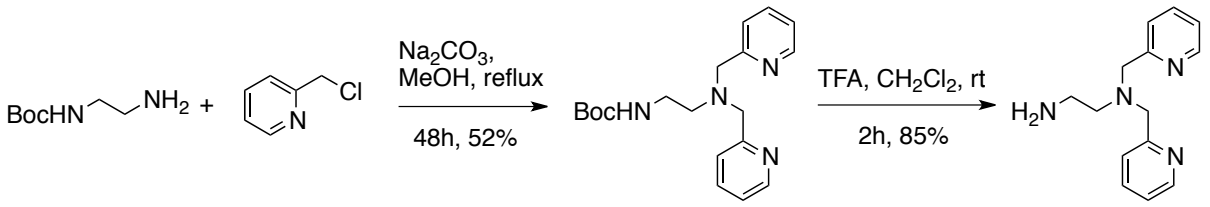

79 **108** **109** **110**

Scheme 3.10: Synthetic scheme of the amine **110**.

To obtain the mono-substituted amino methyl pyridine **111**, 2-chloropyridine **108** was replaced by 2-pyridine carboxaldehyde **96** and the product was obtained by reductive amination using $NaBH(OAc)_3$ in methanol.[136] The selective methylation was done by reaction with iodomethane and Na_2CO_3 as a base, heating to reflux for 72 hours to yield the product **112**. Other stronger bases like diisopropylethylamine were tested to increase the rate of the reaction but the product was not obtained. The desired amine **113** could be obtained under

standard deprotection condition using TFA in CH_2Cl_2 (Scheme 3.11) but it was used without purification for the next step of the synthesis.

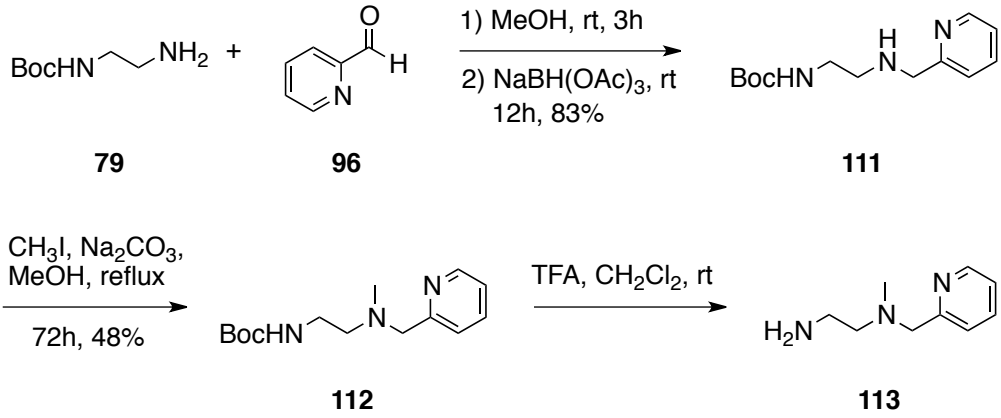

Scheme 3.11: Synthetic scheme of the amine **113**.

Both target compounds **EnDiPic** and **EnMePic** were obtained by the reaction of the amines **110** and **113** respectively, with the common precursor **94** (Scheme 3.12).

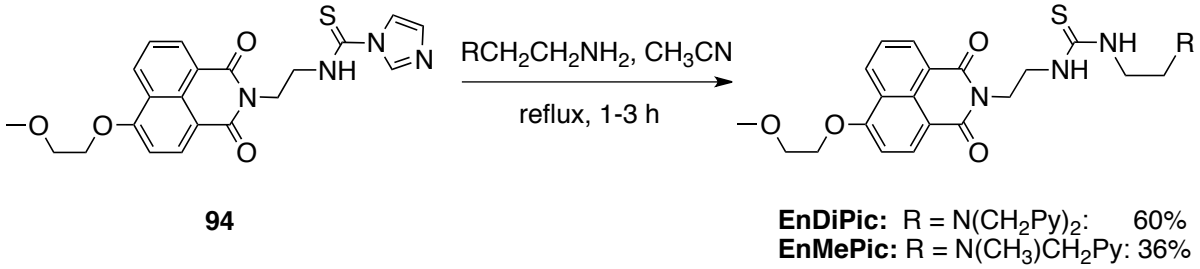

Scheme 3.12: Synthesis of the two compounds of the second series of chemosensors with an ethyl group spacer; Py = 2-pyridyl.

The obtained target had to be kept in the freezer to prevent slow decomposition. The observed decomposition process was leading to the formation of a guanidinium-based compound **114** through elimination of sulfur (Figure 3.35).

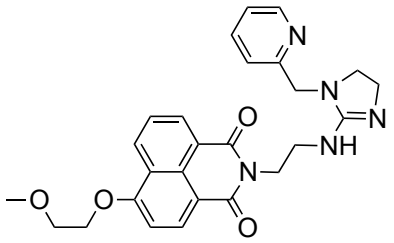

114

Figure 3.35: Guamidinium decomposition product **114**.

The synthesis of the two other amines needed to complete the second series was intended but the target compounds **EnHomoPic** and **EnNS2** were not obtained during this work. The synthesis of the amine needed to obtain **EnHomoPic**, was started with 2-pyridine ethanol **115**. The alcohol was transformed in a good leaving group by reaction with *p*-toluensulfonyl chloride in CH_2Cl_2 in presence of triethylamine as a base. The tosylated compound **116** was obtained in a good yield and has to be kept at 4°C in order to prevent decomposition.[143] In the next step, **116** reacts with the mono-protected *N*-Boc-1,2-diaminoethane **79**. Different reaction conditions have been tested for this step but no optimal conditions giving good yields were found. The reaction with Na_2CO_3 as a base in methanol did not show any reaction between the starting materials after 3 days. The use of potassium tert-butoxide in DMF leads to the formation of the desired product **117** in a very low yield (15%). The use of KF activated on Celite in acetonitrile improved the yield to 25 % but the conditions are still not optimal (Scheme 3.13).[144]

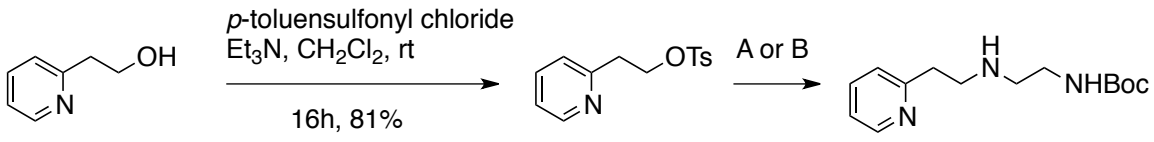

115 **116** **117**

Scheme 3.13: Synthetic scheme of the amine **117**. A) **79**, KO-*t*-Bu, DMF, 100°C, 24h, 15%. B) **79**, KF/Celite, acetonitrile, 72h, 25%.

The obtained compound could not lead to the formation of the target **EnHomoPic**, the deprotection step was yielding to an important lost of compound and the synthesis without isolation of the free amine was intended. Only the fluorophore starting material could be isolated from this reaction and no formation of new non-fluorescent product was observed.

Since the reaction was done in a very small scale, the amine could not be recovered. This reaction was intended many times but was always showing the same problem.

For the synthesis of the target **EnN2S**, the amine **118** has to be formed. To achieve this synthesis, 3,6-dithia-1,8-octanediol **119** was selected as the best starting material. This compound is commercially available, it is a white powder, it doesn't have a strong smell and this makes it easy to handle. To distinct pathways were explored as shown in the retrosynthetic scheme (Scheme 3.14). In the first one, a stepwise formation of the ring with the formation of an intermediate compound **120** was intended. In the second pathway, a direct cyclisation with two simultaneous reactions of the nitrogen of compound **79** was explored.

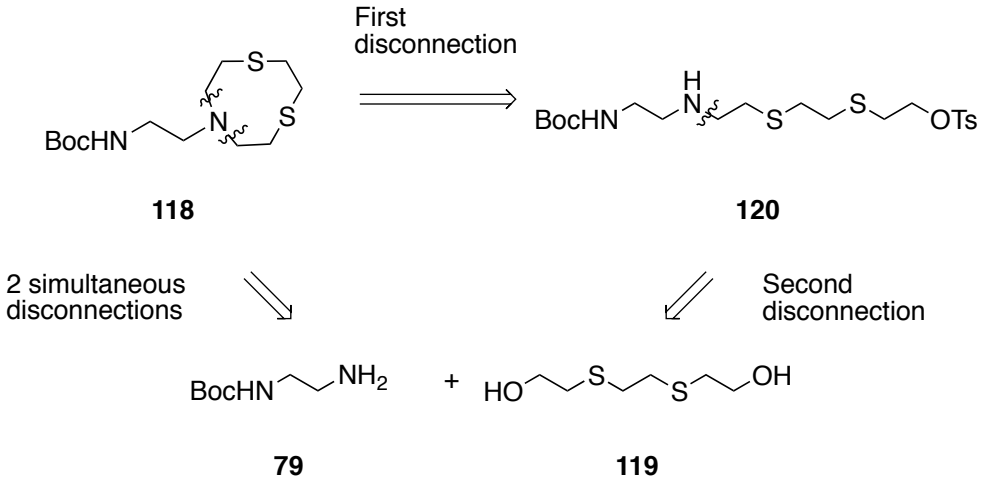

Scheme 3.14: Retrosynthetic scheme of the amine **118**.

The first reaction intended was the selective oxidation of the alcohol functional groups over the thioether in compound **119**, which is common to both reaction pathways. It has been previously reported using IBX as oxidative agent in ethylacetate.[145] The same paper reports that the addition of cetyltrimethylammonium bromide (CTAB) allows conversion to the sulfoxide without oxidation of the alcohol.

The use of IBX for the oxidation of various alcohols was previously report in our group, so 3,6-dithia-1,8-octanediol was oxidized following our procedure.[146] We observed that oxidation was occurring only at the alcohol and in a stepwise manner allowing the isolation of the mono- and di-oxidized compounds **121** and **122** respectively (Scheme 3.15).

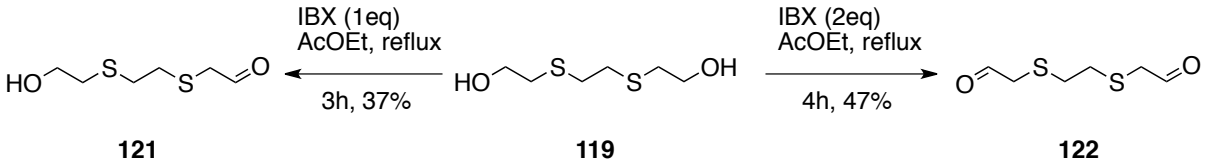

Scheme 3.15: Selective oxidation from 3,6-dithia-1,8-octanediol **119**.

In the stepwise procedure, the monoaldehyde compound **121** was elongated by reductive amination reaction with the mono Boc-protected 1,2-aminoethane **79**. The cyclisation of the obtained compound **123** was intended via different ways. An oxidation of the second alcohol with IBX followed by a second reductive amination did not lead to the desired product. The formation of the aldehyde of compound **124** could not be observed by NMR and the end product **118** could not be obtained.

Another possibility to achieve the ring closing was to activate the alcohol group via direct Mitsunobu reaction or tosylation. The Mitsunobu did not lead to the target compound but the tosylated compound **120** could be isolated and characterized. Many attempt to close the ring from the toslyated compound **120** have been done using various bases and various solvents in high dilution conditions. With Na_2CO_3 in MeOH and K_2CO_3 in DMF as well as with KF on activated Celite in acetonitrile, the starting material was recovered. The reaction with sodium *tert*-butoxide in DMF and sodium hydride in THF leads to complex mixtures and the desired compound **118** could not be identified. The only product, which could be isolated, is losing the Boc protection and supposedly a five-membered ring was formed with the nitrogen (Scheme 3.16).

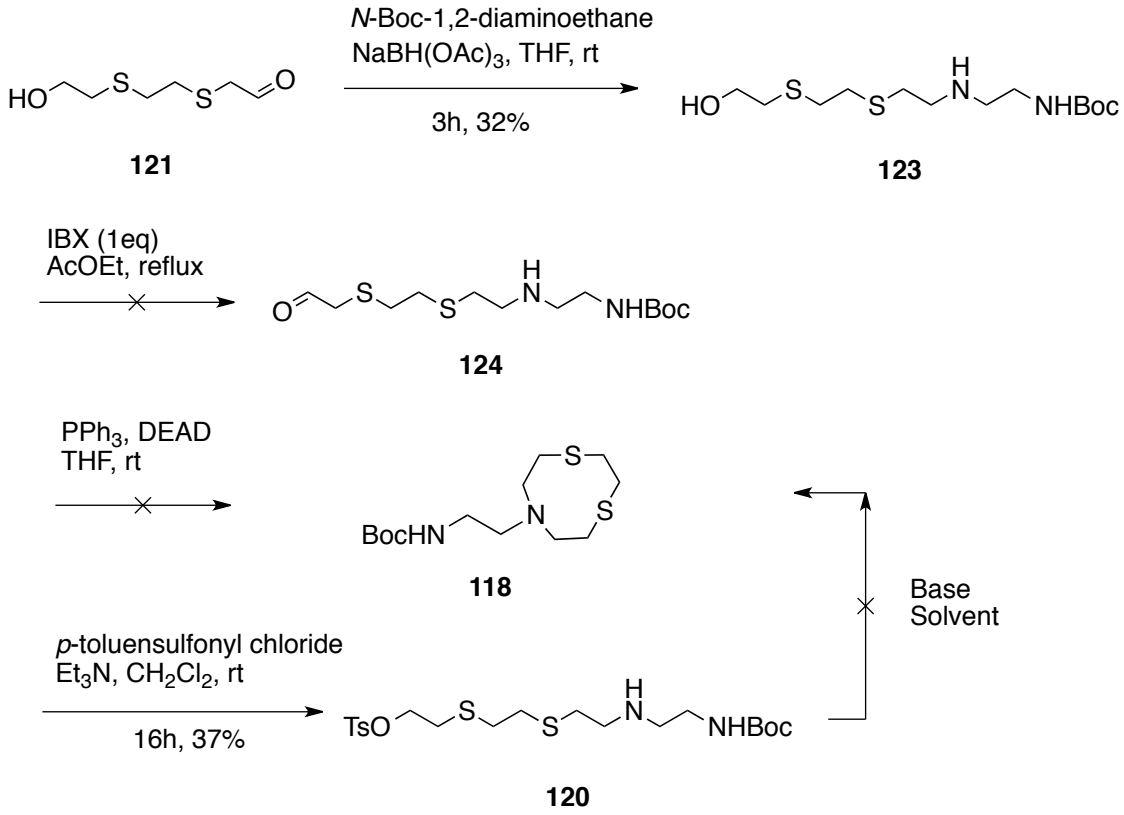

Scheme 3.16: Stepwise synthetic pathways of compound **118**.

In the case of the one step cyclization pathway, the reductive amination reaction between the dialdehyde **122** and the mono Boc-protected 1,2-aminoethane **79** was intended using $NaBH(OAc)_3$ as reductive agent. Many spots were obtained on TLC and the product could not be isolated. However the addition of acetic acid as reported by Painter for similar ring closing, leads to a TLC showing only one apolar spot and a large spot on the baseline.[147] The desired product **118** could be isolated in an extremely low yield and low degree of purity. After many trials of improving the reaction yield, no sufficient amount of the compound was obtained to continue the synthesis of the target chemosensor.

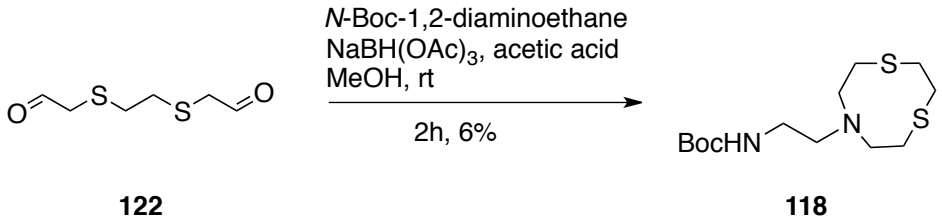

Scheme 3.17: Synthetic scheme of **118**.

3.4.3 Photophysical Properties of EnDiPic and EnMePic

The optical properties of **EnDiPic** and **EnMePic** were investigated in methanol. The UV-visible absorption spectrum and the fluorescence emission spectrum are similar to the spectrum of the compounds of the first series. A broad band with a maximum at 368 nm is observed in the absorption spectrum and a broad band with a maximum at 446 mn for the fluorescence emission (Table 3.8). Both compounds have relatively low quantum yields.

Table 3.8: Photophysical properties of **EnDiPic** and **EnMePic** in methanol.

Compounds	λ_{abs} / nm	ε^a/ $M^{-1}cm^{-1}$	λ_{em} / nm	ϕ_F [b]
EnDiPic	368	14500	446	0.04
EnMePic	368	13800	446	0.03

[a] For longest wavelength λ_{max} . [b] Relative to anthracene in methanol $\phi = 0.30$.[89]

3.4.4 Fluorescence Titrations of the Second Series of Targets with Metal Ions in Methanol

The response of the second series of chemosensors was investigated by addition of various metal ions in the same way as previously described for **PTU** and the first series. The cations used are again Li^+, Na^+, K^+, Mg^{2+}, Ca^{2+}, Ag^+, Zn^{2+}, Cd^{2+}, Hg^{2+} and Pb^{2+} and the anions are Cl^-, ClO_4^- or NO_3^-. The titrations were carried out with a 3µM solution of the fluorophore in methanol. The salts were added as 5 µl aliquots of solutions in methanol with an increasing concentration from $2 \cdot 10^{-4}$ M to 2 M depending on the response observed. In the same way as previously described (Chapter 3.3.4) all the titrations presented in this section are showing modifications in the fluorescence intensities but no modification of their absorbance properties. The dissociation constants were obtained in the same way as described for **PTU** using the program Prism6. The results are summarized in Table 3.9 for the binding affinities and in Figure 3.36 for the maximum of fluorescence enhancement.

Table 3.9: Apparent log K_d (M) for the titrations of **EnDiPic** and **EnMePic** in methanol with responsive metal ions.

Compounds	Zn^{2+}	Cd^{2+}	Hg^{2+}	Ag^{+}	Pb^{2+}
EnDiPic	-7.1	-7.0	-6.0	-5.7	-5.4
EnMePic	-5.0	-6.9	-5.9	-5.6	–

Titration at 3µM of the chemosensor in methanol. Entries marked ”-“ indicates an absence of fluorescence response

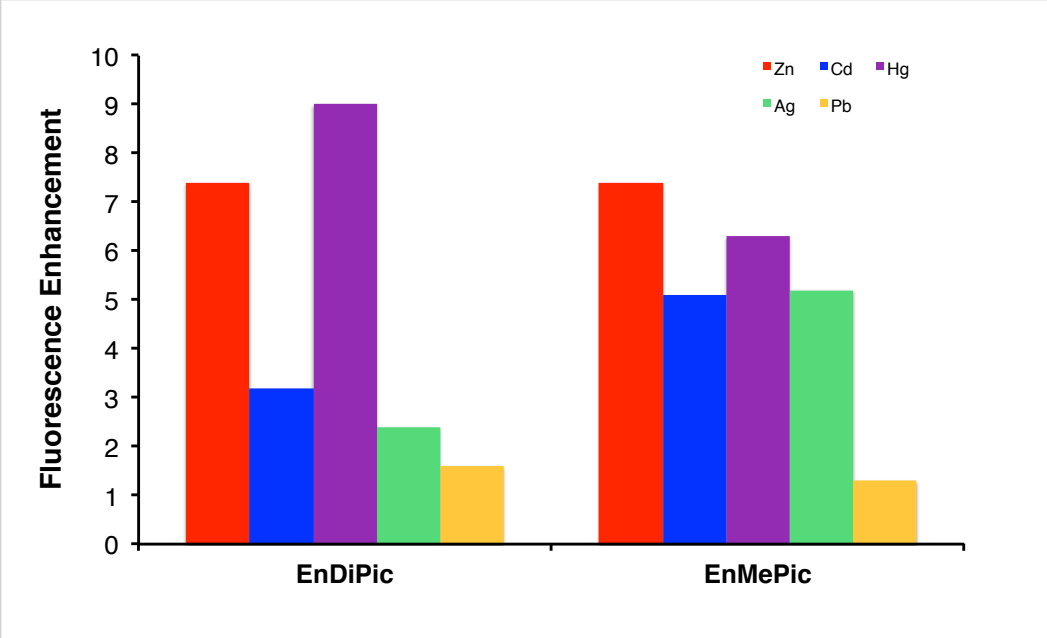

Figure 3.36: Metal-induced ratiometric fluorescence enhancement of **EnDiPic** and **EnMePic** in methanol.

Table 3.10: Values of $(I/I_0)_{max}$ and (ϕ_{max}) for titrations of **EnDiPic** and **EnMePic** in methanol.[a,b,c]

Compounds	Zn^{2+}	Cd^{2+}	Hg^{2+}	Ag^{+}	Pb^{2+}
EnDiPic	7.4 (0.30)	3.2 (0.13)	9 (0.36)	2.4 (0.10)	1.6 (0.06)
EnMePic	7.4 (0.22)	5.1 (0.15)	6.3 (0.19)	5.2 (0.16)	–

[a] Maximum observed I/I_0 as shown in Figure 3.36. [b] $\phi_{max} = \phi_{initial} \times (I/I_0)_{max}$. ϕ_{max} in parentheses. [c] Entries marked ‘–‘ indicate that saturated binding, and thus I/I_0(max), was not reached.

The compounds of the second series **EnDiPic** and **EnMePic** have high binding affinities for Hg^{2+}, Zn^{2+} and Cd^{2+}. Both compound show the same response to Hg^{2+}, Ag^{+} and Cd^{2+} but there is a significant difference observed for the affinity towards Zn^{2+}. In the case of the presence of the dipicolylamine moiety in **EnDiPic**, the affinity is higher due to the fact that dipicolylamine is a very high affinity ligand for Zn^{2+}. For compound **EnMePic** the observed dissociation constant was higher by about 10^2 relative to **EnDiPic**. This is explained by the fact that only a single pyridine ring is present (Figure 3.37).

In comparison with the first series of chemosensors, a high affinity response is also observed for other metal ions like Ag^{+} and Pb^{2+}.

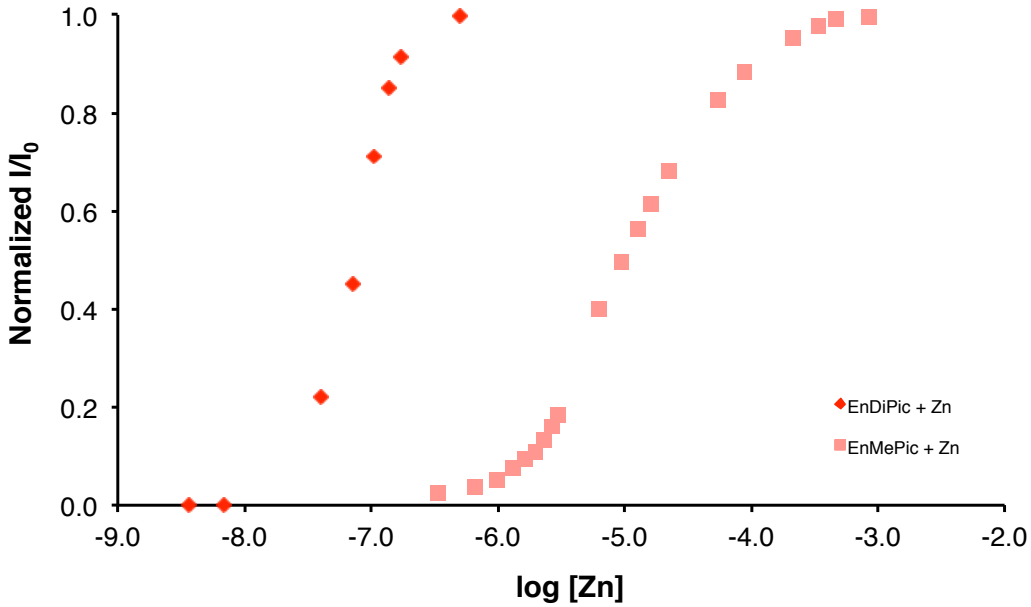

Figure 3.37: Ratiometric fluorescence enhancement for the titrations of **EnDiPic** and **EnMePic** with $ZnCl_2$ in methanol.

In general lower increase in the fluorescence emission was observed for this series in comparison with the series where the binding moiety was directly appended to the thiourea. This can be explained by the fact that the metal ion is coordinating to ligand, which is farther away from the sulfur and therefore the equilibrium between the fluorescent state of the chemosensor (with sulfur binding the metal) and the non-fluorescent state of the sensor lies more towards the non-emissive configuration.

No crystal structure could be obtained to study the binding mode of this ligand with the metal ions but the geometry of the complex is expected to be as drawn in Figure 3.38 for a Zn:**EnDiPic** complex. In this case the efficient binding of the DPA moiety is showing very high affinity for Zn^{2+} whereas **EnMePic** is showing reduced affinity.

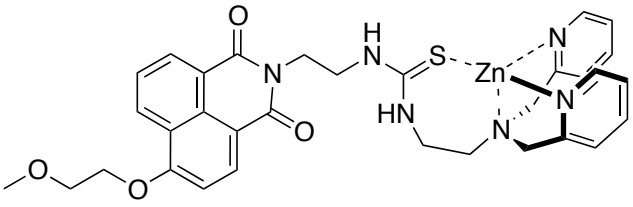

Figure 3.38: Proposed structure of the Zn:**EnDiPic** complex.

3.4.5 Fluorescence Titrations of the Second Series of Targets with Metal Ions in Water

The titrations done in Chapter 3.4.4 were repeated in a water:methanol 90:10 solvent mixture. In other to be able to make comparison with the titration of the first series the compounds of the second series **EnDiPic** and **EnMePic** in water were prepared again by serial dilution with water from a 30 μM solution of the chemosensors in methanol. The titrations were done in the same way as reported for the titrations the previous titrations and the dissociation constants were calculated for all the experiment showing response to the added salt using the program Prism6. The results are summarized in Table 3.11 for the binding affinities and in Figure 3.39 for the maximum of fluorescence enhancement.

Table 3.11: Apparent log K_d (M) for the titrations of **EnDiPic** and **EnMePic** in a mixture water:methanol 90:10 with responsive metal ions.

Compounds	Zn^{2+}	Cd^{2+}	Hg^{2+}
EnDiPic	-6.9	-7.2	-6.1
EnMePic	-2.4	-	-5.9

Titration at 3μM of the chemosensor in methanol. Entries marked ”-“ indicates an absence of fluorescence response

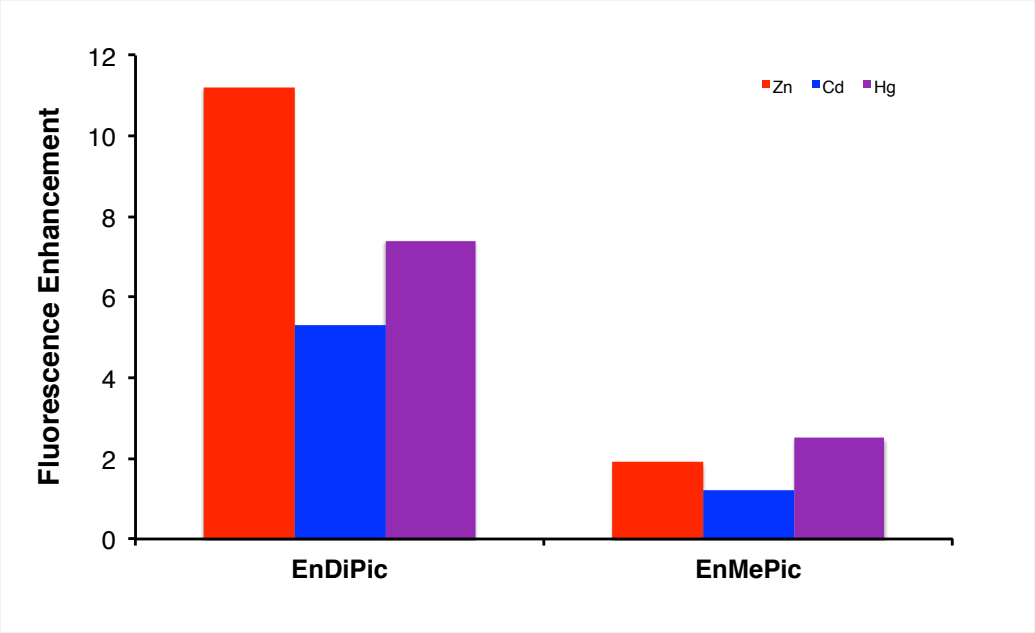

Figure 3.39: Metal-induced ratiometric fluorescence enhancement of **EnDiPic** and **EnMePic** in water:methanol 90:10.

Table 3.12: Values of $(I/I_0)_{max}$ and (ϕ_{max}) for titrations of **EnDiPic** and **EnMePic** in water:methanol 90:10.[a,b,c]

Compounds	Zn^{2+}	Cd^{2+}	Hg^{2+}
EnDiPic	11.2 (0.45)	5.3 (2.21)	7.4 (0.30)
EnMePic	1.9 (0.06)	-	2.5 (0.08)

[a] Maximum observed I/I_0 as shown in Figure 3.39. [b] $\phi_{max} = \phi_{initial} \times (I/I_0)_{max}$. ϕ_{max} in parentheses. [c] Entries marked '–' indicate that saturated binding, and thus I/I_0(max), was not reached.

For this series in a water:methanol 90:10 mixture an important difference was observed for the titrations with Zn^{2+}. As for **EnMePic** the dissociation constant K_d was increased from 10^2 M with the change to a water environment as observed for **MePic** (log K_d = 3.2 in methanol and 1.1 in aquous media for **MePic**:Zn), the dissociation constant of **EnDiPic** stays similar in both media (Figure 3.40).

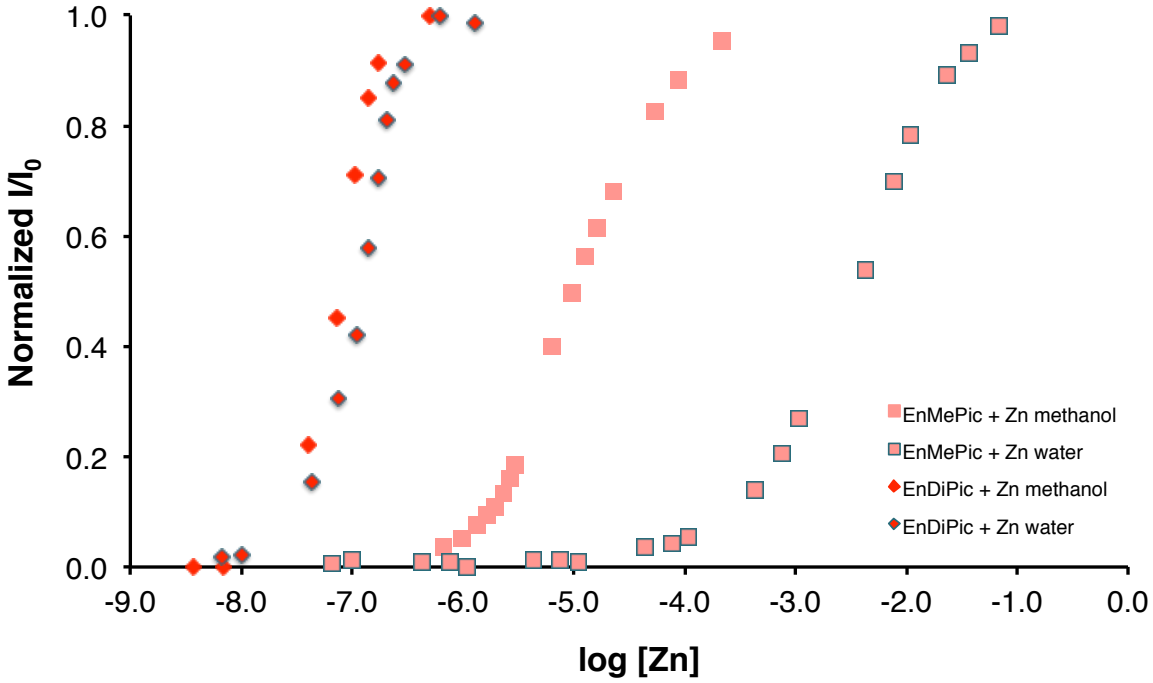

Figure 3.40: Comparison of the ratiometric fluorescence enhancement for the titrations of **DiPic** and **MePic** with $ZnCl_2$ in water:methanol 90:10 and in methanol.

The reversibility of the binding of **EnDiPic** with Cd^{2+} was tested in the aqueous media by the addition of dipicolylamine (DPA) as competitive ligand. After the addition of Cd^{2+} leading to the maximum of the fluorescence enhancement, DPA was added and a decrease of the fluorescence emission was observed. After further addition of Cd^{2+}, enhancement of the fluorescence emission was observed again showing the reversibility of the binding event between **EnDiPic** and Cd^{2+}. This result is indicating that the formed complex is stable and that no decomposition is occurring.

3.4.6 Fluorescence Titrations of the Second Series of Targets with Hydrochloric Acid in Methanol

The sensitivity to acid was tested in methanol for **EnDiPic** and **EnMePic**. A fluorescence enhancement could be observed after the addition of HCl with a dissociation constant corresponding to the pK_a of dipicolylamine in the case of **EnDiPic**. However, further protonation of the chemosensors are leading to decrease of the fluorescence emission (Figure 3.41). For **EnMePic** a similar increase after addition of HCl was observed with lower enhancement maximum. In this case further addition of HCl did not lead to decrease of the fluorescent emission.

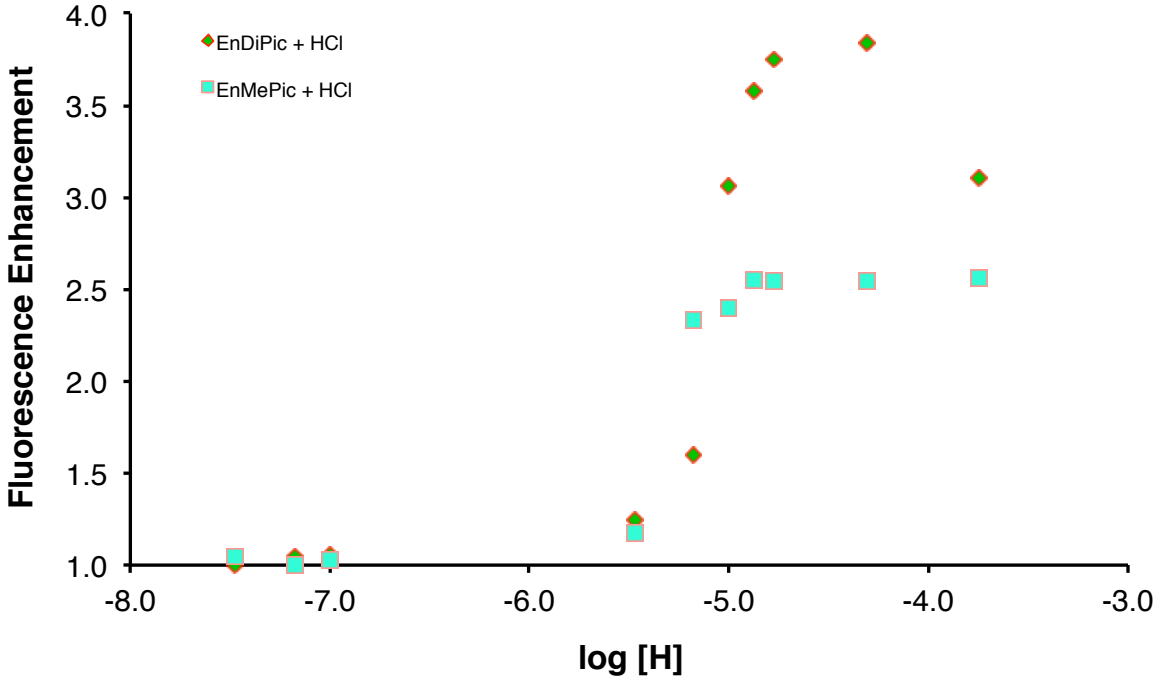

Figure 3.41: Fluorescence enhancement upon addition of HCl to the chemosensors of the second series **EnDiPic** and **EnMePic** in methanol.

This phenomena was previously observed and described as an OFF-ON-OFF sensor by de Silva.[148] The fluorescence decrease is due to the protonation of the pyridine. In fact the protonation is leading to significant changes in the reduction potential. For a non protonated pyridine ring the reduction potential is -2.62 eV and it changes to -1.25 eV when it is protonate. As a result, the LUMO state of the pyridine is now available for a non emissive electron transfer pathway and therefore the fluorescence is quenched.[149]

The compound studied by de Silva with its different protonation states is shown in Figure 3.42. Special feature of this compound is that after the protonation of the benzylic amine and subsequent recovery of the fluorescence, PET quenching occurs from the protonation of a pyridine. The fluorescence of this compound is increasing with the addition of Zn^{2+} and the observed log K_d is -5.3. A 1:1 complex is formed. The quantum yield is 0.01 and a 77-fold increase of the fluorescence enhancement is observed.

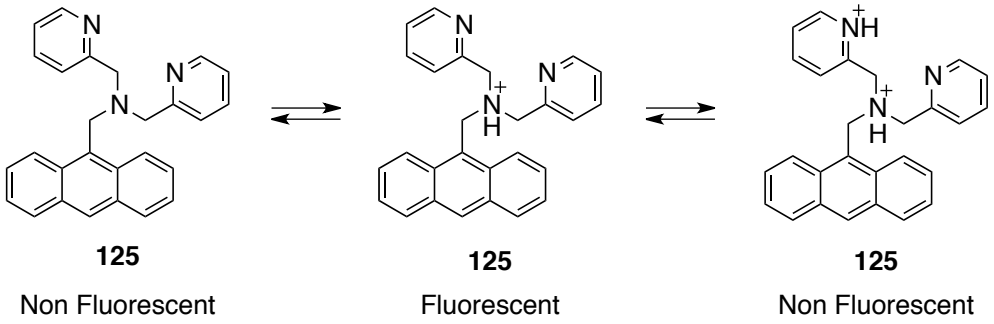

Figure 3.42: Fluorescent state upon protonation of di-2-picolylamine based chemosensor from de Silva.[148]

The same behavior was observed the compound shown in Figure 3.43 containing one more nitrogen atom and an ethyl spacer.[150] After determination of the pKa for all four nitrogen atoms, it was shown that the most fluorescent state is the LH_2^{2+} state, when the benzylic nitrogen atom as well as the tertiary nitrogen atom are protonated but not the pyridine's nitrogen atoms. When the compound is protonated further, the pyridinium ions formed are capable of quenching the fluorescence.

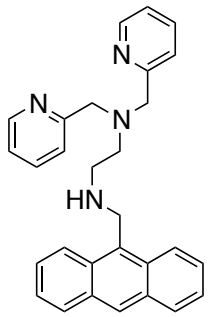

126

Figure 3.43: Fluorescent chemosensor studied by Fabbrizzi.[150]

3.5 Comparisons between the First and the Second Series of Targets and Conclusions

3.5.1 Comparison of the Response to Zn^{2+}

The first target of the thiourea-naphthalimide construct **PTU** was showing low affinity response to Zn^{2+} with a log K_d = -1.2. The addition of pyridine as a binding moiety in the compounds **DiPic** and **MePic** leads to an increase of the complex stability with a log K_d = -3.0. However the expected effect of two pyridines vs. one pyridine was not observed. A crystal structure of a complex of a ligand related to **DiPic** with Zn^{2+} is proving that only one pyridine is involved in the coordination of **DiPic** with Zn^{2+} (Figure 3.44).

A further change in the structure by the introduction of an ethyl bridge between the thiourea and the additional coordination moiety is leading to better ligand conformation for the coordination event. The second series of targets are tetradentate ligand for the coordination of metals. The binding affinity from **EnMePic** (log K_d = -5.0) is higher than for its analogue **MePic** (log K_d = -3.2). In this case the effect of the second pyridine was marked, and **EnDiPic** (log K_d = -7.1) shows an increased affinity for Zn^{2+} in comparison with **EnMePic** (Figure 3.44).

The presence of the ethyl bridge has also an effect on the maximum of the fluorescence enhancement. An approximately 2-fold lowering of the maximum fluorescence intensity was observed in methanol in the case of **EnDiPic** and **EnMePic** in comparison with **DiPic** and **MePic** respectively. This could be due to the fact that the metal ion is bound more tightly with the nitrogen atoms and is affecting less the electronic environment of the sulfur from the thiourea (Figure 3.46).

Our chemosensors also show a response to metal ion in a water:methanol 90:10 solvent mixture. This mixture was chosen for solubility and practical reason. The solutions of the chemosensor were prepared with water by serial dilution from a 30 μM solution of the compound in methanol. The response observed is showing lower affinity in aqueous media than in methanol (for **MePic** log K_d = -3.2 in methanol and log K_d = -1.1 in water:methanol 90:10) with an at least 2-fold decrease of the maximum fluorescence enhancement except for **EnDiPic**. This can be explained by the fact that water is a better competing ligand for the thiourea than methanol. However a high affinity and fluorescence enhancement from **EnDiPic** for Zn^{2+} in water was observed. This is an interesting result since this affinity is high

enough and may have practical use for the detection of Zn^{2+}. Moreover the apparent K_d measured in this case is at the lower limit of our experimental conditions and therefore the binding event could be even tighter (Figure 3.45 and Figure 3.46).

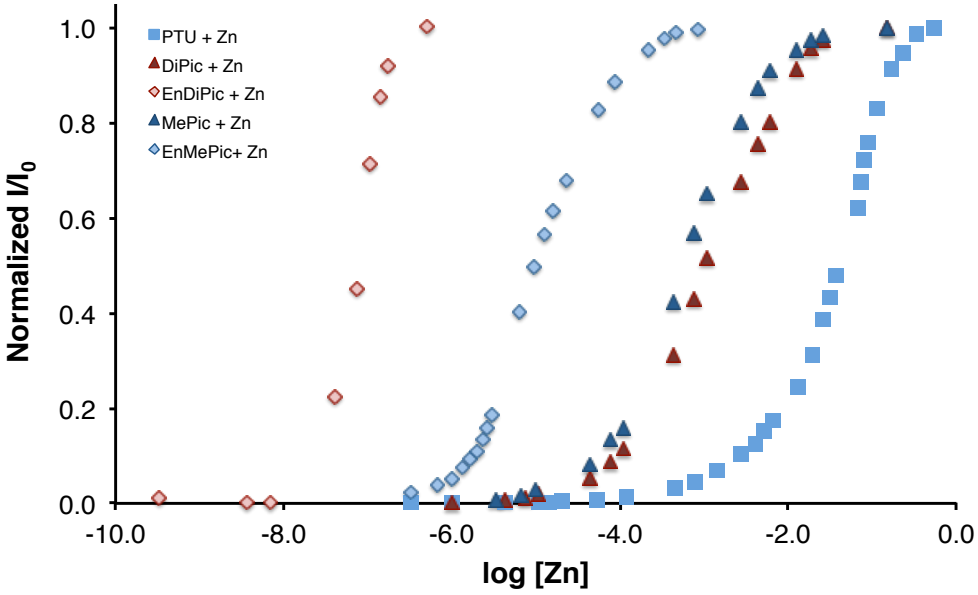

Figure 3.44: Comparison of the response of **PTU**, **DiPic**, **MePic**, **EnDiPic** and **EnMePic** to Zn^{2+} in methanol.

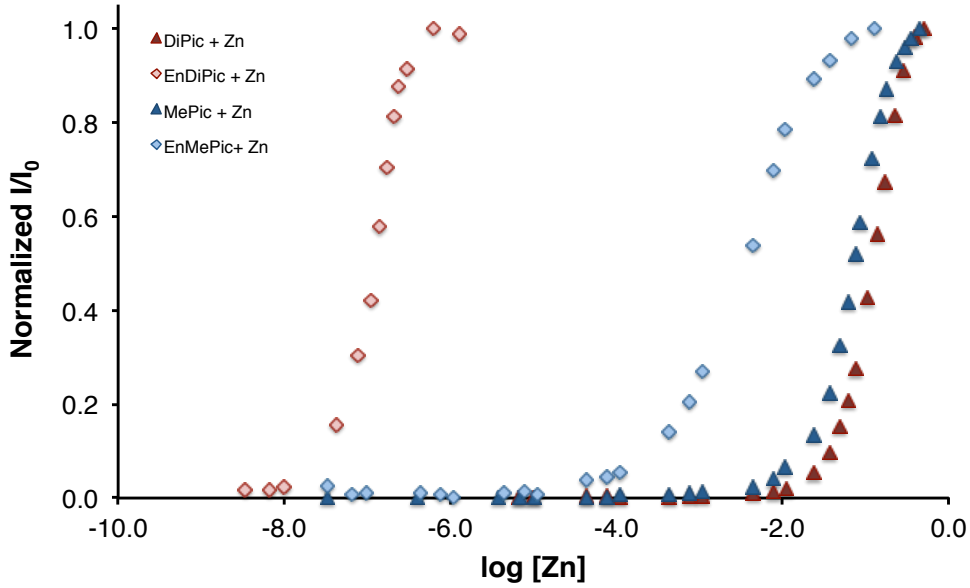

Figure 3.45: Comparison of the response of **PTU**, **DiPic**, **MePic**, **EnDiPic** and **EnMePic** to Zn^{2+} in water:methanol 90:10.

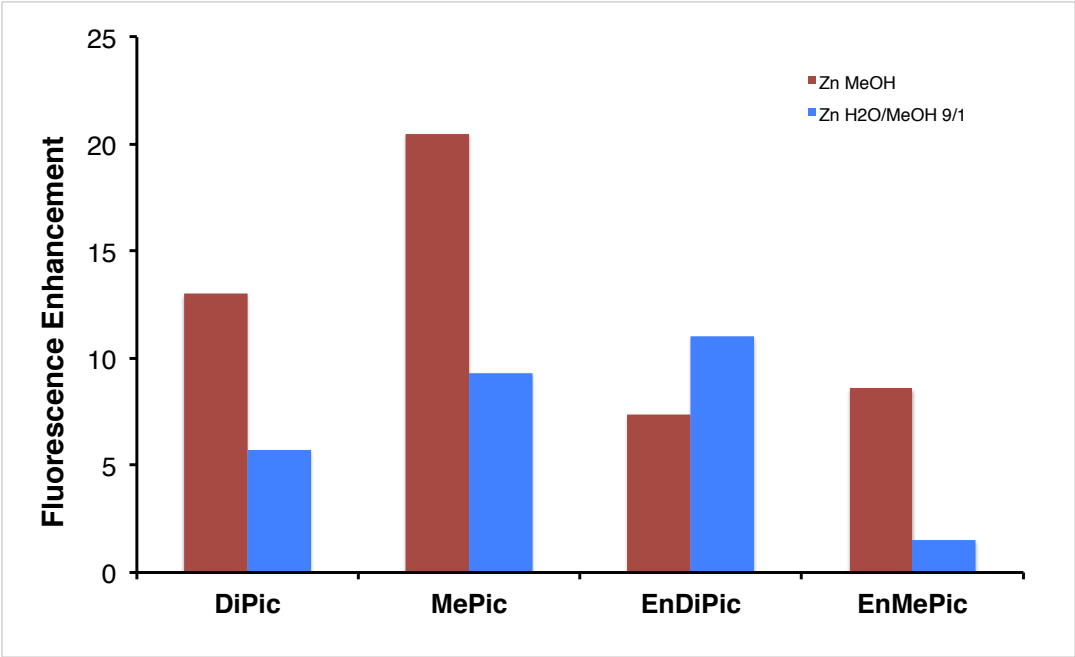

Figure 3.46: Comparison of the fluorescence enhancement of **DiPic**, **MePic**, **EnDiPic** and **EnMePic** in methanol (red) and in a water:methanol 90:10 mixture (blue).

3.5.2 Comparison of the Response to Hg^{2+}

The responses of all our chemosensors obtained in the first and in the second series are showing a similar response to the addition of Hg^{2+}, an approximated log K_d = -6.0 and high maximum fluorescence enhancement. Those results indicate that the interaction of the thiourea with Hg^{2+} is directed efficiently by the S-Hg coordination due to the efficient soft base to soft acid type interaction (Figure 3.47). The additional binding moiety is influencing the response to Hg^{2+} since PTU was not showing fluorescence enhancement towards the addition of Hg^{2+}. However, the apparent response of the different chemosensors with different binding moiety to the addition Hg^{2+} cannot be differentiated in our experimental conditions. Differences between them may appear if the experiment could be done in lower concentrations of the fluorophore.

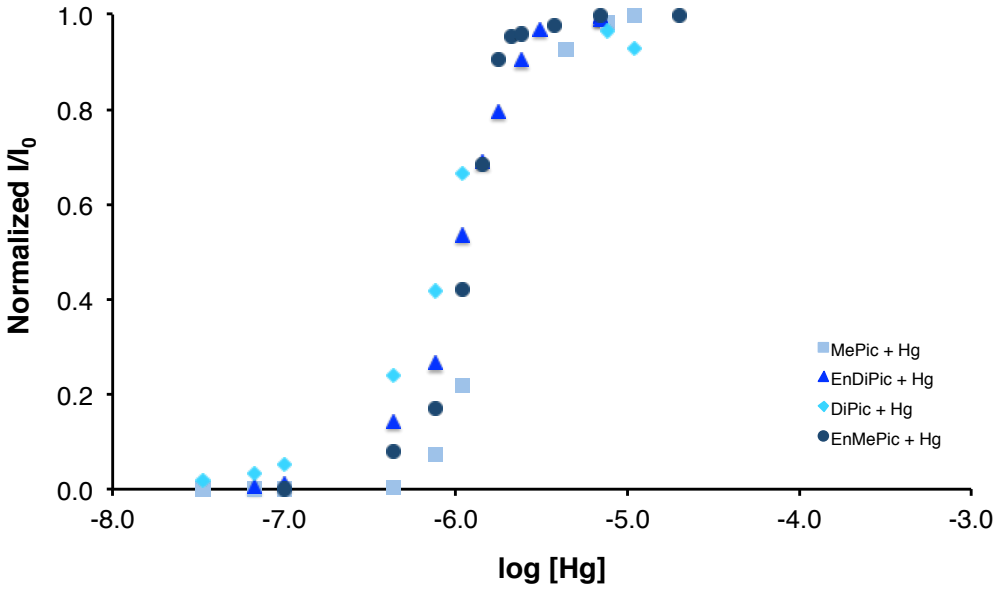

Figure 3.47: Comparison of the response of **PTU**, **DiPic**, **MePic**, **EnDiPic** and **EnMePic** to Hg^{2+} in methanol.

3.5.3 Conclusions

The chemosensors obtained in this chapter are showing that thiourea can be modulated to show significant differences in the fluorescence response to the addition of metal ions. At least one of the sensor is showing a very high affinity for Zn^{2+} in aqueous solution and could have practical use. The binding affinity towards Hg^{2+} is as well promising. The apparent binding affinities are very high and perspective of using them with a fluorophore with higher absorbance at lower concentration open the possibilities of practical use. This is significant in that most known metal-responsive chemosensors rely on binding to a nitrogen atom, and the coordination chemistry of nitrogen has dominated fluorescent chemosensor development to date. The addition of sulfur to the group of viable reporting heteroatoms is significant expansion, and will have an impact beyond the present work.

It is expected that further variation of binding domain and fluorophore will lead to the development of additional practical probes for metal ion detection and visualization. To this end the exploration of different binding domains as recognition elements will be presented in Chapter 4.

Chapter 4

Variations of the Structure of the Thiourea-Based Chemosensors

4.1 Introduction

In other to modulate to response of the thiourea based chemosensor system, we have tried to introduce various other modifications and they will be summarized in this Chapter. In the first part, crown ether binding moieties were introduced in order to bind selectively different metal ions like alkali metal ions. Then a following section will resume the efforts towards the synthesis of an analogue containing ester functionality.

4.2 Crown Ether Containing Binding Moiety

4.2.1 Introduction

The crown ethers are a large family of marocyclic compounds with a variety of size and coordinating atoms and typically ethyl bridges in ring systems. This kind of ligand has been discovered by Charles Pedersen and is at the origin of his Nobel Prize in 1987. They are very effective ligand due to the chelating effect. The selectivity of cation complexation is due to the size complementarity between the cation and the host size, to electronic complementarity, to the solvent and to the enthalpic and entropic contribution of the cation-host interaction.[151] The most widely used representative of the crow ether family is the 18C6 compound known as excellent ligand for the coordination of potassium ions and it is used in organic synthesis in order to improve the basic effect of various potassium counter ions. Modulating the size and ligating atoms of the crown ether allow complexation of various metal ions as summarized in a very long review illustrating the numerous possibilities of this kind of compound.[152-154] In the specific field of fluorescent chemosensors, various crown ether binding domains have been involved as well in order to target various metal ions.[155] Alkali metal ions as well as alkaline-earth metal ions are detected using various crown ether containing oxygen as heteroatom coupled to various fluorophores.[156-158] By inserting other

heteroatom like nitrogen or sulfur in the system, different metal ions like Ag^{+} or Hg^{2+} are also going to interact with crown ether moieties.[159-161] In general tuning of the response to various metal ions should be possible with the condition that the metal also interacts with our thiourea-reporting element.[162]

The targets designed in this section are containing a 12C4 crown ether for **En12C4** and a 15C5 crown ether for **En15C5** containing both one nitrogen allowing the link to the fluorophore system developed in Chapter 3 (Figure 4.1). The link using an ethyl bridge will be kept and the targeted metal ions are going to be Na^{+}, K^{+} or Li^{+} but as well the now standard response to Zn^{2+} or Hg^{2+} are expected.

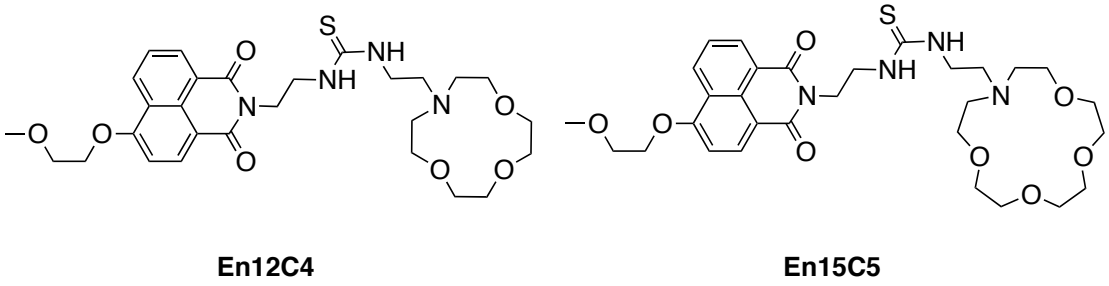

En12C4 **En15C5**

Figure 4.1: Structures of the target compounds containing crown ether binding moieties.

4.2.2 Synthesis of the Target Compounds En12C4 and En15C5

As described in Chapter 3, the synthesis of the target compounds started from the mono imidazole thiourea **94** with the corresponding free amines, which can be synthesized from the commercially available 1-aza-12-crown-4 **127** and 1-aza-15-crown-4 **131** amines respectively.

In the first step of this synthesis for both compounds, the starting materials were first alkylated with chloroacetonitrile to form the corresponding nitriles **128** and **132** respectively (Scheme 4.1 and Scheme 4.2).[144]

The next step was the hydrogenation of the cyano group using ethanol as solvent and Raney Nickel as catalyst under molecular hydrogen pressure, which proved to be a problematic step.

In the first approach following the pathway A from Scheme 4.1, the direct synthesis of the free amine **130** was intended, but the formation of the dimeric form of the desired

compound was observed as side product and the desired compound could not be purified. In order to avoid this problem, pathway B with the formation of the Boc protected amine **129** as intermediate was explored (Scheme 4.1).

The addition of Boc_2O to the reaction mixture had the expected effect and no dimer was obtained but another side reaction was observed. Due to the presence of traces of aldehyde impurity in the solvent, reductive amination took place, leading to an undesired ethylated side product. The presence of the ethyl group could be determined my mass spectrometry. This compound was very difficult to purify by column chromatography and since it was oily, it could not be recrystallized.

Therefore different reaction conditions were tested for pathway B in order to avoid the formation of this side product. The reaction was carried out in freshly distilled ethanol leading to the formation of less side product but the purity was not considered as sufficient for the next step. Then THF was used as a solvent and the same side product was observed. The reaction in methanol was tested and a peak in the mass spectra corresponding to the addition of a methyl group was observed. This result is the confirmation of the hypothesis that the reaction with the solvent was taking place. Finally, to avoid completely this side reaction, *tert*-butanol was selected as solvent and this reaction leads to the desired product **129** in 20 % yield. After deprotection, the free amine **130** could finally be obtained in a good purity.

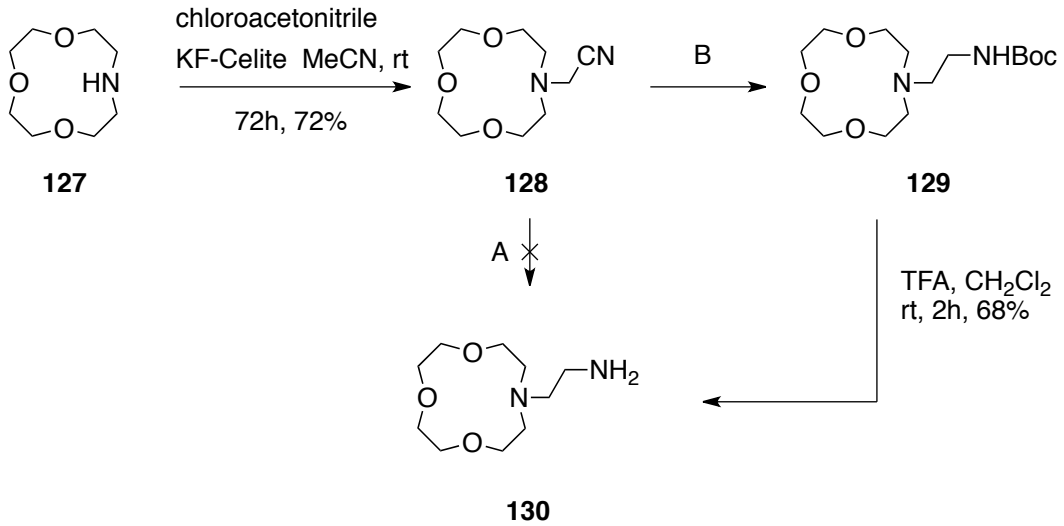

Scheme 4.1: Synthetic scheme of the amine **130**. A) Raney Nickel, H_2, ethanol. B) Raney Nickel, H_2, Boc_2O, *tert*-butanol, 14 h, 20%.

The reaction conditions for the synthesis of the amine **129** were used for the synthesis of the boc protected amine needed for the larger crown ether **133**. The free amine **134** was obtained in a good purity after deprotection under standard conditions (Scheme 4.2).

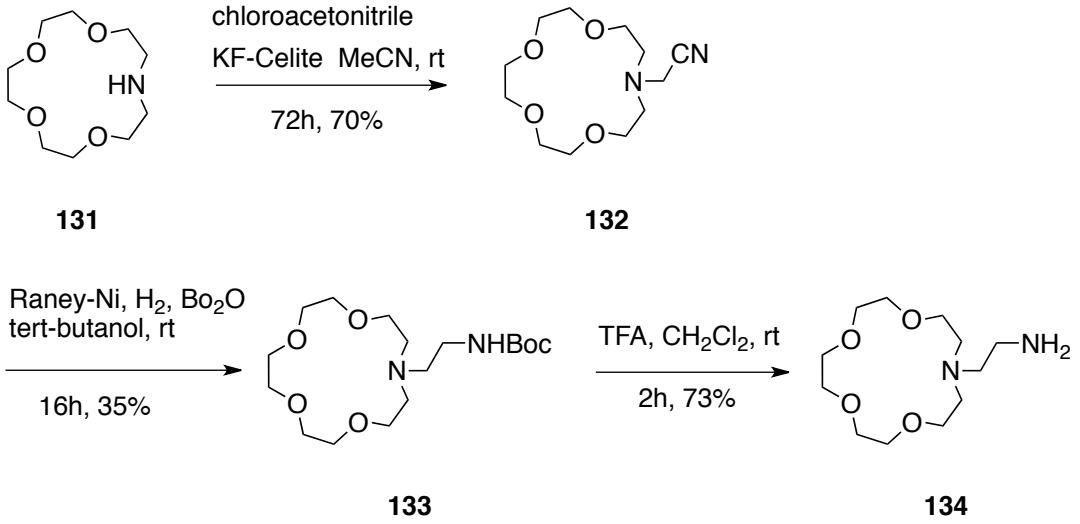

Scheme 4.2: Synthetic scheme of the amine **134**.

Target compounds **En12C4** and **En15C5** were obtained by the reaction of the amines **130** and **134** respectively, with the common precursor **94**, the thiourea bearing an imidazole as previously described in Chapter 3.3.2 (Scheme 4.3).

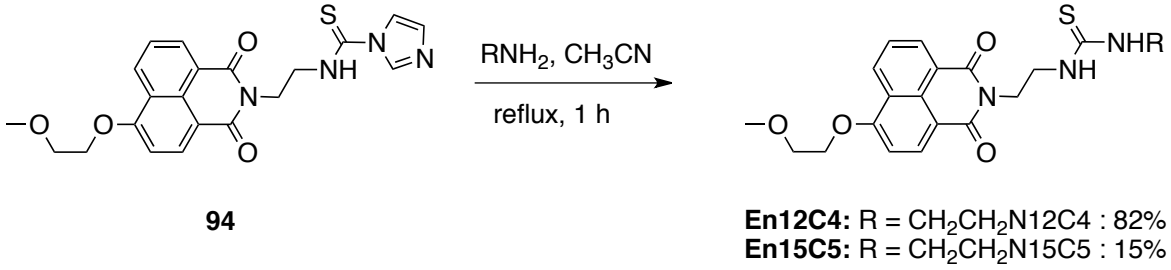

Scheme 4.3: Synthesis of the target compounds bearing crown ether as additional binding moieties.

4.2.3 Photophysical Properties of En12C4 and En15C5

The optical properties of **En12C4** and **En15C5** were investigated in methanol. The UV-visible absorption spectrum is characterized by a broad band with a maximum at 368 nm. The fluorescence emission spectrum is characterized by broad band with a maximum at 446 mn. All the compounds are showing relatively low quantum yield (Table 4.1). The

photophysical properties of those compounds are very similar to the ones of all the thiourea based compounds presented in Chapter 3.

Table 4.1: Photophysical properties of **En12C4** and **En15C5** in methanol.

Compounds	λ_{abs} / nm	ε^{a}/ $M^{-1}cm^{-1}$	λ_{em} / nm	ϕ_F [b]
En12C4	368	12600	446	0.03
En15C5	368	13500	446	0.02

[a] For longest wavelength λ_{max} . [b] Relative to anthracene in methanol $\phi = 0.30$.[89]

4.2.4 Fluorescence Titrations of En12C4 and En15C5 with Metal Ions in Methanol

The response of the second series of chemosensors was investigated by addition of various metal ions in the same way as previously described for **PTU** and for the first series. The cations used are again Li^+, Na^+, K^+, Mg^{2+}, Ca^{2+}, Ag^+, Zn^{2+}, Cd^{2+}, Hg^{2+} and Pb^{2+} and the anions are Cl^-, ClO_4^- or NO_3^-. The titrations were carried out in a 3μM solution of the fluorophore in methanol. The salts were added as 5 μl aliquots of solutions in methanol with an increasing concentration from $2 \cdot 10^{-4}$ M to 2 M depending on the response observed. In the same way as described in Chapter 3.2.3, all the titrations presented in this section are showing modifications in the fluorescence intensities but no modification of their absorbance properties. The dissociation constants were obtained in the same way as described for **PTU** using the program Prism6. The results are summarized in Table 4.2 for the binding affinities and Figure 4.2 for the maximum of the fluorescence enhancement.

Table 4.2: Apparent log K_d (M) for the titrations of **En12C4** and **En15C5** in methanol with responsive metal ions.

Compounds	Zn^{2+}	Cd^{2+}	Hg^{2+}	Ag^+	Pb^{2+}	Mg^{2+}	Na^+
En12C4	[a]	-3.5	-6.0	-6.0	-4.0	-3.7	–
En15C5	[a]	[a]	-6.3	[a]	–	–	–

Titration at 3μM of the chemosensor in methanol. Entries marked ”-“ indicates an absence of fluorescence response. Entries marked [a] indicates that the observed increase was not sigmoidal and log K_d could not be determined.

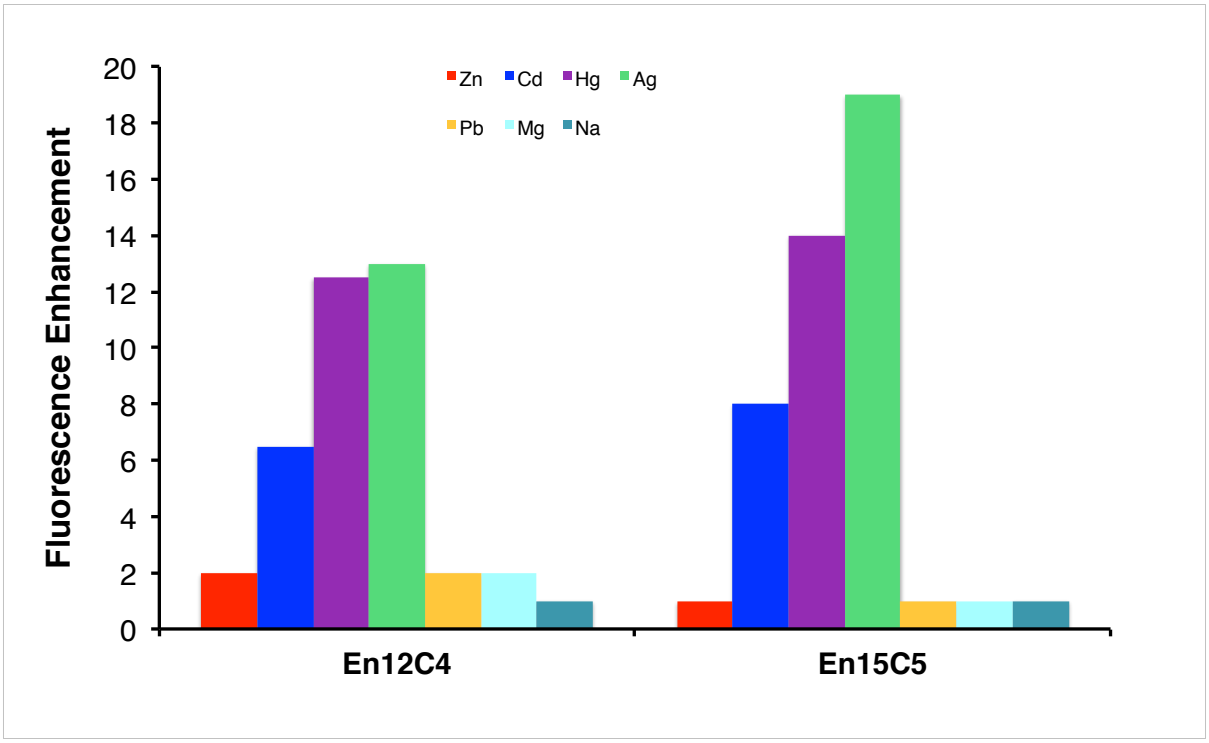

Figure 4.2: Metal-induced ratiometric fluorescence enhancement of **En12C4** and **En15C5** in methanol.

For both new chemosensors **En12C4** and **En15C5**, a response to Hg^{2+} was observed with similar affinity (**Figure 4.3**) and maximum of the fluorescence enhancement as observed for both series thiourea based chemosensors of Chapter 3. A high affinity response was also observed for Ag^{+} with 14 to 18 folds increase of the fluorescence emission.

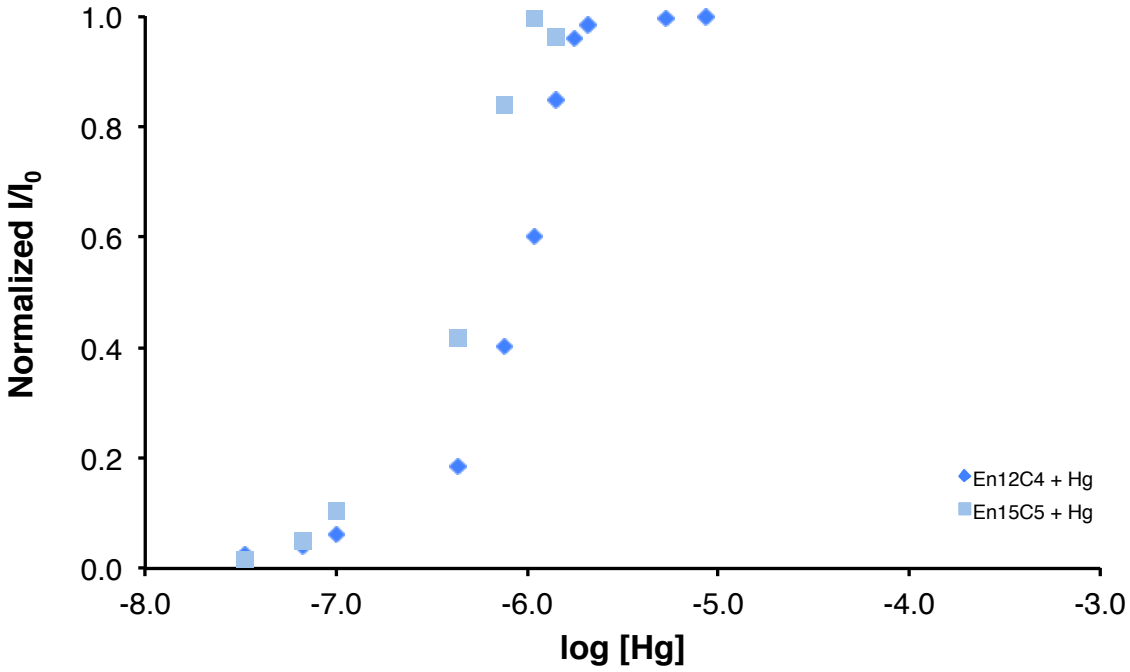

Figure 4.3: Ratiometric fluorescence enhancement for the titrations of **En12C4** and **En15C5** with $HgCl_2$ in methanol.

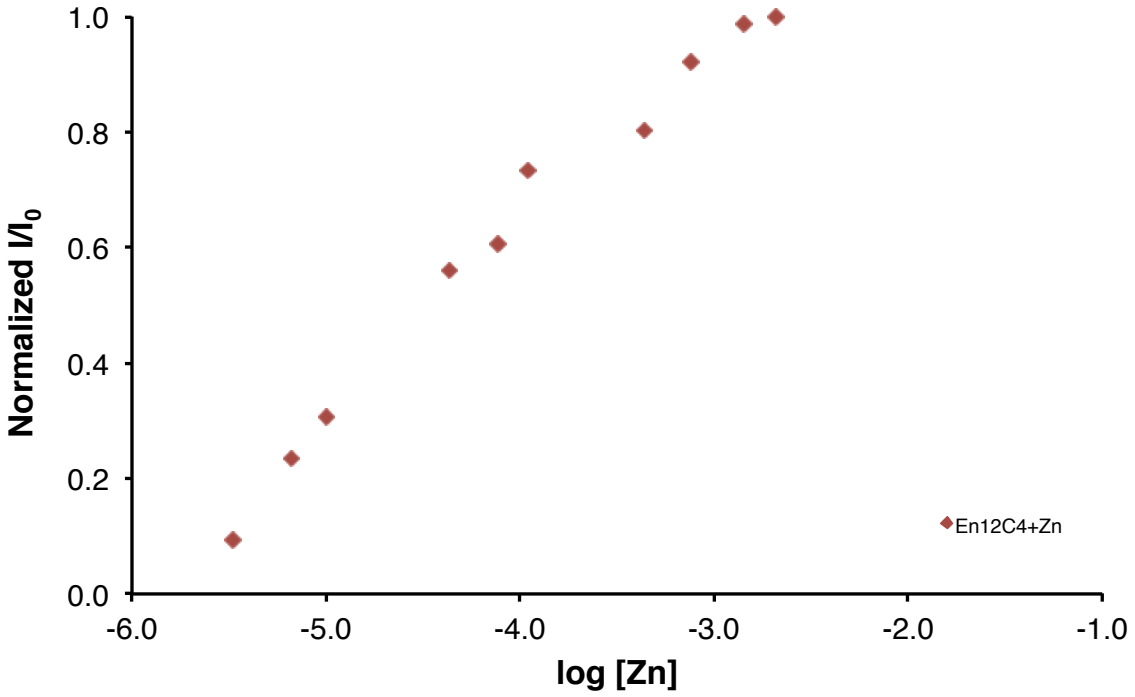

Figure 4.4: Ratiometric fluorescence enhancement for the titrations of **En12C4** with $ZnCl_2$ in methanol.

For the response to Zn^{2+}, a low regular increase of the fluorescence emission was observed while increasing the concentration of the added solution of metal ion until a maximum of 2 times increase of the fluorescence emission. For both compounds, no sigmoidal curve was obtained from the plot of the normalized integrated fluorescence as function of the logarithm of the metal ion concentration (Figure 4.4). The response to Cd^{2+} is interesting because the maximum of the fluorescence enhancement was higher than for Zn^{2+}. This was not observed with the previous series and as discussed in the previous chapter, the effect of Zn^{2+} complexation was generally observed to be higher than for Cd^{2+}, leading to higher increase of the fluorescence upon addition of Zn^{2+}. A possible explanation for this observation is that when Zn^{2+} is forming a complex with the crown ether moiety, it fits better inside the ring than Cd^{2+} due to the size (ionic radii for Zn^{2+}: 83 pm; for Cd^{2+}: 103 pm)[163] and therefore Zn^{2+} is less involved in coordination with the sulfur than Cd^{2+}, leading to less disruption of the PET process in the case of Zn^{2+}.

According to the known affinity of 12C4 and 15C5 crown ether with alkali and earth-alkali metal ions, a response to those classes of compound was expected. However, compound **En12C4** is showing less than 2 times increase of fluorescence emission upon addition of metal ions such as Pb^{2+} and Mg^{2+} and no response to Na^{+} or K^{+}. In the case of compound **En15C5** no response to this category of metal ions was observed.

The fact that no fluorescence increase is observed after the addition of alkali and earth-alkali metal ions does not necessarily means that there is no interaction between this class of elements and the chemosensor. A possible explanation of this observation is that the metal ion is complexed by the crown ether but doesn't interact with the sulfur moiety responsible of PET quenching and therefore is not able of restoring the fluorescence emission (Scheme 4.4). As alkali metal ions are hard cations, it is reasonable that they do not interact with a soft base like sulfur, in accord with the hard-soft interaction principle.

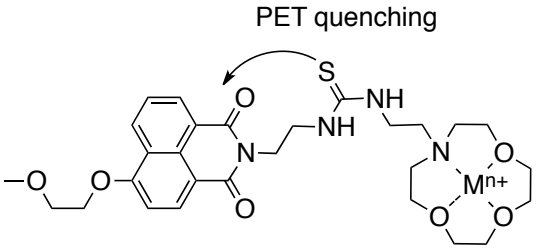

Scheme 4.4: Possible explanation for the absence of fluorescence enhancement upon addition of crown ether complexing metal ions.

4.2.5 Fluorescence Titrations of En12C4 and En15C5 with Metal Ions in Water

The titrations done in Chapter 4.2.4 were repeated in a water:methanol 90:10 solvent mixture. In other to be able to make comparison with the titration of the previous Chapter (3.3.5 and 3.4.5), the compounds **En12C4** and **En15C5** in water were prepared again by serial dilution with water from a 30 μM solution of the chemosensors in methanol. The titrations were done in the same way as reported for the titrations the previous titrations and the dissociation constants were calculated for all the experiment showing response to the added salt using the program Prism6. The results are summarized in Table 4.3 for the binding affinities and in Figure 4.5 for the maximum of the fluorescence enhancement.

Table 4.3: Apparent log K_d (M) for the titrations of **En12C4** and **En15C5** in a mixture water:methanol 90:10 with responsive metal ions.

Compounds	Zn^{2+}	Cd^{2+}	Hg^{2+}	Ag^{+}	Pb^{2+}	Mg^{2+}	Na^{+}
En12C4	[a]	[a]	-5.8	–	–	–	–
En15C5	[a]	[a]	-5.6	–	–	–	–

Titration at 3μM of the chemosensor in water:methanol 90:10. Entries marked ”-“ indicates an absence of fluorescence response. Entries marked [a] indicates that the observed increase was not sigmoidal and log K_d could not be determined.

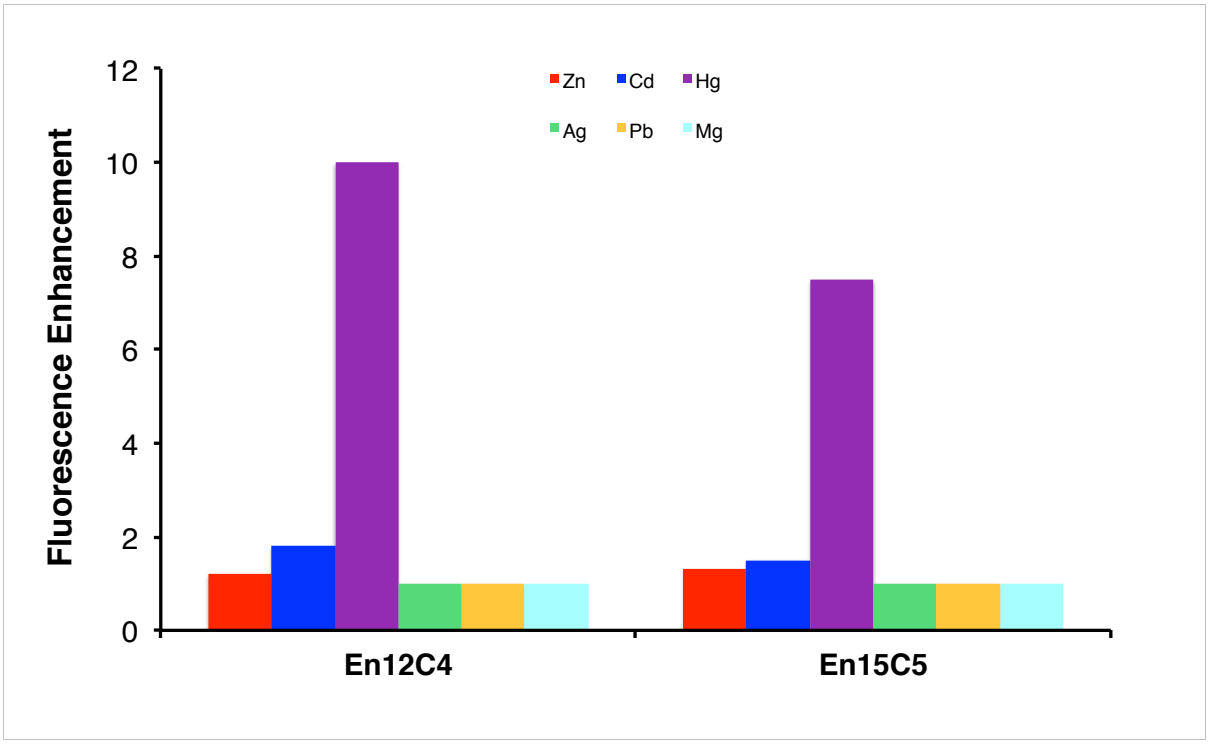

Figure 4.5: Metal-induced ratiometric fluorescence enhancement of **En12C4** and **En15C5** in water:methanol 90:10.

The same effect of water as for the series of thiourea chemosensors from Chapter 3 was observed for **En12C4** and **En15C5**. A similar response to Hg^{2+} is the only observed response for those compounds in water and therefore they can be defined as Hg^{2+} specific probes. The response to other metal ions was already very low in pure methanol and is reduced to no response in most of the cases.

4.2.6 Conclusions

The combination of sulfur as soft donor for the fluorescence reporting element with a crown ether as hard donor as additional binding moieties did not lead to the sensing of hard metal ions. However the obtained sensors are selective for the detection of Hg^{2+} in an aqueous media. With those results, it seems that the use of thiourea will not lead to the response for alkali metal ions. However as outlook of this chapter, the crown ether moiety could be introduced directly to incorporate the nitrogen atom of the crown ether to the thiourea or with more geometrical restriction directing the crown ether towards the sulfur atom. This could bring the two moieties closer together and maybe could lead to response and fluorescence enhancement as response to alkali metal ions.

4.3 Carboxyl Group Containing Binding Moiety

4.3.1 Introduction

Another possible binding moiety to add to our chemosensor system is a carbonyl group. This moiety is present in the well-known ethylenediamine tetraacetate (EDTA) ligand which is a very powerful ligand through its chelating ability to Ca^{2+} and earth-alkali metal ions. As analogy with the **Fura** series from Tsien (Chapter 1.5.2), the targets designed in this section are containing a diacetate moiety. In the first targets **135** and **136**, the binding moiety is directly appended to the thiourea moiety and in target **137** the ethyl bridge is introduced between both moieties in analogy to the second series of Chapter 3. The targeted metal ions are going to be Ca^{2+}or Mg^{2+} but as well the standard response to Zn^{2+} or Hg^{2+} were expected. However the synthesis of those compounds appeared to be problematic and systematic degradation by Edman mechanism was observed. The efforts towards the synthesis of those compounds will be presented in this section.

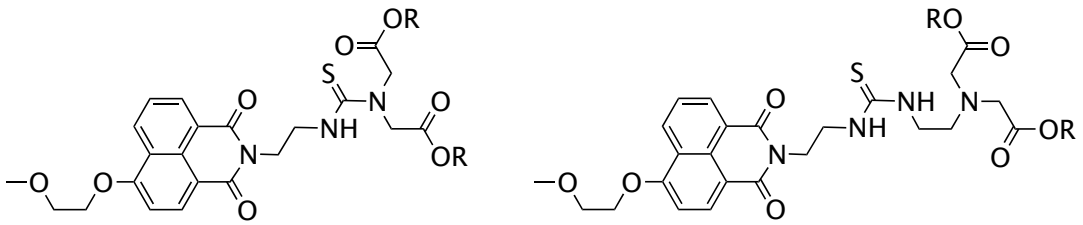

135 R = Et
136 R = *t*-bu

137 R = Et

Figure 4.6: Structures of the target compounds containing carbonyl groups as binding moieties.

4.3.2 Effort Towards the Synthesis of Target Compound 135, 136 and 137

As described in Chapter 3, the synthesis of the target compounds will be attempted starting from the mono imidazole thiourea **94** with the corresponding free amines. For the formation of **135** and **136**, the amine di-methyl iminodiacetate and di-tert-butyl iminodiacetate are commercially available and can be used to form the deired product in one step. In the case where an ethylene spacer is introduced, the corresponding amine can be synthesized in two steps starting from mono Boc-protected 1,2-aminoethane **79** and ethylchloroacetate.

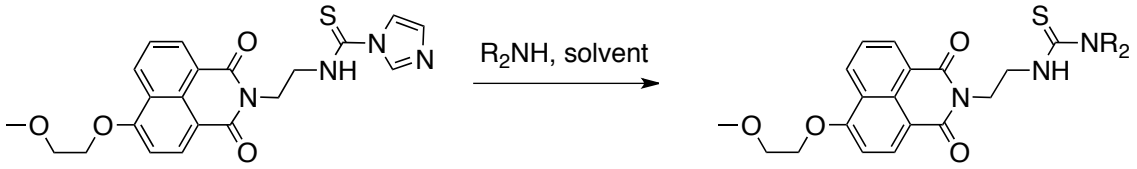

94

135 R = Et
136 R = t-bu
137 R = $CH_2CH_2N(COOEt)_2$

Scheme 4.5: Synthetic scheme for the synthesis of the carbonyl containing targets

The targets were synthesized from **94** in acetonitrile but after reaction another undesired reaction took place know as the Edman degradation. This reaction was developed and is used for the sequencing of peptides. Phenylthiourea reacts with the terminal amino group from a peptide and is then cleaved from the rest of the peptide without causing other bond breaking in the molecule. The residue can then be analyzed for sequencing. The reaction mechanism for this degradation is depicted in Scheme 4.6. In our case the bond disruption occurs to eliminate an alcohol instead of the amine. The use of ethanol as a solvent and room temperature conditions did not avoid this degradation process observed directly in the reaction mixture.

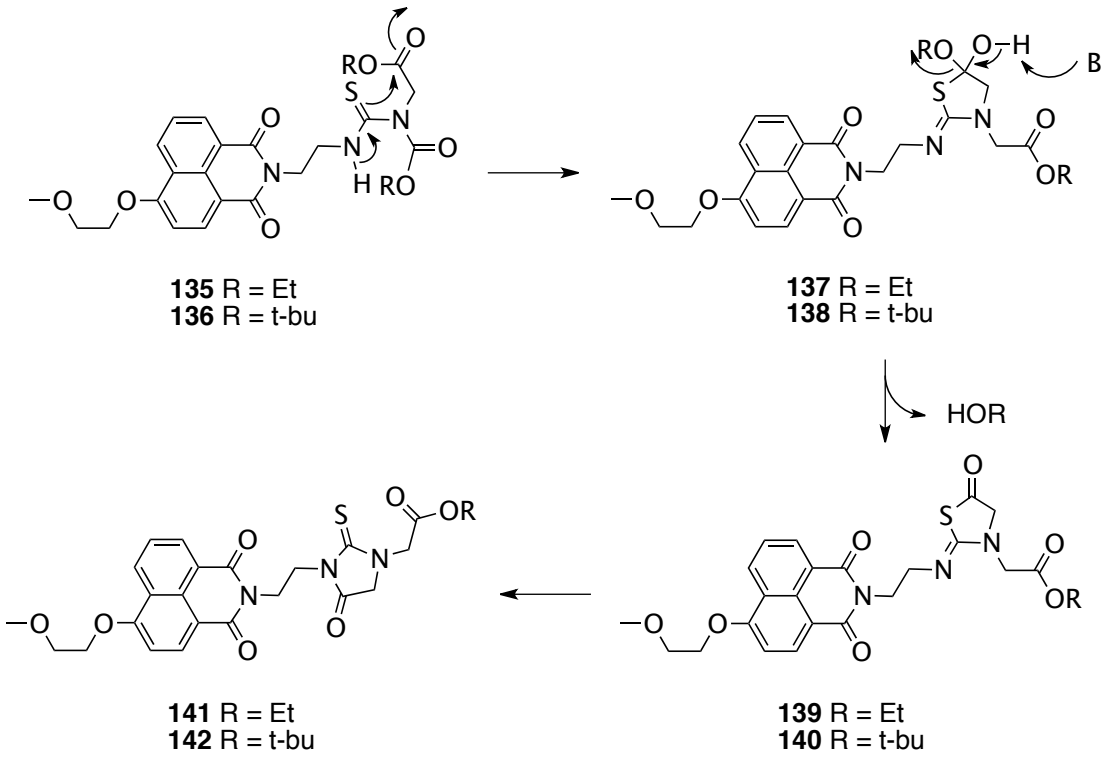

135 R = Et
136 R = t-bu

137 R = Et
138 R = t-bu

141 R = Et
142 R = t-bu

139 R = Et
140 R = t-bu

Scheme 4.6: Scheme of the Edman-like degradation.

4.3.3 Conclusion

The target compounds bearing an ester functional group as additional binding moiety are not stable compounds. This group is not compatible with the presence of thiourea and no further investigations could be done on this kind of constructs.

Chapter 5

Experimental Data

5.1 General notes and procedures

Synthetic procedures were carried out under an inert atmosphere, in dry solvent, using standard Schlenk techniques, unless otherwise noted. All reagents and solvents were reagent grade and were used without further purification unless otherwise specified. Flash chromatographic purification was performed using silica gel Merck 60 (particle size 0.040–0.063 mm), deactivated (20% triethylamine in hexane) silica gel Merck 60 (particle size 0.040–0.063 mm) or deactivated (5% water by weight) neutral aluminum oxide Sigma-Aldrich, Brockmann I, packed in glass columns; eluting solvent for each purification was determined by thin layer chromatography (TLC). Analytical thin-layer chromatography was performed using Merck TLC silica gel 60 F254 or Macherey–Nagel POLYGRAM ALOX N/UV254.

^{1}H NMR spectra were obtained on Bruker AV2-400 (400 MHz) or AV2-500 (500 MHz) spectrometers. Chemical shifts are reported in parts per million (ppm) relative to the solvent residual peak ($CDCl_3$, 7.26 ppm). Multiplicities are given as: s (singlet), d (doublet), t (triplet), q (quartet), dd (doublet of doublets), m (multiplet), and the coupling constants, *J*, are given in Hz. ^{1}H-decoupled ^{13}C NMR spectra were obtained on Bruker AV2-400 (100 MHz) or AV2-500 (125 MHz) spectrometers. ^{13}C NMR chemical shifts are reported relative to the solvent residual peak ($CDCl_3$, 77.0 ppm).

IR frequencies are given in cm^{-1}; spectra of thin films or KBr pellets for solids were obtained on a Perkin-Elmer Spectrum One spectrometer.

The cyclic voltammograms were performed in a CH1600C CH-Instrument, Electrochemical Analyzer. Conditions: 1mM compound, 0.1 M Bu_4NClO_4 as supporting electrolyte in ACN, scan rate 100 mV s^{-1}, glassy carbon working electrode (Ø = 0.3 cm), Pt wire counter electrode, Ag/AgCl reference electrode, added ferrocene (Fc) as internal reference.

Fluorescence measurements were carried out in spectroscopic grade methanol on an Edinburgh FLS920 spectrophotometer, using 450W Xenon lamp excitation, 1 nm excitation and 1 nm emission slit widths. Emission spectra were obtained by exciting at the longest-wavelength absorption maxima. Quantum yields were determined by standard methods,[6] using anthracene (ϕ = 0.3, in methanol) or 9,10-diphenylanthracene DPA (ϕ = 0.83, in methanol) as the standards.[164] The samples were diluted to optical transparency ($A \leq 0.05$), and the integrated emission intensity was compared to an iso-absorptive solution of the standards in degassed solvent.

UV/Vis measurements were carried out on an Agilent 8453 UV/VIS spectrophotometer. For extinction coefficient determination, four independent solutions of different concentration were prepared, with absorption between 0.04-0.10 AU. The value of ε was calculated by linear least-squares fitting of plots of A vs. concentration. All fits gave R^2 values of $\geq$0.98.

X-Ray structure analyses was carried out by the Laboratorium für Computerchemie und Roentgenstrukturanalyse of the Orgnisch-chemisches Institut of the University of Zurich. The measurement was made on an *Agilent Technologies SuperNova* area-detector diffractometer2 using Mo *K*α radiation (λ = 0.71073 Å) from a micro-focus X-ray source and an *Oxford Instruments Cryojet XL* cooler.

General Protocol for Metal Ion Titrations: 3.00 ml of chemosensor solution (ca. 3.0 μM in CH_3OH, prepared by serial dilution) were placed in a quartz cuvette and the initial fluorescence emission spectra was recorded. Aliquots of metal salt (3×5 μl, 20 μM to 2M in 10-folds increments, in CH_3OH) were then added sequentially (i.e. 3×5 μl×20 μM, then 3×5 μl×200 μM, etc.), until maximum fluorescence increase or a total volume of 4 ml was reached. After each addition of the metal ion solutions, the fluorescence emission spectra were recorded.

5.2 Synthesis of the Thioether Based Series

5.2.1 *N*-acetylcysteamine 23

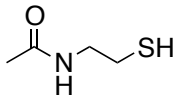

Cysteamine hydrochloride **21** (3.10 g, 27.43 mmol, 1.4 eq.) was solved in THF (70 ml). The white cloudy mixture was cooled to 0°C and acetic anhydride **22** (2.00 g, 19.61 mmol, 1 eq.) is added dropwise as a solution in THF (10 ml). The reaction mixture was stirred 1 hour at 0°C and allowed to warm at room temperature over night. An aqueous solution of NaOH (2N) (6 ml) was added to neutralize the reaction mixture until the white precipitate has disappeared. It was then stirred at room temperature over night. Water (50 ml) was added and the product was extracted with ethylacetate. The organic phase was dried over $MgSO_4$ and concentrated under vacuum. The crude product was dried with the vacuum pump and was considered pure enough for the next reaction. The product **23** is a colorless oil (670 mg, 29 %).[ii] The obtained data are consistent with the value reported in the literature.[165]

^{1}H NMR (δ ppm, 400 MHz, $CDCl_3$): 5.98 (s, br, 1H), 3.44 (q, 2H, J = 6.2), 2.68 (dt, 2H, J = 8.5, J = 6.4), 2.01 (s, 3H), 1.35 (t, 1H, J = 8.5). R_f (CH_2Cl_2/MeOH: 8/2): 0.78.

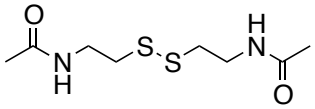

^{1}H NMR (δ ppm, 400 MHz, $CDCl_3$): 6.35 (s, br, 1H), 3.57 (q, 2H, J = 6.3), 2.82 (t, 2H, J = 6.4), 2.02 (s, 3H). ^{13}C NMR (δ ppm, 125 MHz, $CDCl_3$): 170.88, 38.65, 37.90, 23.39. R_f (CH_2Cl_2/MeOH: 95/5): 0.31.

5.2.2 *N*-(2-((2-(ethylthio)ethyl)thio)ethyl)acetamide 24

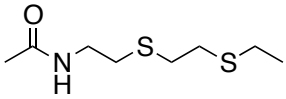

Compound **23** (660 mg, 5.54 mmol) was solved in DMF (20 ml), sodium carbonate (1.76 g, 16.63 mmol) was added and the reaction mixture was stirred for 15 minutes at room temperature. 2-Chloroethyl ethyl sulfide (688 mg, 5.54 mmol) was added dropwise and the

[ii] Since 2012 compound **23** is commercially available.

reaction mixture was stirred at room temperature over night. Water (60 ml) was added and the product was extracted with ethylacetate. The organic phase was dried over $MgSO_4$ and concentrated under vacuum. The crude product was purified by column chromatography (eluent: CH_2Cl_2/Acetone: 9/1) to give the product **24** as a white solid (853 mg, 74 %).

^{1}H NMR (δ ppm, 400 MHz, $CDCl_3$): 5,91 (s, br, 1H), 3.45 (q, 2H, J = 6.2), 2.75 (s, 4H), 2,71 (t, 2H, J = 6.3), 2,58 (q, 2H, J = 7.4), 2.00 (s, 3H), 1,27 (t, 3H, J = 7.4). ^{13}C NMR (δ ppm, 100 MHz, $CDCl_3$): 170.3, 38.6, 32.1, 31.9, 31.8, 26.2, 23.5, 14.9. HRMS-ESI: Calculated for $C_8H_{17}NNaOS_2$ $[M+Na]^+$ 230.06438, found 230.06451. R_f (CH_2Cl_2/AcOEt: 9/1): 0.27.

5.2.3 2-((2-(ethylthio)ethyl)thio)ethanamine 25

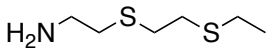

Sodium hydroxide (290 mg, 7.24 mmol) was solved in water and **24** (150 mg, 0.72 mmol) was added. The reaction mixture was heated at reflux overnight. The product was extracted with ethylacetate and the organic phase was washed with a saturated solution of sodium hydrogen carbonate, dried over $MgSO_4$ and concentrated under vacuum to give compound **25** (80 mg, 67 %) as a light yellow oil.

^{1}H NMR (δ ppm, 400 MHz, $CDCl_3$): 2.90 (dd, 2H, J = 6.8, J = 5.8), 2.74 (s, 4H), 2.67 (dd, 2H, J = 6.8, J = 5.8), 2.58 (q, 2H, J = 7.4), 1.27 (t, 3H, J = 7.4). ^{13}C NMR (δ ppm, 100 MHz, DMSO): 39.5, 31.9, 31.7, 29.0, 25.9, 15.8. MS-ESI: $[M+H]^+$: 166.

5.2.4 4,4'-oxybis(2-(2-((2-(ethylthio)ethyl)thio)ethyl)diphthalimide 20

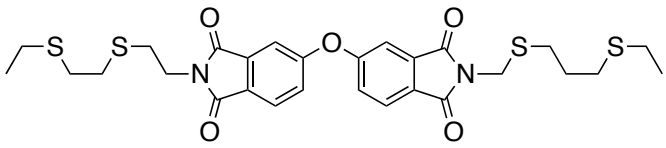

Compound **25** (128 mg, 0.41 mmol) was solved in DMF (10 ml) and 4,4'-oxydiphthalic anhydride (200 mg, 0.99 mmol) was added as a solid. The reaction mixture was stirred at 130°C for 24 hours and the solvent was distilled. CH_2Cl_2 (20 ml) was poured to the yellow residue and the organic phase was washed with water, dried over $MgSO_4$ and concentrated under vacuum. The crude product was purified by column chromatography (eluent: CH_2Cl_2/Acetone: 99/1) to give the product **20** as a white solid (115 mg, 46 %).

^{1}H NMR (δ ppm, 400 MHz, $CDCl_3$): 7.89 (d, 2H, *J* = 8.2), 7.45 (d, 2H, *J* = 2.0), 7.38 (dd, 2H, *J* = 8.2, *J* = 2.0), 3.90 (t, 4H, *J* = 7.0), 2.87 (t, 4H, *J* = 7.0), 2.84-2.73 (m, 8H), 2.59 (q, 4H, *J* = 7.4), 1.28 (t, 6H, *J* = 7.4). ^{13}C NMR (δ ppm, 100 MHz, $CDCl_3$): 167.27, 167.12, 161.09, 134.99, 127.68, 125.91, 124.47, 113.91, 37.37, 31.79, 31.59, 30.17, 26.17, 14.93. IR (KBr) cm^{-1}: 2923w, 1769m, 1710s, 1608m, 1475w, 1445m, 1397m, 1350m, 1277m, 1242m, 1090m, 974w, 823w, 742w, 695w, 613w, 549w. ESI-MS: M + H$^+$: 627 (measured with acetonitrile, avoid methanol). HRMS-ESI: Calculated for $C_{28}H_{32}N_2NaO_5S_4$ $[M+Na]^+$ 627.10863, found 627.10849. R_f (CH_2Cl_2/Acetone: 99/1): 0.32.

5.2.5 4-Bromo-*N*-2-(2-((2-(ethylthio)ethyl)thio)ethyl)naphthalimide 39

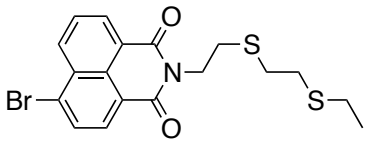

A solution of **29** as hydrochloride salt (60 mg, 0.30 mmol) and triethylamine (30 mg, 0.30 mmol) in DMF (10 ml) was stirred for 1 hour at room temperature. 4-bromo-1,8-phthalic anhydride **38** (68 mg, 0.25 mmol) was added as a solid and the color turn to orange. The reaction mixture was heated to 100 °C and stirred at this temperature for 24 hours. After cooling to room temperature the solvent was distilled. The crude product was purified by column chromatography (eluent: CH_2Cl_2/Hexane: 6/4) to give the product **39** as a white solid (80 mg, 76 %).

^{1}H NMR (δ ppm, 400 MHz, $CDCl_3$): 8.67 (dd, 1H, *J* = 1.2, *J* = 7.3), 8.60 (dd, 1H, *J* = 1.2, *J* = 8.5), 8.43 (d, 1H, *J* = 7.8), 8.06 (d, 1H, *J* = 7.8), 7.86 (dd, 1H, *J* = 7.3, *J* = 8.5), 4.39 (t, 2H, *J* = 7.5), 2.93-2.87 (m, 4H), 2.83-2.79 (m, 2H), 2.62 (q, 2H, *J* = 7.4), 1.29 (t, 3H, *J* = 7.4). ^{13}C NMR (δ ppm, 125 MHz, $CDCl_3$): 163.68, 163.66, 133.68, 132.37, 131.55, 131.32, 130.85, 130.70, 129.22, 128.29, 123.04, 122.16, 39.84, 32.06, 31.65, 29.51, 26.10, 14.96. IR (KBr) cm^{-1}: 2924w, 1699m, 1650s, 1592m, 1568m, 1502w, 1434w, 1402w, , 1374m, 1342m, 1255m, 1231m, 1169w, 1107m, 1090 m, 1046w, 872w, 856w, 785m, 751w. HRMS-ESI: Calculated for $C_{18}H_{18}BrNNaO_2S_2$ $[M+Na]^+$ 445.98534, found 445.98545. R_f (CH_2Cl_2/Hexane: 6/4): 0.16.

5.2.6 4-(2-methoxyethoxy)-*N*-2-(2-((2-(ethylthio)ethyl)thio)ethyl)naphthalimide 34

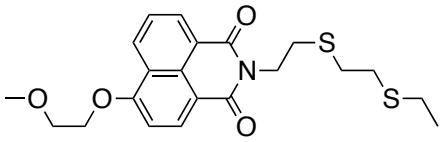

A solution of **39** (50 mg, 0.12 mmol) and potassium carbonate (163 mg, 1.12 mmol) in methoxyethanol was heated to 100 °C for 2 hours and a color change to orange is observed. After cooling to room temperature water was added and the product was extracted with CH_2Cl_2. The organic phase was washed with water, dried over $MgSO_4$ and concentrated under vacuum. The crude product was purified by column chromatography (silica gel deactivated with 20% Et_3N, eluent: CH_2Cl_2/Hexane: 1/1) give the product **34** as a white solid (26 mg, 53 %).

^{1}H NMR (δ ppm, 400 MHz, $CDCl_3$): 8.62 (m, 2H), 8.55 (d, 1H, J = 8.3), 7.72 (dd, 1H, J = 8.3, J = 7.5), 7.06 (d, 1H, J = 8.3), 4.45-4.43 (m, 2H), 4.40-4.37 (m, 2H), 3.95-3.93 (m, 2H), 3.52 (s, 3H), 2.92-2.83 (m, 6H), 2.63-2.61 (m, 2H), 1.29 (t, 3H, J = 7.4). ^{13}C NMR (δ ppm, 125 MHz, $CDCl_3$): 164.54, 163.91, 160.31, 133.69, 131.91, 129.63, 129.22, 126.12, 123.72, 122.31, 115.14, 106.13, 70.77, 68.55, 59.54, 39.71, 32.06, 31.68, 29.57, 26.06, 14.96. IR (KBr) cm^{-1}: 2925w, 1697m, 1654s, 1596m, 1514w, 1423w, 1388m, 1355m, 1274m, 1248m, 1232m, 1202m, 1128m, 1106m, 1079m, 1056m, 1033m, 994w, 910w, 860m, 817w, 783m, 757w, 585w, 474w. HRMS-ESI: Calculated for $C_{21}H_{25}NNaO_4S_2$ $[M+Na]^+$ 442.11172, found 442.11224. R_f (deactivated silica gel, CH_2Cl_2/Hexane: 1/1): 0.4.

5.2.7 *N*-(3-mercaptopropyl) acetamide 42

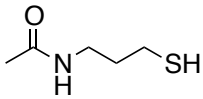

3-bromopropylamine hydrobromide **40** (3.00 g, 13.70 mmol) and potassium thioacetate **41** (1.12 g, 9.79 mmol) were mixed in THF (80 ml) under argon. The reaction mixture was heated to reflux and stirred for 24 hours. After cooling to room temperature, water was added (100 ml) and the organic phase was extracted and with ethylacetate, dried over $MgSO_4$ and concentrated under vacuum. The crude product was purified by column chromatography (eluent: CH_2Cl_2/MeOH 98/2) to give the product **42** as a yellow oil (210 mg, 16 %).

^{1}H NMR (δ ppm, 400 MHz, $CDCl_3$): 3.36 (dt, 2H, *J* = 6.7), 2.56 (dt, 2H, *J* = 7.0, *J* = 7.9), 1.98 (s, 3H), 1.82 (quint, 2H, *J* = 6.9), 1.47 (t, 1H, *J* = 8.0). ^{13}C NMR (δ ppm, 125 MHz, $CDCl_3$): 170.37, 38.11, 33.54, 23.33, 22.03. R_f (CH_2Cl_2/MeOH: 98/2): 0.08.

5.2.8 *N*-(3-((2-(ethylthio)ethyl)thio)propyl)acetamide 43

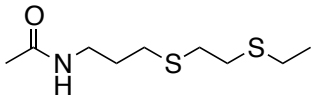

Compound **42** (320 mg, 2.41 mmol) was solved in DMF (8 ml), sodium carbonate (789 mg, 7.44 mmol) was added and the reaction mixture was stirred for 15 minutes at room temperature. 2-Chloroethyl ethyl sulfide (308 mg, 2.41 mmol) was added dropwise and the reaction mixture was stirred at room temperature over night. Water (60 ml) was added and the product was extracted with ethylacetate. The organic phase was dried over $MgSO_4$ and concentrated under vacuum. The crude product was purified by column chromatography (eluent: CH_2Cl_2/MeOH: 98/2) to give the product **43** as a yellow oil (130 mg, 25 %).

^{1}H NMR (δ ppm, 400 MHz, $CDCl_3$): 3.36 (dt, 2H, *J* = 6.7), 2.74 (s, 4H), 2.60 (t, 4H, *J* = 7.1), 2.58 (q, 2H, *J* = 7.4), 1.98 (s, 3H), 1.81 (quint, 2H, *J* = 7.0), 1.27 (t, 3H, *J* = 7.4). ^{13}C NMR (δ ppm, 125 MHz, $CDCl_3$): 170.33, 38.71, 32.13, 31.64, 29.68, 29.19, 26.10, 23.44, 14.84. HRMS-ESI: Calculated for $C_9H_{19}NNaOS_2$ $[M+Na]^+$ 244.08003, found 244.07995. R_f (CH_2Cl_2/MeOH: 98/2): 0.08.

5.2.9 3-((2-(ethylthio)ethyl)thio)propanamine 44

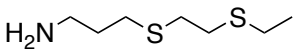

Sodium hydroxide (140 mg, 3.62 mmol) was solved in water (3 ml) and **43** (80 mg, 0.36 mmol) was added. The reaction mixture was heated at reflux overnight. The product was extracted with ethylacetate and the organic phase was washed with a saturated solution of sodium hydrogen carbonate, dried over $MgSO_4$ and concentrated under vacuum to give compound **44** (48 mg, 74 %) as a light yellow oil.

^{1}H NMR (δ ppm, 400 MHz, $CDCl_3$): 2.81 (t, 2H, *J* = 6.9), 2.74 (s, 4H), 2.62 (t, 2H, *J* = 7.2), 2.58 (q, 2H, *J* = 7.4), 1.75 (quint, 2H, *J* = 7.0), 1.27 (t, 3H, *J* = 7.4). ^{13}C NMR (δ ppm, 125 MHz, $CDCl_3$): 170.33, 38.71, 32.13, 31.64, 29.68, 29.19, 26.10, 23.44, 14.84. HRMS-ESI: Calculated for $C_7H_{18}NNaS_2$ $[M+H]^+$ 180.08728, found 180.08752.

5.2.10 4-Bromo-*N*-3-(2-((2-(ethylthio)ethyl)thio)propyl)naphthalimide 45

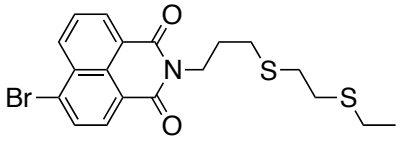

A solution of **44** (48 mg, 0.27 mmol) and triethylamine (27 mg, 0.27 mmol) in DMF (10 ml) was stirred for 1 hour at room temperature. 4-bromo-1,8-phthalic anhydride (62 mg, 0.22 mmol) was added as a solid and the color turn to orange. The reaction mixture was heated to 100 °C and stirred at this temperature for 24 hours. After cooling to room temperature the solvent was distilled. The crude product was purified by column chromatography (eluent: CH_2Cl_2/Hexane: 1/1) to give the product **45** as a yellow solid (54 mg, 55 %).

^{1}H NMR (δ ppm, 400 MHz, $CDCl_3$): 8.67 (dd, 1H, *J* = 1.1, *J* = 7.3), 8.59 (dd, 1H, *J* = 1.1, *J* = 8.5), 8.42 (d, 1H, *J* = 7.8), 8.06 (d, 1H, *J* = 7.8), 7.86 (dd, 1H, *J* = 7.3, *J* = 8.5), 4.29 (t, 2H, *J* = 7.3), 2.76-2.74 (m, 4H), 2.69 (t, 2H, *J* = 7.3), 2.57 (q, 2H, *J* = 7.4), 2.05 (quint, 2H, *J* = 7.3), 1.25 (t, 3H, *J* = 7.4). ^{13}C NMR (δ ppm, 125 MHz, $CDCl_3$): 164.54, 163.91, 160.31, 133.54, 132.28, 131.46, 131.30, 130.85, 130.53, 129.21, 128.27, 123.21, 122.34, 39.81, 32.18, 31.82, 29.94, 28.14, 26.17, 14.94. R_f (CH_2Cl_2/Hexane: 1/1): 0.08.

5.2.11 4-(2-methoxyethoxy)-*N*-3-(2-((2-(ethylthio)ethyl)thio)propyl)naphthalimide 35

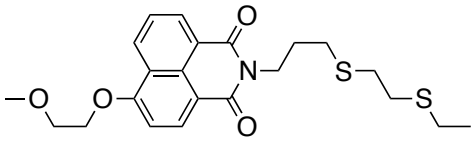

A solution of **45** (50 mg, 0.11 mmol) and potassium carbonate (157 mg, 1.11 mmol) in methoxyethanol was heated to 100 °C for 2 hours and a color change to orange is observed. After cooling to room temperature water was added and the product was extracted with CH_2Cl_2. The organic phase was washed with water, dried over $MgSO_4$ and concentrated under vacuum. The crude product was purified by column chromatography (silica gel

deactivated with 20% Et_3N, eluent: CH_2Cl_2/Hexane: 1/1) to give the product **35** as a light yellow solid (20 mg, 40 %).

^{1}H NMR (δ ppm, 400 MHz, $CDCl_3$): 8.63 (dd, 1H, *J* = 1.3, *J* = 8.3), 8.61 (dd, 1H, *J* = 1.3, *J* = 7.3), 8.55 (d, 1H, *J* = 8.3), 7.72 (dd, 1H, *J* = 7.3, *J* = 8.4), 7.06 (d, 1H, *J* = 8.3), 4.48-4.40 (m, 2H), 4.32-4.24 (m, 2H), 3.98-3.91 (m, 2H), 3.53 (s, 3H), 2.76-2.74 (m, 4H), 2.68 (t, 2H, *J* = 7.4), 2.57 (q, 2H, *J* = 7.4), 2.05 (quint, 2H, *J* = 7.4), 1.25 (t, 3H, *J* = 7.4). ^{13}C NMR (δ ppm, 125 MHz, $CDCl_3$): 164.68, 164.07, 160.24, 133.62, 131.85, 129.59, 129.12, 126.12, 123.71, 122.43, 115.29, 106.13, 70.80, 68.54, 59.56, 39.52, 32.07, 31.74, 29.91, 28.27, 26.11, 14.94. IR (KBr) cm^{-1}: 2925w, 1692s, 1652s, 1621m, 1593m, 1513m, 1453m, 1424m, 1390m, 1355s, 1272m, 1245m, 1203m, 1103m, 1074m, 1028m, 916w, 854w, 781m, 757m, 581w, 501w. HRMS-ESI: Calculated for $C_{22}H_{27}NO_4S_2$ $[M+Na]^+$ 456.12373, found 456.12773. R_f (deactivated silica gel, CH_2Cl_2/Hexane: 1/1): 0.4.

5.2.12 4-Bromo-*N*-propylnaphthalimide 46

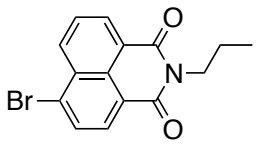

A solution of 4-bromo-1,8-naphthalic anhydride **38** (200 mg, 0.72 mmol) was prepared in ethanol (15 ml). A color change to orange was observed after the addition of 1-aminopropane (43 mg, 0.72 mmol). The reaction mixture was refluxed overnight. After cooling to room temperature a solid precipitated in the reaction mixture. It was filtered and the obtained solid was purified by column chromatography (eluent: CH_2Cl_2/Hexane: 1/1) to give the product **46** as a white solid (200 mg, 88 %).

^{1}H NMR (δ ppm, 400 MHz, $CDCl_3$): 8.67 (dd, 1H, *J* = 1.1, *J* = 7.3), 8.58 (dd, 1H, *J* = 1.1, *J* = 8.5), 8.42 (d, 1H, *J* = 7.9), 8.05 (d, 1H, *J* = 7.9), 7.85 (dd, 1H, *J* = 7.3, *J* = 8.5), 4.17-4.13 (m, 2H), 1.82-1.73 (m, 2H), 1.02 (t, 3H, *J* = 7.4). ^{13}C NMR (δ ppm, 125 MHz, $CDCl_3$): 163.73 (2), 133.30, 132.11, 131.31, 131.19, 130.76, 130.27, 129.15, 128.18, 123.30, 122.44, 42.19, 21.48, 11.61. IR (KBr) cm^{-1}: 3054w, 2950m, 2869w, 1699s, 1659s, 1586s, 1568s, 1503m, 1460m, 1437m, 1397m, 1358s, 1287m, 1240s, 1165m, 1152w, 1101w, 1072s, 1044m, 1015w, 934w, 907w, 864m, 784s, 749m, 734w, 714w, 666w, 571w, 504w. HRMS-ESI: Calculated for $C_{15}H_{13}BrNNaO_2$ $[M+Na]^+$ 339.99436, found 339.99412. R_f (CH_2Cl_2/Hexane: 1/1): 0.42.

5.2.13 4-(2-((2-((2-(ethylthio)ethyl)thio)ethyl)amino)-*N*-propylnaphthalimide 36

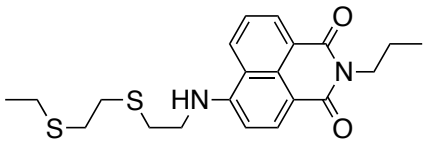

A solution of **46** (30 mg, 0.09 mmol) and **25** (78 mg, 0.47 mmol) in DMSO (3 ml) was stirred at 80°C overnight. Water (10 ml) was added and the precipitate was filtered. The solid residue was dissolved in CH_2Cl_2 and concentrated under vacuum. The crude product was purified by column chromatography (eluent: CH_2Cl_2/MeOH: 99/1) and by recrystallization from hexane and ethylacetate to give product **36** as a yellow solid (17 mg, 48 %).

^{1}H NMR (δ ppm, 400 MHz, $CDCl_3$): 8.61 (dd, 1H, J = 1.1, J = 7.3), 8.48 (d, 1H, J = 8.3), 8.16 (dd, 1H, J = 1.1, J = 8.4), 7.66 (dd, 1H, J = 7.3, J = 8.4), 6.74 (d, 1H, J = 8.3), 4.19-4.08 (m, 2H), 3.62 (t, 2H, J = 6.3), 3.10-2.99 (m, 2H), 2.85-2.71 (m, 4H), 2.56 (q, 2H, J = 7.4), 1.83-1.71 (m, 2H), 1.25 (t, 3H, J = 7.4), 1.01 (t, 3H, J = 7.4). ^{13}C NMR (δ ppm, 125 MHz, $CDCl_3$): 164.79, 164.28, 148.80, 134.39, 131.38, 129.92, 126.12, 125.18, 123.42, 120.70, 111.41, 104.90, 41.85, 41.65, 31.86, 31.65, 31.33, 26.30, 21.58, 14.89, 11.71. IR (KBr) cm^{-1}: 3745w, 3331m, 2959w, 1685m, 1635s, 1585s, 1546s, 1428m, 1395m, 1377m, 1357m, 1245m, 1107m, 1072m, 780m, 757w. HRMS-ESI: Calculated for $C_{21}H_{26}N_2NaO_2S_2$ $[M+Na]^+$ 425.13279, found 425.13280. R_f (CH_2Cl_2/MeOH: 99/1): 0.11.

5.2.14 4-(3-((2-((2-(ethylthio)ethyl)thio)propyl)amino)-*N*-propylnaphthalimide 37

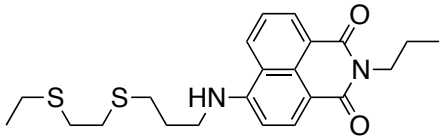

A solution of **46** (15 mg, 0.05 mmol) and **44** (60 mg, 0.34 mmol) in DMSO (3 ml) was stirred at 80°C overnight. Water (10 ml) was added and the precipitate was filtered. The solid residue was dissolved in CH_2Cl_2 and concentrated under vacuum. The crude product was purified by column chromatography (eluent: CH_2Cl_2/Hexane: 6/4 to CH_2Cl_2) to give the product **37** as a yellow solid (8 mg, 40 %).

^{1}H NMR (δ ppm, 400 MHz, $CDCl_3$): 8.60 (dd, 1H, J = 1.1, J = 7.3), 8.48 (d, 1H, J = 8.4), 8.12 (dd, 1H, J = 1.1, J = 8.4), 7.63 (dd, 1H, J = 7.3, J = 8.4), 6.75 (d, 1H, J = 8.4), 4.19-4.08 (m, 2H), 3.59 (t, 2H, J = 6.6), 2.87-2.69 (m, 6H), 2.57 (q, 2H, J = 7.4), 2.13 (quint, 2H, J =

6.6), 1.85-1.67 (m, 2H), 1.26 (t, 3H, *J* = 7.4), 1.01 (t, 3H, *J* = 7.4). ^{13}C NMR (δ ppm, 125 MHz, $CDCl_3$): 164.83, 164.30, 149.30, 134.52, 131.28, 129.98, 126.04, 124.97, 123.44, 120.48, 110.85, 104.39, 43.09, 41.84, 32.56, 31.82, 30.27, 28.07, 26.30, 21.60, 14.93, 11.71. IR (KBr) cm^{-1}: 2925w, 1692s, 1652s, 1621m, 1593m, 1513m, 1453m, 1424m, 1390m, 1355s, 1272m, 1245m, 1203m, 1103m, 1074m, 1028m, 916w, 854w, 781m, 757m, 581w, 501w. HRMS-ESI: Calculated for $C_{22}H_{28}N_2NaO_2S_2$ $[M+Na]^+$ 439.14844, found 439.14810. R_f (CH_2Cl_2/MeOH: 99/1): 0.13.

5.2.15 4-((propyl)amino)-*N*-propylnaphthalimide 47

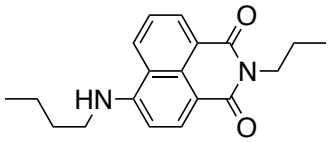

A solution of **46** (40 mg, 0.13 mmol) and 1-aminobutylamine (92 mg, 1.26 mmol) in DMSO (5 ml) was stirred at 80°C overnight. The solvent was distilled and the crude product was purified by column chromatography (eluent: CH_2Cl_2/Hexane: 6/4) to give product **47** as a yellow solid (35 mg, 90 %).

^{1}H NMR (δ ppm, 400 MHz, $CDCl_3$): 8.59 (dd, 1H, *J* = 1.1, *J* = 7.3), 8.48 (d, 1H, *J* = 8.4), 8.07 (dd, 1H, *J* = 1.1, *J* = 8.4), 7.62 (dd, 1H, *J* = 7.3, *J* = 8.4), 6.74 (d, 1H, *J* = 8.4), 4.15-4.12 (m, 2H), 3.42 (t, 2H, *J* = 7.3), 1.85-1.72 (m, 4H), 1.59-1.50 (m, 2H), 1.04 (t, 3H, *J* = 7.3), 1.01 (t, 3H, *J* = 7.4). ^{13}C NMR (δ ppm, 125 MHz, $CDCl_3$): 164.85, 164.34, 149.49, 134.61, 131.61, 129.95, 125.77, 124.83, 123.43, 120.28, 110.51, 104.48, 43.56, 41.82, 31.19, 21.59, 20.48, 14.00, 11.72. IR (KBr) cm^{-1}: 3376m, 2960m, 2932w, 2872w, 1683m, 1635s, 1570s, 1544s, 1463w, 1476w, 1427m, 1396m, 1384s, 1353s, 1295w, 1244m, 1191w, 1150w, 1129m, 1097w, 1071m, 910w, 888w, 829w, 776m, 761w, 749w, 668w, 610w, 579w, 493w. HRMS-ESI: Calculated for $C_{19}H_{23}N_2O_2$ $[M+H]^+$ 311.17540, found 311.17495. R_f (CH_2Cl_2/Hexane: 6/4): 0.27.

5.2.16 7-methoxycoumarin-3-carboxylic acid 58

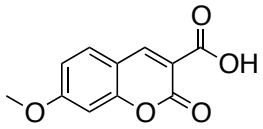

Meldrum's acid (2,2-dimethyl-1,3-dioxane-4,6-dione) **56** (568 mg, 3.95 mmol) and 2-hydroxy-4-methoxybenzaldehyde **57** (600 mg, 3.95 mmol) were solved in ethanol (10 ml). Catalytic amount of piperidine and acetic acid were added and the color turns to yellow. The reaction mixture was stirred for 30 min at room temperature and heated to reflux for 2 hours. After cooling to room temperature, the precipitate was filtered, washed 3 times with ethanol and the product **58** was obtained as a white solid (590 mg, 68 %).[91]

^{1}H NMR (δ ppm, 400 MHz, DMSO): 12,97 (s, 1H), 8.72 (s, 1H), 7.83 (d, 1H, *J* = 8.6), 7.04 (d, 1H, *J* = 2.4), 7.01 (dd, 1H, *J* = 8.6, *J* = 2.4), 3.89 (s, 3H). ^{13}C NMR (δ ppm, 125 MHz, DMSO): 165.13, 164.61, 157.68, 157.36, 149.53, 132.03, 114.30, 113.76, 112.08, 100.76, 56.71.

5.2.17 *N*-2-(2-((2-(ethylthio)ethyl)thio)ethyl)-7-methoxycoumarin-3-carboxamide 52

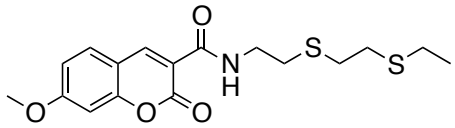

A solution of **25** (80 mg, 0.49 mmol) in CH_2Cl_2 (5 ml) was cooled to 0°C. 4-dimethylaminopyridine (50 mg, 0.40 mmol), *N*,*N'*-dicyclohexylcarbodiimide (83 mg, 0.40 mmol) and **58** (89 mg, 0.40 mmol) were added successively and the reaction mixture was stirred at room temperature overnight. The reaction mixture was filtered over Celite and the filtrate was concentrated under vacuum. The crude product was purified by column chromatography (silica gel deactivated with 20% Et_3N, eluent: CH_2Cl_2/Hexane: 1/1) and crystalized from cyclohexane to give the product **52** as a white solid (103 mg, 70 %).

^{1}H NMR (δ ppm, 400 MHz, $CDCl_3$): 9.03 (s, 1H), 8.88 (d, 1H, *J* = 0.6), 7.59 (d, 1H, *J* = 8.7), 6.95 (dd, 1H, *J* = 2.4, *J* = 8.7), 6.87 (dd, 1H, *J* = 0.6, *J* = 2.4), 3.92 (s, 3H), 3.67 (td, 2H, *J* = 5.9, *J* = 6.9), 2.88-2.71 (m, 6H), 2.59 (q, 2H, *J* = 7.4), 1.27 (t, 3H, *J* = 7.4). ^{13}C NMR (δ ppm, 125 MHz, $CDCl_3$): 165.05, 162.33, 161.93, 156.85, 148.55, 131.09, 114.73, 114.24, 112.51, 100.43, 56.18, 39.54, 32.15, 31.79, 31.74, 26.17, 14.94. HRMS-ESI: Calculated for

$C_{17}H_{21}NNaO_4S_2$ $[M+Na]^+$ 390.08042, found 390.08064. R_f (deactivated silica gel, CH_2Cl_2/Hexane: 1/1): 0.28.

5.2.18 *N*-3-(2-((2-(ethylthio)ethyl)thio)propyl)-7-methoxycoumarin-3-carboxamide 53

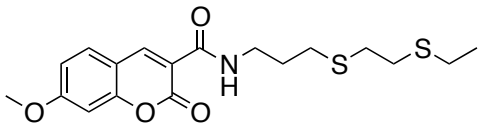

A solution of **44** (15 mg, 0.08 mmol) in CH_2Cl_2 (2 ml) was cooled to 0°C. 4-Dimethylaminopyridine (9 mg, 0.07 mmol), *N*,*N'*-dicyclohexylcarbodiimide (14 mg, 0.07 mmol) and **58** (15 mg, 0.07 mmol) were added successively and the reaction mixture was stirred at room temperature overnight. The reaction mixture was filtered over Celite and the filtrate was concentrated under vacuum. The crude product was purified by column chromatography (silica gel deactivated with 20% Et_3N, eluent: CH_2Cl_2/hexane: 1/1) and crystalized from cyclohexane to give the product **53** as a white solid (8 mg, 30 %).

^{1}H NMR (δ ppm, 400 MHz, $CDCl_3$): 8.84 (d, 1H, *J* = 0.7), 7.59 (d, 1H, *J* = 8.7), 6.95 (dd, 1H, *J* = 2.4, *J* = 8.7), 6.87 (dd, 1H, *J* = 0.6, *J* = 2.4), 3.92 (s, 3H), 3.57 (td, 2H, *J* = 5.9, *J* = 6.9), 2.75 (s, 4H), 2.65 (t, 2H, *J* = 7.4), 2.58 (q, 2H, *J* = 7.4), 1.93 (quint, 2H, *J* = 7.0), 1.27 (t, 3H, *J* = 7.4). ^{13}C NMR (δ ppm, 125 MHz, $CDCl_3$): 165.00, 162.29, 162.04, 156.80, 148.46, 131.07, 114.87, 114.20, 112.56, 100.45, 56.16, 38.83, 32.31, 31.77, 29.75, 29.55, 26.18, 14.94. IR (KBr) cm^{-1}: 3345m, 3051w, 2964w, 2933w, 1701s, 1654m, 1602m, 1567m, 1527s, 1459w, 1442w, 1372m, 1256w, 1220m, 1140m, 1115w, 1026w, 908w, 844w, 815w, 799w, 770w, 746w, 676w, 638w, 507w, 482w. HRMS-ESI: Calculated for $C_{18}H_{23}NNaO_4S_2$ $[M+Na]^+$ 404.09596, found 404.09607. R_f (deactivated silica gel, CH_2Cl_2/Hexane: 1/1): 0.22.

5.2.19 *N*-(2-((2-(ethylthio)ethyl)thio)ethyl)-*N*-methylacetamide 59

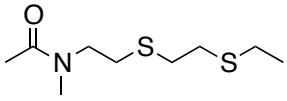

A solution of **25** (200 mg, 0.97 mmol) in THF (6 ml) was cooled to -70°C and n-butyllithium (1.6 M in hexane) (0.75 ml, 1.16 mmol) was added with a syringe. The reaction mixture was stirred for 20 min at -70°C and iodomethane (550 mg, 3.86 mmol) was added. The reaction mixture was stirred 10 min and then it was allowed to warm up to room temperature and

stirred overnight. The reaction was quenched with a saturated solution of NH_4Cl and the product was extracted with ethylacetate. The organic phase was washed with a saturated solution of NaCl, dried over $MgSO_4$ and the solvent was evaporated. The crude product was purified by column chromatography (eluant: CH_2Cl_2/MeOH: 99/1) to give the product **59** as a colorless oil (130 mg, 59 %).

^{1}H NMR (δ ppm, 400 MHz, $CDCl_3$): 3.56-3.47 (m, 2H), 3.05 (rotamer A, s, 2H), 2.94 (rotamer B, s, 1H), 2.78-2.70 (m, 6H), 2.59 (q, 2H, *J* = 7.4), 2.13 (rotamer B, s, 1H), 2.08 (rotamer A, s, 2H), 1.30-1.25 (m, 3H). ^{13}C NMR (δ ppm, 125 MHz, $CDCl_3$): 172.53, 38.25, 32.54, 31.35, 29.98, 29.23, 26.50, 23.14, 14.64. ESI-MS: M+Na^+: 244. R_f (CH_2Cl_2/AcOEt: 9/1): 0.27.

5.2.20 2-((2-(ethylthio)ethyl)thio)-*N*-methylethanamine 60

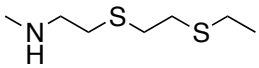

Sodium hydroxide (235 mg, 5.88 mmol) was solved in water (4 ml) and **59** (130 mg, 0.59 mmol) was added. The reaction mixture was heated at reflux overnight. The product was extracted with ethylacetate and the organic phase was washed with a saturated solution of sodium hydrogen carbonate, dried over $MgSO_4$ and concentrated under vacuum to give compound **60** (60 mg, 57 %) as a light yellow oil.

^{1}H NMR (δ ppm, 400 MHz, $CDCl_3$): 2.82-2.70 (m, 8H), 2.58 (q, 2H, *J* = 7.4), 2.46 (s, 3H), 1.27 (t, 3H, *J* = 7.4). ^{13}C NMR (δ ppm, 125 MHz, $CDCl_3$): 51.17, 36.55, 32.80, 32.60, 32.31, 26.58, 15.31.

5.2.21 *N*-2-(2-((2-(ethylthio)ethyl)thio)ethyl)-*N*-methyl-7-methoxycoumarin-3-carboxamide 54

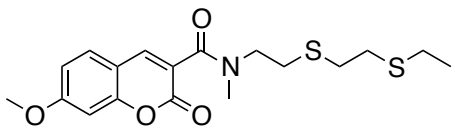

A solution of **60** (60 mg, 0.34 mmol) in CH_2Cl_2 (5 ml) was cooled to 0°C. 4-Dimethylaminopyridine (34 mg, 0.28 mmol), *N*,*N*'-dicyclohexylcarbodiimide (58 mg, 0.28 mmol) and **58** (62 mg, 0.28 mmol) were added successively and the reaction mixture was stirred at room temperature overnight. The reaction mixture was filtered over Celite and the

filtrate was concentrated under vacuum. The crude product was purified by column chromatography (silica gel deactivated with 20% Et_3N, eluent: CH_2Cl_2/Hexane: 1/1) and crystalized from cyclohexane to give the product **54** as a yellow solid (40 mg, 37 %).

^{1}H NMR (δ ppm, 400 MHz, $CDCl_3$): 8.89 (m, 1H), 7.44 (d, 1H, *J* = 8.7), 6.90 (dd, 1H, *J* = 2.4, *J* = 8.7), 6.84 (d, 1H, *J* = 2.4), 3.90 (s, 3H), 3.70 (rotamer A, t, 2H *J* = 6.9), 3.48 (rotamer B, t, 1H, *J* = 6.9), 3.10 (rotamer B, s, 1H), 3.05 (rotamer A, s, 2H), 2.88-2.81 (m, 4H), 2.65-2.60 (m, 2H), 2.50 (rotamer B, q, 1H, *J* = 7.4), 1.28 (rotamer A, t, 2H, *J* = 7.4), 1.22 (rotamer B, t, 1H, *J* = 7.4). ^{13}C NMR (δ ppm, 125 MHz, $CDCl_3$): 165.71, 163.90, 158.20, 156.36, 144.08, 1143.64, 129.73, 113.51, 112.07, 100.79, 56.07, 50.98, 48.09, 37.29, 33.42, 33.05, 32.57, 32.28, 31.82, 30.43, 29.08, 26.18, 25.46, 24.73, 14.90. HRMS-ESI: Calculated for $C_{18}H_{23}NNaO_4S_2$ $[M+Na]^+$ 404.09596, found 404.0960. R_f (deactivated silica gel, CH_2Cl_2/Hexane: 1/1): 0.26.

5.3 Synthesis of the Thiourea Based Series

General Procedures

A. The *N*-Boc protected amine (1 eq.) was solved in DMF and triethylamine (1.2 eq.) was added. The reaction mixture was stirred at room temperature for 30 min. The 4-bromo-1,8-naphthalic anhydride (1 eq.) was added as a solid and the reaction mixture was heated to 100°C for 48 h. The solvent was removed and the crude product was purified by column chromatography.

B. A solution of the *N*-Boc protected naphthalimide (1 eq.) and potassium carbonate (10 eq.) in 2-methoxyethanol was heated to 100 °C for 2 hours. After cooling to room temperature water was added and the product was extracted with CH_2Cl_2. The organic phase was washed with water, dried over $MgSO_4$ and concentrated under vacuum. The crude product was purified by column chromatography.

C. A solution of the *N*-Boc protected 4-(2-methoxyethoxy) naphthalimide (1eq.) in CH_2Cl_2 was cooled to 0°C and trifluoroacetic acid (25 eq.) was added. The reaction mixture was stirred for 2 hours at room temperature. The reaction was quenched by the adding of a solution of NaOH (2N) and the product was extracted with CH_2Cl_2. The organic phase was dried over $MgSO_4$ and concentrated under vacuum. The product was obtained without purification.

D. Phenylisothiocyanate (1 eq.) was added to a suspension of the free amino 4-(2-methoxyethoxy) naphthalimide (1 eq.) in acetonitrile. The reaction mixture was stirred at room temperature for 30 minutes. The solid was filtered and purified by recrystallization from isopropanol.

E. To a mixture of **94** (1 eq.) and acetonitrile was added a solution of the corresponding amine (1 eq.) in acetonitrile. The reaction mixture was refluxed and became clear. After cooling to room temperature, the reaction mixture was concentrated under vacuum. The residue was solved in CH_2Cl_2 (20 ml), washed with water, dried over $MgSO_4$ and concentrated under vacuum. The crude was purified to give the products as yellow solids.

5.3.1 N-Boc-1,2-diaminoethane 79

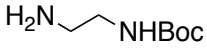

Prepared according to the literature:[123] 1,2-diaminoethane (14.0 ml, 209.77 mmol) was solved in chloroform (200 ml); di-*tert*-butyldicarbonate (4.37 g, 20.05 mmol) was solved in chloroform (100 ml); *N*-Boc-1,2-diaminoethane **79** is obtained without purification as a colorless oil (3.05 g, 95 %).

^{1}H NMR (δ ppm, 400 MHz, $CDCl_3$, 300 K): 4.92 (s, br, 1H), 3.15 (q, 2H, *J* = 5.8), 2.78 (t, 2H, *J* = 5.8), 1.43 (s, 9H), 1.19 (s, br, 2H). ^{13}C NMR (δ ppm, 100 MHz, $CDCl_3$): 156.3, 79.3, 43.6, 42.0, 28.5 (3).

5.3.2 4-Bromo-*N*-(*N*-Boc-aminoethyl)naphthalimide 82

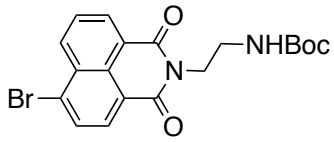

Prepared according to the general procedure A: *N*-Boc-1,2-diaminoethane **79** (400 mg, 2.71 mmol) was solved in DMF (20 ml); triethylamine (328 mg, 3.25 mmol); 4-bromo-1,8-naphthalic anhydride (750 mg, 2.71 mmol). The crude product was purified by column chromatography (eluent: CH_2Cl_2/MeOH: 99.5/0.5) to give the product **82** as a yellow solid (782 mg, 69 %).

^{1}H NMR (δ ppm, 400 MHz, $CDCl_3$): 8.66 (dd, 1H, *J* = 7.3, J = 0.9), 8.57 (dd, 1H, *J* = 8.4, *J* = 0.8), 8.42 (d, 1H, *J* = 7.8), 8.04 (d, 1H, *J* = 7.8), 7.86 (dd, 1H, *J* = 8.4, *J* = 7.3), 4.93 (s, br, 1H), 4.35 (t, 2H, *J* = 5.7), 3.55-3.52 (m, 2H), 1.28 (s, 9H). ^{13}C NMR (δ ppm, 125 MHz,): 164.15 (2), 156.20, 133.56, 132.39, 131.57, 131.26, 130.76, 130.57, 129.23, 128.23, 123.06, 122.19, 79.33, 40.16, 39.64, 28.33 (3). R_f (CH_2Cl_2/MeOH: 99.5/0.5): 0.23.

5.3.3 4-(2-methoxyethoxy)-*N*-(*N*-Boc-aminoethyl)naphthalimide 85

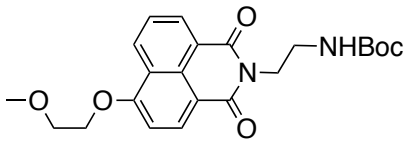

Prepared according to the general procedure B: **82** (800 mg, 1.90 mmol); potassium carbonate (2.63g, 19.00 mmol); methoxyethanol (50 ml). The crude product was purified by column

chromatography (eluent: CH_2Cl_2/AcOEt: 9/1) to give the product **85** as a light yellow solid (665 mg, 84 %).

^{1}H NMR (δ ppm, 400 MHz, $CDCl_3$): 8.61 (dd, 1H, *J* = 1.2, *J* = 8.3), 8.60 (dd, 1H, *J* = 1.2, *J* = 7.4), 8.54 (d, 1H, *J* = 8.3), 7.70 (dd, 1H, *J* = 7.4, *J* = 8.3), 7.04 (d, 1H, *J* = 8.3), 5.02 (s, 1H, br), 4.44-4.42 (m, 2H), 4.35 (t, 2H, *J* = 5.7), 3.95-3.93 (m, 2H), 3.54-3.49 (m, 5H), 1.31 (s, 9H). ^{13}C NMR (δ ppm, 100 MHz, $CDCl_3$): 165.03, 164.40, 160.28, 156.1, 133.74, 131.96, 129.67, 129.14, 126.07, 123.68, 122.34, 115.20, 106.13, 79.17, 70.81, 68.57, 59.53, 40.07, 39.80, 28.40 (3). IR (KBr) cm^{-1}: 3346m, 2979m, 2932m, 2889m, 1698s, 1655s, 1622m, 1595s, 1582s, 1535s, 1453m, 1428m, 1390s, 1362s, 1270s, 1237s, 1180s, 1129m, 1087m, 1054m, 1037m, 995w, 906w, 864m, 815s, 779m, 758w, 735w, 668w, 614w, 583w, 497w, 457w. HRMS-ESI: Calculated for $C_{22}H_{26}N_2NaO_6$ $[M+Na]^+$ 437.16831; found 437.16787. R_f (CH_2Cl_2/AcOEt: 9/1): 0.14.

5.3.4 4-(2-methoxyethoxy)-*N*-(aminoethyl)naphthalimide 88

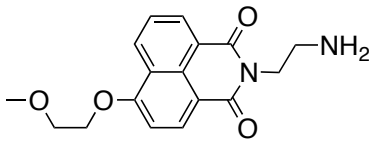

Prepared according to the general procedure C: **85** (640 mg, 1.54 mmol) in CH_2Cl_2 (5 ml); trifluoroacetic acid (4.40 g, 38.60 mmol). The product **88** was obtained without purification as a yellow solid (393 mg, 81 %).

^{1}H NMR (δ ppm, 400 MHz, $CDCl_3$): 8.62 (dd, 1H, *J* = 1.2, *J* = 8.3), 8.60 (dd, 1H, *J* = 1.2, *J* = 7.4), 8.54 (d, 1H, *J* = 8.3), 7.70 (dd, 1H, *J* = 7.4, *J* = 8.3), 7.04 (d, 1H, *J* = 8.3), 4.44-4.42 (m, 2H), 4.28 (t, 2H, *J* = 6.5), 3.95-3.93 (m, 2H), 3.52 (s, 3H), 3.08 (t, 2H, *J* = 6.5). ^{13}C NMR (δ ppm, 100 MHz, $CDCl_3$): 164.97, 164.36, 160.26, 133.65, 131.88, 129.64, 129.10, 126.09, 123.71, 122.42, 115.26, 106.14, 70.81, 68.56, 59.52, 43.12, 40.75. IR (KBr) cm^{-1}: 3366m, 3299w, 2953w, 2878w, 2821w, 1696s, 1656s, 1622m, 1514s, 1473m, 1457m, 1427m, 1386s, 1356s, 1310m, 1263s, 1233s, 1200m, 1172m, 1124s, 1106s, 1093s, 1075s, 1033s, 995m, 971w, 889m, 861m, 827w, 785s, 758m, 733m, 669w, 650w, 609w, 582w, 501w, 470w, 455w. HRMS-ESI: Calculated for $C_{17}H_{19}N_2O_4$ $[M+H]^+$ 315.13393; found 315.13342.

5.3.5 4-(2-methoxyethoxy)-*N*-(ethyl-3-phenylthiourea)naphthalimide PTU

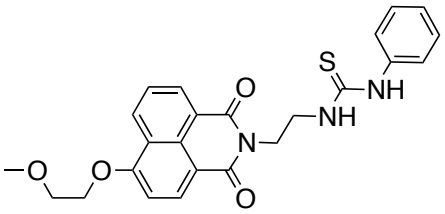

Prepared according to the general procedure D: Phenylisothiocyanate (86 mg, 0.64 mmol); **88** (200 mg, 0.64 mmol); acetonitrile (8 ml). The reaction mixture is stirred at room temperature for 30 minutes. The crude product was purified by recrystallization from isopropanol to give the product **PTU** as a cream white solid (185 mg, 65 %).

^{1}H NMR (δ ppm, 400 MHz, $CDCl_3$): 8.65 (dd, 1H, *J* = 1.2, *J* = 8.3), 8.54 (dd, 1H, *J* = 1.2, *J* = 7.4), 8.48 (d, 1H, *J* = 8.3), 7.72 (dd, 1H, *J* = 7.4, J = 8.3), 7.43-7.34 (m, 3H), 7,20 (s, br), 7.07 (d, 1H, *J* = 8.3), 6.85 (s, 1H, br), 4.46-4.41 (m, 4H), 4.01-3.94 (m, 4H), 3.53 (s, 3H). ^{13}C NMR (δ ppm, 125 MHz, $CDCl_3$): 181.36, 165.13, 164.46, 160.56, 136.05, 133.97, 132.11, 130.07 (2), 129.64, 129.54, 127.46, 126.14, 125.97 (2), 123.72, 121.99, 114.79, 106.20, 70.77, 68.62, 59.56, 45.98, 38.70. IR (KBr) cm^{-1}: 3361m, 3193m, 3003w, 2935w, 2885w, 1690s, 1651s, 1620m, 1595s, 1549s, 1515s, 1471m, 1453m, 1427m, 1398m, 1385s, 1362s, 1345s, 1321s, 1298m, 1271s, 1238s, 1202m, 1174m, 1124s, 1081s, 1033m, 991w, 933w, 873m, 843w, 835w, 781s, 756m, 736m, 728w, 695w, 678w, 639w, 609w, 569w, 508w, 490w. HRMS-ESI: Calculated for $C_{24}H_{23}N_3NaO_4S$ $[M+Na]^+$ 472.13015; found, 437.12983. R_f (deactivated silica gel, CH_2Cl_2/Hexane/Et_3N: 3.5/1.5/0.1): 0.42.

5.3.6 *N*-Boc-1,2-diaminopropane 80

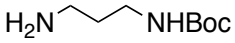

Prepared according to the literature:[125] 1,3-diaminopropane (16.97 g, 229.32 mmol) was solved in chloroform (200 ml); di-*tert*-butyldicarbonate (5.00 g, 22.94 mmol) was solved in chloroform (100 ml); *N*-Boc-1,3-diaminopropane **80** is obtained without purification as a colorless oil (3.50 g, 88 %).

^{1}H NMR (δ ppm, 400 MHz, $CDCl_3$, 300 K): 4.91 (s, br, 1H), 3.23-3.15 (m, 2H), 2.75 (t, 2H, *J* = 6.6), 1.60 (quint, 2H, *J* = 6.6), 1.43 (s, 9H), 1.29 (s, br, 2H). ^{13}C NMR (δ ppm, 100 MHz, $CDCl_3$): 156.1, 79.1, 39.7, 38.5, 33.4, 28.4 (3).

5.3.7 4-Bromo-*N*-(*N*-Boc-aminopropyl)naphthalimide 83

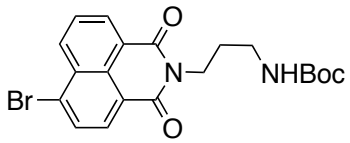

Prepared according to the general procedure A: *N*-Boc-1,3-diaminopropane **80** (1.00 g, 5.74 mmol) was solved in DMF (20 ml); triethylamine (0.58 g, 5.74 mmol); 4-bromo-1,4-naphthalic anhydride (1.59 g, 5.74 mmol) The crude product was purified by column chromatography (eluent: CH_2Cl_2/MeOH: 99.5/0.5) to give the product **83** as a yellow solid (2.38 g, 94 %).

^{1}H NMR (δ ppm, 400 MHz, $CDCl_3$): 8.66 (dd, 1H, *J* = 7.3, J = 1.2), 8.58 (dd, 1H, *J* = 8.5, *J* = 1.2), 8.41 (d, 1H, *J* = 7.8), 8.05 (d, 1H, *J* = 7.8), 7.85 (dd, 1H, *J* = 8.5, *J* = 7.3), 5.20 (s, br, 1H), 4.26 (t, 2H, *J* = 6.6), 3.19-3.14 (m, 2H), 1.93 (quint, 2H, *J* = 6.5), 1.45 (s, 9H). ^{13}C NMR (δ ppm, 125 MHz, $CDCl_3$): 163.95 (2), 155.99, 133.51, 132.25, 131.42, 131.16, 130.67, 130.53, 129.02, 128.14, 122.87, 122.00, 79.08, 37.75(2), 37.46, 28.43 (3). IR (KBr) cm^{-1}: 3359m, 2968m, 2926w, 1704s, 1684s, 1652s, 1618m, 1592m, 1571m, 1526s, 1460m, 1447m, 1436m, 1361s, 1349s, 1283s, 1269s, 1251m, 1230s, 1171s, 1101m, 1080m, 1065m, 1044m, 1001w, 900m, 855w, 782s, 750w, 731w, 714w, 635w, 568w. HRMS-ESI: Calculated for $C_{20}H_{21}BrN_2NaO_4$ $[M+Na]^+$ 455.05769; found 455.05746. R_f (CH_2Cl_2/MeOH: 99.5/0.5): 0.23.

5.3.8 4-(2-methoxyethoxy)-*N*-(*N*-Boc-aminopropyl)naphthalimide 86

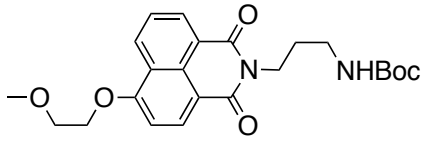

Prepared according to the general procedure B: **83** (1.00 g, 2.30 mmol); potassium carbonate; (3.18 g, 23.00 mmol); methoxyethanol (60 ml). The crude product was purified by column chromatography (eluent: CH_2Cl_2/MeOH: 99/1) to give the product **86** as a light yellow solid (720 mg, 73 %).

^{1}H NMR (δ ppm, 500 MHz, $CDCl_3$): 8.63 (dd, 1H, *J* = 1.2, *J* = 8.3), 8.61 (dd, 1H, *J* = 1.2, *J* = 7.4), 8.55 (d, 1H, *J* = 8.3), 7.72 (dd, 1H, *J* = 7.4, *J* = 8.3), 7.06 (d, 1H, *J* = 8.3), 5.31 (s, 1H, br), 4.45-4.43 (m, 2H), 4.26 (t, 2H, *J* = 6.5), 3.95-3.93 (m, 2H), 3.52 (s, 3H), 3.18-3.14 (m, 2H), 1.93 (quint, 2H, *J* = 6.4), 1.45 (s, 9H). ^{13}C NMR (δ ppm, 100 MHz, $CDCl_3$): 164.97,

164.37, 160.33, 156.19, 133.72, 131.92, 129.60, 129.19, 126.12, 123.71, 122.33, 115.16, 106.18, 79.09, 70.80, 68.59, 59.52, 37.56 (3), 28.60 (3). IR (KBr) cm^{-1}: 3309m, 2930m, 2895w, 2819w, 1688s, 1658s, 1623w, 1598m, 1538m, 1442m, 1398m, 1363s, 1324w, 1290m, 1267m, 1244s, 1180m, 1165m, 1127s, 1097m, 1084m, 1060w, 1036w, 982w, 937w, 893w, 864w, 845w, 821w, 781s, 756m, 736w, 691w, 669w, 617w, 582w, 508w. HRMS-ESI: Calculated for $C_{23}H_{28}N_2NaO_6$ $[M+Na]^+$ 451.18369; found 451.18363. R_f (CH_2Cl_2/AcOEt: 9/1): 0.16.

5.3.9 4-(2-methoxyethoxy)-*N*-(aminopropyl)naphthalimide 89

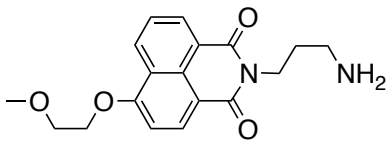

Prepared according to the general procedure C: **86** (350 mg, 0.82 mmol) in CH_2Cl_2 (8 ml); trifluoroacetic acid (2.33 g, 38.60 mmol). The product **89** was obtained without purification as a yellow solid (220 mg, 81 %).

^{1}H NMR (δ ppm, 500 MHz, $CDCl_3$): 8.63 (dd, 1H, *J* = 1.2, J = 8.3), 8.61 (dd, 1H, *J* = 1.2, *J* = 7.4), 8.55 (d, 1H, *J* = 8.3), 7.72 (dd, 1H, *J* = 7.4, J = 8.3), 7.06 (d, 1H, *J* = 8.3), 4.45-4.42 (m, 2H), 4.28 (t, 2H, *J* = 6.8), 3.95-3.93 (m, 2H), 3.53 (s, 3H), 2.76 (t, 2H, *J* = 6.7). ^{13}C NMR (δ ppm, 125 MHz, $CDCl_3$): 164.86, 164.27, 160.23, 133.63, 131.86, 129.59, 129.11, 126.12, 123.69, 122.43, 115.29, 106.12, 70.80, 68.54, 59.55, 39.54, 37.66, 32.26. IR (KBr) cm^{-1}: 3372w, 3308w, 2955w, 2934w, 2896w, 2866,w 2822w, 1695s, 1658s, 1621m, 1594s, 1579m, 1515w, 1472w, 1454w, 1431m, 1389s, 1354s, 1271s, 1240m, 1199m, 1129m, 1094m, 1044m, 1034m, 902m, 863m, 828w, 782s, 758m, 677w, 665w, 606w, 583w, 500w, 461w. HRMS-ESI: Calculated for $C_{18}H_{20}N_2O_4$ $[M+H]^+$ 329.14958; found 329.14967.

5.3.10 4-(2-methoxyethoxy)-*N*-(propyl-3-phenylthiourea)naphthalimide PTU3C

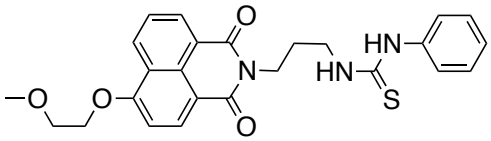

Prepared according to the general procedure D: Phenylisothiocyanate (37 mg, 0.27 mmol); **89** (90 mg, 0.27 mmol); acetonitrile (6 ml). The reaction mixture is stirred at room temperature

for 30 minutes. The crude product **PTU3C** was purified by recrystallization from isopropanol to give the product as a yellow solid (75 mg, 59 %).

^{1}H NMR (δ ppm, 400 MHz, $CDCl_3$): 8.63 (d, 1H, *J* = 8.3), 8.52 (d, 1H, *J* = 7.4), 8.46 (d, 1H, *J* = 8.3), 7.70 (dd, 1H, *J* = 7.4, *J* = 8.3), 7.56 (s, 1H, br), 7.52-7.48 (m, 2H), 7.35-7.30 (m, 3H), 7.05 (d, 1H, *J* = 8.3), 4.44-4.42 (m, 2H), 4.16 (t, 2H, *J* = 6.1), 3.95-3.93 (m, 2H), 3.69-3.67 (m, 2H), 3.52 (s, 3H), 2.09-2.06 (m, 2H). ^{13}C NMR (δ ppm, 125 MHz, $CDCl_3$): 180.64, 165.05, 164.41, 160.42, 136.29, 133.87, 132.03, 130.21 (2), 129.52, 129.45, 127.19, 126.10, 125.32 (2), 123.64, 122.08, 114.88, 106.14, 70.75, 68.57, 59.54, 42.30, 37.36, 27.45. IR (KBr) cm^{-1}: 3308m, 3198m, 3104w, 3025w, 2932w, 1689s, 1653s, 1591s, 1548s, 1532s, 1513s, 1457m, 1395s, 1376m, 1357s, 1343s, 1327s, 1315s, 1266s, 1237s, 1171s, 1123m, 1081s, 1051m, 985m, 955m, 900w, 861m, 818m, 787m, 761m, 728m, 675m, 604w, 596w, 500w. HRMS-ESI: Calculated for $C_{25}H_{25}N_3NaO_4S$ $[M+Na]^+$ 486.1458; found, 486.14522. R_f (deactivated silica gel, CH_2Cl_2/Hexane/Et_3N: 3.5/1.5/0.1): 0.44.

5.3.11 *N*-Boc-1,2-diaminobutane 81

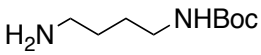

Prepared according to the literature:[126] 1,4-diaminobutane (10.15 g, 115.14 mmol) was solved in chloroform (100 ml); di-*tert*-butyldicarbonate (2.50 g, 11.47 mmol) was solved in chloroform (50 ml); *N*-Boc-1,4-diaminobutane **81** is obtained without purification as a light yellow oil (1.80 g, 83 %).

^{1}H NMR (δ ppm, 400 MHz, $CDCl_3$, 300 K): 4.61 (s, br, 1H), 3.15-3.11 (m, 2H), 2.71 (t, 2H, *J* = 6.6), 1.50-1.46 (m, 4H), 1.44 (s, 9H), 1.31 (s, br, 2H). ^{13}C NMR (δ ppm, 100 MHz, $CDCl_3$): 156.1, 79.1, 42.0, 40.6, 31.0, 28.6 (3), 27.6.

5.3.12 4-Bromo-*N*-(*N*-Boc-aminobutyl)naphthalimide 84

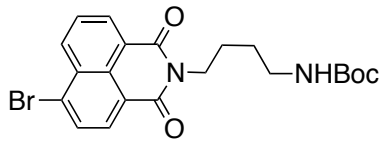

Prepared according to the general procedure A: *N*-Boc-1,4-diaminobutane **81** (1.30 g, 6.91 mmol) was solved in DMF (20 ml); triethylamine (0.70 g, 6.91 mmol); 4-bromo-1,4-naphthalic anhydride (1.91 g, 6.90 mmol). The crude product was purified by

column chromatography (eluent: CH_2Cl_2/MeOH: 99.5/0.5) to give the product **84** as a light yellow solid (2.10 g, 68 %).

^{1}H NMR (δ ppm, 400 MHz, $CDCl_3$): 8.65 (dd, 1H, *J* = 7.3, *J* = 1.1), 8.57 (dd, 1H, *J* = 8.5, *J* = 1.1), 8.41 (d, 1H, *J* = 7.8), 8.04 (d, 1H, *J* = 7.8), 7.85 (dd, 1H, *J* = 8.5, *J* = 7.3), 4.61 (s, br, 1H), 4.19 (t, 2H, *J* = 7.4), 3.20 (q, 2H, *J* = 6.5), 1.80-1.73 (m, 2H), 1.65-1.57 (m, 2H), 1.43 (s, 9H). ^{13}C NMR (δ ppm, 125 MHz, $CDCl_3$): 163.77 (2), 156.08, 133.47, 132.23, 131.41, 131.26, 130.81, 130.46, 129.17, 128.24, 123.22, 122.35, 79.23, 40.36, 40.18, 28.56 (3), 27.73, 25.55. IR (KBr) cm^{-1}: 3358m, 2971w, 2934w, 1703s, 1682s, 1650s, 1591m, 1570m, 1532m, 1460w, 1435w, 1389m, 1364m, 1263m, 1233m, 1177m, 1104w, 1066m, 996w, 949w, 878w, 857w, 783m, 753w, 732w, 711w, 631w, 568w. HRMS-ESI: Calculated for $C_{21}H_{23}BrN_2NaO_4$ $[M+Na]^+$ 469.07334; found 469.07344. R_f (CH_2Cl_2/MeOH: 99.5/0.5): 0.23.

5.3.13 4-(2-methoxyethoxy)-*N*-(*N*-Boc-aminobutyl)naphthalimide 87

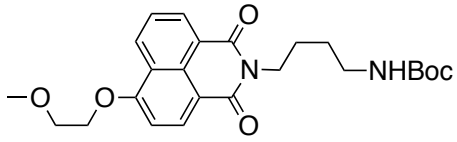

Prepared according to the general procedure B: **84** (1.75 g, 3.91 mmol); potassium carbonate (5.4 g, 39.10 mmol); methoxyethanol (60 ml). The crude product was purified by column chromatography (eluant: CH_2Cl_2/AcOEt: 9/1) to give the product **87** as a light yellow solid (1.37 g, 79 %).

^{1}H NMR (δ ppm, 500 MHz, $CDCl_3$): 8.62 (dd, 1H, *J* = 1.2, *J* = 8.3), 8.61 (dd, 1H, *J* = 1.2, *J* = 7.4), 8.54 (d, 1H, *J* = 8.3), 7.71 (dd, 1H, *J* = 7.4, *J* = 8.3), 7.06 (d, 1H, *J* = 8.3), 4.63 (s, 1H, br), 4.45-4.43 (m, 2H), 4.18 (t, 2H, *J* = 7.4), 3.95-3.93 (m, 2H), 3.52 (s, 3H), 3.20-3.19 (m, 2H), 1.80-1.74 (m, 2H), 1.64-1.58 (m, 2H), 1.43 (s, 9H). ^{13}C NMR (δ ppm, 100 MHz, $CDCl_3$): 164.65, 164.05, 160.18, 156.08, 133.51, 131.76, 129.56, 129.00, 126.07, 123.69, 122.49, 115.35, 106.11, 79.14, 70.81, 68.54, 59.52, 40.39, 39.86, 28.56 (3), 27.69, 25.63. IR (KBr) cm^{-1}: 3347m, 2980m, 2936m, 2893w, 1683s, 1652s, 1623m, 1596m, 1541s, 1453m, 1393s, 1358s, 1292m, 1274s, 1248s, 1175s, 1125m, 1097m, 1085m, 1052m, 1032m, 996w, 905w, 854w, 814w, 779m, 757m, 667w, 647w, 611w, 583w, 504w. HRMS-ESI: Calculated for $C_{24}H_{30}N_2NaO_6$ $[M+Na]^+$ 465.19961; found 465.19935. R_f (CH_2Cl_2/AcOEt: 9/1): 0.16.

5.3.14 4-(2-methoxyethoxy)-*N*-(aminobutyl)naphthalimide 90

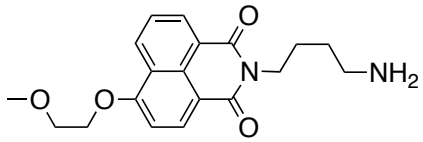

Prepared according to the general procedure C: **87** (560 mg, 1.26 mmol) in CH_2Cl_2 (10 ml); trifluoroacetic acid (3.6 g, 31.60 mmol). The product **90** was obtained without purification as a yellow solid (560 mg, 84 %).

^{1}H NMR (δ ppm, 500 MHz, $CDCl_3$): 8.57 (dd, 1H, *J* = 1.2, *J* = 8.3), 8.55 (dd, 1H, *J* = 1.2, *J* = 7.4), 8.49 (d, 1H, *J* = 8.3), 7.67 (dd, 1H, *J* = 7.4, J = 8.3), 7.02 (d, 1H, *J* = 8.3), 4.42-4.40 (m, 2H), 4.17 (t, 2H, *J* = 7.3), 3.94-3.92 (m, 2H), 3.52 (s, 3H), 2.91 (t, 2H, *J* = 7.0), 1.85-1.79 (m, 2H), 1.72-1.66 (m, 2H). ^{13}C NMR (δ ppm, 100 MHz, $CDCl_3$): 164.69, 164.10, 160.18, 133.50, 131.76, 129.57, 129.00, 126.08, 123.70, 122.52, 115.39, 106.12, 70.80, 68.54, 59.52, 41.92, 40.04, 31.07, 25.54. IR (KBr) cm^{-1}: 3340w, 2928w, 1694s, 1657s, 1622m, 1594s, 1514m, 1454m, 1429m, 1389s, 1354s, 1271s, 1240m, 1200m, 1181m, 1129m, 1094m, 1080m, 1032m, 1053m, 942w, 902w, 860w, 832w, 802w, 782m, 758w, 736w, 722w, 667w, 609w, 581w, 496w. HRMS-ESI: Calculated for $C_{19}H_{22}N_2O_4$ $[M+H]^+$ 343.16523; found 343.6529.

5.3.15 4-(2-methoxyethoxy)-*N*-(butyl-3-phenylthiourea)naphthalimide PTU4C

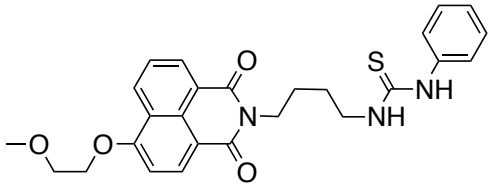

Prepared according to the general procedure D: Phenylisothiocyanate (100 mg, 0.73 mmol); **90** (252 mg, 0.73 mmol); acetonitrile (10 ml). The reaction mixture is stirred at room temperature for 30 minutes. The crude product was purified by recrystallization from isopropanol to give the product **PTU4C** as a cream white solid (175 mg, 50 %).

^{1}H NMR (δ ppm, 400 MHz, $CDCl_3$): 8.63 (dd, 1H, *J* = 1.2, *J* = 8.3), 8.56 (dd, 1H, *J* = 1.2, *J* = 7.4), 8.49 (d, 1H, *J* = 8.3), 7.71 (dd, 1H, *J* = 7.4, *J* = 8.3), 7.56 (s, 1H, br), 7.44-7.40 (m, 2H), 7.31-7.22 (m, 3H), 7.05 (d, 1H, *J* = 8.3), 6.26 (s, 1H, br), 4.45-4.43 (m, 2H), 4.17 (t, 2H, *J* = 7.0), 3.95-3.93 (m, 2H), 3.78-3.73 (m, 2H), 3.52 (s, 3H), 1.81-1.68 (m, 4H). ^{13}C NMR (δ

ppm, 125 MHz, $CDCl_3$): 180.90, 164.69, 164.09, 160.27, 136.25, 133.65, 131.86, 130.33 (2), 129.56, 129.16, 127.41, 126.09, 125.58 (2), 123.68, 122.36, 115.21, 106.10, 70.79, 68.55, 59.56, 45.09, 39.50, 26.40, 25.50. IR (KBr) cm^{-1}: 3379m, 3159m, 2933m, 1692s, 1650s, 1595s, 1578s, 1541s, 1513s, 1450m, 1397s, 1386s, 1358s, 1320s, 1266s, 1235s, 1189m, 1126s, 1087s, 1060m, 1029m, 901w, 859w, 813w, 781s, 757m, 739m, 694m, 667w, 642w, 617w, 605w, 512w. HRMS-ESI: Calculated for $C_{26}H_{27}N_3NaO_4S$ $[M+Na]^+$ 500.16145; found, 500.16158. R_f (deactivated silica gel, CH_2Cl_2/Hexane/Et_3N: 3.5/1.5/0.1): 0.36.

5.3.16 4-(2-methoxyethoxy)-*N*-propylnaphthalimide 49

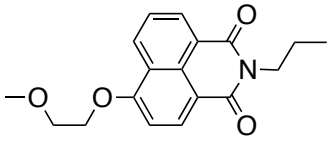

Prepared according to the general procedure B: **46** (100 mg, 0.32 mmol); potassium carbonate (435 mg, 19.00 mmol); methoxyethanol (10 ml). The crude product was purified by column chromatography (eluent: CH_2Cl_2 to CH_2Cl_2/MeOH: 99/1) to give the product **49** as a light yellow solid (71 mg, 72 %).

^1H NMR (δ ppm, 400 MHz, $CDCl_3$): 8.67-8.59 (m, 2H), 8.55 (d, 1H, J = 8.2), 7.71 (t, 1H, J = 7.8), 7.05 (d, 1H, J = 8.3), 4.51-4.36 (m, 2H), 4.17-4.18 (m, 2H), 4.04-3.87 (m, 2H), 3.52 (s, 3H), 1.88-1.66 (m, 2H), 1.01 (t, 3H, J = 7.4). ^{13}C NMR (δ ppm, 125 MHz, $CDCl_3$): 164.73, 164.15, 160.13, 133.47, 131.75, 129.62, 128.93, 126.09, 123.73, 122.65, 115.53, 106.11, 70.84, 68.54, 59.55, 41.96, 21.59, 11.70. IR (KBr) cm^{-1}: 2960w, 2931w, 2900w, 2875w, 1699s, 1660s, 1595s, 1580m, 1514w, 1455m, 1432m, 1387s, 1354s, 1287s, 1236s, 1200m, 1130m, 1091s, 1045m, 1037m, 908w, 887w, 781s, 758m, 677w, 666w, 609w, 583w, 498w. HRMS-ESI: Calculated for $C_{18}H_{19}NNaO_4$ $[M+Na]^+$ 336.12063, found 336.12065. R_f (CH_2Cl_2/MeOH: 99/1): 0.28.

5.3.17 4-(2-methoxyethoxy)-*N*-(ethyl-(imidazole-1-carbothioamide)naphthalimide 94

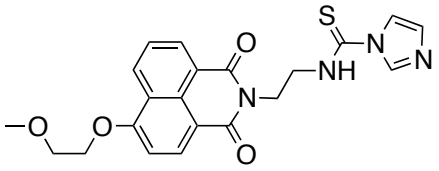

1,1- Thiocarbonyldiimidazole (187 mg, 1.05 mmol) and **88** (330 mg, 1.05 mmol) were mixed in acetonitrile (5 ml). The reaction mixture was stirred for 1 hour at room temperature and the solid was filtered. **94** was obtained as a yellow solid without any further purification (365 g, 82 %).

^{1}H NMR (δ ppm, 400 MHz, $CDCl_3$): 9.13 (s, 1H), 8.62 (dd, 1H, *J* = 1.2, *J* = 8.3), 8.60 (dd, 1H, *J* = 1.2, *J* = 7.4), 8.54 (d, 1H, *J* = 8.3), 8.42 (s, 1H), 7.70 (dd, 1H, *J* = 7.4, *J* = 8.3), 7.64 (s, 1H), 7.04 (d, 1H, *J* = 8.3), 4.63-4.60 (m, 2H), 4.47-4.44 (m, 2H), 4.05-4.04 (m, 2H), 3.96-3.93 (m, 2H), 3.52 (s, 3H). ^{13}C NMR (δ ppm, 100 MHz, $CDCl_3$): 165.95, 161.09, 136.67, 134.64, 132.62, 130.08, 129.66, 126.35, 123.73, 121.69, 116.98, 114.37, 106.48, 70.73, 68.77, 59.55, 47.82, 38.77. HRMS-ESI: Calculated for $C_{21}H_{20}N_4O_4S$ $[M+H]^+$ 425.12780; found, 425.12724.

5.3.18 4-(2-methoxyethoxy)-*N*-(ethyl-1,1'bis(pyridin-2-ylmethyl)thiourea)naphthalimide DiPic

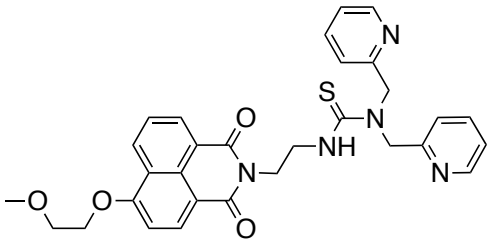

Prepared according to the general procedure E: **94** (150 mg, 0.35 mmol); acetonitrile (10 ml); di-(2-picolyl)amine (70 mg, 0.35 mmol); acetonitrile (3 ml). The reaction mixture is stirred for 1 hour at reflux. The crude product was purified by column chromatography (silica gel deactivated with 20% Et_3N, eluent: CH_2Cl_2/hexane/Et_3N: 3.5/1.5/0.1) to give the product **DiPic** as a yellow solid (180 mg, 82 %).

^{1}H NMR (δ ppm, 500 MHz, $CDCl_3$): 8.77 (t, 1H, *J* = 4.8), 8.63 (dd, 1H, *J* = 1.2, *J* = 8.4), 8.52 (dd, 1H, *J* = 1.2, *J* = 7.3), 8.48 (d, 1H, *J* = 8.3), 8.32-8.28 (m, 2H), 7.68 (dd, 1H, *J* = 7.3, *J* = 8.4), 7.48 (td, *J* = 1.8, *J* = 7.6, 2H), 7.26-7.23 (m, 2H), 7.06-7.02 (m, 3H), 4.97 (s, 4H), 4.55-

4.53 (m, 2H), 4.45-4.42 (m, 2H), 4.16-4.12 (m, 2H), 3.96-3.93 (m, 2H), 3.53 (s, 3H). ^{13}C NMR (δ ppm, 100 MHz, $CDCl_3$): 184.94, 165.08, 164.42, 160.27 (3), 149.03 (2), 136.93 (2), 133.70, 131.92, 129.67, 129.13, 126.09, 123.70, 122.89 (2), 122.54 (2), 122.44, 115.27, 106.15, 70.82, 68.60, 59.54, 45.92, 45.56 (2), 39.62. IR (KBr) cm^{-1}: 3374w, 2924m, 1695s, 1656s, 1592s, 1516m, 1473m, 1440m, 1384s, 1355s, 1267s, 1325s, 1201m, 1179m, 1125m, 1081s, 1031m, 992m, 936m, 859w, 779m, 755m, 661w, 614w, 539w, 498w. HRMS-ESI: Calculated for $C_{30}H_{29}N_5O_4S$ $[M+H]^+$ 556.2013; found 556.20181. R_f (deactivated silica gel, CH_2Cl_2/Hexane/Et_3N: 3.5/1.5/0.1): 0.26.

5.3.19 4-(2-methoxyethoxy)-*N*-(ethyl-1-methyl-1-(pyridin-2-ylmethyl)thiourea) naphthalimide MePic

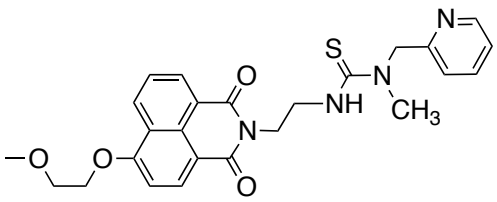

Prepared according to the general procedure E: **94** (150 mg, 0.35 mmol); acetonitrile (10 ml); 2-[(Methylamino)methyl]pyridine (43 mg, 0.35 mmol); acetonitrile (3 ml). The reaction mixture is stirred for 1 hour at reflux. The crude product was purified by column chromatography (silica gel deactivated with 20% Et_3N, CH_2Cl_2/hexane/Et_3N: 3.5/1.5/0.1) to give the product **MePic** as a yellow solid (138 mg, 82 %).

^{1}H NMR (δ ppm, 400 MHz, $CDCl_3$): 8.65 (dd, 1H, *J* = 1.2, *J* = 8.4), 8.58 (dd, 1H, *J* = 1.2, *J* = 7.3), 8.53 (d, 1H, *J* = 8.3), 8.44-8.43 (m, 1H), 7.72 (dd, 1H, *J* = 7.3, *J* = 8.4), 7.58 (td, *J* = 1.6, *J* = 7.6, 1H), 7.37-7.32 (m, 2H), 7.14-7.11 (m, 1H), 7.06 (d, 1H, *J* = 8.4), 5.13 (s, 2H), 4.55-4.52 (m, 2H), 4.46-4.43 (m, 2H), 4.04-4.01 (m, 2H), 3.96-3.94 (m, 2H), 3.53 (s, 3H), 3.21 (s, 3H). ^{13}C NMR (δ ppm, 100 MHz, $CDCl_3$): 182.92, 165.60, 164.97, 160.61 (2), 149.27, 136.98, 134.03, 132.17, 129.66, 129.53, 126.20, 123.74, 122.50, 122.26, 122.13, 114.93, 106.29, 70.79, 68.67, 59.55, 58.63, 47.38 (2), 39.39. IR (KBr) cm^{-1}: 3343w, 2925w, 1693s, 1652s, 1621m, 1593s, 1534s, 1472m, 1436m, 1386s, 1354s, 1269s, 1236s, 1179m, 1125m, 1081s, 1031m, 982m, 934w, 869w, 779m, 756m, 647w, 580w, 494w. HRMS-ESI: Calculated for $C_{25}H_{26}N_4O_4S$ $[M+H]^+$ 479.17475; found 479.17452. R_f (deactivated silica gel, CH_2Cl_2/Hexane/Et_3N: 3.5/1.5/0.1): 0.26.

5.3.20 Thiacrown amine

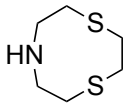

Prepared according to the literature.[137] The ^{1}H NMR is consistent with previously reported data.[135]

^{1}H NMR (δ ppm, 400 MHz, $CDCl_3$): 3.02-2.99 (m, 8H), 2.82-2.79 (m, 4H).

5.3.21 4-(2-methoxyethoxy)-*N*-(ethyl-1,4,7-dithiazonane-7-carbothioamide NS2

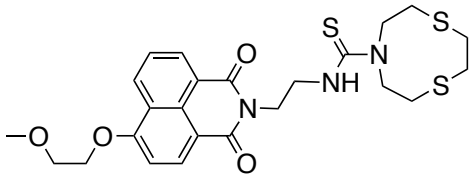

Prepared according to the general procedure E: **94** (50 mg, 0.12 mmol); acetonitrile (3 ml); thiacrown amine (19 mg, 0.12 mmol); acetonitrile (3 ml). The reaction mixture is stirred for 30 minutes at reflux. The solvent was removed under vacuum and the solid crude product was washed with acetonitrile and purified by recrystallization from isopropanol to give the product **NS2** (42 mg, 69 %) as a yellow solid.

^{1}H NMR (δ ppm, 400 MHz, $CDCl_3$): 8.66 (dd, 1H, J = 1.2, J = 8.4), 8.62 (dd, 1H, J = 1.2, J = 7.4), 8.56 (d, 1H, J = 8.3), 7.73 (dd, 1H, J = 7.4, J = 8.4), 7.33 (s, 1H), 7.07 (d, 1H, J = 8.4), 4.55-4.53 (m, 2H), 4.45-4.43 (m, 2H), 4.02-3.94 (m, 8H), 3.53 (s, 3H), 3.31-3.30 (m, 2H), 2.80 (s, 4H). ^{13}C NMR (δ ppm, 100 MHz, $CDCl_3$): 183.95, 165.35, 164.76, 160.47, 133.87, 132.00, 129.51, 129.41, 126.06, 123.60, 122.00, 114.79, 106.14, 70.62, 68.49, 59.39, 56.48 (2), 46.75, 39.16, 34.03, 30.72 (2), 25.36. IR (KBr) cm^{-1}: 3399m, 2921w, 1691s, 1647s, 1619m, 1594s, 1580s, 1525s, 1470m, 1441m, 1421m, 1384s, 1345s, 1330s, 1265s, 1238s, 1198m, 1166m, 1134s, 1082s, 1054m, 1031m, 950w, 905w, 841w, 778m, 755w, 733w, 675w, 645w, 579w, 488w. HRMS-ESI: Calculated for $C_{24}H_{29}N_3NaO_4S_3$ $[M+Na]^+$ 542.12124; found 542.12083. R_f (deactivated silica gel, CH_2Cl_2/Hexane/Et_3N: 3.5/1.5/0.1): 0.64.

5.3.22 4-(2-methoxyethoxy)-*N*-(ethyl-3-(2-(pyridin-2-yl)ethyl)thiourea)naphthalimide HomoPic

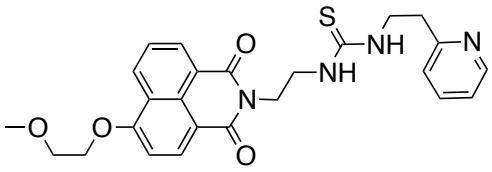

Prepared according to the general procedure E: **94** (150 mg, 0.35 mmol); acetonitrile (10 ml); 2-(aminoethyl)pyridine (43 mg, 0.35 mmol); acetonitrile (3 ml). The reaction mixture is stirred for 1 hour at reflux. The solvent was removed under vacuum and the solid crude product was washed with acetonitrile and purified by recrystallization from isopropanol to give the product **HomoPic** as a yellow solid (96 mg, 57 %).

^{1}H NMR (δ ppm, 500 MHz, $CDCl_3$): 8.64 (dd, 1H, *J* = 1.2, *J* = 8.4), 8.60 (dd, 1H, *J* = 1.2, *J* = 7.3), 8.55 (d, 1H, *J* = 8.3), 8.54-8.52 (m, 1H), 7.72 (dd, 1H, *J* = 7.3, *J* = 8.4), 7.63 (td, *J* = 1.6, *J* = 7.6, 1H), 7.24-7.22 (m, 2H), 7.16-7.13 (m, 1H), 7.06 (d, 1H, *J* = 8.4), 5.13, 4.46-4.42 (m, 4H), 3.96-3.93 (m, 4H), 3.80-3.70 (m, 2H), 3.53 (s, 3H), 3.15-3.12 (m, 2H). ^{13}C NMR (δ ppm, 100 MHz, $CDCl_3$): 181.71, 165.29, 164.66, 160.36 (2), 149.30, 136.80, 134.11, 132.20, 129.61, 126.17, 123.68, 123.64, 121.95, 121.76, 114.73, 106.25, 70.76, 68.63, 59.56, 53.58, 38.79, 36.67, 25.51. IR (KBr) cm^{-1}: 3350m, 3210w, 2928w, 1692s, 1657s, 1593s, 1581s, 1518s, 1474m, 1425m, 1386s, 1346s, 1272s, 1239s, 1196m, 1124m, 1083s, 1054m, 997w, 873w, 857w, 780m, 758m, 711w, 674w, 581w, 493w. HRMS-ESI: Calculated for $C_{25}H_{26}N_4O_4S$ $[M+H]^+$ 479.17475; found 479.17497. R_f (deactivated silica gel, CH_2Cl_2/Hexane/Et_3N: 3.5/1.5/0.1): 0.09.

5.3.23 *N*-(phenyl-1,1'bis(pyridin-2-ylmethyl)thiourea 107

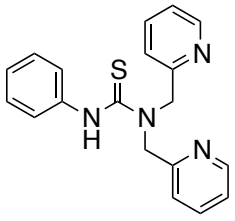

Prepared according to the general procedure D: Phenylisothiocyanate (34 mg, 0.16 mmol); di-(2-picolyl)amine (50 mg, 0.16 mmol); acetonitrile (8 ml). The reaction mixture is stirred at room temperature for 30 minutes. The crude product was purified by column chromatography (CH_2Cl_2/hexane: 7/3) to give the product **107** as a white solid (69 mg, 82 %).

^{1}H NMR (δ ppm, 400 MHz, $CDCl_3$): 11.52 (s, 1H), 8.60 (s, 2H), 7.66 (dt, 2H, *J* = 1.2, *J* = 8.4), 7.58 (d, 2H, *J* = 7.3), 7.38 (m, 4H), 7.27 (m, 2H), 7.17 (m, 1H), 5.11 (s, 4H). ^{13}C NMR (δ ppm, 100 MHz, $CDCl_3$): 184.67, 156.79, 148.89, 141.01, 137.30, 128.59, 124.74, 124.17, 123.59, 123.04, 56.17. IR (KBr) cm^{-1}: 3207w, 2948m, 1594s, 1569s, 1498s, 1475s, 1436s, 1398s, 1349s, 1268m, 1197s, 1152w, 1098w, 1007m, 993w, 839w, 735m, 691w, 627w, 550w. R_f (CH_2Cl_2/Hexane: 7/3): 0.15.

5.4 Synthesis or the Second Series of Thiourea

5.4.1 *N,N*-di-(2-picolyl)-*N'*-Boc-ethylenediamine 109

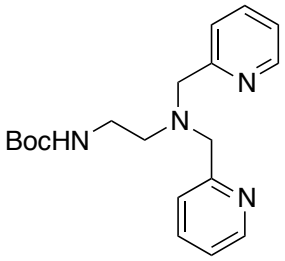

Prepared according to the literature:[142] 2-chloromethylpyridine hydrochloride (451 mg, 2.75 mmol) and Na_2CO_3 (530 mg, 5.00 mmol) were added to a solution of *N*-Boc-1,2-diaminoethane **79** (200 mg, 1.25 mmol) in methanol (20 ml), and the reaction mixture was heated to reflux for 48 hours. A 2N solution of NaOH (20 ml) was added and the product was extracted with CH_2Cl_2. The organic phase was swashed with brine, dried over $MgSO_4$ and concentrated under vacuum. The crude product was purified by column chromatography (aluminum oxide; eluent: Hexane/CH_2Cl_2: 1/1 and increase polarity to CH_2Cl_2/MeOH: 99/1) to give the product **109** as a brown-yellow oil (220 mg, 52 %).

^{1}H NMR (δ ppm, 400 MHz, $CDCl_3$): 8.55 (ddd, 2H, *J* = 4.9, *J* = 1.8, *J* = 0.9), 7.64 (td, 2H, *J* = 7.6, *J* = 1.8), 7.43 (d, 2H, *J* = 7.8), 7.16 (ddd, 2H, *J* = 7.5, *J* = 4.9, *J* = 1.2), 5.80 (s, 1H), 3.89 (s, 4H), 3.25-3.22 (m, 2H), 2.75-2.72 (m, 2H), 1.44 (s, 9H). ^{13}C NMR (δ ppm, 125 MHz, $CDCl_3$): 159.19 (2), 156.24, 149.14 (2), 136.52 (2), 123.16 (2), 122.14 (2), 78.75, 60.20 (2), 53.51, 38.49, 28.54 (3). HRMS-ESI: Calculated for $C_{19}H_{27}N_4O_2$ $[M+H]^+$ 343.21333, found 343.21285, calculated for $C_{19}H_{27}N_4NaO_2$ $[M+Na]^+$ 365.19510, found 365.19480. R_f (CH_2Cl_2/MeOH: 99/1): 0.2.

5.4.2 *N,N*-di-(2-picolyl)ethylenediamine 110

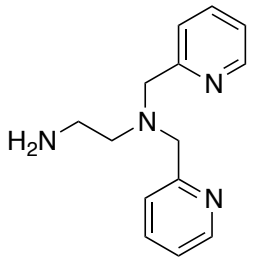

Prepared according to the general procedure D: **109** (80 mg, 0.23 mmol) in CH_2Cl_2 (2 ml); trifluoroacetic acid (660 mg, 5.85 mmol). The product **110** was obtained without purification as a yellow oil (48 mg, 85 %).

^{1}H NMR (δ ppm, 400 MHz, $CDCl_3$): 8.54 (dd, 2H, *J* = 4.9, *J* = 1.3), 7.65 (td, 2H, *J* = 7.7, *J* = 1.8), 7.48 (d, 2H, *J* = 7.8), 7.15 (ddd, 2H, *J* = 7.4, *J* = 4.9, *J* = 1.2), 3.86 (s, 4H), 2.82 (t, 2H, *J* = 6.0), 2.69 (t, 2H, *J* = 6.0). ^{13}C NMR (δ ppm, 100 MHz, $CDCl_3$): 159.46 (2), 149.11 (2), 136.53 (2), 123.03 (2), 122.12 (2), 60.51 (2), 56.25, 39.26. HRMS-ESI: Calculated for $C_{14}H_{19}N_4$ $[M+H]^+$ 243.16020, found 243.160452.

5.4.3 4-(2-methoxyethoxy)-*N*-(ethyl-1-(2-(bis(pyridin-2-ylmethyl)amino)ethyl)thiourea) naphthalimide EnDiPic

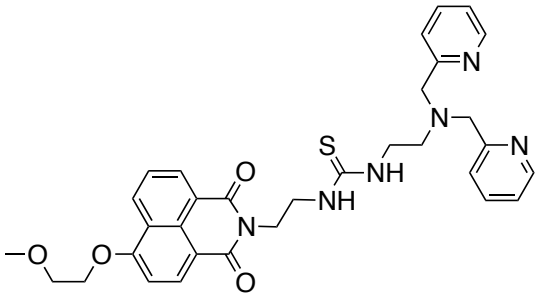

Prepared according to the general procedure F: **94** (53 mg, 0.12 mmol); acetonitrile (5 ml); **110** (30 mg, 0.12 mmol); acetonitrile (5 ml). The reaction mixture is stirred for 2 hour at reflux. The crude product was purified by column chromatography (aluminium oxide, eluent: CH_2Cl_2 to CH_2Cl_2/MeOH: 99/1) to give the product **EnDiPic** (45 mg, 60 %) as a yellow solid.

^{1}H NMR (δ ppm, 400 MHz, $CDCl_3$): 8.64 (dd, 1H, *J* = 1.6, *J* = 8.4), 8.59 (dd, 1H, *J* = 1.2, *J* = 7.3), 8.57-8.56 (m, 2H), 8.54 (d, 1H, *J* = 8.3), 7.71 (dd, 1H, *J* = 7.3, *J* = 8.4), 7.59 (dt, 2H, *J* = 1.8, *J* = 7.6), 7.35-7.33 (m, 2H), 7.12-7.09 (m, 2H), 7.04 (d, 1H, J = 8.3), 4.50-4.48 (m, 2H), 4.45-4.43 (m, 2H), 3.96-3.93 (m, 4H), 3.85 (s, 4H), 3.53 (s, 3H), 2.82 (t, 2H, *J* = 5.6).

^{13}C NMR (δ ppm, 100 MHz, $CDCl_3$): 181.88, 165.41, 164.80, 160.59, 158.96 (2), 149.32 (2), 136.74 (2), 134.01, 132.14, 129.69, 129.52, 126.17, 123.75, 123.34 (2), 122.30 (2), 122.14, 114.94, 106.26, 70.79, 68.65, 59.90, 59.55, 52.27, 43.04, 39.17. IR (film) cm^{-1}: 3343m, 3052m, 2939m, 1693s, 1657s, 1593s, 1549s, 1515s, 1471m, 1433m, 1387s, 1357s, 1270s, 1238s, 1198m, 1128m, 1085s, 1034m, 996w, 860w, 780m, 758m, 734m, 701w, 676w, 581w. HRMS-ESI: Calculated for $C_{32}H_{34}N_6O_4S$ $[M+H]^+$ 599.24350, found 599.24344; calculated for $C_{32}H_{33}N_6NaO_4S$ $[M+Na]^+$ 621.22545, found 621.22522. R_f (Aluminium oxide, CH_2Cl_2/MeOH: 99.5/0.5): 0.25.

5.4.4 *N*-(2-picolyl)-*N'*-Boc-ethylenediamine 111

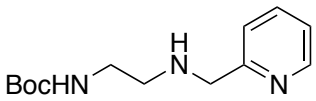

N-Boc-1,2-diaminoethane **79** (627 mg, 3.92 mmol) was solved in methanol (15 ml) and 2-pyridine carboxaldehyde (350 mg, 3.27 mmol) was added at 0°C. The reaction mixture was stirred at room temperature for 3 hours, sodium triacetoxyborohydride (970 mg, 4.57 mmol) was added and the reaction mixture was stirred over night. The solvent was concentrated under vacuum and the residue was treated with a saturated solution of Na_2CO_3. The product was extracted with CH_2Cl_2, the organic phase was dried over $MgSO_4$ and concentrated under vacuum. The crude product obtained was considered to be enough pure for the next step, **111** was obtained as a brawn oil (680 mg, 83 %). The obtained data are consistent with those previously reported.[166]

^{1}H NMR (δ ppm, 400 MHz, $CDCl_3$): 8.56 (dd, 1H, J = 5.0, J = 1.2), 7.65 (td, 1H, J = 7.7, J = 1.8), 7.29 (d, 1H, J = 7.8), 7.18 (ddd, 1H, J = 7.5, J = 4.9, J = 1.1), 5.17 (s, 1H), 3.93 (s, 2H), 3.39-3.36 (m, 2H), 2.82-2.80 (m, 2H), 1.44 (s, 9H). ^{13}C NMR (δ ppm, 125 MHz, $CDCl_3$): 158.88, 156.20, 149.39, 136.64, 122.42, 122.21, 79.21, 54.46, 48.76, 40.17, 28.44 (3). R_f (aluminium oxide, CH_2Cl_2/MeOH: 99.5/0.5): 0.11.

5.4.5 *N*-methyl-*N*-(2-picolyl)-*N'*-Boc-ethylenediamine 112

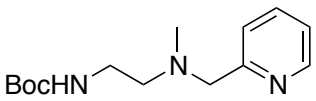

Iodomethane (34 mg, 0.24 mmol) and sodium carbonate (85 mg, 0.80 mmol) were added to a solution of **111** (50 mg, 0.20 mmol) in methanol (20 ml) and the reaction mixture was heated

to reflux for 72 hours. The solvent was concentrated under vacuum and the crude product was purified by column chromatography (aluminium oxide, eluent: CH_2Cl_2/MeOH 99/1). The product **112** was obtained as a light yellow oil (25 mg, 48 %).

^{1}H NMR (δ ppm, 400 MHz, $CDCl_3$): 8.57-8.55 (m, 1H), 7.67 (td, 1H, *J* = 7.7, *J* = 1.8), 7.38 (d, 1H, *J* = 7.9), 7.18 (dd, 1H, *J* = 7.4, J = 3.0), 3.71 (s, 2H), 3.27-3.25 (m, 2H), 2.59-2.57 (m, 2H), 2.32 (s, 3H), 1.45 (s, 9H). ^{13}C NMR (δ ppm, 125 MHz, $CDCl_3$): 159.03, 156.18, 149.33, 136.57, 123.17, 122.20, 79.19, 63.78, 56.47, 42.43, 38.18, 28.56 (3). IR (film) cm^{-1}: 3353 (m), 2978m, 2847m, 2806m, 1698s, 1592m, 1571m, 1520m, 1476m, 1435m, 1392m, 1366m, 1251m, 1174m, 1046w, 995w, 863w, 759m, 612s, 503w. HRMS-ESI: Calculated for $C_{14}H_{24}N_3O_2$ $[M+H]^+$ 266.1863, found 266.1864. R_f (aluminium oxide: CH_2Cl_2/MeOH 99/1): 0.31.

5.4.6 *N*-methyl-*N*-(2-picolyl)ethylenediamine 113

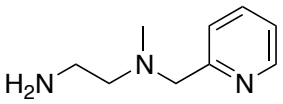

Prepared according to the general procedure D: **112** (150 mg, 0.57 mmol) in CH_2Cl_2 (10 ml); trifluoroacetic acid (1.61 g, 14.15 mmol). The product **113** was obtained without purification as a yellow oil (48 mg, 50 %). This compound was not purified and used for the next reaction.

^{1}H NMR (δ ppm, 400 MHz, $CDCl_3$): 8.57-8.55 (m, 1H), 7.68-7.64 (m, 1H), 7.38 (d, 1H, *J* = 7.9), 7.19-7.17 (m, 1H), 3.68 (s, 2H), 2.56-2.54 (m, 4H), 2.26 (s, 3H).

5.4.7 4-(2-methoxyethoxy)-*N*-(ethyl-1-(2-methyl(2-picolyl)amino)ethyl) thiourea) naphthalimide EnMePic

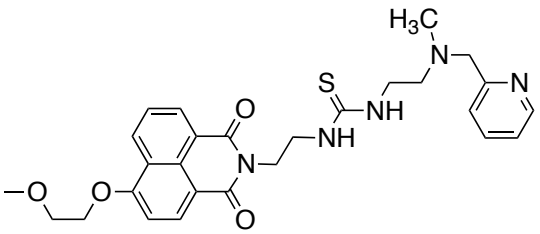

Prepared according to the general procedure F: **94** (103 mg, 0.24 mmol); acetonitrile (5 ml); **113** (40 mg, 0.24 mmol); acetonitrile (5 ml). The reaction mixture is stirred for 2 hour at reflux. The crude product was purified by column chromatography (aluminium oxide, eluent:

CH_2Cl_2 to CH_2Cl_2/MeOH: 99/1) to give the product **EnMePic** as a yellow solid (45 mg, 36 %).

^{1}H NMR (δ ppm, 400 MHz, $CDCl_3$): 8.66 – 8.55 (m, 3H), 8.53 (d, 1H, *J* = 8.3), 7.70 (dd, 1H, *J* = 7.3, *J* = 8.4), 7.62 (td, 1H, *J* = 1.8, *J* = 7.7), 7.34 (d, 1H, *J* = 7.8), 7.14 (dt, *J* = 2.9, *J* = 8.1), 7.05 (d, 1H, *J* = 8.3), 4.57-4.36 (m, 4H), 4.01-3.81 (m, 4H), 3.73 (s, 2H), 3.52 (s, 5H), 2.71 (s, 2H), 2.31 (s, 3H). ^{13}C NMR (δ ppm, 125 MHz, $CDCl_3$): 181.97, 165.37, 164.74, 160.57 (2), 149.37, 136.77, 134.02, 132.13, 129.62, 129.55, 126.16, 123.68, 123.35, 122.38, 122.04, 114.83, 106.02, 70.75, 68.61, 63.29, 59.56, 55.44, 53.58, 42.20, 39.09. IR (film) cm^{-1}: 3343m, 3052m, 2939m, 1693s, 1657s, 1593s, 1549s, 1515s, 1471m, 1433m, 1387s, 1357s, 1270s, 1238s, 1198m, 1128m, 1085s, 1034m, 996w, 860w, 780m, 758m, 734m, 701w, 676w, 581w. HRMS-ESI: Calculated for $C_{27}H_{32}N_5O_4S$ $[M+H]^+$ 522.21695, found 522.21711. R_f (CH_2Cl_2/MeOH: 99.5/0.5): 0.25.

5.4.8 2-(2-Pyridinyl)ethyl tosylate 116

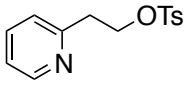

Triethylamine (812 mg, 8.12 mmol) was added to a solution of 2-pyridine ethanol **115** (500 mg, 4.06 mmol) in dry CH_2Cl_2 (10 ml) and p-toluensulfonyl chloride (1.161 g, 6.09 mmol) was added portionwise as a solid. The reaction mixture was stirred at room temperature over night. The organic phase was washed with water and brine, dried over $MgSO_4$ and concentrated under vacuum. The crude product was purified by column chromatography (eluent: CH_2Cl_2 / Hexane: 3/7 then CH_2Cl_2 and CH_2Cl_2/MeOH: 99.5/0.5) to give the product **116** as yellow oil (910 mg, 81 %). This product has to be stored at 4°C. The obtained data are consistent with those previously reported.[143]

^{1}H NMR (δ ppm, 400 MHz, $CDCl_3$): 8.42 (ddd, 1H, *J* = 4.9, *J* = 1.9, *J* = 1.0), 7.71-7.65 (m, 2H), 7.58 (td, 1H, *J* = 7.7, *J* = 1.9), 7.31-7.25 (m, 2H), 7.16 -7.09 (m, 2H), 4.43 (t, 2H, *J* = 6.6), 3.12 (t, 2H, *J* = 6.6), 2.43 (s, 3H). ^{13}C NMR (δ ppm, 125 MHz, $CDCl_3$): 156.66, 149.54, 144.73, 136.60, 133.04, 129.89, 128.00, 123.93, 121.94, 77.48, 77.16, 76.85, 69.55, 37.56, 21.74. R_f (CH_2Cl_2/MeOH: 99.5/0.5): 0.15.

5.4.9 *N*-2-((2-pyridinyl)ethyl))-*N'*-Boc-ethylenediamine 117

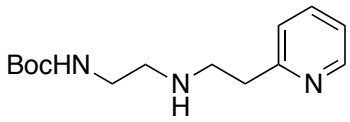

Celite (500 mg) and KF (500 mg, 8.77 mmol) were sonicated in acetonitrile (10 ml) for 20 min and stirred under Ar for 10 min. **79** (116 mg, 0.72 mmol) was added as a solid. A solution of **116** (200 mg, 0.72 mmol) solved in acetonitrile (1 ml) was added dropwise to the reaction mixture and it was stirred at room temperature for 5 days. The precipitate was filtered, washed with acetonitrile and the filtrate was concentrated under vacuum. The crude product was purified by column chromatography (aluminium oxide; eluent: CH_2Cl_2/MeOH: 99.5/0.5) to give product **117** as a colorless oil (45 mg, 23 %).

^{1}H NMR (δ ppm, 400 MHz, $CDCl_3$): 8.53 (ddd, 1H, J = 4.9, J = 1.9, J = 1.0), 7.60 (td, 1H, J = 7.7, J = 1.9), 7.16 (dt, 1H, J = 7.8, J = 1.1), 7.12 (ddd, 1H, J = 7.5, J = 4.9, J = 1.2), 5.18 (s, 1H), 3.23 (q, 2H, J = 5.9), 3.09-2.92 (m, 4H), 2.78 (t, 2H, J = 5.8), 1.44 (s, 9H). ^{13}C NMR (δ ppm, 125 MHz, $CDCl_3$): 160.23, 156.23, 149.41, 136.55, 123.44, 121.43, 79.17, 48.66, 48.55, 40.07, 37.94, 28.54 (3). IR (KBr) cm^{-1}: 3312m, 2975m, 2932m, 1707s, 1593m, 1525m, 1476m, 1436m, 1391m, 1366m, 1275m, 1252m, 1173s, 1051w, 995w, 865w, 758w. HRMS-ESI: Calculated for $C_{14}H_{24}N_3O_2$ $[M+H]^+$ 266.18595, found 266.18630. R_f (CH_2Cl_2/MeOH: 99.5/0.5): 0.22.

5.4.10 *o*-iodoxybenzoic acid (IBX)

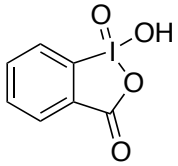

Prepared according to the literature:[167] Iodobenzoic acid (2.00 g, 8.06 mmol) and Oxone (14.88 g, 27.76 mmol) were heated to 70°C in water (100 ml). The precipitate is dissolving slowly and the reaction mixture is stirred at this temperature for 2 hours. The solution is becoming clear but the product start to precipitate immediately. The solution is cooled overnight to room temperature and the product is filtered and wash with water and acetone. **IBX** is obtained as a white solid (1.53, 68 %).

^{1}H NMR (δ ppm, 400 MHz, $CDCl_3$): 8.16-8.14 (m, 1H), 8.04-7.98 (m, 2H), 7.84 (t, 1H, *J* = 7.3).

5.4.11 2-((2-((2-hydroxyethyl)thio)ethyl)thio)acetaldehyde 121

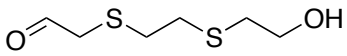

IBX (1.000 g, 3.57 mmol) was added as a solid to a solution of 3,6-dithia-1,8-octanediol (650 mg, 3.57 mmol) in ethylacetate (20 ml) and the reaction mixture was heated to reflux for 4 hours. After cooling down to room temperature, the precipitate is filtered and washed with ethylacetate. The organic phase containing the product is washed with a saturated solution of $NaHCO_3$, water, dried over $MgSO_4$ and concentrated under vacuum. The crude product was purified by column chromatography (eluent: CH_2Cl_2; CH_2Cl_2/MeOH: 99/1) and **121** is obtained as a yellow oil (158 mg, 25 %).

^{1}H NMR (δ ppm, 400 MHz, $CDCl_3$): 9.49 (t, 1H, *J* = 3.5), 3.76 (t, 2H, *J* = 5.9), 3.24 (d, 2H, *J* = 3.5), 2.81-2.71 (m, 4H), 2.71-2.63 (m, 2H). ^{13}C NMR (δ ppm, 125 MHz, $CDCl_3$): 193.65, 60.87, 41.19, 35.36, 31.52, 31.30. IR (film): 3406br, 2920m, 1714m, 1416m, 1107m, 1035m, 600s, 499s. EI-MS: 180 (5, M^+), 160 (53), 131 (55), 105 (71), 103 (61), 84 (49), 76 (52), 71 (47), 61(79), 60 (99), 59 (100). R_f (CH_2Cl_2/MeOH: 99/1): 0.15.

5.4.12 2,2'-(ethane-1,2-diylbis(sulfanediyl))diacetaldehyde 122

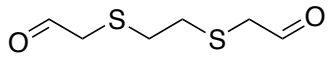

IBX (1.015 g, 3.63 mmol) was added as a solid to a solution of 3,6-dithia-1,8-octanediol (300 mg, 1.65 mmol) in ethylacetate (20 ml) and the reaction mixture was heated to reflux for 4 hours. After cooling down to room temperature, the precipitate is filtered and washed with ethylacetate. The organic phase containing the product is washed with a saturated solution of $NaHCO_3$, water, dried over $MgSO_4$ and concentrated under vacuum. The crude product was purified by column chromatography (eluent: CH_2Cl_2; CH_2Cl_2/MeOH: 99/1) and the product **122** is obtained as a yellow oil (140 mg, 47 %).

^{1}H NMR (δ ppm, 500 MHz, $CDCl_3$): 9.50 (t, 2H, *J* = 3.4), 3.24 (d, 4H, *J* = 3.4), 2.65 (s, 4H). ^{13}C NMR (δ ppm, 125 MHz, $CDCl_3$): 193.54, 41.23, 31.03. IR (film) cm^{-1}: 3417br, 2921s, 2723w, 1714s, 1583m, 1424m, 1246m, 1015m, 744m, 551w. EI-MS: 178 (16, M^+), 160 (5), 136 (33), 103 (100), 92 (11), 75 (28), 61 (45). R_f (CH_2Cl_2/MeOH: 99/1): 0.20.

5.4.13 2-((2-((2-((2-hydroxyethyl)thio)ethyl)thio)ethyl)-*N'*-Boc-ethylendiamine 123

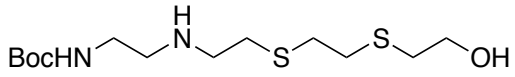

N-Boc-1,2-diaminoethane **79** (106 mg, 0.67 mmol) was solved in THF (15 ml) and **121** (120 mg, 0.67 mmol) was added at 0°C. Sodium triacetoxyborohydride (970 mg, 4.57 mmol) was added and the reaction mixture was stirred at room temperature for 3 hours. The solvent was concentrated under vacuum and the residue was treated with a saturated solution of Na_2CO_3. The product was extracted with ether, the organic phase was dried over $MgSO_4$ and concentrated under vacuum. The crude product was purified by column chromatography (aluminium oxide, eluent: CH_2Cl_2 to CH_2Cl_2/MeOH: 95/5) **123** was obtained as a brawn oil (70 mg, 32 %).

^{1}H NMR (δ ppm, 400 MHz, $CDCl_3$): 4.99 (s, 1H), 3.76 (t, 2H, *J* = 5.9), 3.23 (q, 2H, *J* = 5.7), 2.90 – 2.60 (m, 12H), 2.02 (s, 2H), 1.45 (s, 9H). ^{13}C NMR (δ ppm, 125 MHz, $CDCl_3$): 165.30, 77.36, 60.94, 48.89, 48.34, 40.40, 35.60, 32.71, 32.38, 32.22, 28.57 (3). HRMS-ESI: Calculated for $C_{13}H_{29}N_2O_3S_2$ $[M+H]^+$ 325.16141, found 325.16158. R_f (CH_2Cl_2/MeOH: 95/5): 0.15.

5.4.14 *N'*-Boc-1,4-diaza-7,10-dithiadodecyl tosylate 120

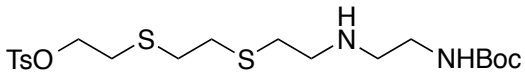

Triethylamine (31 mg, 0.31 mmol) was added to a solution of **123** (50 mg, 0.15 mmol) in CH_2Cl_2 (10 ml) at 0°C and p-toluensulfonyl chloride (44 mg, 0.23 mmol) was added portionwise as a solid. The reaction mixture was stirred at room temperature over night. The organic phase was washed with water and brine, dried over $MgSO_4$ and concentrated under vacuum. The crude product was purified by column chromatography (eluent: CH_2Cl_2/Hexane: 3/7 then CH_2Cl_2 and CH_2Cl_2/MeOH: 99/1) to give the product **120** as a white solid (25 mg, 37 %). This product has to be stored at 4°C.

^{1}H NMR (δ ppm, 400 MHz, $CDCl_3$): 7.69 (d, 2H, *J* = 8.1), 7.33 (d, 2H, *J* = 8.0), 3.79 (q, 2H, *J* = 5.7), 3.33-3.26 (m, 4H), 3.21-3.18 (m, 2H), 2.85 – 2.70 (m, 7H), 2.55 (s, 1H), 2.44 (s, 3H), 1.45 (s, 9H). ^{13}C NMR (δ ppm, 125 MHz, $CDCl_3$): 156.28, 143.96, 135.85, 130.07 (2), 127.32(2), 79.94, 61.58, 50.13, 49.07, 40.17, 35.31, 32.32, 32.19, 31.22, 28.54 (3), 21.68.

HRMS-ESI: Calculated for $C_{20}H_{34}N_2NaO_5S_3$ $[M+Na]^+$ 501.15221, found 501.15198. R_f (CH_2Cl_2/MeOH 99/1): 0.14.

5.4.15 *N*'-Boc-*N*-dithiacrownm-ethylendiamine 118

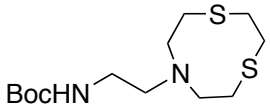

A solution of **122** (35 mg, 0.20 mmol) and sodium triacetoxyborohydride (125 mg, 0.59 mmol) in methanol (10 ml) was prepared and acetic acid (20 µl) was added and the reaction mixture was cooled to -78°C. A solution of **79** (28 mg, 0.18 mmol) in methanol (1 ml) was added dropwise very slowly. The reaction mixture was stirred 2 hours at room temperature. The solvent was concentrated under vacuum and the residue was treated with NaOH (2N) solution. The product was extracted with ether, the organic phase was dried over $MgSO_4$ and concentrated under vacuum. The crude product was purified by column chromatography (aluminium oxide, CH_2Cl_2/MeOH: 99/1) **118** was obtained as a brawn oil (4 mg, 6 %).

^{1}H NMR (δ ppm, 400 MHz, $CDCl_3$): 3.25-3.22 (m, 2H), 3.13 (s, 4H), 2.88-2.80 (m, 8H), 2.63 (t, 2H, J = 7.8), 1.45 (m, 9H). ESI-MS: $M+H^+$: 251. R_f (aluminum oxide, CH_2Cl_2/MeOH 99/1): 0.32.

5.4.16 *N*-(1-aza-12-crown-4)acetonitrile 128

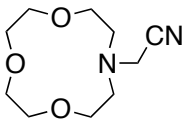

Celite (500 mg) and KF (500 mg, 8.77 mmol) were sonicated in acetonitrile (10 ml) for 20 min and stirred under Ar for 10 min. 1-Aza-12-crown-4 **127** (250 mg, 1.43 mmol) was added as a solid. A solution of chloroacetonitrile (118 mg, 1.57 mmol) solved in acetonitrile (1 ml) was added dropwise to the reaction mixture and it was stirred at room temperature for 72 hours. The precipitate was filtered, washed with acetonitrile and the filtrate was concentrated under vacuum. The crude product was purified by column chromatography (eluent: CH_2Cl_2/MeOH: 99/1) to give product **128** as a yellow oil (220 mg, 72 %).

^{1}H NMR (δ ppm, 400 MHz, $CDCl_3$): 3.68-3.62 (m, 14H), 2.83-2.81 (m, 4H). ^{13}C NMR (δ ppm, 125 MHz, $CDCl_3$): 115.77, 70.78 (2), 70.48 (2), 68.96 (2), 54.30 (2), 44.80. IR (film) cm^{-1}: 3480m, 2919s, 2858s, 1668s, 1455m, 1363m, 1306m, 1127m, 918m, 839m, 752w.

HRMS-ESI: Calculated for $C_{10}H_{18}N_2NaO_3$ $[M+Na]^+$ 237.12096, found 237.12085. R_f (CH_2Cl_2/MeOH: 99/1): 0.35.

5.4.17 *N*'-Boc-*N*-(1-aza-12-crown-4)ethylendiamine 129

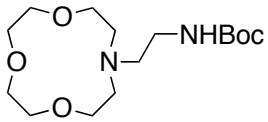

Raney nickel was introduced in a flask for hygrogenator and solved in *tert*-butanol. **128** (100 mg, 0.47 mmol) and di-tert-butyl dicarbonate (500 mg, 2.35 mmol) were added and the flask was submit to 55 psi of hydrogen pressure and stirred at room temperature over night. The solution was filtered over Celite while keeping the maximum of Raney nickel in the flask to avoid danger of combustion. The filtrate was concentrated under vacuum and the residue was purified by column chromatography (eluent: CH_2Cl_2/MeOH: 99/1 to 95/5) to give the product **129** as a colorless oil (29 mg, 20 %).

^{1}H NMR (δ ppm, 400 MHz, $CDCl_3$): 3.76-3.64 (m, 8H), 3.63-3.53 (m, 4H), 3.28-3.14 (m, 2H), 2.68 (t, 4H, *J* = 4.5), 2.62 (d, 2H, *J* = 6.0), 1.44 (s, 9H). ^{13}C NMR (δ ppm, 125 MHz, $CDCl_3$): 156.34, 78.50, 71.24 (2), 70.43 (2), 69.87 (2), 55.50 (2), 54.66, 38.53, 28.53 (3). IR (film) cm^{-1}: 3354m, 2859s, 1714s, 1516m, 1365m, 1251m, 1133m, 918w, 615m. HRMS-ESI: Calculated for $C_{15}H_{31}N_2O_5$ $[M+H]^+$ 319.22275, found 319.22296. R_f (CH_2Cl_2/MeOH: 98/2): 0.15.

5.4.18 *N*-(1-aza-12-crown-4)ethylendiamine 130

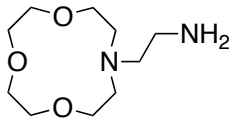

Prepared according to the general procedure D: **129** (54 mg, 0.17 mmol) in CH_2Cl_2 (10 ml); trifluoroacetic acid (484 mg, 4.25 mmol). The product **130** was obtained without purification as a yellow oil (25 mg, 68 %).

^{1}H NMR (δ ppm, 400 MHz, $CDCl_3$): 3.73-3.69 (m, 8H), 3.68-3.62 (m, 4H), 2.82-2.79 (m, 2H), 2.72-2.20 (m, 4H), 2.63-2.60 (m, 2H). ^{13}C NMR (δ ppm, 125 MHz, $CDCl_3$): 68.92 (2), 68.59 (2), 67.70 (2), 53.46 (2), 49.51, 37.69. IR (film) cm^{-1}: 3396m, 2873s, 1694s, 1465m, 1365m, 1293m, 1202m, 1129s, 1096, 918m, 835w, 800w, 719w. ESI-MS: $M+H^+$: 219.

5.4.19 4-(2-methoxyethoxy)-*N*-(ethyl-1-(2-(1-aza-12-crown-4)amino)ethyl) thiourea) naphthalimide En12C4

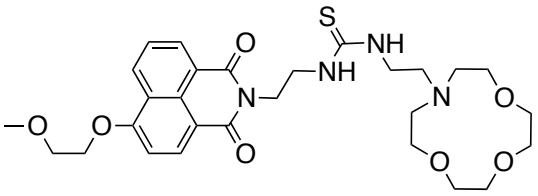

Prepared according to the general procedure E: **94** (43 mg, 0.10 mmol); acetonitrile (2 ml); **130** (22 mg, 0.10 mmol); acetonitrile (0.5 ml). The reaction mixture is stirred for 2 hour at reflux. The crude product was purified by column chromatography (aluminium oxide, eluent: CH_2Cl_2 to CH_2Cl_2/MeOH: 99/1) to give the product **En12C4** as a yellow solid (48 mg, 82 %).

^{1}H NMR (δ ppm, 400 MHz, $CDCl_3$): 8.66-8.56 (m, 2H), 8.53 (d, 1H, *J* = 8.2), 7.69 (dd, 1H, *J* = 7.3, *J* = 8.3), 7.04 (d, 1H, *J* = 8.3), 4.43 – 4.39 (m, 4H), 3.99-3.92 (m, 4H), 3.70-3.66 (m, 4H), 3.61-3.53 (m, 8H), 3.52 (s, 3H), 3.43-3.41 (m, 4H), 2.68-2.62 (m, 6H). ^{13}C NMR (δ ppm, 125 MHz, $CDCl_3$): 180.45, 164.09, 160.13, 133.48, 131.72, 129.62, 128.99, 126.03, 123.68, 122.53, 115.39, 106.10, 70.96, 70.81, 70.58, 70.43, 69.82, 68.54, 68.30, 59.52, 55.51, 53.50, 42.02, 39.65. IR (film) cm^{-1}: 3289s, 2920s, 1734s, 1695s, 1657s, 1593s, 1470m, 1397m, 1357m, 1270m, 1127m, 1084m, 1043m, 916w, 861w, 781m, 758w, 700w, 606w, 513w. HRMS-ESI: Calculated for $C_{28}H_{39}N_4O_7S$ $[M+H]^+$ 575.25340, found 575.25277; calculated for $C_{28}H_{38}N_4NaO_7S$ $[M+Na]^+$ 597.23534, found 597.23431. R_f (Aluminium oxide, CH_2Cl_2/MeOH: 99.5/0.5): 0.25

5.4.20 *N*-(1-aza-15-crown-5)acetonitrile 132

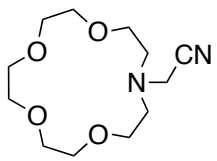

Celite (325 mg) and KF (325 mg, 5.70 mmol) were sonicated in acetonitrile (10 ml) for 20 min and stirred under Ar for 10 min. 1-Aza-15-crown-5 **131** (250 mg, 1.14 mmol) was added as a solid. A solution of chloroacetonitrile (95 mg, 1.25 mmol) in acetonitrile (1 ml) was added dropwise to the reaction mixture and it was stirred at room temperature for 72 hours. The precipitate was filtered, washed with acetonitrile and the filtrate was concentrated under

vacuum. The crude product was purified by column chromatography (eluent: CH_2Cl_2/MeOH: 98/2) to give product **132** as a yellow oil (205 mg, 70 %).

^{1}H NMR (δ ppm, 400 MHz, $CDCl_3$): 3.75-3.65 (m, 18H), 2.83-2.81 (m, 4H). ^{13}C NMR (δ ppm, 125 MHz, $CDCl_3$): 116.00, 70.92 (2), 70.47 (2), 70.36 (2), 69.13 (2), 54.28 (2), 44.59. IR (film) cm^{-1}: 3397m, 2878s, 1652w, 1455w, 1357m, 1248w, 1117s, 996w, 940m, 853w. HRMS-ESI: Calculated for $C_{12}H_{22}N_2NaO_4$ $[M+Na]^+$ 281.14733, found 281.14718. R_f (CH_2Cl_2/MeOH: 99/1): 0.35.

5.4.21 *N*'-Boc-*N*-(1-aza-15-crown-5)ethylendiamine 133

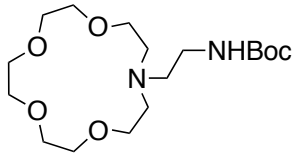

Raney nickel was introduced in a flask for hygrogenator and solved in *tert*-butanol. **132** (100 mg, 0.39 mmol) and di-tert-butyl dicarbonate (415 mg, 1.95 mmol) were added and the flask was submit to 55 psi of hydrogen pressure and stirred at room temperature over night. The solution was filtered over Celite while keeping the maximum of Raney nickel in the flask to avoid danger of combustion. The filtrate was concentrated under vacuum and the residue was purified by column chromatography (eluent: CH_2Cl_2/MeOH: 99/1 to 95/5) to give the product **133** as a colorless oil (50 mg, 35 %).

^{1}H NMR (δ ppm, 400 MHz, $CDCl_3$): 3.70-3.57 (m, 16H), 3.18-3.16 (m, 2H), 2.74-2.70 (m, 4H), 2.63-2.59 (m, 2H), 1.44 (s, 9H). IR (film) cm^{-1}: 3354m, 2862s, 1712s, 1514m, 1365m, 1248m, 1128m, 917w, 605m. ESI-MS: M+H$^+$: 363, M+Na$^+$: 385. R_f (CH_2Cl_2/MeOH: 98/2): 0.15.

5.4.22 *N*-(1-aza-15-crown-5)ethylendiamine 134

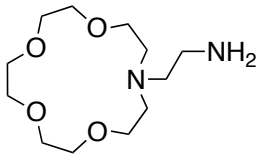

Prepared according to the general procedure D: **133** (75 mg, 0.21 mmol) in CH_2Cl_2 (10 ml); trifluoroacetic acid (484 mg, 4.25 mmol). The product **134** was obtained without purification as a yellow oil (45 mg, 83 %).

^{1}H NMR (δ ppm, 400 MHz, $CDCl_3$): 3.73-3.62 (m, 16H), 3.46-3.43 (m, 4H), 3.03-2.99 (m, 2H), 2.92-2.89 (m, 2H), 2.88-2.81 (m, 4H). ^{13}C NMR (δ ppm, 125 MHz, $CDCl_3$): 70.58 (2), 70.17 (2), 70.11 (2), 70.01 (2), 57.32 (2), 55.42, 39.32. IR (film) cm^{-1}: 3385m, 2875s, 1467m, 1455m, 1355m, 1301m, 1117s, 939m, 623s, 514w. ESI-MS: M+H$^+$: 263.

5.4.23 4-(2-methoxyethoxy)-*N*-(ethyl-1-(2-(1-aza-15-crown-5)amino)ethyl) thiourea) naphthalimide En15C5

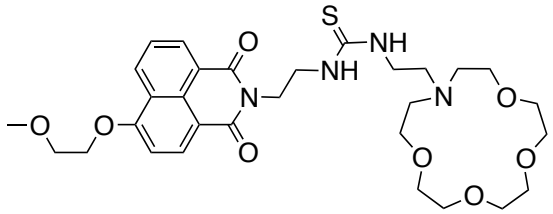

Prepared according to the general procedure E: **94** (43 mg, 0.10 mmol); acetonitrile (2 ml); **134** (22 mg, 0.10 mmol); acetonitrile (0.5 ml). The reaction mixture is stirred for 2 hour at reflux. The crude product was purified by column chromatography (aluminium oxide, eluent: CH_2Cl_2 to CH_2Cl_2/MeOH: 99/1) to give the product **En15C5** as a yellow solid (17 mg, 15 %).

^{1}H NMR (δ ppm, 400 MHz, $CDCl_3$): 8.62-8.56 (m, 2H), 8.52 (d, 1H, *J* = 8.2), 7.68 (dd, 1H, *J* = 7.3, *J* = 8.3), 7.03 (d, 1H, *J* = 8.3), 4.44-4.31 (m, 4H), 3.94-3.92 (m, 4H), 3.70-3.53 (m, 16H), 3.52 (s, 3H), 3.45-3.42 (m, 4H), 2.67-2.63 (m, 6H). ^{13}C NMR (δ ppm, 125 MHz, $CDCl_3$): 182.71, 164.71, 160.08, 133.46, 131.70, 129.59, 128.93, 126.01, 123.62, 122.57, 115.42, 106.07, 70.81, 70.35, 69.84, 69.74, 69.26, 69.15, 68.53, 59.52, 55.23, 53.81, 42.53, 39.64. IR (film) cm^{-1}: 3315m, 2875s, 1734m, 1694s, 1657s, 1593s, 1470m, 1433m, 1386m, 1356m, 1269m, 1238m, 1125m, 1084m, 1034m, 933w, 841w, 781m, 758w, 734w, 633w, 581w. HRMS-ESI: Calculated for $C_{30}H_{43}N_4O_8S$ $[M+H]^+$ 619.27961, found 619.27910; calculated for $C_{30}H_{42}N_4NaO_8S$ $[M+Na]^+$ 641.26156, found 641.26053. R_f (Aluminium oxide, CH_2Cl_2/MeOH: 99.5/0.5): 0.22.

5.5 Crystallographic Data

Table 5.1: *Crystallographic Data of MV412:Zn*

Crystallised from	Slow diffusion from Hexane in CH_2Cl_2
Empirical formula	$C_{19}H_{18}Cl_2N_4SZn$
Formula weight [g mol^{-1}]	470.72
Crystal colour, habit	colourless, prism
Crystal dimensions [mm]	0.15 × 0.18 × 0.20
Temperature [K]	160(1)
Crystal system	monoclinic
Space group	$P2_1/c$ (#14)
Z	4
Reflections for cell determination	11047
2θ range for cell determination [°]	4−57
Unit cell parameters a [Å]	11.10561(17)
b [Å]	12.50496(19)
c [Å]	14.4266(2)
α [°]	90
β [°]	97.9938(14)
γ [°]	90
V [Å^3]	1984.03(5)
$F(000)$	960
D_x [g cm^{-3}]	1.576
μ(Mo $K\alpha$) [mm^{-1}]	1.624
Scan type	ω
$2\theta_{(max)}$ [°]	56.6
Transmission factors (min; max)	0.859; 1.000
Total reflections measured	19445
Symmetry independent reflections	4480
R_{int}	0.023
Reflections with $I > 2\sigma(I)$	3885
Reflections used in refinement	4480
Parameters refined	248
Final $R(F)$ [$I > 2\sigma(I)$ reflections]	0.0260
$wR(F^2)$ (all data)	0.0627

Weights: $w = [\sigma^2(F_o^2) + (0.0237P)^2 + 1.1698P]^{-1}$ where $P = (F_o^2 + 2F_c^2)/3$

Goodness of fit	1.055
Final Δ_{max}/σ	0.001
$\Delta\rho$ (max; min) [e Å^{-3}]	0.46; -0.26
$\sigma(d_{(C-C)})$ [Å]	0.002 – 0.003

References

(1) IUPAC; Compendium of Chemical Technology, 2nd ed., compiled by McNaught, A. D. and Wilkinson, A. Blackwell Scientific Publications, Oxford, **1997**, Online version: *goldbook.iupac.org* created by Nic, N.; Jirat, J. an Kosata, B.

(2) Bell, T. W.; Hext, N. M. *Chem. Soc. Rev.* **2004**, *33*, 589–598.

(3) de Silva, A. P.; Gunaratne, H. Q. N.; Gunnlaugsson, T.; Huxley, A. J. M.; McCoy, C. P.; Rademacher, J. T.; Rice, T. E. *Chem. Rev.* **1997**, *97*, 1515–1566.

(4) de Silva, A. P. *J. Phys. Chem. Lett.* **2011**, *2*, 2865–2871.

(5) Czarnik, A. W. *Fluorescent Chemosensors for Ion and Molecule Recognition*; American Chemical Society: Waschington, DC, 1993.

(6) Lakowicz, J. R. *Principles of Fluorescence Spectroscopy*; Springer, 2006.

(7) Cowan, O. D.; Drisko, R. L. *Elements of Organic Photochemistry*; New York: Plenum Press, 1976.

(8) Kasha, M. *Discuss. Faraday Soc.* **1950**, *9*, 14–19.

(9) Bissell, R. A.; de Silva, A. P.; Gunaratne, H. Q. N.; Lynch, P. L. M.; Maguire, G. E. M.; Sandanayake, K. R. A. S. *Chem. Soc. Rev.* **1992**, *21*, 187–195.

(10) Amiot, C. L.; Xu, S.; Liang, S.; Pan, L.; Zhao, J. X. *Sensors* **2008**, *8*, 3082–3105.

(11) Valeur, B.; Leray, I. *Coord. Chem. Rev.* **2000**, *205*, 3–40.

(12) Stokes, G. G. *Philosophical Transactions of the Royal Society of London* **1852**, *142*, 463–562.

(13) Bissell, R. A.; de Silva, A. P. *Top. Curr. Chem.* **1993**, *168*, 223–264.

(14) Selinger, B. K. *Aust. J. Chem.* **1977**, *30*, 2087–2090.

(15) Sousa, L. R.; Larson, J. M. *J. Am. Chem. Soc.* **1977**, *99*, 307–310.

(16) Ghosh, S.; Petrin, M.; Maki, A. H.; Sousa, L. R. *J. Chem. Phys.* **1987**, *87*, 4315-4323.

(17) Shizuka, H.; Nakamura, M.; Morita, T. *J. Phys. Chem.* **1979**, *83*, 2019–2024.

(18) Konopelski, J. P.; Kotzyba-Hibert, F.; Lehn, J.-M.; Desvergne, J.-P.; Fag s, F. D. R.; Castellan, A.; Bouas-Laurent, H. *J. Chem. Soc., Chem. Commun.* **1985**, 433-436.

(19) Fages, F.; Desvergne, J. P.; Bouas-Laurent, H.; Marsau, P.; Lehn, J. M.; Kotzyba-Hibert, F.; Albrecht-Gary, A. M.; Al-Joubbeh, M. *J. Am. Chem. Soc.* **1989**, *111*, 8672–8680.

(20) de Silva, A. P.; Rupasinghe, R. A. D. D. *J. Chem. Soc., Chem. Commun.* **1985**, 1669–1670.

(21) de Silva, A. P.; de Silva, S. A. *J. Chem. Soc., Chem. Commun.* **1986**, 1709–1710.

(22) Huston, M. E.; Akkaya, E. U.; Czarnik, A. W. *J. Am. Chem. Soc.* **1989**, *111*, 8735-8737.

(23) Nanjappan, P.; Czarnik, A. W. *J. Am. Chem. Soc.* **1987**, *109*, 1826–1833.

(24) Huston, M. E.; Haider, K. W.; Czarnik, A. W. *J. Am. Chem. Soc.* **1988**, *110*, 4460-4462.

(25) Akkaya, E. U.; Huston, M. E.; Czarnik, A. W. *J. Am. Chem. Soc.* **1990**, *112*, 3590-3593.

(26) Czarnik, A. W. *Acc. Chem. Res.* **1994**, *27*, 302–308.

(27) Formica, M.; Fusi, V.; Giorgi, L.; Micheloni, M. *Coord. Chem. Rev.* **2012**, *256*, 170–192.

(28) Jeong, Y.; Yoon, J. *Inorg. Chim. Acta* **2012**, *381*, 2–14.

(29) Demchenko, A. P. *Introduction to Fluorescence Sensing*; Springer, 2009.

(30) Valeur, B.; Berberan-Santos, M. *Molecular Fluorescence*; Wiley-VCH, 2012.

(31) Kavarnos, G. J. *Fundamentals of Photoinduced Electron Transfer*; VCH Publishers, 1993.

(32) Weller, A. *Pure Appl. Chem* **1968**, *16*, 115–123.

(33) Rehm, D.; Weller, A. *Isr. J. Chem.* **1970**, *8*, 259–271.

(34) Oevering, H.; Paddon-Row, M. N.; Heppener, M.; Oliver, A. M.; Cotsaris, E.; Verhoeven, J. W.; Hush, N. S. *J. Am. Chem. Soc.* **1987**, *109*, 3258–3269.

(35) Marcus, R. A. *Angew. Chem. Int. Ed. Engl.* **1993**, *32*, 1111–1121.

(36) Grampp, G. *Angew. Chem. Int. Ed. Engl.* **1993**, *32*, 691–693.

(37) Kavarnos, G. J.; Turro, N. J. *Chem. Rev.* **1986**, *86*, 401–449.

(38) Beeson, J. C.; Huston, M. E.; Pollard, D. A.; Venkatachalam, T.; Czarnik, A. W. *J Fluoresc.* **1993**, *3*, 65–68.

(39) Vanderauwera, P.; DeSchryver, F. C.; Weller, A.; Winnik, M. A.; Zachariasse, K. A. *J. Phys. Chem.* **1984**, *88*, 2964–2970.

(40) Brimage, D. R. G.; Davidson, R. S. *J. Chem. Soc., Chem. Commun.* **1971**, 1385-1386.

(41) Davidson, R. S.; Trethewey, K. R. *J. Chem. Soc., Chem. Commun.* **1976**, 827–829.

(42) Closs, G. L.; Miller, J. R. *Science* **1988**, *240*, 440–447.

(43) Suppan, P. *Top. Curr. Chem.* **1992**, 95–130.

(44) Callan, J. F.; de Silva, A. P.; Magri, D. C. *Tetrahedron* **2005**, *61*, 8551–8588.

(45) Bryan, A. J.; de Silva, A. P.; de Silva, S. A.; Rupasinghe, R.; Sandanayake, K. *Biosensors* **1989**, *4*, 169–179.

(46) Walkup, G. K.; Burdette, S. C.; Lippard, S. J.; Tsien, R. Y. *J. Am. Chem. Soc.* **2000**, *122*, 5644–5645.

(47) Burdette, S. C.; Walkup, G. K.; Spingler, B.; Tsien, R. Y.; Lippard, S. J. *J. Am. Chem. Soc.* **2001**, *123*, 7831–7841.

(48) Burdette, S. C.; Frederickson, C. J.; Bu, W.; Lippard, S. J. *J. Am. Chem. Soc.* **2003**, *125*, 1778–1787.

(49) Nolan, E. M.; Jaworski, J.; Racine, M. E.; Sheng, M.; Lippard, S. J. *Inorg. Chem.* **2006**, *45*, 9748–9757.

(50) Kim, S. Y.; Hong, J. I. *Tetrahedron Lett.* **2009**, *50*, 2822–2824.

(51) Ji, H. F.; Dabestani, R.; Brownxy, G. M.; Hettich, R. L. *Photochem. Photobiol.* **1999**, *69*, 513–516.

(52) Le, T. P.; Rogers, J. E.; Kelly, L. A. *J Phys Chem A* **2000**, *104*, 6778–6785.

(53) Jones, G., II; Jackson, W. R.; Kanoktanaporn, S.; Bergmark, W. R. *Photochem. Photobiol.* **1985**, *42*, 477–483.

(54) Grabowski, Z. R. *Pure Appl. Chem* **1992**, *64*, 1249–1255.

(55) Grabovski, Z. R.; Dobkowski, J. *Pure Appl. Chem.* **1983**, *55*, 245–252.

(56) Rettig, W. *Angew. Chem. Int. Ed. Engl.* **1986**, *25*, 971–988.

(57) Grabowski, Z. R.; Rotkiewicz, K.; Rettig, W. *Chem. Rev.* **2003**, *103*, 3899–4032.

(58) Martin, M. M.; Plaza, P.; Meyer, Y. H.; Badaoui, F.; Bourson, J.; Lefevre, J. P.; Valeur, B. *J. Phys. Chem.* **1996**, *100*, 6879–6888.

(59) Létard, J.; Lapouyade, R.; Rettig, W. *Pure Appl. Chem.* **1993**, *65*, 1705–1705.

(60) Dumon, P.; Jonusauskas, G.; Dupuy, F.; Pée, P.; Rulliere, C.; Létard, J. F.; Lapouyade, R. *J. Phys. Chem.* **1994**, *98*, 10391–10396.

(61) Minta, A.; Tsien, R. Y. *J. Biol. Chem.* **1989**, *264*, 19449–19457.

(62) Grynkiewicz, G.; Poenie, M.; Tsien, R. Y. *J. Biol. Chem.* **1985**, *260*, 3440–3450.

(63) Van den Bergh, V.; Boens, N.; De Schryver, F. C.; Ameloot, M.; Steels, P.; Gallay, J.; Vincent, M.; Kowalczyk, A. *Biophys. J.* **1995**, *68*, 1110–1119.

(64) Tsien, R. Y.; Poenie, M. *Trends in Biochem. Sci.* **1986**, *11*, 450–455.

(65) Lemieux, G. A.; de Graffenried, C. L.; Bertozzi, C. R. *J. Am. Chem. Soc.* **2003**, *125*, 4708–4709.

(66) Soh, N.; Sakawaki, O.; Makihara, K.; Odo, Y.; Fukaminato, T.; Kawai, T.; Irie, M.; Imato, T. *Bioorg. Med. Chem.* **2005**, *13*, 1131–1139.

(67) Akasaka, K.; Suzuki, T.; Ohrui, H.; Meguro, H. *Anal. Lett.* **1987**, *20*, 731–745.

(68) Hoffmann, C.; Gaietta, G.; Bünemann, M.; Adams, S. R.; Oberdorff-Maass, S.; Behr, B.; Vilardaga, J.-P.; Tsien, R. Y.; Ellisman, M. H.; Lohse, M. J. *Nat. Methods* **2005**, *2*, 171–176.

(69) Griffin, B. A. *Science* **1998**, *281*, 269–272.

(70) Murray, S. G.; Hartley, F. R. *Chem. Rev.* **1981**, *81*, 365–414.

(71) Cooper, S. R. *Acc. Chem. Res.* **1988**, *21*, 141–146.

(72) Pearson, R. G. *J. Am. Chem. Soc.* **1963**, *85*, 3533–3539.

(73) Pearson, R. G. *J. Chem. Ed.* **1968**, *45*, 581.

(74) Griesbeck, A. G.; Schieffer, S. *Photochem. Photobiol. Sci.* **2003**, *2*, 113–117.

(75) Lee, M. S.; Qin, G.; Nakanishi, K.; Zagorski, M. G. *J. Am. Chem. Soc.* **2001**, *111*, 6234–6241.

(76) Martin, R. B.; Hedrick, R. I. *J. Am. Chem. Soc.* **1962**, *84*, 106–110.

(77) Mathew, E.; Meriwether, B. P.; Park, J. H. *J. Biol. Chem.* **1967**, *242*, 5024–5033.

(78) Qiao, W.; Zheng, J.; Wang, Y.; Zheng, Y.; Song, N.; Wan, X.; Wang, Z. Y. *Org. Lett.* **2008**, *10*, 641–644.

(79) Loving, G.; Imperiali, B. *J. Am. Chem. Soc.* **2008**, *130*, 13630–13638.

(80) Philipova, T.; Karamancheva, I.; Grabchev, I. *Dyes Pigm.* **1995**, *28*, 91–99.

(81) Alexiou, M. S.; Tychopoulos, V.; Ghorbanian, S.; Tyman, J. H. P.; Brown, R. G.; Brittain, P. I. *J. Chem. Soc., Perkin Trans. 2* **1990**, 837–842.

(82) Gao, Y. Q.; Marcus, R. A. *J. Phys Chem A* **2002**, *106*, 1956–1960.

(83) de Silva, A. P.; Gunaratne, H. Q.; Habib Jiwan, J. L.; McCoy, C. P.; Rice, T. E.; Soumillion, J. P. *Angew. Chem. Int. Ed. Engl.* **1995**, *34*, 1728–1731.

(84) Veale, E. B.; Tocci, G. M.; Pfeffer, F. M.; Kruger, P. E.; Gunnlaugsson, T. *Org. Biomol. Chem.* **2009**, *7*, 3447–3454.

(85) Xiao, Y.; Fu, M.; Qian, X.; Cui, J. *Tetrahedron Lett.* **2005**, *46*, 6289–6292.

(86) Ramachandram, B.; Saroja, G.; Sankaran, B.; Samanta, A. *J. Phys. Chem. B* **2000**, *104*, 11824–11832.

(87) Benanti, T. L.; Saejueng, P.; Venkataraman, D. *Chem. Commun.* **2007**, 692.

(88) Wolter, M.; Nordmann, G.; Job, G. E.; Buchwald, S. L. *Org. Lett.* **2002**, *4*, 973-976.

(89) Boens, N.; Qin, W.; Basarić, N.; Hofkens, J.; Ameloot, M.; Pouget, J.; Lefèvre, J.-P.; Valeur, B.; Gratton, E.; vandeVen, M.; Silva, N. D.; Engelborghs, Y.; Willaert, K.; Sillen, A.; Rumbles, G.; Phillips, D.; Visser, A. J. W. G.; van Hoek, A.; Lakowicz, J. R.; Malak, H.; Gryczynski, I.; Szabo, A. G.; Krajcarski, D. T.; Tamai, N.; Miura, A. *Anal. Chem.* **2007**, *79*, 2137–2149.

(90) Lim, N. C.; Br ckner, C. *Chem. Commun.* **2004**, 1094.

(91) Song, A.; Wang, X.; Lam, K. S. *Tetrahedron Lett.* **2003**, *44*, 1755–1758.

(92) Akita, S.; Umezawa, N.; Higuchi, T. *Org. Lett.* **2005**, *7*, 5565–5568.

(93) Phuong, T.; Khac-Minh, T.; Van Ha, N. T.; Ngoc Phuong, H. T. *Bioorg. Med. Chem. Lett.* **2004**, *14*, 653–656.

(94) Rodríguez-Fernández, E.; Manzano, J. L.; Benito, J. J.; Hermosa, R.; Monte, E.; Criado, J. J. *J. Inorg. Biochem.* **2005**, *99*, 1558–1572.

(95) Huebner, C. F.; Marsh, J. L.; Mizzoni, R. H.; Mull, R. P.; Schroeder, D. C.; Troxell, H. A.; Scholz, C. R. *J. Am. Chem. Soc.* **1953**, *75*, 2274–2275.

(96) Venkatachalam, T. K.; Sudbeck, E. A.; Uckun, F. M. *Tetrahedron Lett.* **2001**, *42*, 6629–6632.

(97) Foye, W. O.; Chao, C. C. *J. Pharm. Sci.* **1984**, *73*, 1284–1286.

(98) Leßmann, F.; Beyer, L.; Sieler, J. *Inorg. Chem. Commun.* **2000**, *3*, 62–64.

(99) Moloto, M. J.; Malik, M. A.; O'Brien, P.; Motevalli, M.; Kolawole, G. A. *Polyhedron* **2003**, *22*, 595–603.

(100) Ashcroft, S. J. *J. Chem. Engin. Data* **1988**, *33*, 73–75.

(101) Salter, M. H.; Reibenspies, J. H.; Jones, S. B.; Hancock, R. D. *Inorg. Chem.* **2005**, *44*, 2791–2797.

(102) Amendola, V.; Bonizzoni, M.; Esteban-Gómez, D.; Fabbrizzi, L.; Licchelli, M.; Sancenón, F.; Taglietti, A. *Coord. Chem. Rev.* **2006**, *250*, 1451–1470.

(103) Fan, E.; Van Arman, S. A.; Kincaid, S.; Hamilton, A. D. *J. Am. Chem. Soc.* **1993**, *115*, 369–370.

(104) Haushalter, K. A.; Lau, J.; Roberts, J. D. *J. Am. Chem. Soc.* **1996**, *118*, 8891–8896.

(105) Bryantsev, V. S.; Hay, B. P. *J. Phys. Chem. A* **2006**, *110*, 4678–4688.

(106) Costero, A. M.; Gaviña, P.; Rodríguez-Muñiz, G. M.; Gil, S. *Tetrahedron* **2007**, *63*, 7899–7905.

(107) Schreiner, P. R. *Chem. Soc. Rev.* **2003**, *32*, 289.

(108) Zhang, Z.; Schreiner, P. R. *Chem. Soc. Rev.* **2009**, *38*, 1187.

(109) Costero, A. M.; Gaviña, P.; Rodríguez-Muñiz, G. M.; Gil, S. *Tetrahedron* **2006**, *62*, 8571–8577.

(110) Gunnlaugsson, T.; Ali, H. D. P.; Glynn, M.; Kruger, P. E.; Hussey, G. M.; Pfeffer, F. M.; Santos, C. M. G.; Tierney, J. *J. Fluoresc.* **2005**, *15*, 287–299.

(111) Duke, R. M.; Veale, E. B.; Pfeffer, F. M.; Kruger, P. E.; Gunnlaugsson, T. *Chem. Soc. Rev.* **2010**, *39*, 3936.

(112) Gunnlaugsson, T.; Glynn, M.; Kruger, P. E.; Pfeffer, F. M. *Coord. Chem. Rev.* **2006**, *250*, 3094–3117.

(113) Ziessel, R.; Bonardi, L.; Retailleau, P.; Ulrich, G. *J. Org. Chem.* **2006**, *71*, 3093-3102.

(114) Profatilova, I.; Bumber, A.; Tolpygin, I.; Rybalkin, V.; Gribanova, T.; Mikhailov, I.; Bren, V. *Russ. J. Gen. Chem.* **2005**, *75*, 1774–1781.

(115) Tolpygin, I.; Shepelenko, E.; Revinskii, Y. V.; Tsukanov, A.; Dubonosov, A.; Bren, V.; Minkin, V. *Russ. J. Gen. Chem.* **2010**, *80*, 765–770.

(116) Del, G. T.; Carlotti, B.; De, S. S.; Barbafina, A.; Elisei, F. *Phys. Chem. Chem. Phys.* **2010**, *12*, 8062–8070.

(117) Sumiya, S.; Sugii, T.; Shiraishi, Y. *J. Photochem. Photobiol.* **2011**, *219*, 154-158.

(118) Lin, W.-C.; Wu, C.-Y.; Liu, Z.-H.; Lin, C.-Y.; Yen, Y.-P. *Talanta* **2010**, *81*, 1209-1215.

(119) Lu, X.; Guo, Z.; Feng, M.; Zhu, W. *ACS Appl Mater Interfaces* **2012,** *4*, 3657-3662.

(120) Hennrich, G.; Walther, W.; Resch-Genger, U.; Sonnenschein, H. *Inorg. Chem.* **2001**, *40*, 641–644.

(121) Koch, K. R. *Coord. Chem. Rev.* **2001**, *216*, 473–488.

(122) Malashikhin, S. A.; Baldridge, K. K.; Finney, N. S. *Org. Lett.* **2010**, *12*, 940–943.

(123) Eisenführ, A.; Arora, P. S.; Sengle, G.; Takaoka, L. R.; Nowick, J. S.; Famulok, M. *Bioorg. Med. Chem.* **2003**, *11*, 235–249.

(124) Jentzsch, E.; Mokhir, A. *Inorg. Chem.* **2009**, *48*, 9593–9595.

(125) Montero, A.; Goya, P.; Jagerovic, N.; Callado, L. F.; Meana, J. J.; Girón, R.; Goicoechea, C.; Martín, M. I. *Bioorg. Med. Chem.* **2002**, *10*, 1009–1018.

(126) West, C. W.; Estiarte, M. A.; Rich, D. H. *Org. Lett.* **2001**, *3*, 1205–1208.

(127) King, R. M.; Hercules, D. M. *Anal. Chem.* **1963**, *35*, 1099–1100.

(128) Kruppa, M.; König, B. *Chem. Rev.* **2006**, *106*, 3520–3560.

(129) Xu, Z.; Yoon, J.; Spring, D. R. *Chem. Soc. Rev.* **2010**, *39*, 1996–2006.

(130) Nolan, E. M.; Lippard, S. J. *J. Am. Chem. Soc.* **2003**, *125*, 14270–14271.

(131) Wu, Y.; Peng, X.; Guo, B.; Fan, J.; Zhang, Z.; Wang, J.; Cui, A.; Gao, Y. *Org. Biomol. Chem.* **2005**, *3*, 1387–1392.

(132) Tang, B.; Huang, H.; Xu, K.; Tong, L.; Yang, G.; Liu, X.; An, L. *Chem. Commun.* **2006**, 3609–3611.

(133) Anderegg, G.; Hubmann, E.; Podder, N. G.; Wenk, F. *Helv. Chim. Acta* **1977**, *60*, 123–140.

(134) Blake, A. J.; Danks, J. P.; Fallis, I. A.; Harrison, A.; Li, W.-S.; Parsons, S.; Ross, S. A.; Whittaker, G.; Schröder, M. *J. Chem. Soc., Dalton Trans.* **1998**, 3969–3976.

(135) McAuley, A.; Subramanian, S. *Inorg. Chem.* **1990**, *29*, 2830–2837.

(136) Abdel-Magid, A. F.; Carson, K. G.; Harris, B. D.; Maryanoff, C. A.; Shah, R. D. *J. Org. Chem.* **1996**, *61*, 3849–3862.

(137) van de Water, L. G. A.; Hoonte, ten, F.; Driessen, W. L.; Reedijk, J.; Sherrington, D. C. *Inorg. Chim. Acta* **2000**, *303*, 77–85.

(138) Collington, E. W.; Middlemiss, D.; Panchal, T. A.; Wilson, D. R. *Tetrahedron Lett.* **1981**, *22*, 3675–3678.

(139) Bourdais, J.; Rajniakova, O.; Povazanec, F. *J. Heterocyclic Chem.* **1980**, *17*, 1351–1353.

(140) Nolan, E. M.; Lippard, S. J. *Inorg. Chem.* **2004**, *43*, 8310–8317.

(141) Macomber, R. S. *J. Chem. Ed.* **1992**, *69*, 375-378.

(142) Hanaoka, K.; Kikuchi, K.; Urano, Y.; Nagano, T. *J. Chem. Soc, Perkin Trans. 2* **2001**, 1840–1843.

(143) Lin, Y.-C.; Yu, K.-H.; Lin, Y.-F.; Lee, G.-H.; Wang, Y.; Liu, S.-T.; Chen, J.-T. *Dalton Trans.* **2012**, *41*, 6661.

(144) Lochner, M.; Geneste, H.; Hesse, M. *Helv. Chim. Acta* **1998**, *81*, 2270–2281.

(145) Ozanne-Beaudenon, A.; Quideau, S. *Tetrahedron Lett.* **2006**, *47*, 5869–5873.

(146) Jesse, D.; Finney, N. S. *Org. Lett.* **2002**, *4*, 3001–3003.

(147) Painter, G. F.; Eldridge, P. J.; Falshaw, A. *Bioorg. Med. Chem.* **2004**, *12*, 225–232.

(148) de Silva, S. A.; Zavaleta, A.; Baron, D. E.; Allam, O.; Isidor, E. V.; Kashimura, N.; Percarpio, J. M. *Tetrahedron Lett.* **1997**, *38*, 2237–2240.

(149) de Silva, A. P.; Gunaratne, H. Q. N.; Lynch, P. L. M. *J. Chem. Soc., Perkin Trans. 2* **1995**, 685–690.

(150) Fabbrizzi, L.; Gatti, F.; Pallavicini, P.; Parodi, L. *New J. Chem.* **1998**, *22*, 1403-1407.

(151) Martell, A. E.; Hancock, R. D.; Motekaitis, R. J. *Coord. Chem. Rev.* **1994**, *133*, 39-65.

(152) Bradshaw, J. S.; Izatt, R. M. *Acc. Chem. Res.* **1997**, *30*, 338–345.

(153) Gokel, G. W.; Leevy, W. M.; Weber, M. E. *Chem. Rev.* **2004**, *104*, 2723–2750.

(154) Reed, M. I.; Pawlak, K.; Bradshaw, J. S. *Chem. Rev.* **1991**, *91*, 1721–2085.

(155) Tsukanov, A. V.; Dubonosov, A. D.; Bren, V. A.; Minkin, V. I. *Chem. Heterocycl. Compd.* **2008**, *44*, 899–923.

(156) Ver Heyen, K.; Cielen, E.; Tahri, A.; Saleh, A.; Boens, N.; Hoornaert, G. J. *Tetrahedron* **1999**, *55*, 5207–5226.

(157) Wu, Y. X.; Cao, J.; Deng, H. Y.; Feng, J. X. *Spectrochim. Acta, part A* **2011**, *82*, 340–344.

(158) Kondo, S.; Takahashi, T.; Takiguchi, Y.; Unno, M. *Tetrahedron Lett.* **2011**, *52*, 453–457.

(159) Park, C. S.; Lee, J. Y.; Kang, E.-J.; Lee, J.-E.; Lee, S. S. *Tetrahedron Lett.* **2009**, *50*, 671–675.

(160) Hou, C.; Urbanec, A. M.; Cao, H. *Tetrahedron Lett.* **2011**, *52*, 4903-4905.

(161) Aragoni, M. C.; Arca, M.; Bencini, A.; Blake, A. J.; Caltagirone, C.; Danesi, A.; Devillanova, F. A.; Garau, A.; Gelbrich, T.; Isaia, F.; Lippolis, V.; Hursthouse, M. B.; Valtancoli, B.; Wilson, C. *Inorg. Chem.* **2007**, *46*, 8088–8097.

(162) Moczar, I.; Peragovics, A.; Baranyai, P.; TOth, K.; Huszthy, P. *Tetrahedron* **2010**, *66*, 2953–2960.

(163) Emsley, J. *The Elements*; 1998.

(164) B, B. I. *Handbook of Fluorescent Spectra*; Accademic Press, New York, 1965.

(165) Lee, M. S.; Qin, G.; Nakanishi, K.; Zagorski, M. G. *J. Am. Chem. Soc.* **1989**, *111*, 6234–6241.

(166) Lim, N. C.; Ewart, C. B.; Bowen, M. L.; Ferreira, C. L.; Barta, C. A.; Adam, M. J.; Orvig, C. *Inorg. Chem.* **2008**, *47*, 1337–1345.

(167) Frigerio, M.; Santagostino, M.; Sputore, S. *J. Org. Chem.* **1999**, *64*, 4537–4538.

Curriculum vitae

Education

July 2008-present	University of Zürich, Switzerland PhD Thesis in Organic Chemistry: Fluorescent Chemosensors for Metal Ions Based on Photoinduced Electron Transfer from Sulfur. PD Dr. Nathaniel Finney
October 2002-July 2007	University of Neuchâtel, Switzerland Diplôme de chimiste Grade: Bien
August 1999- June 2002	Gymnase de Bienne (High School), Bienne, Switzerland

Work Experience

July 2008-present	University of Zürich, Switzerland Doctoral Research on fluorescent chemosensors for metal ions and teaching assistant in the general chemistry laboratories for medicine students.
Sept 2007 – Feb 2008	Training in Industry: Merck OLED, Frankfurt, Germany Work in organic synthesis in a research group for the development of compounds for OLED.
September 2006- May 2007	Diploma Work: Synthesis and Study of Liquid Crystalline Dendrimers (Polyarylester and Polybenzylether) for the Functionalization of Gold Nanoparticules Prof. Robert Deschenaux, University of Neuchâtel

Publications

Liquid-Crystalline Thiol- and Disulfide-Based Dendrimers for the Functionalization of Gold Nanoparticules, Frein, S. Boudon, J. Vonlanthen, M. Scharf, T. Barbera, J. Süss-Fink, G. Bürgi, T. Deschenaux, R. *Helv. Chim. Acta*, **2008**, *91*, 2321.

Thioureas as Reporting Elements for Metal-Responsive Fluorescent Chemosensors, Vonlanthen, M. Finney, N. S. *J. Org. Chem*. **2013**, 78, 3980-3988.

Modulation of the Response of Thiourea Based Fluorescent Chemosensor for Metal Ions in Aqueous Media, Vonlanthen, M. Finney N. S. *manuscript in preparation.*

Oral Presentations and Poster

Oral Presentation:	Swiss Chemical Society Meeting, Zürich, September 2010 Doktorandentag, University of Zürich, June 2011.
Posters:	Swiss Chemical Society Meeting, Lausanne, September 2009 and 2011 EuCheMS Chemistry Congress Nürnberg, August 2010 Gordon Conference on Physical Organic Chemistry, Holderness, NH, June 2011 Dorothy Crowfoot Hodgkin Symposium, Zurich, November 2010 and 2011